
PhD Thesis

School of Chemistry

Cardiff University

# Heterogeneous Nanoalloyed Precious Metal Catalysts

Thesis submitted in accordance with the requirements of Cardiff University for the degree of Doctor of Philosophy by:

Alexander G. R. Howe

October 2018

## *Acknowledgements*

Pursing a PhD at Cardiff University has been a thoroughly enjoyable, yet challenging experience. I'd like to thank my supervisors Dr Jennifer Edwards and Dr Jonathon Bartley for providing me with the opportunity and their advice, guidance and encouragement along the way.

I would also like the thank Dr Qian He, Dr Andrew Logsdail, Dr Richard Lewis and Dr Nick Dummer for their valuable insight provided throughout my three years of experimental work. Their expansive knowledge of the areas of electron microscopy, computational, and experimental chemistry have been indispensable in shaping the direction of my research during my time at Cardiff.

Many thanks also go to Dr Sarwat Iqbal and Dr Peter Miedziak, for their training and support in the lab whilst undertaking my PhD. Similar thanks are extended to Dr Thomas Davies and Dr David Morgan for their critical insight into the operation and analysis of electron microscopy and x-ray photoelectron spectroscopy respectively, without which this work would not have been possible.

I would also like to express my gratitude to all the students, postdocs and staff at the CCI for their assistance and encouragement in preparing this work. Special thanks go to Dr Greg Shaw and Mr Christopher Morgan for their aid in the practical aspects of my study.

Finally, I would like to thank my friends and family for their love, understanding and enduring support during this time.

## *Summary*

Hydrogen peroxide is a commodity chemical that is currently produced industrially using a complex and relatively inefficient process. The direct synthesis of hydrogen peroxide from molecular hydrogen and oxygen therefore represents a more environmentally friendly, atom efficient alternative. The aim of this thesis is to explore the preparation of highly active catalysts for the direct synthesis of hydrogen peroxide.

Chapter 3 investigates microwave assisted solvothermal methods as a possible preparation protocol for catalysts for the direct synthesis of hydrogen peroxide. It was found that mono- and bimetallic supported catalysts could be readily prepared in a one pot method, with the use of a microwave reactor greatly increase the speed and ease of catalyst preparation in comparison to conventional heating. $PdAu/TiO_2$ and $PdX/TiO_2$ catalysts, where X= Sn, Ni or In catalysts were explored, given their high activity for hydrogen peroxide synthesis when prepared by other methods. Preparation parameters such as solvent choice, the presence of stabilisers and metal loadings were all investigated with their regard to catalyst activity.

Chapter 4 focuses on the development of $PdAu/TiO_2$ catalysts using the sol immobilisation preparation technique. The protocol is commonly used as a recipe in literature to prepare catalysts, with little thought given to the nature of the preparation. Herein, factors such as preparation temperature, choice of reductant and the presence of stabilisers are considered in producing active catalysts. The optimised catalysts were found to be highly active for hydrogen peroxide synthesis but entirely inactive towards the non-productive hydrogen peroxide hydrogenation pathway, indicating that they are highly selective towards hydrogen peroxide. The catalysts were found to contain a unique agglomerated chain nanostructure, which was in part responsible for the high selectivity of the catalyst.

Chapter 5 investigates the preparation of PdAu/C catalysts for the direct synthesis of hydrogen peroxide. Catalysts prepared by wet impregnation and sol immobilisation, supported on various commercial carbons, were evaluated for their activity, finding that the choice of carbon support material greatly defines activity of the final catalyst. In the case of catalysts prepared by impregnation, the nanostructuring, oxidation state and surface composition of the PdAu nanoparticles varies wildly between catalyst, making identification of the factors important in preparing active catalysts difficult. In comparison, preparing using the sol immobilisation method yields catalysts containing nanoparticles of the same size,

oxidation state and surface composition. In this case, the activity of the catalysts was found to correlate with the oxygen surface concentration of the support material.

# *List of abbreviations*

| | |
|---|---|
| 1,3-BeD | 1,3-Butanediol |
| 1,5-PeD | 1,5-Pentanediol |
| AB | Ammonia borane complex, formula $NH_3BH_3$ |
| ADF | Angular dark field |
| AES | Atomic emission spectroscopy |
| AO | Anthraquinone oxidation process |
| AQ | Anthraquinone |
| BE | Binding energy |
| BET | Brunauer-Emmett-Teller surface area |
| BF | Bright field |
| Black Pearl | Black Pearl commercial carbon |
| CO-DRIFTS | Carbon monoxide diffuse reflectance infrared fourier transform spectroscopy |
| CTAB | Cetyltriammonium bromide |
| DMF | Dimethylformamide |
| DMFC | Direct methanol fuel cell |
| DMSO | Dimethyl sulfoxide |
| DP | Deposition precipitation |
| EDX | Energy dispersive x-ray spectroscopy |
| EG | Ethylene glycol |
| GC-TCD | Gas chromatography thermal conductivity detector |
| Glyc | Glycerol |
| GNP | Graphene nanoplatelets |
| Graphite (BNFL) | Graphite supplied by BNFL |
| Graphite(Sigma) | Graphite supplied by Sigma Aldrich |
| HAADF | High angle angular dark field |
| HG | Hexylene glycol |
| HPPO | Hydrogen peroxide to propylene oxide process |
| IMFP | Inelastic mean free path |
| KBB | KBB Black commercial carbon |
| MP-AES | Microwave plasma atomic emission spectroscopy |
| MWCNT | Multiwalled carbon nanotube commercial carbon |
| MWCNT-OH | Hydroxyl functionalised multiwalled carbon nanotube commercial carbon |
| NP | Nanoparticles |
| PAA | Polyacrylic acid |
| PTFE | Polytetrafluoroethylene |
| PVA | Polyvinyl alcohol |
| PVP | Polyvinylpyrrolidone |
| SDP500 | SDP500 commercial carbon |
| SDP500-COOH | Carboxylic acid functionalised SDP500 commercial carbon |
| SEM | Scanning electron microscopy |

| | |
|---|---|
| STEM | Scanning transmission electron microscopy |
| TEG | Tetraethylene glycol |
| TEM | Transmission electron microscopy |
| TOF | Turnover frequency |
| TPR | Temperature programmed reduction |
| XAFS | X-ray absorption fine structure spectroscopy |
| XC72R | XC72R commercial carbon |

# 1. Introduction

## *1.1. Catalysis*

The concept of catalysis was first introduced into common use over 170 years ago by Swedish scientist Jons Jakob Berzelius in 1836.[1] J. J. Berzelius was tasked of preparing an annual report on the entirety of chemical knowledge for the Stockholm Academy of Sciences. One section of this report summarised recent findings on the nature of chemical change in homo- and heterogeneous systems, and in doing so introduced the concept of catalysis to account for the experimental observations.

The report went on to also introduce the phrase 'catalytic force', and that the physical contact of the material with the catalyst was crucial in the transformations of the material. The world 'catalysis' is derived from the Greek – '*kata'* meaning down and *'lyein'* meaning loosen.

Prior to this observation, catalysis had been utilised but largely unnoticed. Perhaps the earliest use of catalysis is the fermentation of sugars to alcohol, with Stone age jug fragments suggesting that fermented drinks were being prepared as early as 12,000 years ago.[2] A more recent chemical advancement includes the medieval preparation of dilute sulfuric acid (vitrol) from the combustion of elemental sulfur and potassium nitrate (saltpetre). In 1648, German industrialist Johann Glauber worked on improving the process, and found that increasing air flow to the crucible resulted in more concentrated vitrol. It was therefore understood that air operated as the oxidant, and nitrate was merely acting as a catalyst.[3]

The modern IUPAC definition of a catalyst is 'A substance that increases the rate of a reaction without modifying the overall standard Gibbs energy change in the reaction'.[4] The potential energy profile of a catalysed and uncatalyzed reaction is presented in Figure 1-1. A catalyst provides access to an alternative reaction pathway with a lower activation energy than the uncatalyzed pathway.

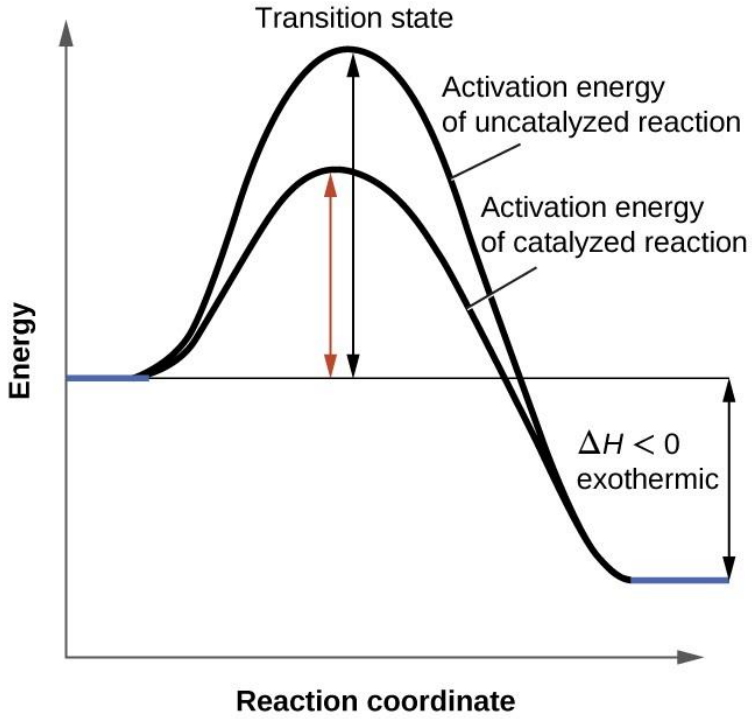


**Figure 1-1 - Reaction coordinate diagram for a reaction in the absence (top) and presence (bottom) of a catalyst**[5]

The thermal energy of reactants in a given state can be described by the Boltzmann Distribution:

$$\frac{Ni}{Nj} = \exp\left(-\frac{Ei - Ej}{kT}\right)$$

*Where*

*Ni and Nj are the populations of species in the respective states i and j*

*Ei and Ej are the energies of the two states i and j*

*And k and T are the Boltzmann constants and temperature respectively.*

It therefore follows that in the presence of a catalyst, the reduced activation energy (Ej) yields a larger Ni/Nj and thus a greater proportion of the reactant species have sufficient energy to proceed through the catalysed pathway in comparison to the uncatalyzed reaction.

The presence of a catalyst also yields kinetic benefits, which can be expressed through the Arrhenius Equation:

$$k = Ae^{-\frac{E_A}{RT}}$$

*Where*

*k is the kinetic rate constant,*

*A is the pre-exponential factor, a constant dependent upon the probability of reactants interacting in the correct orientation,*

*$E_A$ is the activation energy,*

*R and T are the ideal gas constant and temperature respectively.*

A decreased activation energy, $E_A$, will result in a larger rate constant *k* and therefore increased reaction rate in comparison to the uncatalyzed pathway.

A heterogeneous catalyst is one which occupies a separate phase from the reactants or products. As a result, diffusion of the reactant to the active site of the catalyst is critical in the enhancement of catalytic activity. Similarly, the strength of the interaction between the reactant and the catalyst surface can have a significant influence on catalyst potency.

An ideal reaction coordinate for a reaction being catalysed by a heterogeneous catalyst is presented below in Figure 1-2. The initial requirement for a heterogeneously catalysed reaction is the adsorption of the reaction species onto the surface of the catalyst. For a multi-reactant reaction, both reactants must adsorb favourably onto the surface of the catalyst in close contact for the chemical transformation to proceed to the product. Typically two reactants will have different affinities for a catalyst surface, and therefore the surface concentration of the reactants is dependent upon their free energy of adsorption.[6] Upon adsorption, the necessary bond breakage and formation can take place to yield the product, albeit bound to the catalyst surface. Finally, the product can desorb from the surface to yield the free product.

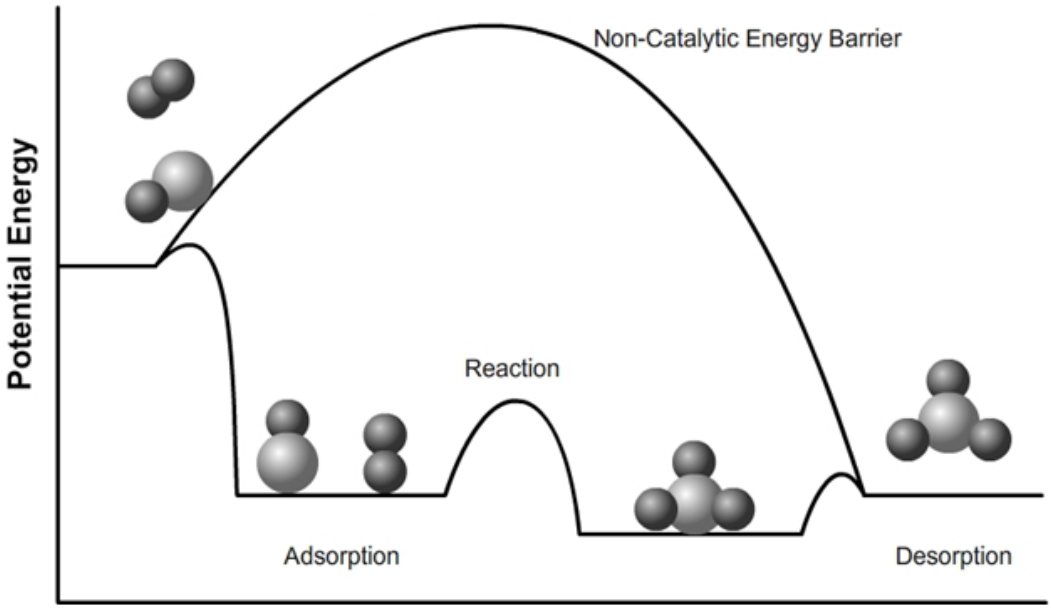


**Figure 1-2 - Reaction coordinate diagram illustrating the fundamental reaction steps for catalysis by a heterogeneous catalyst**[5]

One critical benefit of heterogeneous catalysis is the ease of separation of catalyst and reactant/product. Catalysts can be recovered using any number of common solid/liquid separation techniques, such as filtration or centrifugation. It is for this reason that heterogeneous catalysts make up around 75 % of catalysts used industrially. The value of chemicals produced by catalytic reactions exceeds $4 trillion annually, highlighting the critical importance of catalysis to the global economy.[7]

## *1.2. Green Chemistry*

The concept of green chemistry was first posited by Anastas and Warner in the book "Green chemistry: theory and practice" in 1998.[8] In this work, the authors propose the future development of chemical processes with a view to minimising waste, reducing energy consumption and avoiding hazardous materials. In doing so, 12 principles were proposed which guide chemical process development.

1. **Prevention** - It is better to prevent waste than to treat or clean up waste after it has been created.
2. **Atom Economy** - Synthetic methods should be designed to maximize the incorporation of all materials used in the process into the final product.
3. **Less Hazardous Chemical Syntheses** - Wherever practicable, synthetic methods should be designed to use and generate substances that possess little or no toxicity to human health and the environment.
4. **Designing Safer Chemicals** - Chemical products should be designed to affect their desired function while minimizing their toxicity.
5. **Safer Solvents and Auxiliaries** - The use of auxiliary substances (e.g., solvents, separation agents, etc.) should be made unnecessary wherever possible and innocuous when used.
6. **Design for Energy Efficiency** - Energy requirements of chemical processes should be recognized for their environmental and economic impacts and should be minimized. If possible, synthetic methods should be conducted at ambient temperature and pressure.
7. **Use of Renewable Feedstocks** - A raw material or feedstock should be renewable rather than depleting whenever technically and economically practicable.
8. **Reduce Derivatives** - Unnecessary derivatization (use of blocking groups, protection/ deprotection, temporary modification of physical/chemical processes) should be minimized or avoided if possible, because such steps require additional reagents and can generate waste.
9. **Catalysis** - Catalytic reagents (as selective as possible) are superior to stoichiometric reagents.
10. **Design for Degradation** - Chemical products should be designed so that at the end of their function they break down into innocuous degradation products and do not persist in the environment.

11. **Real-time analysis for Pollution Prevention** - Analytical methodologies need to be further developed to allow for real-time, in-process monitoring and control prior to the formation of hazardous substances.
12. **Inherently Safer Chemistry for Accident Prevention** - Substances and the form of a substance used in a chemical process should be chosen to minimize the potential for chemical accidents, including releases, explosions, and fires.

The principles of green chemistry were further explored by the Nobel laureate Ryoji Noroyi, who identified three key areas.[9] In addition to asymmetric hydrogenation reactions and the use of supercritical $CO_2$ as a solvent, Noroyi emphasized the importance of hydrogen peroxide ($H_2O_2$) as a green oxidant. Particularly in the field of organic synthesis, toxic oxidants such as chromates or permanganates are commonly used. Whilst these oxidants can be handled easily on the laboratory scale, translation of these transformations to the industrial scale results in the formation of large quantities of highly toxic waste solutions that are hazardous to human life and the environment. In contrast, using hydrogen peroxide, the only by-product of oxidation is water. There are also chemical benefits to using hydrogen peroxide as an oxidant, as oxidations using hydrogen peroxide are often more selective, and this is critical in minimising chemical process waste.[9]

### *1.3. The Properties of Hydrogen Peroxide*

Hydrogen Peroxide, chemical formula $H_2O_2$, was first discovered by Thenard in 1818. It is a clear, colourless liquid. Hydrogen peroxide is miscible with water but can be readily separated by distillation. It is a potent oxidant, with a high oxidation potential across a range of pHs, $E_o$=1.77 V at pH 0 and $E_o$=0.88 V at pH 14. As a result, it can readily oxidise a range of organic and inorganic species in the liquid phase under mild conditions.

| | |
|---|---|
| Decomposition | $2\ H_2O_2 \rightarrow 2H_2O + O_2$ |
| Oxidation | $M + H_2O_2 \rightarrow MO + H_2O$ |
| Addition | $H_2O_2 + A \rightarrow AH_2O_2$ |
| Reduction | $H_2O_2 + R \rightarrow RH_2 + O_2$ |
| Substitution | $H_2O_2 + RX \rightarrow ROOX + HX$ |

**Table 1-1 - General reactions of hydrogen peroxide**[10]

Hydrogen peroxide readily undergoes a range of reactions, as seen in Table 1-1, making it a versatile reactant and as a result hydrogen peroxide is a valuable commodity chemical. In 2005, world output reached 2.2 million metric tons, with demand continually increasing in

the following decade due to increased usage in commodity chemical synthesis.[11] Currently more than 60 % of produced hydrogen peroxide is used for bleaching in the paper and textile industries.

Propene epoxidation represents a current area of interest which is expected to significantly increase industrial demand for hydrogen peroxide. Propylene oxide, a large scale chemical intermediate, is currently prepared through the dehydrochlorination of chlorohydrins. The by-product of this process is contaminated brine solution, which is difficult to dispose of.[12] The use of hydrogen peroxide for propene epoxidation represents a greener alternative in which the only by-product is water. The so-called hydrogen peroxide-propylene oxide (HPPO) process is reaching industrial maturity and as a result demand for hydrogen peroxide is set to surge.

### *1.4. The Anthraquinone Process*

Currently, more than 95 % of industrial hydrogen peroxide is prepared using anthraquinone oxidation. The use of anthraquinone oxidation (AO) was pioneered industrially in the 1940s by BASF, who filed a patent in 1939 and subsequently developed a 1ton/day $H_2O_2$ plant.[13] The core of the process is the hydrogenation of anthraquinone to yield a quinol, which then undergoes oxidation to regenerate the quinone and liberate hydrogen peroxide. Since its inception, the AO process has displaced all other methods as the market dominant means of hydrogen peroxide production.[14] The AO process requires three inputs – alkylated anthraquinones, air and hydrogen. Industrially, hydrogen is typically prepared on-site using steam reforming. The transformation from oxygen to hydrogen peroxide is realised through the sequential hydrogenation and oxidation of the anthraquinone carrier species, and as such the various reactions take place independently in separate reactor vessels, typically slurry or fixed bed reactors. The reaction takes place in the so called working solution, a highly optimised and complex mixture of alkylated anthraquinones, aromatics and long chain alcohol species. The solvent ratios must be such that both anthraquinone and the diol reduction product remain in solution throughout the process. Common solvents include hydroterpineol and trioctyl phosphate.[15]

The selectivity of the initial hydrogenation step is critical in determining system performance. The over hydrogenation of the anthraquinone ring may occur which prevents the species from being further oxidised to yield hydrogen peroxide. Originally, Raney nickel was used as the hydrogenation catalyst, but was replaced by palladium on alumina over subsequent decades.[16]

Palladium based catalysts are considerably more active for hydrogenation reactions and as a result readily facilitate unwanted ring hydrogenation of the alkyl anthraquinone species. This deactivates anthraquinone to the overall process and introduces further costs in wasted anthraquinone and hydrogen. As a result, the hydrogenation reaction is typically controlled to around 60% conversion to minimise anthraquinone decomposition.

Considerable effort has been made to improve the selectivity of palladium catalysts for alkylanthraquinone hydrogenation due to the highly developed nature of the technology; selectivity improvements of a few percent could yield savings of tens of millions of dollars per year on the industrial scale.

Alumina and silica supported palladium catalysts are commonly used industrially. It has been found that metal oxide supports with low isoelectric points supress AQ decomposition in comparison to acidic supports.[17] Yuan *et al.* found that in preparing $Pd/Al_2O_3$ by coprecipitation, the number of alumina acid sites was greatly reduced versus a catalyst prepared by the impregnation of commercial alumina. This translated into a selectivity increase to 93% versus 62% for the impregnation catalyst.[18] Pursiainen and co-workers afforded a similar effect from the treatment of palladium on alumina catalysts with water and base prior to heat treatment, finding that residual base improved selectivity for the hydrogenation of the C=O double bond whilst minimising tautomerisation of the quinol product which leads to ring decomposition.[19]

Similarly, Kosydar *et al.* explored the doping of $Pd/Al_2O_3$ catalysts with alkali metals to afford a selectivity improvement.[20] It was found that over hydrogenation of ethylanthraquinone decreased significantly with the incorporation of at least one equivalent of alkali metal. The selectivity was more pronounced with increased atomic weight, and therefore follows the trend Cs > K > Na > Li. Incorporation of Cs into a $2\%Pd/Al_2O_3$ catalyst in a 2:1 weight ratio reduced the rate of formation of the inactive anthrone over-hydrogenation product from 0.29 to 0.05 mol/min/$g_{cat}$, increasing the lifetime of the anthraquinone oxygen carrier and therefore improving $H_2O_2$ yield.

Polymer supported palladium catalysts have also been explored as efficient alkylanthraquinone hydrogenation catalysts.[21] Drelinkiewicz *et al.* reported that palladium nanoparticles supported on polyaniline (PANI) foams were highly selective for ethylanthraquinone hydrogenation and found that the rate of formation of the ring hydrogenation product ethyltetrahydroanthraquinone was greatly reduced versus $Pd/SiO_2$

catalysts prepared by impregnation, and as a result hydrogen efficiency is significantly greater.[22] The catalyst exhibited a small and narrow size distribution, thought to be a consequence of pre-coordination of the anionic palladium precursor with the aniline functional group minimising the presence of large particles active for ring hydrogenation.[23] Further work has looked at immobilising these catalysts as silica/PANI composites to improve their robustness for incorporation into $H_2O_2$ production on an industrial scale.

More recently, Ni-B bulk alloy materials have been investigated as alternatives, principally in a drive to reduce costs. Hou *et al.* have shown that the activity of Ni-B bulk materials is improved considerably through the doping of lanthanum into the catalyst material, which improves nickel dispersion.[24,25] The improved Ni dispersion resulted in a decrease in the $H_2$ TPR reduction temperature and an increase in AQ hydrogenation TOF from 1110 to 2350 $g_{H_2O_2}/g_{cat}/min$ in the case of the La promoted catalyst. He and co-workers observed a similar effect with the incorporation of chromium into a Ni-B amorphous catalyst, and also ascribed the activity improvement to Ni dispersion improvements.[26]

After hydrogenation, the subsequent reaction is the oxidation of the resultant alkylanthroquinol to regenerate the quinone and liberate hydrogen peroxide. This is achieved stoichiometrically using autooxidation in air at relatively low pressures (5 bar) and temperature (50°C).[14] Owing to the low oxygen solubility of the working solution, mass transfer at the gas/liquid interface determines oxidation rates.[27] As a result great effort has been undertaken to maximise gas/liquid interface surface area to improve rates of oxidation.[28] A three phase oxidation/extraction system has also been investigated, where a two phase system of working solution and water is subjected to oxidative conditions, performing oxidation and extraction simultaneously rather than sequentially. Cheng *et al.* observed in using simultaneous oxidation and extraction, that the organic phase forms droplets in the aqueous phase, with droplet size decreasing with increasing agitation, resulting in increased interfacial surface area and therefore faster extraction.[29]

Alternative work has investigated the addition of initiators to accelerate the rate of autooxidation. Degussa has reported that the addition of organic soluble amines to the working solution drastically improves the rates of autooxidation.[30] The rate improvements were observed at concentrations as low as 0.001 molar equivalents, with the oxidation proceeding through a radical mechanism.

The final step in the process is the extraction of hydrogen peroxide from the working solution followed by the recirculation of the working solution back to the hydrogenation reactor. This is typically achieved in a column, which is fed water from the top. Due to the relative low density of water in comparison to the organic phase, the water flows to the bottom, where it can be pumped back to the top of the column to further extract hydrogen peroxide from the working solution. Finally the aqueous phase is siphoned from the bottom of the column, and the working solution introduced back into the hydrogenation vessel.[14] The amount of residual hydrogen peroxide that remains in the working solution should be minimised to maximise profitability on a plant scale. The concentration of the hydrogen peroxide extract is typically 25-45% $H_2O_2$ and varies from plant to plant. Whilst the rates of the hydrogenation and oxidation steps influence the amount of hydrogen peroxide produced, the choice of anthraquinone carrier and extraction regime are equally important in maximising hydrogen peroxide yield.[31]

### *1.5. Electrochemical Generation of Hydrogen Peroxide*

The synthesis of hydrogen peroxide by electrolysis was first reported in 1853, and prior to the invention of the anthraquinone process was the sole industrial route to hydrogen peroxide.[32] In this process the bisulphate anion is oxidised to form peroxydisulphuric acid which undergoes hydrolysis to form peroxymonosulphuric acid and sulfuric acid. The former further hydrolyses to yield hydrogen peroxide and regenerate the acid.

$$H_2SO_4 \leftrightharpoons H^+ + HSO_4^-$$

$$2HSO_4^- \rightarrow H_2S_2O_4 + 2e^- \qquad E = 2.01V \; vs \; SHE$$

$$H_2S_2O_4 + H_2O \rightarrow H_2SO_5 + H_2SO_4$$

$$H_2SO_5 + H_2O \rightarrow H_2SO_4 + H_2O_2$$

Hydrogen peroxide can also be prepared by electrochemical oxygen reduction which was first reported in 1939 and represents a considerably less hazardous and more economical alternative to sulfuric acid oxidation.[33] Oxygen can be reduced by either a two or four electron process to yield hydrogen peroxide and water respectively.

$$O_2 + 2H^+ + 2e^- \rightarrow H_2O_2 \qquad E = 0.7V \; vs \; RHE$$

$$O_2 + 4H^+ + 4e^- \rightarrow H_2O \qquad E = 1.23V \; vs \; RHE$$

Industrialisation of this process began in earnest in the 1980s, with DOW preparing alkaline hydrogen peroxide solutions for use in the paper and textile industries.[34] These sectors consume more than 60% of annual global hydrogen peroxide demand, and tolerate a wide range of hydrogen peroxide purities. Furthermore hydrogen peroxide for bleaching is required in alkaline solutions, and therefore the prepared solutions can be sold as is without any further purification.[11] This criteria is largely unique to the paper and textiles industries as hydrogen peroxide decomposes rapidly under basic conditions, and therefore alkaline solutions must be prepared close to the point of use.[35] The added complexity of having to neutralise the prepared solution for use in other applications and the corrosive properties of the caustic solution has resulted in the process being abandoned in favour of hydrogen peroxide prepared by the AO process in all but a few specialist use cases. One such case is in water treatment, where electrochemically generated hydrogen peroxide is generated and subsequently treated with iron species to generate hydroxyl radicals.[36] Fenton's chemistry occurs optimally around pH 3 and therefore the process is carried out at considerably lower pH than the Dow process. A secondary benefit of this is that the Fenton active Fe(III) species can be catalytically regenerated at the cathode. This results in the process being considerably more efficient than conventional Fenton water purification.[36]

The efficiency of electrochemical $H_2O_2$ manufacturing is largely determined by Faradaic efficiency ($\lambda_{Faradaic}$), which is the relative proportion of charge transferred to the final product with respect to the charge input to the system. A faradaic efficiency of 100% indicates that every electron which passes through the cell is incorporated into the final hydrogen peroxide product. This is especially significant because the price of electricity represents a major cost in operating oxygen reduction cells.[37] Efficiency losses in oxygen reduction electrolysers are typically a consequence of further reduction of hydrogen peroxide to water at the cathode or thermal decomposition of hydrogen peroxide in the electrolyte.

Precious metals are commonly used as effective electrocatalysts for hydrogen peroxide production. Most commonly carbon is used as a conductive carrier to immobilise precious metals owing to its high surface area. Supported Pt, Pd, Au, Ir and Rh materials have been shown to be highly active, though often accompanied with poor faradaic efficiency, and therefore reduced $H_2O_2$ yields.[38] Yamanaka *et al.* investigated the activity of precious metal nanoparticles supported on carbon electrodes for the electrochemical synthesis of $H_2O_2$, reporting that Au/C and Pd/C cathodes achieved Faradaic efficiencies of 10.1 and 9.0% respectively.[39] For comparison, analogous Rh/C, Pt/C and Ir/C electrodes displayed

efficiencies of 0.6, 0.3 and 0% respectively, indicating that these materials were almost entirely selective towards the water producing four electron pathway. Furthermore, the activity of precious metal electrocatalysts is highly pH dependent. For example operating a Pt/C electrode under basic conditions results in the reaction proceeding almost exclusively through the four electron pathway to yield water.[40] Conversely, Au electrocatalysts have been found to display the opposite trend – that selectivity and activity towards hydrogen peroxide improves considerably at higher pH.[41] This is a consequence of the mechanism of oxygen reduction, where the rates of fundamental mechanistic steps vary with pH. Under basic conditions the rate determining step in electrochemical hydrogen peroxide synthesis is the reduction of adsorbed oxygen to yield a dioxy anion. The selectivity is therefore driven largely by the strength of $O_2$ and $O_2^-$ adsorption. In the case of platinum catalysts, the interaction is between the dioxygen species and metal surface is stronger than for gold, and as a result the bound hydrogen peroxide is further protonated and reduced to form water. For gold however, the species is loosely bound, sufficiently so that hydrogen peroxide readily desorbs before further reduction.

The high cost and low faradaic efficiency of precious metal electrodes reduces the economic viability of their industrial usage, and therefore recent attention has turned to non-precious electrocatalysts for oxygen reduction. Precious metal free electrode materials have been investigated for more than 50 years, with Jasinski *et al.* reporting electrocatalytic oxidation of organic species using metal phthalocyanines in 1964.[42] Work over the following decades has focused on developing more active and stable materials as well as building an understanding of origin of their catalytic activity. Examples are generally limited to a selective number of metals, Fe, Co, Ni and Mn.[43–45]

It is worth noting that often catalyst development is undertaken with a view to minimising the hydrogen peroxide producing 2 electron pathway, in favour of the water producing 4 electron one. This is particularly true for the case of power generating fuel cells such as the direct methanol fuel cell (DMFC).[46] As a consequence, many catalysts that perform poorly in fuel cell applications may produce significant quantities of hydrogen peroxide as a side effect. Wan and co-workers recently reported a range of Fe derived electrocatalysts for ORR for use in fuel cells, prepared through the pyrolysis of iron impregnated carbon nanotubes, finding that increased iron loadings resulted in superior performance for power generation owing to increased dominance of the 4 electron pathway.[47] The poorly performing catalysts were however highly active for hydrogen peroxide synthesis, with faradaic efficiency towards

$H_2O_2$ in excess of than 60%, versus 10% for the Pt/C reference electrode. For this application, hydrogen peroxide production should be minimised as its decomposition is responsible for degradation of the electrode surface and thus activity.

Interestingly, carbon materials originally intended to act as charge carrier support materials, display significant activity for the oxygen reduction reaction under basic conditions. Gorlin *et al.* found in the preparation of $MnO_x$/C electrodes that the glassy carbon electrodes alone exhibited hydrogen peroxide synthesis activity.[48] Further analysis indicated that the faradaic efficiency of the process was approaching 100%, likely limited by diffusion of reactants in the cell.

Improvements in faradaic efficiency are largely driven by the choice of electrode material. Current density (A $cm^{-2}$) is a critical parameter to afford efficient charge transfer and therefore high surface area materials are best suited for electrode construction. Carbonaceous materials are commonly uses owing to their low cost, tuneable properties and high surface areas.[49,50,] Pérez *et al.* investigated the effect carbon structure on the activity of a rotating disc electrode (RDE) cell for oxygen reduction to hydrogen peroxide.[51] For low surface area carbons, energy consumption rapidly increases with increasing current density, resulting in a decreased faradaic efficiency and the generation of excess heat. Increased surface area resulted in significantly reduced energy consumption at a given current density up to a point. This was attributed to reactant flux at the surface of the electrodes which is dependent upon agitation speed.

In addition to physical properties, the surface functionality of carbon electrodes has also been found to have a significant effect on catalytic activity. Sheng *et al.* found that carbon-PTFE composite electrodes were significantly more stable than carbon only electrodes over 50 uses. [52] The stability of the composite electrodes was attributed to the hydrophobic nature of PTFE which allows the gas to diffuse into carbon micropores without wetting by the electrolyte, resulting in improved diffusion characteristics. Likewise, the hydrophobicity of the electrode surface minimises surface oxidation by the formed $H_2O_2$ which deactivates the surface for electrocatalysis. Murayama *et al.* further developed this work by investigating a range of different carbons in the preparation of carbon-PTFE composite electrodes.[53] Similar to the work by Sheng *et al.*, addition of PTFE to the electrode material improved activity and selectivity for the two electron hydrogen peroxide synthesis pathway. The surface functionality of the carbons used in the electrodes were modified by oxidation using $O_2$ or

$HNO_3$ and their composition analysed by TPR. The most active carbon material, a vapor grown carbon fibre, contained predominantly phenolic and quinonic oxygens at its surface. For comparison, activated carbons were found to have a much broader range of oxygen surface groups and in much lower concentration, and as a result these carbons displayed diminished activity as a cathode material.

Chemical modification of carbon electrode surfaces has been shown to affect faradaic efficiency. This can include doping of the carbon with heteroatoms such as nitrogen or the tethering of organic species.[54,55] Wang *et al.* reported that the surface adsorption of anthraquinone and riboflavin molecules to the surface of a carbon electrode significantly improved activity and selectivity for electrochemical hydrogen peroxide synthesis.[56] The optimised riboflavin modified electrode exhibited a faradaic efficiency of 80% versus 57% for the unfunctionalized carbon electrode, which was attributed to the oxidation of the anthraquinone group in a manner analogous to the anthraquinone oxidation process itself, albeit proceeding through the formation of bound peroxide radicals rather than sequential oxidation and hydrogenation.

Zhou *et al.* reported improvement in activity of carbon electrons upon the incorporation of nitrogen, using hydrazine as the nitrogen source.[55] Hydrogen peroxide yield tripled upon incorporation of nitrogen into the electrode, from 45 mg/L to 160 mg/L over the course of a 2 h reaction, whilst faradaic efficiency remained constant at 80%. As a result the nitrogen doped cathode exhibited superior performance for the organic pollutant decontamination of water.

The principal of electrochemical reduction of oxygen has further been applied to prepare hydrogen peroxide generating fuel cells. In 1990, Yamanaka and co-workers demonstrated the direct synthesis of hydrogen peroxide from $H_2$ and $O_2$ using proton exchange membranes to facilitate the simultaneous oxidation and reduction of oxygen and hydrogen respectively under acidic conditions.[57] The prepared cell operated at ambient conditions and was demonstrated to perform stably for over 24h. A considerable benefit of the operation of membrane fuel cells is the physical isolation of molecular oxygen and hydrogen which allows the use of high pressures within the $H_2/O_2$ explosive regime and therefore a wider range of operating conditions in comparison to direct synthesis. Furthermore the production of hydrogen peroxide is accompanied by the generation of electrical power which, for example, could be integrated into further electrochemical processes in a cascade reaction. Yamanaka

and co-workers reported that the cathodic oxygen reduction reaction proceeded selectively towards hydrogen peroxide initially, but decreased steadily to less than 50% after 5 h on stream due to oxidation of the electrode surface.[58] The low activity of the hydrogen peroxide fuel cell in comparison to direct synthesis reactors was attributed principally to limiting dissolved oxygen concentration.

Later work found that porous membrane electrodes can be used to operate a three phase gaseous oxygen/aqueous/solid carbon cathode system that is considerably more active and displayed a maximum hydrogen peroxide selectivity of 93%.[59] More recently, Li *et al.* demonstrated the production of $H_2O_2$ in a fuel cell at neutral conditions under flow conditions.[60] This approach presents a number of significant advantages over traditional alkaline cells. By preparing hydrogen peroxide at neutral conditions, the need for purification and neutralisation eliminated, and therefore process costs are reduced. Likewise, several applications specifically require neutralised hydrogen peroxide, such as water purification and electronics manufacturing. The relative simplicity of flow systems in comparison to batch make this technology suitable for the on-site generation of hydrogen peroxide for these applications.

### *1.6. The Direct Synthesis of $H_2O_2$*

The direct synthesis of hydrogen peroxide was first discovered in 1914 by Henkel, who observed during investigations into the electrochemical synthesis of hydrogen peroxide that the electrical potential was not necessary in the presence of palladium cathode materials.[61] The discovery was patented as a new method to prepare hydrogen peroxide from gaseous hydrogen and oxygen in the presence of a precious metal catalyst. The development of this field in the subsequent decades has been hindered by several fundamental challenges. The first is the dangerous combination of the two reactant gasses. Hydrogen-oxygen gas mixtures are explosive between 5 and 95 mol% $H_2$ and as a result the direct synthesis of hydrogen peroxide has inherent safety challenges to overcome.[61] To overcome this, direct synthesis reactions are typically carried out in the presence of diluent gasses such as nitrogen or carbon dioxide such that the hydrogen/oxygen mixture is below the lower explosive concentration limit.[62,63] The second issue is the presence of thermodynamically favourable reaction pathways for the reaction of hydrogen and oxygen, which do not yield hydrogen peroxide.

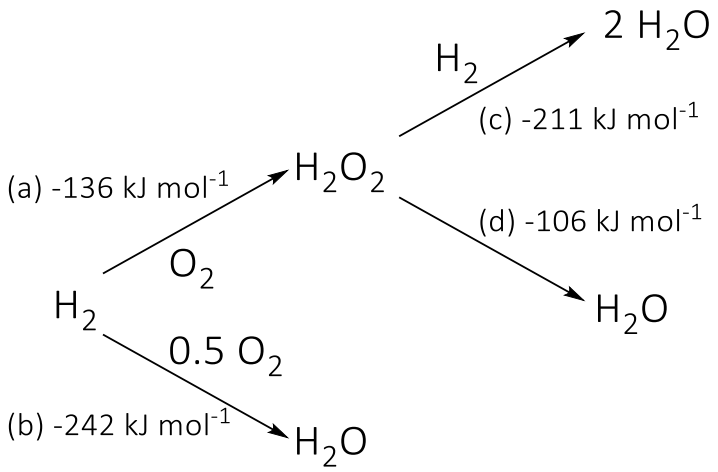


**Figure 1-3 - Reaction pathways and enthalpies of reactions of hydrogen and oxygen [64]**

The potential products of the direct reaction of oxygen and hydrogen are illustrated in Figure 1-3. Although the direct synthesis of hydrogen peroxide is thermodynamically favourable (a), the combustion of hydrogen to form water is even more so (b). In addition, hydrogen peroxide, once formed can undergo further favourable transformations, namely hydrogenation (c) and catalytic decomposition (d) to also yield water. Therefore the yield of hydrogen peroxide during direct synthesis is highly dependent upon the balance between the four pathways.[64]

The catalytic direct synthesis of hydrogen peroxide is intimately dependent upon the use of precious metals. Early work by ICI Ltd employed a supported palladium catalyst and an aqueous acidic reaction medium to afford direct synthesis as early as 1962.[65] To date no single example of precious metal free direct hydrogen peroxide synthesis has been reported, despite theoretical evidence suggesting that it should be feasible.[66]

### *1.6.1. Palladium Catalysed Direct Synthesis of Hydrogen Peroxide*

Palladium is well known to be a highly active hydrogenation metal, with early work on direct synthesis showing that the palladium based catalysts are active for the hydrogenation of oxygen to yield hydrogen peroxide.[67–69] Since then monometallic palladium catalysts have been exhaustively studied for direct synthesis. Work by DuPont in the late 1980s found that palladium supported on carbon, $SiO_2$, $Al_2O_3$ (various phases) and $TiO_2$ were active for direct synthesis.[70–74] Further work by Choudhary and co-workers expanded the range of potential metal oxide supports by demonstrating the activity of palladium supported on $Ga_2O_3$, $ZrO_2$, $CeO_2$, $ThO_2$ and $Y_2O_3$.[75–77] Other notable examples include catalysts supported on mixed metal oxides, zeolites and organic polymers.[78–80] Importantly, the choice of support has a considerable effect on decomposition activity during the direct synthesis reaction, and as a

result overall selectivity towards hydrogen peroxide. Such an effect is commonly attributed to variations in catalyst structure during preparation (such as particle size) or electronic interactions between the metal and support during use (strong metal support interaction)[81–83]

More recently Edwards *et al.* suggested a correlation between the isoelectric point of the support and hydrogen peroxide decomposition activity finding that catalysts supported on supports with low isoelectric points, such as $TiO_2$, were considerably less active for hydrogen peroxide decomposition than those with high isoelectric points such as MgO.[84] A similar observation was reported by Park *et al.*, who found that for palladium supported on zeolite ZSM-5, variation of the Si/Al ratio resulted in increased Brönsted acidity, which was accompanied by increased hydrogen peroxide synthesis activity and decreased decomposition activity, resulting in an increase in hydrogen peroxide yield.[85] Catalyst $H_2O_2$ selectivity was maximum with an Si/Al ratio of 30, 16 %, falling to 9 and 2 % upon further increase in the Si/Al ratio to 80 and 150 respectively.

Variation in the Si/Al ratio of the zeolite altered a number of factors influential in driving direct hydrogen peroxide synthesis. Palladium dispersion decreased with increasing Si content, however $H_2O_2$ yield increased. The authors also showed that the activity of the catalyst could be replicated by the addition of strong acids to the reaction mixture, indicating that the surface acidity of the support plays a fundamental role in the stabilisation of formed hydrogen peroxide, in addition to influencing the activity of the supported nanoparticles.

Palladium oxidation state has also been shown to also influence hydrogen peroxide yield from the direct synthesis reaction. Work by Gaikwad and co-workers found that catalysts prepared with oxidative or reductive heat treatments had significantly different activity and selectivity profiles.[86] Reduced monometallic Pd catalysts prepared on a range of zeolites exhibited significantly higher $H_2$ conversions, but very poor selectivity towards $H_2O_2$. The reduced form of a Pd/ZSM-5 catalyst was shown to be active, but entirely selective towards water formation, with $H_2$ conversion and $H_2O_2$ selectivity of 59% and 0% respectively. The oxidised analogue, PdO/ZSM-5 was less active, achieving $H_2$ conversion of only 9.2% but critically an $H_2O_2$ selectivity of 72.2%.

Similar Pd oxidation state effects have also been observed in flow systems. Centi *et al.* investigated membrane immobilised palladium nanoparticles for direct synthesis for water purification, showing that oxidative pretreatment of the catalyst membrane yielded 200 ppm

of hydrogen peroxide after 420 min on stream, in comparison to only 110 ppm $H_2O_2$ for the reduced membrane under the same conditions.[87,88]

Centomo *et al.* investigated palladium oxidation state under operando conditions using x-ray absorption fine structure spectroscopy (XAFS).[89] The monometallic polymer supported palladium catalyst had a 2:1 Pd(0):Pd(II) ratio before reaction, which remained constant after three hours on stream. Solution phase additives are commonly used in direct hydrogen peroxide synthesis to improve yield and reduce hydrogen peroxide decomposition, and it was shown in follow up work that the presence of bromide ions during reaction decreased the Pd(0):Pd(II) ratio for monometallic catalysts from 2:1 to 4:1 over a period of three hours.[90,91] It was also shown that the presence of even low concentrations of bromide ions (10 ppm) results in metal leaching from catalysts that are indefinitely stable in their absence.

### *1.6.2. Exploration of Other Metals for the Direct Synthesis of Hydrogen Peroxide*

Owing to its high activity, palladium has been used most extensively for direct synthesis. Theoretical work has however suggested that other metals can catalyse the reaction. Early work by Sellers and co-workers concluded that $H_2O_2$ formation from $H_2$ and $O_2$ should be preferable over Au, Ag and Pt surfaces.[92] This was experimentally confirmed by Edwards *et al.* across a number of publications, who showed that both Au and Pt monometallic catalysts are capable of catalysing the direct synthesis reaction.[93–96] In the case of monometallic catalysts of Au, Ag or Pt, the rate of hydrogen peroxide synthesis is generally an order of magnitude lower than for Pd, and as a result hydrogen peroxide yields are significantly lower. This is however coupled with a decrease in $H_2O_2$ hydrogenation and decomposition activity in the presence of these metals. Li *et al.* investigated monometallic zeolite supported catalysts for direct synthesis, showing that Cu, Rh and Ru also exhibit some activity for direct synthesis, typically below 1 mol$H_2O_2$/h/$kg_{cat}$. Analogous Pt or Au catalysts had activities of 3.5 and 3 mol$H_2O_2$/h/$kg_{cat}$ respectively, and a monometallic Pd catalyst 8 mol$H_2O_2$/h/$kg_{cat}$.[97]

Hutchings and co-workers reported that the alloying of Au and Pd significantly improved hydrogen peroxide direct synthesis yield through a reduction in the catalyst hydrogenation and decomposition activity.[98] The author's showed that the addition of Au to a 2.5%Pd/C catalyst increased $H_2O_2$ selectivity from 34 to 80 % and hydrogen peroxide synthesis activity from 55 to 110 mol$H_2O_2$/h/$kg_{cat}$. Similar improvements in selectivity and activity were also observed for $TiO_2$ and $Al_2O_3$ supported analogues. This represented a paradigm shift in catalyst design for direct hydrogen peroxide synthesis which would be extensively explored

over the coming decade. AuPd bimetallic catalysts have been tested on a range of support materials including $Fe_2O_3$, $TiO_2$, $SiO_2$, carbon and mixed metal oxides.[99,94,100] Similar to monometallic Pd catalysts, acidic supports are preferable to basic oxides such as MgO, which exhibit very poor performance for hydrogen peroxide synthesis.

Nanoparticle structure is critical in affording highly active AuPd catalysts for direct synthesis. Most commonly, catalysts are prepared by impregnation of the support material with metal precursors, followed by heat treatment to decompose the precursors and afford supported nanoparticles. In work by Hutchings and co-workers, XPS analysis of AuPd/$TiO_2$ catalysts showed a significant decrease in Au(4f) signal after heat treatment.[101] STEM imaging of the prepared catalyst found that the heat treatment afford Pd-core Au-shell catalysts. These catalysts were more active for direct synthesis than their monometallic palladium counterparts, 124 versus 99 mol$H_2O_2$/h/$kg_{cat}$. This suggests that despite the direct synthesis reaction proceeding on an effectively monometallic palladium surface in both catalysts, the presence of the Au core affords electronic changes in the case of the AuPd catalyst. Core-shell nanoparticles were also prepared on $Fe_2O_3$ and $Al_2O_3$ in further work, both of which benefitted from the incorporation of Au into the Pd catalyst.[99,102] Pritchard *et al.* showed that the choice of heat treatment regime is critical in determining the activity and reusability of PdAu/$TiO_2$ catalysts.[103] Catalyst activity was greatest for untreated catalysts however this was accompanied leaching of more than 75% of the initial metal loading into solution, resulting in rapid catalyst deactivation.

Tiruvalam *et al.* used a colloidal preparation method to carefully control AuPd nanoparticle structure, yielding catalysts highly active for hydrogen peroxide synthesis.[104] Similar to the catalysts prepared by impregnation, it was shown that alloyed AuPd nanoparticle catalysts are more active than either Pd core-Au shell or Au core-Pd shell catalysts. Interestingly the Pd core-Au shell catalysts were reasonably active in comparison to the Au core-Pd shell catalysts, the former displaying hydrogen peroxide synthesis activity of 29 mol$H_2O_2$/h/$kg_{cat}$ and the latter 25 mol$H_2O_2$/h/$kg_{cat}$. The activity difference between monometallic Au and Pd catalysts suggests that the Au shell catalyst should be considerably less active, however STEM-EDX data indicated the presence of small amounts of Pd in an otherwise Au rich shell, which could account for the relatively high activity of the catalyst.

Edwards *et al.* reported further optimisation of AuPd catalysts prepared by impregnation.[105] The authors showed that in the case of carbon supported catalysts, acid pretreatment of the

support yielded catalysts that were significantly more selective than those without pretreatment. Treatment of the carbon support with formic or nitric acid resulted in $H_2O_2$ selectivities >98% versus 80% for the untreated catalyst, whilst phosphoric and hydrochloric acids reduced hydrogen peroxide selectivity to 30 and 15% respectively. The acid treated catalyst was shown by XPS to have a smaller Pd(0):Pd(II) ratio than the untreated catalyst. Previous work has shown that Pd(0) is not only less active for the direct synthesis pathway, but also more active for hydrogenation and decomposition, and therefore the author's suggest that the presence of Pd(II) is critical in preparing selective catalysts.

### *1.6.3. Beyond Gold Palladium Bimetallic Catalysts*

The synergistic effect between gold and palladium is well established for the direct synthesis of hydrogen peroxide with further work investigating the potential use of other secondary metals. Choudhary *et al.* investigated the addition of Au, Pt, Rh and Ru to $Pd/ZrO_2$ catalysts during preparation.[77] Consistent with previous work by Hutchings and co-workers, the addition of Au results in an increased hydrogen peroxide yield and decreased decomposition activity.[106] Addition of Pt to a $Pd/TiO_2$ catalyst increased hydrogen peroxide decomposition activity and resulted in a increase in hydrogen peroxide yield up to 0.02 Pt/Pd mol ratio, unlike Au which promoted hydrogen peroxide synthesis activity across all PdAu compositions. The addition of Rh or Ru in any amount resulted in increased decomposition and therefore a reduction in hydrogen peroxide yield.

Gosser *et al.* found that under industrial conditions, incorporation of 0.1-0.2 mol eq Pt into a Pd catalyst was optimum for maximising $H_2O_2$ yield.[107] Similarly, Melada *et al.* reported that incorporation of 0.05-0.1 mol eq Pt into a membrane derived Pd catalyst resulted in an increase in $H_2O_2$ yield of 25% over the course of 7h on stream.[108] Hölderich and co-workers investigated PtPd catalysts for the oxidation of propylene from in-situ generated hydrogen peroxide from $H_2$ and $O_2$.[109,110] XPS analysis of the fresh and used catalyst revealed that the incorporation of Pt increases the surface concentration of Pd(II) and makes these species resistant to reduction to Pd(0) which is less active for hydrogen peroxide synthesis.

Industrial researchers have exhaustively explored bimetallic Pd containing catalysts for direct synthesis, including the addition of Au, Ag, Pt, Rh, Ru, Ir and Os as evidenced by patent filing over the last two decades.[107,111–116] More recently, attention has turned to preparing bimetallic catalysts using Pd and non-precious metals. A significant barrier to adoption of

direct hydrogen peroxide synthesis on an industrial scale is the use of large amounts of precious metals required, which are not only expensive, but often geopolitically sensitive.

A recent patent filing by the Cardiff Catalysis Institute reports that catalysts comprised of Pd, Pt, Sn and Ni are highly selective for direct synthesis.[117] Complimentary work published by Freakley *et al.* found that $PdSn/TiO_2$ catalysts were highly selective towards hydrogen peroxide synthesis in comparison to $PdAu/TiO_2$ catalysts.[118] Heat treatment was found to play a pivotal role in preparing an active catalyst and that by subjecting the catalyst to three sequential heat treatments, an oxidation, reduction and another final oxidation, selectivity improved from 46 to 96%. Such an aggressive heat treatment regime could be thought to deactivate a catalyst by sintering, however it was found that the synthesis activity of the catalyst differed by 10% between one and three heat treatments. STEM-EDX interrogation of the prepared catalyst showed that successive heat treatments afford a $SnO_2$ overlayer that encapsulates small particles highly active for hydrogen peroxide hydrogenation and decomposition, whilst larger PdSn alloy particles remain uncovered.

Recently, Huang and co-workers prepared a number of novel $PdSn/TiO_2$ catalysts through the solvothermal decomposition of Pd and Sn precursors.[119] The resultant PdSn particles were found to be hollow, a result of the slow and controlled decomposition of the precursors. It was found that the hydrogenation activity of the catalyst could be minimised by varing the Pd:Sn ratio, yielding a maximum activity of 160 $molH_2O_2/h/kg_{cat}$ and selectivity above 95% achieved with a ratio of 1:6. Tian *et al.* have also recently reported highly active palladium tellurium bimetallic catalysts for hydrogen peroxide synthesis.[120] Addition of Te in a Pd:Te ratio of 100:1 resulted in an increase in hydrogen peroxide selectivity to 99%+ versus 65% for the unmodified catalyst. Average particle size was found to decrease from 2.1 to 1.4 nm in the presence of the Te additive, whilst accompanying computational evidence suggests that the presence of Te may slow O-O dissociation, a key intermediate in $H_2O_2$ decomposition.

### *1.6.4. The Effect of Additives on the Direct Synthesis of Hydrogen Peroxide*

The presence of solution phase additives exhibits a remarkable effect on hydrogen peroxide decomposition and hydrogenation rates, and therefore yield. Halides or pseudohalides have been thoroughly explored for their promotional effect on hydrogen peroxide synthesis. Choudhary *et al.* investigated the addition of acid halides/pseudohalides for aqueous palladium catalysed direct synthesis of hydrogen peroxide and showed that hydrogen peroxide decomposition activity decreased by two orders of magnitude in the presence of

acids in comparison to water alone.[121] The observed selectivity improvements followed the trend:

$$HBr > HI > HCl \gg HF$$

Hydrogen peroxide decomposition increased in the presence of fluoride ions, thought to be a consequence of interactions with the metal surface resulting in a change in oxidation state. The authors postulate that the remaining halides poison $H_2O_2$ decomposition sites on the metal surface and as a result improve selectivity.[122,123] The observed decrease in hydrogen peroxide decomposition is also a product of increased acidity, which stabilises $HOO^-$ species formed during the decomposition pathway, to reform hydrogen peroxide.[124,125]

The role of acids and halides was deconvoluted in further work by Samata *et al.*, who showed that potassium halides also exhibit a promotional effect for direct synthesis, but to a lesser extent than acid halides.[126] Pseudohalides have also been shown to decrease hydrogen peroxide decompositions rates, but unlike halides were thought to be non-coordinating to the active metal surface.[77]

### *1.6.5. Solvent Effects in the Direct Synthesis of Hydrogen Peroxide*

Direct synthesis principally takes place in a three-phase system, and therefore catalyst activity is highly dependent upon the mass transfer of the reactant gasses to the catalyst surface. Gas solubility can be improved by operating at elevated pressures or moving to solvent systems with improved $H_2$ and $O_2$ solubility. Whilst the direct synthesis of hydrogen peroxide would be more industrially applicable in the aqueous phase, the poor solubility of $H_2$ and $O_2$ severely hinder catalyst activity.[127] As a result it is more favourable to conduct direct synthesis in an organic solvent, owing to the considerable improvement in $H_2$ and $O_2$ solubility.

Krishnan *et al.* investigated the effect on organic solvents on the palladium catalysed direct synthesis of hydrogen peroxide, and found that generally, reactions in solvents with higher $H_2$ solubility yield a greater hydrogen peroxide yield. Reactions in methanol or acetone produced 200 ppm $H_2O_2$ over six hours, versus 100 ppm for ethanol or dioxane in the same time frame.[128] Acetone is known to be a superior solvent for hydrogen peroxide synthesis, however has inherent safety issues. Acetone reacts readily with hydrogen peroxide to form oligomers that are highly explosive both in solution and the solid phase, which are highly

shock sensitive.[129] Therefore despite its superior performance, acetone is unsuitable for use as a solvent for direct synthesis.

Nijhuis and co-workers further investigated organic solvent effects using AuPd/C catalysts and showed that water/aprotic polar solvent mixtures of DMSO, acetone and acetonitrile significantly improved selectivity, thought to be a consequence of interactions between the solvent and active metal surface.[130] At high concentrations, the coordinating solvents are strongly bound to catalyst surface and as a result activity decreased significantly. Intermediate chain length alcohols were found to be accommodating to use both neat and as a solution with water and exhibited good gas solubility. Further work by Edwards *et al.* investigated the effect of varying water-methanol ratio for AuPd catalysed direct synthesis.[131] For an AuPd/$TiO_2$ catalyst the optimum water/methanol ratio was observed to be 0.2, yielding an activity of 90 mol$H_2O_2$/h/$kg_{cat}$. The system was shown to be highly sensitive to variation in solvent composition around this point, with water/methanol ratios of 0.3 and 0.1 resulting in activities of 55 and 15 mol$H_2O_2$/h/$kg_{cat}$ respectively.

### *1.7. Aims and Objectives*

Chapter 1 has provided an overview of the challenges in preparing active catalysts for the direct synthesis of hydrogen peroxide from molecular hydrogen and oxygen. Given that factors such as choice of metal, metal oxidation state and nanoparticle size have a profound effect on catalyst activity, the aim of this work is to investigate the preparation of novel materials catalytically active for the direct synthesis reaction.

Chapter 2 describes the catalyst preparation protocols, activity evaluation conditions and catalyst characterisation techniques used throughout this thesis. Chapter 3 investigates the solvothermal synthesis of bimetallic catalysts for hydrogen peroxide direct synthesis and the activity of the resultant catalysts in comparison to previously reported materials prepared by alternative means. Chapter 4 looks at optimising a commonly used catalyst preparation technique, sol immobilisation. Particular attention is paid to variables commonly overlooked in literature, namely the effect of choice of reductant, stabiliser and preparation temperature. Both Chapters 3 and 4 explore the activity of gold-free bimetallic catalysts, showing that although PdAu catalysts are most commonly reported, cheaper, more abundant metals can provide reasonable alternatives.

Chapter 5 aims to further understanding of the activity of PdAu/C catalysts for the direct synthesis of hydrogen peroxide. The chapter provides an overview of catalysts prepared on numerous commercial carbons, with a view to determining which factors are important in maximising the activity of carbon supported catalysts.

## *1.8. References*

1 J. Berzelius, *Anuls. Chim. Phys.*, 1836, **61**, 146.
2 C. H. Patrick, *Alcohol, Culture, and Society*, Ams Pr Inc, 1970.
3 H. W. Dickinson, *Trans. Newcom. Soc.*, 1937, **18**, 43–60.
4 K. J. Laidler, *Pure Appl. Chem.*, 1996, **68**, 149–192.
5 W. R. Robinson, P. Flowers, K. Theopold and R. Langley, in *Chemistry*, Rice University.
6 J. R. H. Ross, *Heterog. Catal.*, 2012, 1–15.
7 U. Dingerdissen, A. Martin, D. Herein and H. J. Wernicke, *Handb. Heterog. Catal.*, 2008.
8 I. T. Horváth and P. T. Anastas, *Green Chemistry Theory and Practice*, American Chemical Society, 2007.
9 R. Noyori, *Chem. Commun.*, 2005, 1807–1811.
10 J. M. Campos-Martin, G. Blanco-Brieva and J. L. G. Fierro, *Angew. Chemie - Int. Ed.*, 2006, **45**, 6962–6984.
11 R. Hage and A. Lienke, *Angew. Chemie - Int. Ed.*, 2005, **45**, 206–222.
12 V. Russo, R. Tesser, E. Santacesaria and M. Di Serio, *Ind. Eng. Chem. Res.*, 2013, **52**, 1168–1178.
13 H.-J. Riedl and G. Pfieiderer, .
14 R. Ciriminna, L. Albanese, F. Meneguzzo and M. Pagliaro, *ChemSusChem*, 2016, **9**, 3374–3381.
15 H. Li, B. Zheng, Z. Pan, B. Zong and M. Qiao, 2018, **12**, 124–131.
16 R. E. Albers, M. Nyström, M. Siverström, A. Sellin, A. C. Dellve, U. Andersson, W. Herrmann and T. Berglin, *Catal. Today*, 2001, **69**, 247–252.
17 Q. Chen, *J. Clean. Prod.*, 2006, **14**, 708–712.
18 E. Yuan, C. Wu, G. Liu and L. Wang, *Appl. Catal. A Gen.*, 2016, **525**, 119–127.
19 A. Drelinkiewicz, R. Laitinen, R. Kangas and J. Pursiainen, *Appl. Catal. A Gen.*, 2005, **284**, 59–67.
20 R. Kosydar, A. Drelinkiewicz, E. Lalik and J. Gurgul, *Appl. Catal. A Gen.*, 2011, **402**, 121–131.
21 D. Simon, DE3538816 A1, 1987.
22 A. Drelinkiewicz and M. Hasik, *J. Mol. Catal. A Chem.*, 2001, **177**, 149–164.
23 A. Drelinkiewicz, A. Waksmundzka-Góra, W. Makowski and J. Stejskal, *Catal. Commun.*, 2005, **6**, 347–356.
24 P. Gallezot, P. Cerino, B. Blanc, G. Fleche And P. Fuertes, *J. Catal.*, 1994, **146**, 93–102.
25 Y. Hou, Y. Wang, W. Mi, Z. Li, S. Han, Z. Mi, W. Wu and E. Min, *React. Kinet. Catal. Lett.*, 2003, **80**, 233–239.
26 J. Fang, X. Chen, B. Liu, S. Yan, M. Qiao, H. Li, H. He and K. Fan, *J. Catal.*, 2005, **229**, 97–104.
27 E. Santacesaria, R. Ferro, S. Ricci and S. Carrã, *Ind. Eng. Chem. Res.*, 1987, **26**, 155–159.
28 E. Santacesaria, M. Di Serio, A. Russo, U. Leone and R. Velotti, *Chem. Eng. Sci.*, 1999, **54**, 2799–2806.
29 Y. Cheng, L. Wang, S. Lü, Y. Wang and Z. Mi, *Ind. Eng. Chem. Res.*, 2008, **47**, 7414–7418.
30 T. Haas, US20020141935, 2002.
31 J. Sheikh, L. S. Kershenbaum and E. Alpay, *Chem. Eng. Sci.*, 1998, **53**, 2933–2939.
32 C. W. Jones, *Applications of Hydrogen Peroxide and Derivatives*, Royal Society of

Chemistry, Cambridge, 1999.
33 E. Berl, *Trans. Electrochem. Soc.*, 1939, **76**, 359.
34 J.A. McIntyre, USP4431494, 1984.
35 P. C. Foller and R. T. Bombard, *J. Appl. Electrochem.*, 1995, **25**, 613–627.
36 E. Brillas, I. Sirés and M. A. Oturan, *Chem. Rev.*, 2009, **109**, 6570–6631.
37 S. You, X. Gong, W. Wang, D. Qi, X. Wang, X. Chen and N. Ren, *Adv. Energy Mater.*, 2016, **6**, 1501497.
38 E. Pizzutilo, O. Kasian, C. H. Choi, S. Cherevko, G. J. Hutchings, K. J. J. Mayrhofer and S. J. Freakley, *Chem. Phys. Lett.*, 2017, **683**, 436–442.
39 I. Yamanaka, T. Hashimoto, R. Ichihashi and K. Otsuka, *Electrochim. Acta*, 2008, **53**, 4824–4832.
40 V. R. Stamenkovic, B. Fowler, B. S. Mun, G. Wang, P. N. Ross, C. A. Lucas and N. M. Marković, *Science*, 2007, **315**, 493 LP-497.
41 P. Quaino, N. B. Luque, R. Nazmutdinov, E. Santos and W. Schmickler, *Angew. Chemie - Int. Ed.*, 2012, **51**, 12997–13000.
42 R. JASINSKI, *Nature*, 1964, **201**, 1212–1213.
43 J. Yu, G. Chen, J. Sunarso, Y. Zhu, R. Ran, Z. Zhu, W. Zhou and Z. Shao, *Adv. Sci.*, 2016, **3**, 1–8.
44 H. Tang, S. Cai, S. Xie, Z. Wang, Y. Tong, M. Pan and X. Lu, *Adv. Sci.*, 2015, **3**, 1–8.
45 H. A. Miller, M. Bellini, W. Oberhauser, X. Deng, H. Chen, Q. He, M. Passaponti, M. Innocenti, R. Yang, F. Sun, Z. Jiang and F. Vizza, *Phys. Chem. Chem. Phys.*, 2016, **18**, 33142–33151.
46 C. Song and J. Zhang, in *PEM Fuel Cell Electrocatalysts and Catalyst Layers*, Springer London, London, pp. 89–134.
47 W. J. Jiang, L. Gu, L. Li, Y. Zhang, X. Zhang, L. J. Zhang, J. Q. Wang, J. S. Hu, Z. Wei and L. J. Wan, *J. Am. Chem. Soc.*, 2016, **138**, 3570–3578.
48 Y. Gorlin, C. J. Chung, D. Nordlund, B. M. Clemens and T. F. Jaramillo, *ACS Catal.*, 2012, **2**, 2687–2694.
49 H. Lan, W. He, A. Wang, R. Liu, H. Liu, J. Qu and C. P. Huang, *Water Res.*, 2016, **105**, 575–582.
50 A. Özcan, Y. Şahin, A. Savaş Koparal and M. A. Oturan, *J. Electroanal. Chem.*, 2008, **616**, 71–78.
51 O. González Pérez and J. M. Bisang, *J. Chem. Technol. Biotechnol.*, 2014, **89**, 528–535.
52 Y. Sheng, S. Song, X. Wang, L. Song, C. Wang, H. Sun and X. Niu, *Electrochim. Acta*, 2011, **56**, 8651–8656.
53 T. Murayama and I. Yamanaka, *J. Phys. Chem. C*, 2011, **115**, 5792–5799.
54 G. Xia, Y. Lu, X. Gao, C. Gao and H. B. Xu, *Clean - Soil, Air, Water*, 2015, **43**, 229–236.
55 L. Zhou, M. Zhou, Z. Hu, Z. Bi and K. G. Serrano, *Electrochim. Acta*, 2014, **140**, 376–383.
56 A. Wang, A. Bonakdarpour, D. P. Wilkinson and E. Gyenge, *Electrochim. Acta*, 2012, **66**, 222–229.
57 K. Otsuka and I. Yamanaka, *Electrochim. Acta*, 1990, **35**, 319–322.
58 K. Otsuka and I. Yamanaka, *Catal. Today*, 1998, **41**, 311–325.
59 I. Yamanaka, T. Onizawa, S. Takenaka and K. Otsuka, *Angew. Chemie - Int. Ed.*, 2003, **42**, 3653–3655.
60 W. Li, A. Bonakdarpour, E. Gyenge and D. P. Wilkinson, *ChemSusChem*, 2013, **6**, 2137–2143.
61 H. Henkel, US1108752, 1914.

62 S. Abate, P. Lanzafame, S. Perathoner and G. Centi, *Catal. Today*, 2011, **169**, 167–174.
63 S. Abate, S. Perathoner and G. Centi, *Catal. Today*, 2012, **179**, 170–177.
64 J. H. Lunsford, *J. Catal.*, 2003, **216**, 455–460.
65 G. W. Hooper, US3361533, 1945.
66 R. B. Rankin and J. Greeley, *ACS Catal.*, 2012, **2**, 2664–2672.
67 D. J. Gavia and Y.-S. Shon, *ChemCatChem*, 2015, **7**, 892–900.
68 A. Schmidt and R. Schomäcker, *Ind. Eng. Chem. Res.*, 2007, **46**, 1677–1681.
69 J. A. Schwarz, C. Contescu and A. Contescu, *Chem. Rev.*, 1995, **95**, 477–510.
70 L. W. Gosser, US4832938, 1980.
71 T. Kanada, US5104635, 1989.
72 L. W. Gosser, US4889705, 1988.
73 L. W. Gosser, US4681751A, 1983.
74 L. W. Gosser, US5135731, 1991.
75 A. G. Gaikwad, S. D. Sansare and V. R. Choudhary, *J. Mol. Catal. A Chem.*, 2002, **181**, 143–149.
76 V. R. Choudhary and C. Samanta, *J. Catal.*, 2006, **238**, 28–38.
77 V. R. Choudhary, C. Samanta and T. V. Choudhary, *Appl. Catal. A Gen.*, 2006, **308**, 128–133.
78 H. Nagashima, US5292496, 1991.
79 T. Danciu, E. J. Beckman, D. Hancu, R. N. Cochran, R. Grey, D. M. Hajnik and J. Jewson, *Angew. Chemie Int. Ed.*, 2003, **42**, 1140–1142.
80 G. Blanco-Brieva, E. Cano-Serrano, J. M. Campos-Martin and J. L. G. Fierro, *Chem. Commun.*, 2004, **4**, 1184–1185.
81 Y. Ryndin, *J. Catal.*, 1981, **70**, 287–297.
82 S. J. Tauster, *Acc. Chem. Res.*, 1987, **20**, 389–394.
83 P. Weerachawanasak, P. Praserthdam, M. Arai and J. Panpranot, *J. Mol. Catal. A Chem.*, 2008, **279**, 133–139.
84 J. K. Edwards, A. Thomas, A. F. Carley, A. A. Herzing, C. J. Kiely and G. J. Hutchings, *Green Chem.*, 2008, **10**, 388–394.
85 S. Park, J. Lee, J. H. Song, T. J. Kim, Y. M. Chung, S. H. Oh and I. K. Song, *J. Mol. Catal. A Chem.*, 2012, **363**–**364**, 230–236.
86 V. R. Choudhary, S. D. Sansare and A. G. Gaikwad, *Catal. Letters*, 2002, **84**, 81–87.
87 G. Centi, R. Dittmeyer, S. Perathoner and M. Reif, *Catal. Today*, 2003, **79**–**80**, 139–149.
88 S. Melada, F. Pinna, G. Strukul, S. Perathoner And G. Centi, *J. Catal.*, 2005, **235**, 241–248.
89 P. Centomo, C. Meneghini, S. Sterchele, A. Trapananti, G. Aquilanti and M. Zecca, *ChemCatChem*, 2015, **7**, 3712–3718.
90 V. Paunovic, J. C. Schouten and T. A. Nijhuis, *Catal. Today*, 2015, **248**, 160–168.
91 P. Centomo, C. Meneghini, S. Sterchele, A. Trapananti, G. Aquilanti and M. Zecca, *Catal. Today*, 2015, **248**, 138–141.
92 P. P. Olivera, E. M. Patrito and H. Sellers, *Surf. Sci.*, 1994, **313**, 25–40.
93 Z. Khan, N. F. Dummer and J. K. Edwards, *Philos. Trans. R. Soc. A Math. Phys. Eng. Sci.*, 2018, **376**.
94 J. K. Edwards, A. F. Carley, A. A. Herzing, C. J. Kiely and G. J. Hutchings, *Faraday Discuss.*, 2008, **138**, 225–239.
95 J. K. Edwards, J. Pritchard, P. J. Miedziak, M. Piccinini, A. F. Carley, Q. He, C. J. Kiely and G. J. Hutchings, *Catal. Sci. Technol.*, 2014, **4**, 3244.
96 T. Ishihara, Y. Ohura, S. Yoshida, Y. Hata, H. Nishiguchi and Y. Takita, *Appl. Catal.*

*A Gen.*, 2005, **291**, 215–221.
97 G. Li, J. Edwards, A. F. Carley and G. J. Hutchings, *Catal. Commun.*, 2007, **8**, 247–250.
98 P. Landon, P. J. Collier, A. J. Papworth, C. J. Kiely and G. J. Hutchings, *Chem. Commun.*, 2002, 2058–2059.
99 J. K. Edwards, B. Solsona, P. Landon, A. F. Carley, A. Herzing, M. Watanabe, C. J. Kiely and G. J. Hutchings, *J. Mater. Chem.*, 2005, **15**, 4595.
100 M. Okumura, Y. Kitagawa, K. Yamagcuhi, T. Akita, S. Tsubota and M. Haruta, *Chem. Lett.*, 2003, **32**, 822–823.
101 J. K. Edwards, B. Solsona, P. Landon, A. F. Carley, A. Herzing, C. J. Kiely and G. J. Hutchings, *J. Catal.*, 2005, **236**, 69–79.
102 B. E. Solsona, J. K. Edwards, P. Landon, A. F. Carley, A. Herzing, C. J. Kiely and G. J. Hutchings, *Chem. Mater.*, 2006, **18**, 2689–2695.
103 J. C. Pritchard, Q. He, E. N. Ntainjua, M. Piccinini, J. K. Edwards, A. A. Herzing, A. F. Carley, J. A. Moulijn, C. J. Kiely and G. J. Hutchings, *Green Chem.*, 2010, **12**, 915.
104 R. C. Tiruvalam, J. C. Pritchard, N. Dimitratos, J. A. Lopez-Sanchez, J. K. Edwards, A. F. Carley, G. J. Hutchings and C. J. Kiely, *Faraday Discuss.*, 2011, **152**, 63.
105 J. K. Edwards, B. Solsona, E. N. Ntainjua, A. F. Carley, A. A. Herzing, C. J. Kiely and G. J. Hutchings, *Science (80-. ).*, 2009, **323**, 1037–1041.
106 P. Landon, P. J. Collier, A. F. Carley, D. Chadwick, A. J. Papworth, A. Burrows, C. J. Kiely and G. J. Hutchings, *Phys. Chem. Chem. Phys.*, 2003, **5**, 1917–1923.
107 US4832938, 1980, 96, 62–66.
108 S. Melada, F. Pinna, G. Strukul, S. Perathoner and G. Centi, *J. Catal.*, 2006, **237**, 213–219.
109 R. Meiers and W. F. Holderich, *Catal. Letters*, 1999, **59**, 161–163.
110 R. Meiers, U. Dingerdissen and W. F. Hölderich, *J. Catal.*, 1998, **176**, 376–386.
111 Z. Bing, US6168775, 2001.
112 M. Nystrom, US6210651, 1997.
113 G. Paparatto, US6284213, 1998.
114 J. Wanngard, US5961948, 1996.
115 U. Luckoff, US5505921, 1991.
116 L. W. Gosser, US5135731, 1991.
117 S. Freakley, EP3033170, 2013.
118 S. J. Freakley, Q. He, J. H. Harrhy, L. Lu, D. A. Crole, D. J. Morgan, E. N. Ntainjua, J. K. Edwards, A. F. Carley, A. Y. Borisevich, C. J. Kiely and G. J. Hutchings, *Science*, 2016, **351**, 965–968.
119 F. Li, Q. Shao, M. Hu, Y. Chen and X. Huang, *ACS Catal.*, 2018, 3418–3423.
120 P. Tian, X. Xu, C. Ao, D. Ding, W. Li, R. Si, W. Tu, J. Xu and Y. F. Han, *ChemSusChem*, 2017, **10**, 3342–3346.
121 V. R. Choudhary, C. Samanta and T. V. Choudhary, *J. Mol. Catal. A Chem.*, 2006, **260**, 115–120.
122 V. R. Choudhary, C. Samanta and P. Jana, *Appl. Catal. A Gen.*, 2007, **332**, 70–78.
123 C. Samanta and V. R. Choudhary, *Appl. Catal. A Gen.*, 2007, **330**, 23–32.
124 M. A. Paoli, 1980, **96**, 62–66.
125 US4336239, 1973.
126 C. Samanta and V. R. Choudhary, *Catal. Commun.*, 2007, **8**, 73–79.
127 P. Luehring and A. Schumpe, *J. Chem. Eng. Data*, 1989, **34**, 250–252.
128 V. V. Krishnan, A. G. Dokoutchaev and M. E. Thompson, *J. Catal.*, 2000, **196**, 366–374.
129 R. Schulte-Ladbeck, M. Vogel and U. Karst, *Anal. Bioanal. Chem.*, 2006, **386**, 559–

565.
130 V. Paunovic, V. V. Ordomsky, V. L. Sushkevich, J. C. Schouten and T. A. Nijhuis, *ChemCatChem*, 2015, **7**, 1161–1176.
131 J. K. Edwards, A. Thomas, B. E. Solsona, P. Landon, A. F. Carley and G. J. Hutchings, *Catal. Today*, 2007, **122**, 397–402.

# 2. Experimental

## 2.1. Summary

In this work, a range of supported metal catalysts were prepared by various methods and their performance evaluated for direct hydrogen peroxide synthesis. These materials were then characterised to determine their physical and chemical properties. The following chapter discusses catalyst precursor specifications, catalyst preparation methods, catalyst evaluation reactor configuration and characterisation techniques.

## 2.2. Materials

The following is a description of the materials used to prepare the catalysts presented in this work.

### 2.2.1. Support Materials

**Table 2-1 - Table of support materials**

| Material | Commercial Name | Supplier |
|---|---|---|
| $TiO_2$ | P25 $TiO_2$ | Degussa |
| Carbon | Synthetic Graphite 20µm | Sigma Aldrich |
| Carbon | Graphite Pellets, 300µm | British Nuclear Fuels Laboratory |
| Carbon | Norit KBB Black | Cabot Corporation |
| Carbon | Vulcan XC72R | Cabot Corporation |
| Carbon | Vulcan Black Pearl | Cabot Corporation |
| Carbon | SDP-500 | Perpetuus Advanced Materials |
| Carbon | SDP 500-COOH | Perpetuus Advanced Materials |
| Carbon | MWCNT | Haydale |
| Carbon | MWCNT-OH | Haydale |

### *2.2.2. Metal Precursors*

Metal precursors were dissolved in 0.2M HCl prior to use as stock solutions.

**Table 2-2 - Table of metal precursors**

| Precursor | Purity | Stock Solution Concentration (mg/mL) | Supplier |
|---|---|---|---|
| $PdCl_2$ | Anhydrous, 60% Pd basis | 15 | Sigma Aldrich |
| $HAuCl_4.H_2O$ | 49% Au basis | 12.5 | Strem Chemicals |
| $NiCl_2.6H_2O$ | >98% | 10 | Sigma Aldrich |
| $In(III)Cl_3$ | >98% | 10 | Sigma Aldrich |
| $Sn(II)Cl_2$ | >98% | 10 | Sigma Aldrich |

### *2.2.3. Reagents*

**Table 2-3 - Table of polymer stabilisers**

| Reagent | Molecular Weight | Supplier |
|---|---|---|
| Polyvinylpyrrolidone | 3,500 MW, K12 | Acros Organics |
| Polyvinylpyrrolidone | 360,000 MW | Sigma Aldrich |
| Polyvinyl Alcohol | 13,000-23,000 MW | Sigma Aldrich |
| Poly(acrylic acid) sodium salt | 15,000 MW, 45% solution | Sigma Aldrich |

**Table 2-4 - Table of reductants**

| Reagent | Purity | Supplier |
|---|---|---|
| Sodium Borohydride | 99% | Acros Organics |
| Ammonia-Borane Complex | >90% | Sigma Aldrich |
| Hydrazine | 50-60% solution | Sigma Aldrich |

**Table 2-5 - Table of solvents**

| Solvent | Purity | Supplier |
|---|---|---|
| Water | HPLC Grade | Fisher Scientific |
| Methanol | HPLC Grade | Fisher Scientific |
| Ethylene Glycol | 99%+ | Acros Organics |
| Hexylene Glycol | 99% | Sigma Aldrich |
| 1,3-Butanediol | >99% | Sigma Aldrich |
| 1,5-Pentanediol | >97% | Sigma Aldrich |
| Tetraethylene Glycol | 99% | Sigma Aldrich |
| Glycerol | >99% | Sigma Aldrich |
| Dimethylformamide | 99.5% | VWR |
| Dimethylsulfoxide | 99% | Fisher Scientific |

## *2.3. Catalyst Preparation*

### *2.3.1. Wet Impregnation*

Wet impregnation is a simple and commonly used catalyst preparation method. The technique relies on the dispersion of metal precursors on an appropriate support material, which yields metal nanoparticles through decomposition of the precursors upon heat treatment, as shown schematically in Figure 2-1.

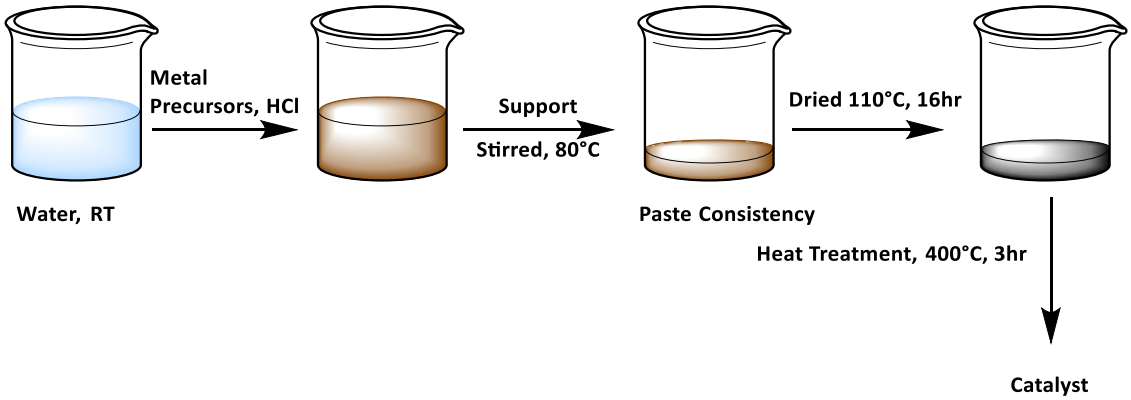


**Figure 2-1 - Illustration of wet impregnation catalyst preparation method**

NOTE – Catalysts prepared by wet impregnation referred to as PdAu are unless otherwise stated, 2.5 % Pd2.5 % Au by weight.

Bi- and monometallic AuPd catalysts were prepared by conventional wet impregnation, previously described elsewhere.[1] 2.5%Pd2.5%Au catalysts were prepared using a standard protocol. $PdCl_2$ (1.66 mL, 15 mg/mL Pd) and $HAuCl_4$ (2.04 mL, 12.5 mg/mL) solutions were added to support (1 g) and gently heated under stirring. The resultant paste was dried for 16 h at 110 °C. The catalyst was then heat treated in a tube furnace. In the case of metal oxide supported catalysts, the resultant catalyst was treated at 400°C for 3h, 20 °C/min ramp rate, under static air conditions. In the case of carbon supported catalysts, the catalysts were treated at 400 °C for 3 h, 20 °C/min ramp rate, with 50 mL/min 5 % $H_2/CO_2$ flow.

In the case of monometallic Pd or Au catalysts, the volume of omitted metal precursor solution was replaced with distilled water such that the aqueous content of the paste remained constant.

### *2.3.2. Sol Immobilisation*

Sol immobilisation is catalyst preparation method that yields, small, well dispersed nanoparticles. The sol immobilisation method requires the formation of a colloidal solution of metal nanoparticles, which is then deposited on an appropriate support material for use as a heterogeneous catalyst. The general scheme of catalyst preparation by sol immobilisation is graphically presented in Figure 2-2. General sol immobilisation protocols have been previously reported for the preparation of supported metal catalysts.[2,3]

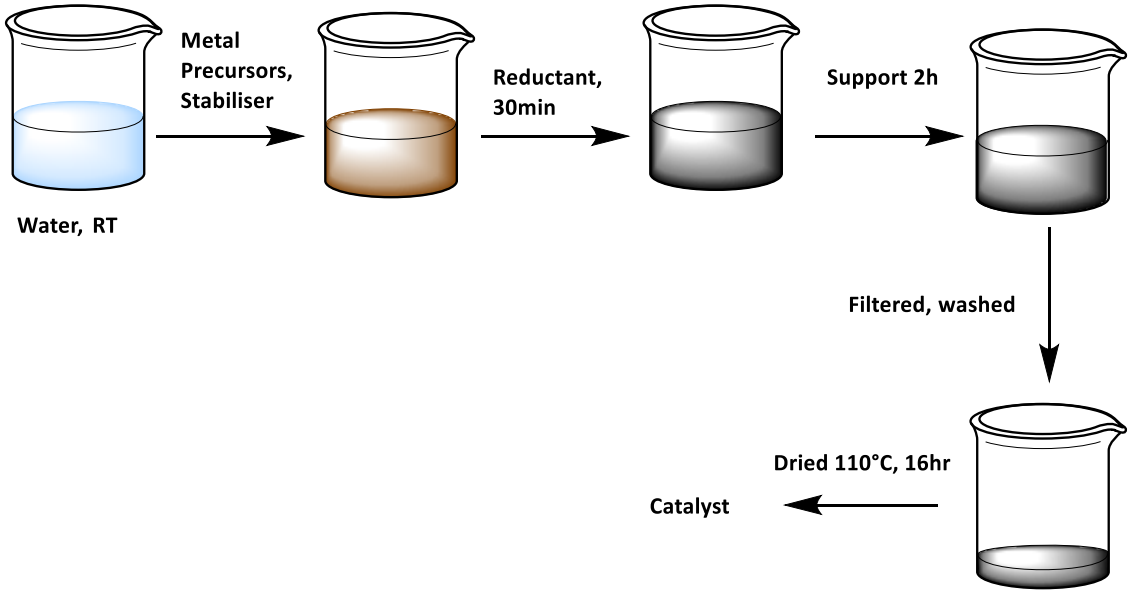


**Figure 2-2 - Illustration of sol immobilisation catalyst preparation method**

NOTE – Unless otherwise stated, bimetallic catalysts prepared by sol immobilisation are 0.5 % Pd 0.5 % Secondary metal by weight.

Mono- and bimetallic catalysts containing Pd, Au, Ni, Sn and/or In were prepared using a modified sol immobilisation procedure, adapted from a previously reported protocol.[4] Metal precursors were used as 0.2 M HCl solutions in all cases. For ease, 1wt% aqueous solutions of polymeric stabiliser were also prepared prior to use. Reductant was added as a freshly prepared 0.3 M solution, such that the [reductant]/[metal] = 5. Catalysts were prepared at varying temperatures. In this case the preparation mixture was kept at 0 °C using an acetone ice bath, or at 25 & 60 °C using a water bath.

An exemplar preparation, 0.5 wt% Pd0.5 wt% Au/$TiO_2$ is outlined below.

$PdCl_2$ (0.33 mL, 15 mg/mL Pd) and $HAuCl_4$ (0.408 mL, 12.5 mg/mL) solutions were added to distilled water (400 mL). Polyvinylpyrrolidone solution (0.8 mL, 1 wt% PVP) was added under vigorous stirring. Sodium borohydride solution (0.3 M, 5 mol eq metal basis) was then added

resulting in the formation of a stabilised colloidal suspension. The dispersion was aged for 30 minutes, followed by the addition of titania (1 g) and subsequent acidification using concentrated $H_2SO_4$. The slurry was stirred for 2h, followed by filtering and thorough washing with distilled water. The resultant solid was dried at 110 °C for 16hr before use.

Catalysts were also prepared with variable total metal loading, with a constant Au:Pd weight ratio 1:1. In this case the precursor solution was scaled such that the precursor concentration remained constant between the higher and low loaded catalysts. Similar to catalysts prepared with a variable metal-stabiliser ratio, the amount of distilled water using in the preparation was reduced to account for additional volume of aqueous stabiliser solution.

*2.3.3. Solvothermal (Polyol) Method*

The polyol method is a versatile preparation method previously used to prepare bulk materials and colloidal and supported nanoparticles.[5] The catalyst preparation procedure requires the heating of metal precursors in oxidizable solvents. Above a given temperature, dependent upon the solvent, the metal precursor is reduced and the solvent oxidized yielding metal nanoparticles. An illustration of the process is presented in Figure 2-3.

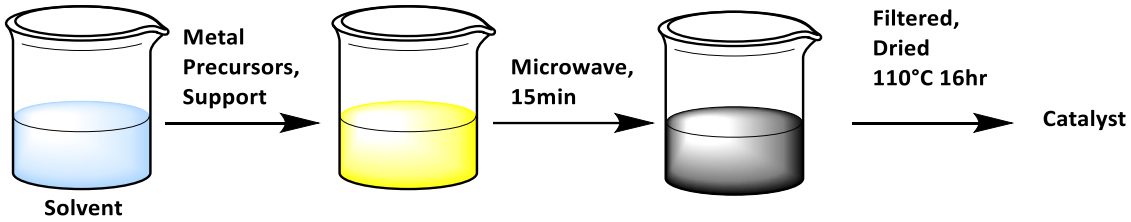


**Figure 2-3 - Illustration of microwave polyol catalyst preparation method**

The preparation can be conducted in the presence of a support material effectively yielding supported metal nanoparticles, or using solvent alone, producing colloidal metal nanoparticles. The preparation method has been further refined through the use of microwave heating which results in more rapid metal precursor decomposition allowing for rapid screening of catalysts.[6,7,8]

In this work, mono- and bimetallic catalysts were prepared using a CEM Discover SP microwave reactor, equipped with a 10mL glass liner and stirrer. The microwave reactor was operated in isothermal mode, with variable power output.

A 0.5 wt% Pd0.5 wt% Au/$TiO_2$ catalyst was prepared using the following procedure. $TiO_2$ (0.245 g) was added to the microwave reaction vessel, followed by the addition of $PdCl_2$ solution (83 µL) and $HAuCl_4$ (102 µL), and DMF (2.8 mL). The mixture then underwent a

microwave treatment, heating to 150 °C in 1 minute, followed by holding at this temperature for 15 minutes. The mixture was cooled, filtered, and washed using 20 mL 4:1 water : ethanol. The resultant catalyst was dried at 110 °C for 16 h before use.

Catalysts were prepared using a range of solvents, with the solvent volume remaining constant (2.8 mL). The addition of stabilisers was also investigated. Where possible the stabilisers were added as solids to the preparation mixture, followed by stirring at room temperature to afford dissolution before microwave irradiation. For the stabilisers received as stock solutions, the volume of solvent was altered such that the concentration of metal precursors remained constant.

For comparison, catalysts were also prepared using conventional heating. In this case, the same amount of metal precursors, solvent and support were added to a round bottom flask with vigorous stirring. The flask was then submerged in an oil bath, pre-heated to 150 °C. The preparation was allowed to proceed for 2 h, before being cooled, filtered, and washed using 20 mL 4:1 water:ethanol. The prepared catalyst was then dried at 110 °C for 16 h before use.

### *2.4. Catalyst Testing*

Catalysts were evaluated for direct hydrogen peroxide synthesis using standard reaction protocols previously published.[9] These conditions have been found to be optimum for legacy catalysts prepared by wet impregnation and so best serve for comparison with previously reported activity data. The prepared catalysts were tested twice for each applicable reaction, with the activity of the catalysts representing the average of these two tests.

#### *2.4.1. Direct Synthesis of Hydrogen Peroxide from Hydrogen and Oxygen*

Catalysts were tested in a stainless steel 100 mL volume Parr autoclave equipped with a Teflon liner – nominal volume ~66 mL. In a typical reaction, the liner was charged with water (2.9 g), methanol (5.6 g) and catalyst (10 mg). The autoclave was purged three times with 5 % $H_2/CO_2$, followed by filling with 30 bar 5 % $H_2/CO_2$ and subsequently 10 bar 25 % $O_2/CO_2$. The autoclave was then chilled to 2 °C then stirring commenced at 1200 rpm for 30min. The catalyst was removed from the reaction mixture after reaction by gravity filtration and the hydrogen peroxide yield was determined by titration of small aliquots of the filtered reaction solution with cerium sulphate ($CeSO_4$) in the presence of ferroin indicator solution, as indicated in Section 2.4.5.

### *2.4.2. Hydrogen Peroxide Hydrogenation*

The hydrogenation activity of catalysts toward hydrogen peroxide was also investigated, using a previously reported method, to enable comparison with previously reported catalysts.[10] In this case the Teflon liner was charged with 50wt % hydrogen peroxide solution (0.68 g), water (2.22 g) and methanol (5.6 g) to yield a 4 wt% hydrogen peroxide solution, followed by the addition of catalyst (10 mg). The autoclave was purged three times with 5 % $H_2/CO_2$, followed by filling with 30 bar 5 % $H_2/CO_2$. The autoclave was chilled to 2 °C then stirred at 1200 rpm for 30min. The catalyst was separated from the reaction mixture after reaction by filtration, and analysis of hydrogen peroxide content of the resultant solution was performed using cerium sulphate titration as presented in Section 2.4.5.

As shown in Section 1.6, hydrogen peroxide can undergo either hydrogenation or catalytic decomposition under direct synthesis conditions, which reduces the final yield of hydrogen peroxide under batch conditions. The catalytic decomposition of hydrogen peroxide occurs under any atmosphere, and therefore the hydrogenation activities of the catalysts include a contribution from both hydrogenation and the decomposition of hydrogen peroxide. Hutchings and co-workers previously found that for carbon and titania supported PdAu catalysts prepared by wet impregnation, the contribution of the catalytic decomposition pathway towards total hydrogen peroxide consumption varied between 8 and 25%, with remainder being due to hydrogenation.

### *2.4.3. Heterogeneous Additive Evaluation for Direct Hydrogen Peroxide Synthesis*

A range of materials were also tested as heterogeneous additives for direct synthesis. In this case 2.5 wt% Pd 2.5 wt% $Au/TiO_2$ was employed as a standard catalyst. Briefly, the autoclave liner was the liner was charged with water (2.9 g), methanol (5.6 g) and catalyst (10 mg) and additive (10 mg). The autoclave was purged three times with 5 % $H_2/CO_2$, followed by filling with 30 bar 5 % $H_2/CO_2$ and subsequently 10 bar 25 % $O_2/CO_2$. The autoclave was then chilled to 2 °C then stirring commenced at 1200 rpm for 30min. The catalyst and additive were separated from the reaction mixture by filtration and the hydrogen peroxide content of the reaction mixture subsequently determined by cerium sulphate titration.

### *2.4.4. Catalyst Reusability*

Catalyst reuse was also investigated using a modified direct synthesis protocol. In this case, the autoclave liner was charged with water (2.9 g), methanol (5.6 g) and catalyst (50 mg).

The autoclave was purged three times with 5 % $H_2/CO_2$, followed by filling with 30 bar 5 % $H_2/CO_2$ and subsequently 10 bar 25 % $O_2/CO_2$. The autoclave was then chilled to 2 °C then stirring commenced at 1200 rpm for 30 min. The catalyst was then filtered from the reaction mixture and washed thoroughly with distilled water before drying at 110 °C for 16 h. The used catalyst was then tested for hydrogen peroxide synthesis activity as outlined in Section 2.4.1.

### *2.4.5. Determination of Hydrogen Peroxide Concentration in Solution*

The amount of hydrogen peroxide present in reaction mixtures was determined by titration with cerium sulphate in the presence of ferroin indicator. Cerium(IV) sulphate stock solution was prepared in 0.75 M $H_2SO_4$ of approximate concentration 0.0085 M. Anhydrous cerium(IV) sulphate is hygroscopic, and therefore the actual concentration of the cerium(IV) sulphate solution was determined at the point of use by titration against ammonium iron(II) sulphate hexahydrate.

The standard protocol for determining hydrogen peroxide content is outlined below. Briefly, reaction mixture (0.5 g) was acidified with 2 drops of 2 % aqueous $H_2SO_4$, followed by the addition of 1 drop 0.35 M ferroin indicator, the structure presented in Figure 2-4. Cerium(IV) sulphate stock solution was then added dropwise, with the end point indicated by transition of the indicator from red to blue.

In the case of highly concentrated hydrogen peroxide solutions, such as those from the evaluation hydrogen peroxide hydrogenation activity, a modified procedure was applied. In this case the amount of reaction mixture was greatly reduced (0.02 g) to conserve cerium(IV) sulphate stock solution.

In all cases, the determination of hydrogen peroxide concentration was repeated to account for experimental error in the protocol. For hydrogen peroxide synthesis activities, the concentration of hydrogen peroxide was determined using the average of three titrations. For hydrogenation reactions, the concentration of hydrogen peroxide was measured five times before and after reaction to ensure accurate results.

$$H_2O_2 + 2Ce(SO_4)_2 \longrightarrow Ce_2(SO_4)_3 + H_2SO_4 + O_2$$

$$Fe(II)(o\text{-}phen)_3(SO_4) \longrightarrow Fe(III)(o\text{-}phen)_3$$

Blue Red

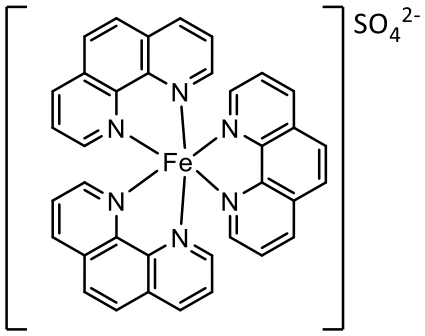


**Figure 2-4 - Hydrogen peroxide - cerium sulphate redox couple and ferroin indicator structure**

## *2.5. Characterisation Techniques*

### *2.5.1. Scanning Electron Microscopy*

Scanning electron microscopy (SEM) is a type of imaging technique that provides invaluable information on elemental composition and structure of a material. In comparison to light microscopy, electron microscopy relies on a highly focused beam of accelerated electrons whose short wavelength enables imaging of materials with greatly improved resolution. The electrons are focused into a narrow beam which scans the surface of the sample. In SEM, the primary electron beam tunnels into the sample in a teardrop volume known as the interaction volume. This volume depends on the nature of the material as well as the kinetic energy of the electrons and beam intensity. These electrons interact with the surface of the material in a variety of ways, as shown in Figure 2-5.

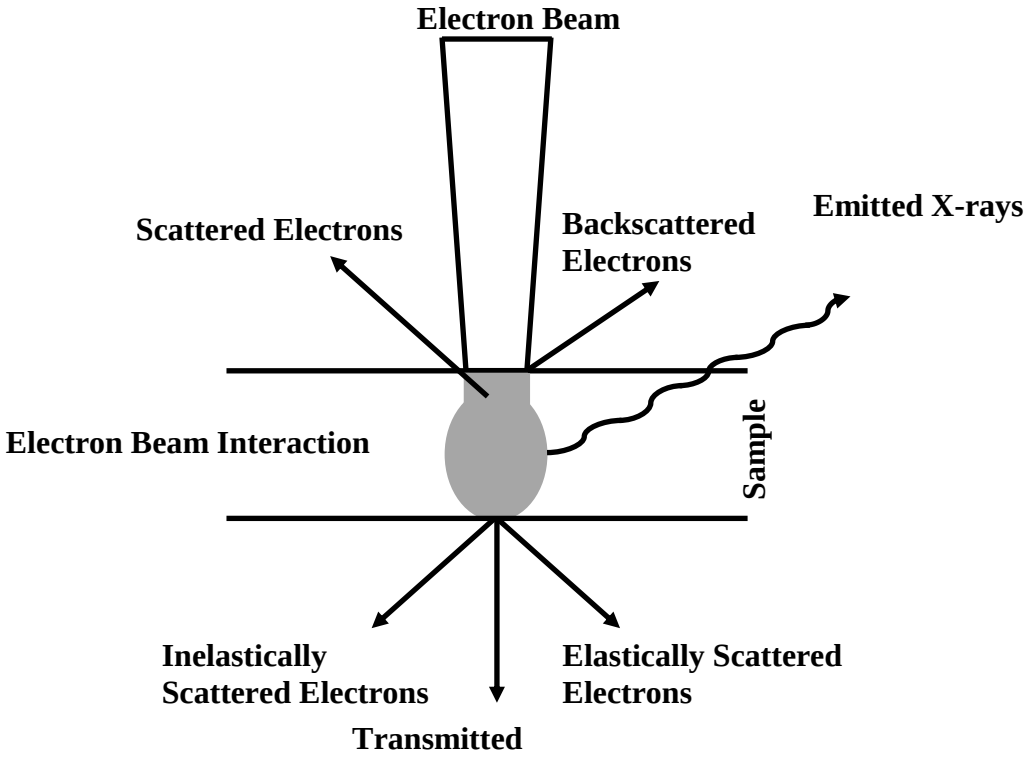


**Figure 2-5 - Diagram illustrating the possible interactions of electrons with materials during electron microscopy**

The irradiation of the sample can result in the elastic scattering of electrons on the surface, the inelastic scattering of electrons, resulting in the emission of secondary electrons, and the emission of x-rays. These three interactions can be recorded using three unique detectors. Backscatter electron detectors (BSD)s record the elastically scattered electrons from the surface of a sample. Critically the intensity of backscattered electrons is dependent on atomic number, as well as other imaging parameters such as electron beam acceleration voltage. As a result, backscattered electrons (BSE) provide compositional contrast between elements in a sample.

Secondary electron detectors record the electrons emitted from inelastic scattering of electrons from a material surface. These electrons are low energy, typically <50 meV, and originate from the atoms present in the first few nanometres of a material surface. Owing to this low depth penetration, secondary electron (SE) images are useful for evaluating topology and morphology, which may be lost in BSE images due to the increased sample penetration. Elemental information can be obtained during SEM due to the emission of x-rays from the sample. This occurs due to the formation of electron holes upon electron emission from the sample during scattering, illustrated in Figure 2-6.

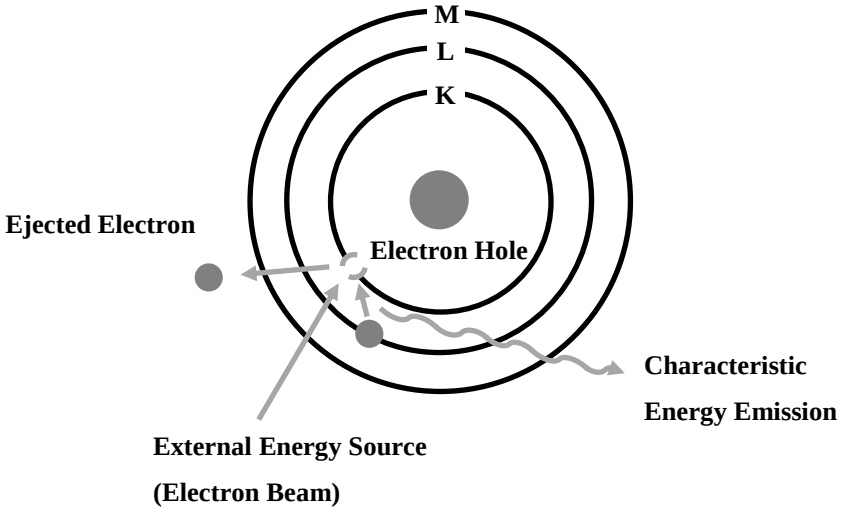


**Figure 2-6 - Diagram of electron scattering processes**

The electron holes are then filled by electrons in higher energy shells accompanied by emission of x-rays of a characteristic energy dependent upon the energy difference of the two shells. The emission of x-rays can be recorded by an x-ray detector, and the energy and intensity of the x-rays mapped to the known emission spectra of elements. This allows the

elemental surface composition of a material to be determined both at a point and across a given area.[11]

Scanning electron microscopy was performed on a Tescan Maia3 field emission gun scanning electron microscope (FEG-SEM) fitted with an Oxford Instruments XMAX$^N$ 80 energy dispersive X-ray detector (EDX). Images were acquired using the secondary electron and backscattered electron detectors. Samples were dispersed as a powder onto 300 mesh copper grids coated with holey carbon film.

### *2.5.2. Transmission Electron Microscopy*

Transmission electron microscopy (TEM) is a second form of electron microscopy in which high energy electrons are transmitted through a thin sample and collected below. As a result, accelerator voltages are high, to provide electrons with sufficiently high energy to penetrate the sample. In contrast to SEM, in TEM the beam is usually spread to encompass the whole sample and as a result does not need to be scanned across the material surface. In addition, the transmission of the electrons through the sample provides more information on the structure of the material, versus SEM, where the poor depth penetration of the beam insists that only morphology and surface composition can be recorded. The electron beam is refocused after passing through the sample and projected onto a screen. TEM has been previously used to assess the structure and morphology of heterogeneous catalysts as atomic weight contrast allows for the determination of particle size for supported metal nanoparticles.[12]

Transmission electron microscopy (TEM) and scanning transmission electron microscopy (STEM) were performed on a JEOL JEM-2100 operating at 200 kV. Energy dispersive X-ray analysis (EDX) was done using an Oxford Instruments X-Max$^N$ 80 detector and the data analysed using the Aztec software. Samples were dispersed as a powder onto 300 mesh copper grids coated with holey carbon film.

### *2.5.3. Scanning Transmission Electron Microscopy*

Scanning transmission electron microscopy (STEM) is a variant of TEM in which the electron beam is focused to a point, which is then scanned across the surface of the thin specimen material. The transmission of the electrons through the sample results in several electron scattering processes, the products of which can be analysed with suitable detectors. The transmitted electrons can be detected using a so called ‘bright field’ detector (BF), whilst scattered electron response can be recorded using angular dark field (ADF) or high angle

angular dark field (HAADF) detectors. Analogous to the back-scatter detectors in SEM, images recorded from these detectors provide atomic weight contrast, which when coupled with the bright field image, can provide more information about the nature of the sample.[13]

Furthermore, elemental analysis can also be performed using a STEM microscope coupled with an energy dispersive x-ray spectroscopy (EDX) detector. As with SEM, the scattering of electrons results in the formation of electron holes and the concomitant emission of X-rays with the filling of these holes. The energy of these x-rays corresponds to the energy difference between atomic energy levels, and as a result, the energy and intensity of the detected x-rays provide a measure of a given material's elemental composition.

The Scanning Transmission Electron Microscopy (STEM) images and X-ray Energy Dispersive Spectra (EDX) were taken using a JEOL® JEM-ARM200F aberration corrected microscope, equipped with an Oxford Instrument® Aztec EDS system.

### *2.5.4. Brunauer–Emmett–Teller (BET) Surface Area Measurements*

Catalyst surface areas were measured using Brunauer–Emmett–Teller theory. BET theory uses the adsorption of non-reactive gases to probe the surface area of a solid. Nitrogen is most commonly used to determine surface area using BET methods, however argon and helium have also been previously used.[14]

In a typical experiment, a known mass of catalyst is dosed with nitrogen to form an equilibrium between surface bound and free nitrogen. The volume of nitrogen added to the cell, and the equilibrium and saturation pressures of nitrogen are recorded. Using a modification to the Langmuir adsorption model yields the following equation:

$$\frac{1}{v[\left(\frac{p_o}{p}\right)-1]} = \frac{c-1}{v_m c}\left(\frac{p}{p_o}\right) + \frac{1}{v_m c}$$

*Where:*

*v is the adsorbed gas volume*

*$v_m$ is the monolayer adsorbed gas volume*

*p is the equilibrium pressure*

*$p_o$ is the saturation pressure*

*and c is the BET constant, where*

$$c = \exp\left(\frac{E_1 - E_L}{RT}\right)$$

*and $E_1$ and $E_L$ are the heat of adsorption of one monolayer and the heat of liquefaction and T is the temperature.*

Plotting $v$ vs $p/p_o$ yields an adsorption/desorption isotherm which expresses the change in volume as a charge in pressure.

The BET approximation is only applicable in regions where the relationship between $v$ and $p/p_o$ is linear, and as a result surface area is typically calculated from $p/p_o = 0.05$ to $p/p_o = 0.35$.

BET Surface area measurements were performed on a Quantachrome Nova 2200 using a multipoint $N_2$ adsorption method. Prior to the analysis, samples were degassed for 24 h at 200 °C under vacuum.

*2.5.5. X-Ray Photoelectron Spectroscopy*

X-Ray Photoelectron Spectroscopy (XPS) is a surface characterisation technique that measures surface elemental composition.[15] The fundamental basis for XPS is the photoelectric effect, the phenomena in which the irradiation of a surface with electromagnetic radiation of sufficiently high energy results in the emission of electrons from the surface. The energy threshold for the emission of an electron is also known as its binding energy (BE).

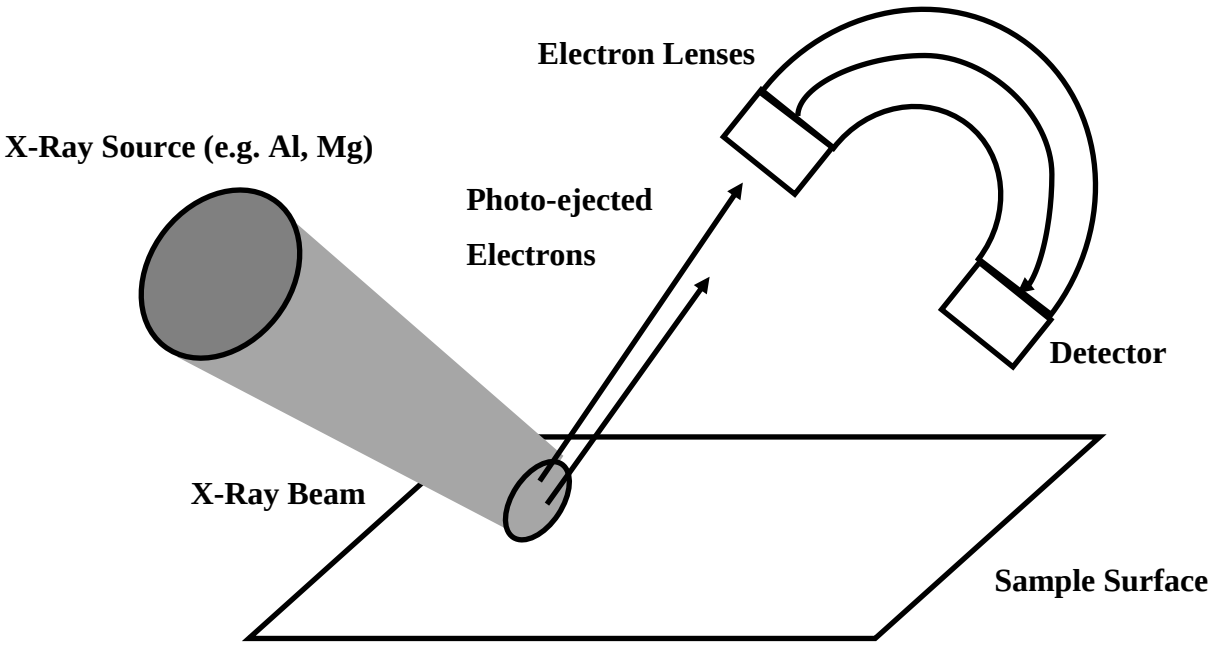


**Figure 2-7 - Schematic of XPS spectrometer operation**

Figure 2-7 illustrates the various components of an XPS system. In the first instance, a beam of x-rays is generated from a source. Typically, the X-ray source is itself a photoelectric device, where a beam of generated electrons strikes a metal anode (typically Aluminium) to yield low energy x-rays. These x-rays are then focused onto the sample resulting in the emission of electrons. The electrons are collected by a detector to yield the number of electrons (count) and energy of the emitted electrons. Given the energy of the generated x-rays and the kinetic energy of the electrons, the binding energy can therefore be determined. This can yield important information on a materials surface, as electron binding energies are specific to given elements. Furthermore, binding energy is dependent upon oxidation state, chemical environment and physical variables such as lattice parameters. As a result, these binding energies can be compared to literature and database values to ascertain elemental information about the nature of the material.

X-ray photoelectron spectroscopy (XPS) data was collected on a Thermo-Fisher Scientific K-Alpha$^+$ X-ray photoelectron spectrometer using a monochromatic Al Kα X-ray source operating at 72 W. Survey scans and high-resolution scans were acquired at a pass energy of 150 eV and 40 eV respectively. Charge neutralization was achieved using a combination of low energy electrons and argon ions, resulting in a C(1s) binding energy of 284.8 eV; experimental binding energies are quoted ±0.2 eV.

### *2.5.6. Microwave Plasma Atomic Emission Spectroscopy (MP-AES)*

Atomic emission spectroscopy (AES) is a technique that allows for the quantitative determination of an element in solution. Analyte solution is introduced to a thermal source, such as flame or plasma, resulting in sample atomisation. This is accompanied by the thermal promotion of electrons to excited states, which then emit light of characteristic wavelengths during decay back to their electronic ground state. The wavelength and intensity of the emitted light therefore directly corresponds to the presence and concentration of given elements in solution.

Microwave plasma AES (MP-AES) is a subset of AES in which the thermal excitation of solution phase species is achieved using a microwave generated plasma. The sample solution is fed into the plasma as an aerosol, and the resultant light emission recorded using a detector.

Elemental concentrations in solution can be determined using the relevant calibration curves. In a standard procedure, commercially available calibration standards (typically 1000 ppm), are diluted to the required concentration and the response recorded.

Microwave Plasma Atomic Emission Spectroscopy (MP-AES) was used to determine the metal loading of the as-prepared catalysts. Analysis was performed on an Agilent 4100 MP-AES equipped with a standard glass concentric nebulizer and cyclonic spay chamber. Samples were prepared by digesting the catalyst (0.01 g) in aqua regia (1 mL) to ensure total metal dissolution followed by dilution with distilled water (9 mL) prior to analysis. Signal response was recorded at two characteristic emission wavelengths for Au (242.8 nm, 267.6 nm) and Pd (340.5 nm, 363.5 nm), and the resultant concentrations averaged. The concentration response of Au and Pd were calibrated using commercial reference standards (Agilent), in all cases $r^2 > 0.999$.

## *2.6. References*

1 J. Edwards, B. Solsona, P. Landon, A. Carley, A. Herzing, C. Kiely and G. Hutchings, *J. Catal.*, 2005, **236**, 69–79.
2 J. Pritchard, L. Kesavan, M. Piccinini, Q. He, R. Tiruvalam, N. Dimitratos, J. A. Lopez-Sanchez, A. F. Carley, J. K. Edwards, C. J. Kiely and G. J. Hutchings, *Langmuir*, 2010, **26**, 16568–16577.
3 D. R. Jones, S. Iqbal, P. J. Miedziak, D. J. Morgan, J. K. Edwards, Q. He and G. J. Hutchings, *Top. Catal.*, 2018, **61**, 833–843.
4 J. Pritchard, M. Piccinini, R. Tiruvalam, Q. He, N. Dimitratos, J. A. Lopez-Sanchez, D. J. Morgan, A. F. Carley, J. K. Edwards, C. J. Kiely and G. J. Hutchings, *Catal. Sci. Technol.*, 2013, **3**, 308–317.
5 B. H. Kim, M. J. Hackett, J. Park and T. Hyeon, *Chem. Mater.*, 2014, **26**, 59–71.
6 J. Yang, T. C. Deivaraj, H. P. Too and J. Y. Lee, *Langmuir*, 2004, **20**, 4241–4245.
7 A. Nirmala Grace and K. Pandian, *Mater. Chem. Phys.*, 2007, **104**, 191–198.
8 K. Patel, S. Kapoor, D. P. Dave and T. Mukherjee, *Res. Chem. Intermed.*, 2006, **32**, 103–113.
9 J. K. Edwards, A. Thomas, B. E. Solsona, P. Landon, A. F. Carley and G. J. Hutchings, *Catal. Today*, 2007, **122**, 397–402.
10 J. K. Edwards, A. F. Carley, A. A. Herzing, C. J. Kiely and G. J. Hutchings, *Faraday Discuss.*, 2008, **138**, 225–239.
11 F. Li, Q. Shao, M. Hu, Y. Chen and X. Huang, *ACS Catal.*, 2018, 3418–3423.
12 S. a. Kondrat, P. J. Miedziak, M. Douthwaite, G. L. Brett, T. E. Davies, D. J. Morgan, J. K. Edwards, D. W. Knight, C. J. Kiely, S. H. Taylor and G. J. Hutchings, *ChemSusChem*, 2014, **7**, 1326–1334.
13 R. C. Tiruvalam, J. C. Pritchard, N. Dimitratos, J. A. Lopez-Sanchez, J. K. Edwards, A. F. Carley, G. J. Hutchings and C. J. Kiely, *Faraday Discuss.*, 2011, **152**, 63.
14 A. M. Kalijadis, M. M. Vukčević, Z. M. Jovanović, Z. V. Laušević and M. D. Laušević, *J. Serbian Chem. Soc.*, 2011, **76**, 757–768.
15 R. Burgess, C. Buono, P. R. Davies, R. J. Davies, T. Legge, A. Lai, R. Lewis, D. J. Morgan, N. Robinson and D. J. Willock, *J. Catal.*, 2015, **323**, 10–18.

# *3. One Pot Microwave Synthesis of Supported Metal Catalysts for Direct Hydrogen Peroxide Synthesis*

## *3.1. Introduction*

Mono and bimetallic nano-alloyed particles (NP) anchored to metal oxide or carbon supports are highly efficient, selective catalysts for a wide-ranging number of environmentally friendly reactions, from upgrading biomass to pioneering new reaction pathways to valuable commodity chemicals such as hydrogen peroxide.[1,2,3,4,5] The preparation route to these supported nanoparticles has been shown to indirectly influence the activity of the final catalyst, through its effect on NP size and composition.

Wet impregnation is a low cost, highly scalable preparation method that is commonly used in the preparation of bimetallic nanoparticle catalysts. The preparation requires the addition of metal precursor solutions to a support material, which upon solvent removal, yields adsorbed metal species. Subsequently the material is dried, and heat treated to yield a supported nanoparticle catalyst. Lack of control over parameters, such as dispersion of the metal precursors, results in the formation of a range of nanoparticulate species with wide particle size distributions (2-1000 nm) of varying composition. In particular the formation of large metal nanoparticles results in a decrease in active metal surface area and therefore catalyst activity.[5]

Hutchings and co-workers previously reported that preparing PdAu catalysts by wet impregnation results in particle size-composition effects, whereby the small particles are palladium rich and large Au rich.[6] Deposition-precipitation (DP) is an analogous method in which the precipitation of metal precursors is instead afforded by pH adjustment, with the resultant metal species adhering to the support material through electrostatic interactions. The DP method yields catalysts with better control of particle size (2-6 nm), but requires the use of very dilute metal salt solutions to prevent the formation of micrometre sized metal particles. The preparation also requires significant washing of the catalyst upon preparation (>200mL/g catalyst), to remove unprecipitated metal precursor, which severely reduces the industrial applicability of the process.[7] For precious metal catalysts, efficient use of the catalytically active metal is of paramount importance and the deposition-precipitation method often results in partial adsorption of the metal precursor species, which introduces further cost to the preparation.

The co-precipitation method has also been reported for the preparation of bi-metallic nanoparticles, where the support is precipitated at the same time as the desired metal complex. In this method some of the active metal can incorporate into the lattice of the support, which is catalytically inactive, and the technique also suffers from the same disadvantages as the deposition precipitation method.[8]

More recently, sol-immobilisation was demonstrated to be effective in yielding highly active catalysts. In this preparation method, aqueous metal salts are subjected to reducing agents in the presence of polymeric stabilising agents to yield metal nanoparticles with exceptionally narrow size distributions (2-4 nm) and uniform particle composition. The simultaneous or subsequent reduction of metal precursors allows for the formation of alloyed or core-shell metal nanoparticles.[9,10] However, the protecting polymer species remain on the metal surface after preparation, which reduces reactant flux to the surface and reduces activity. Catalyst heat treatment or reflux can be used to remove remaining stabiliser, but this introduces further energy cost and complexity into the preparation process.[11]

An alternative preparation method is the solvothermal reduction of metal precursors. The most notable example of this is the so-called polyol method, in which metal precursors are reduced through the oxidation of an organic species, typically polyols, at elevated temperatures.[12] The method is highly versatile, being previously used to prepare monometallic catalysts of Ag, Au, Pd, Pt, Fe, Ni, Co and Sn.[13,14,15] Bimetallic materials have also been prepared, as the controlled growth kinetics yield materials with specific magnetic and crystallographic properties.[16] A wide range of alcohols have been previously used, as well as other organic species such as N,N-Dimethylformamide (DMF).[17] The nature of DMF is similar to polyols (high boiling, polar and forms reductive species), which makes it a viable alternative in the preparation of a variety of metal nanoparticles, most notably silver.[18]

The solvothermal preparation of metal nanoparticles can be further improved through the utilisation of microwave heating. Microwave irradiation affords rapid and uniform heating during preparation, resulting in improved nucleation and crystallisation.[19] The improved crystallisation effect is principally achieved through faster ramping temperatures, achieving temperatures of 150-200°C in typically less than 1 minute as compared to 30 minutes for conventional heating. Humphrey and co-workers previously investigated the benefits of microwave heating in the preparation of Rh nanoparticles and showed that the microwave prepared nanoparticles were more than twice as active for cyclohexene hydrogenation versus

the conventionally heated analogues.[20] This activity improvement was attributed to improved nanoparticle morphology and size control. The microwave assisted preparation yielded highly faceted nanoparticles 5-7 nm in diameter, whereas the conventional heat preparation resulted in formation of a wide range of particle morphologies and sizes.

PdAu bimetallic nanoparticles have also been previously prepared by the polyol method. Ferrer *et al.* showed that careful variation of catalyst preparation temperature could be used to prepare alloyed, core-shell and three-layered core-shell PdAu nanoparticles, highlighting the broad scope of the polyol preparation method.[21] Mukherjee *et al.* reported the preparation of colloidal PdAu alloyed nanoparticles using an analogous method, and showed that the preparation tolerated large variations in the ratio of Pd and Au precursors, enabling access to alloyed nanoparticles of varying composition.[22] PdAu bimetallic nanoparticles are known to be highly active catalysts for the direct synthesis of hydrogen peroxide from hydrogen and oxygen. Hydrogen peroxide is a green oxidant and a major commodity chemical. It can be used as an environmentally friendly alternative to oxidants such as chromates and percarbonates, as its oxidation by-product is water, avoiding potential toxicity issues.[23,24] Hydrogen peroxide is currently produced industrially using the anthraquinone process, which requires energy intensive purification processes, such as distillation, to prepare concentrated hydrogen peroxide. The direct synthesis of hydrogen peroxide therefore offers a more atom efficient alternative to this process.

The aim of this work is to investigate microwave assisted solvothermally prepared catalysts for the direct synthesis of hydrogen peroxide, and to assess the versatility of the microwave assisted polyol method for the preparation of a range of active bimetallic materials.

## *3.2. Results*

### *3.2.1. PdAu Bimetallic Catalysts for Hydrogen Peroxide Synthesis*

#### *3.2.1.1. Catalyst Preparation Optimisation*

Catalyst preparation significantly influences final catalyst activity for metal oxide supported PdAu catalysts. For example, Pritchard *et al.* reported a thorough investigation of catalyst preparation parameters for $PdAu/TiO_2$ catalysts prepared by wet impregnation for hydrogen peroxide synthesis, showing that precursor concentration, drying time and preparation scale all had a profound effect on hydrogen peroxide synthesis and hydrogenation activity.[25] Such work has not been previously explored for metal oxide supported PdAu catalysts prepared by solvothermal methods, either using conventional or microwave-assisted heating. Indeed, examples exist of the optimisation of PdAu nanostructures from a materials perspective, but not from a catalytic one.[26,27]

#### *3.2.1.2. The Effect of Catalyst Composition on Hydrogen Peroxide Synthesis Activity*

The effect of varying Pd:Au ratio was investigated in order to improve the hydrogen peroxide synthesis and hydrogenation activities of the bimetallic catalysts. PdAu catalysts prepared by wet impregnation or sol immobilisation, with a 1:1 Pd:Au ratio by mass, are known to exhibit optimal hydrogen peroxide synthesis activity.[28,25] Increasing palladium content results in increased hydrogenation activity, and therefore decreased synthesis activity. Likewise, decreasing palladium content also results in a decrease in synthesis activity. Figure 3-1 displays the synthesis and hydrogenation activities of PdAu bimetallic catalysts of varying composition in addition to monometallic catalysts. In agreement with previous work, the addition of Au to Pd catalysts results in a significant improvement in their hydrogen peroxide synthesis performance. The monometallic Au and Pd catalysts exhibit synthesis activities of 5 and 35 $molH_2O_2/h/kg_{cat}$, respectively. It is noteworthy that the monometallic palladium catalyst displays activity comparable to that of $AuPd/TiO_2$ catalysts prepared by sol immobilisation previously reported by Tiruvalam *et al.*, who reported that a 0.5 wt% Pd0.5 wt% $Au/TiO_2$ catalyst prepared by conventional sol immobilisation had an activity of 31 $molH_2O_2/h/kg_{cat}$ under identical reaction conditions .[11] This emphasises the critical importance of optimising catalyst preparation to improve activity.

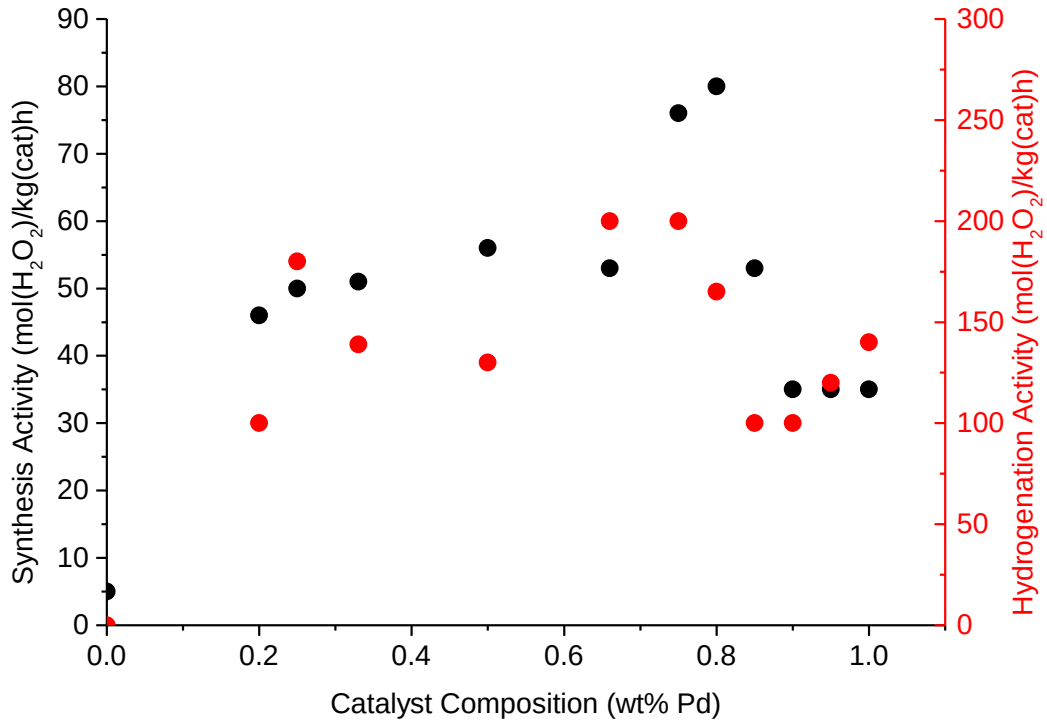


**Figure 3-1 - Hydrogen peroxide synthesis and hydrogenation activity of 1 wt% PdAu/$TiO_2$ catalysts with varying Pd content**

**Reaction Conditions – Hydrogen peroxide synthesis: 5 % $H_2/CO_2$ (2.9 MPa) and 25 % $O_2/CO_2$ (1.1 MPa), 8.5 g solvent (2.9 g $H_2O$, 5.6 g MeOH) 0.01 g catalyst, 2 °C, 1200 rpm, 30 min. Hydrogen peroxide hydrogenation: 5% $H_2/CO_2$ (2.9 MPa), 8.5 g solvent (2.22 g $H_2O$, 5.6 g MeOH and 0.68 g 50% $H_2O_2$), 0.01 g catalyst, 2 °C, 1200 rpm, 30 min.**

Interestingly, despite exhibiting a clear synergistic effect, variation of the Pd:Au ratio does not produce the 'volcano' trend observed for other preparation methods. At low Pd content, 0.25 to 0.66 wt%, increasing palladium content only results in marginal increases in activity, from 50 to 56 mol$H_2O_2$/h/$kg_{cat}$. Although the sluggish improvement in activity suggests the presence of Au is beneficial to hydrogen peroxide synthesis activity, the relative invariance of activity towards Au content suggests that only a small amount of Au may be required to afford improved performance; a possible consequence could be the presence of monometallic Au spectator species in the catalyst.

Above 0.75 wt% Pd, the synthesis activity is considerably greater, 80 mol$H_2O_2$/h/$kg_{cat}$, up to a maximum Pd content of 0.80 wt%. Increasing the Pd content even further results in a decrease in synthesis activity from 53 mol$H_2O_2$/h/$kg_{cat}$ for 0.85wt%Pd to 35 mol$H_2O_2$/h/$kg_{cat}$ for 0.9 wt% Pd. The activity of the 0.95 wt% Pd 0.05 wt% Au/$TiO_2$ catalyst is indistinguishable from the monometallic Pd catalyst. The catalysts were also tested for hydrogen peroxide hydrogenation activity. Hydrogenation is the dominant pathway for the

decomposition of hydrogen peroxide produced during synthesis reactions and, as a result, hydrogenation activity is a good indicator for overall catalyst selectivity.[29] The catalysts exhibit varying hydrogenation activity; however, the trend observed was largely indifferent to Pd content, with all palladium containing catalysts exhibiting hydrogenation activities between 100-200 mol$H_2O_2$/h/$kg_{cat}$. Likewise, the hydrogenation activity of the monometallic Pd catalyst is similar to that of the PdAu counterparts, suggesting that the synthesis activity improvements produced by the addition of Au are a result of factors other than simply a reduction in hydrogenation activity. Previous work by Tiruvalam *et al.* found that a 0.5 wt% Pd 0.5 wt% Au/$TiO_2$ catalyst prepared by sol immobilisation displayed synthesis and hydrogenation activities of 31 and 384 mol$H_2O_2$/h/$kg_{cat}$ under the same conditions.[11] For comparison, the 0.5 wt% Pd 0.5 wt% Au/$TiO_2$ catalyst prepared by microwave irradiation exhibited synthesis and hydrogenation activities of 56 and 130 mol$H_2O_2$/h/$kg_{cat}$. The increased synthesis and decreased hydrogenation activities imply that the catalyst is more active for direct synthesis, less active towards the hydrogenation of the formed hydrogen peroxide and therefore more selective towards hydrogen peroxide. The selectivity of the catalyst could be a consequence of differing nanoparticle structure, such as surface composition or particle size compared to those previously reported in literature. Overall, the results suggest that microwave solvothermal catalyst preparation is a viable alternative to commonly reported catalyst preparation methods.

Given the high cost of precious metals, it can often be more useful to express activity per metal mass as opposed to per catalyst mass. Expressing activity in this manner also allows for accurate comparison between catalysts of differing total metal loading. Considering the relative inactivity of Au, activity is most commonly reported as catalyst activity per gram of Pd. The hydrogen peroxide synthesis activity of PdAu/$TiO_2$ catalysts of varying composition are shown in Figure 3-2.

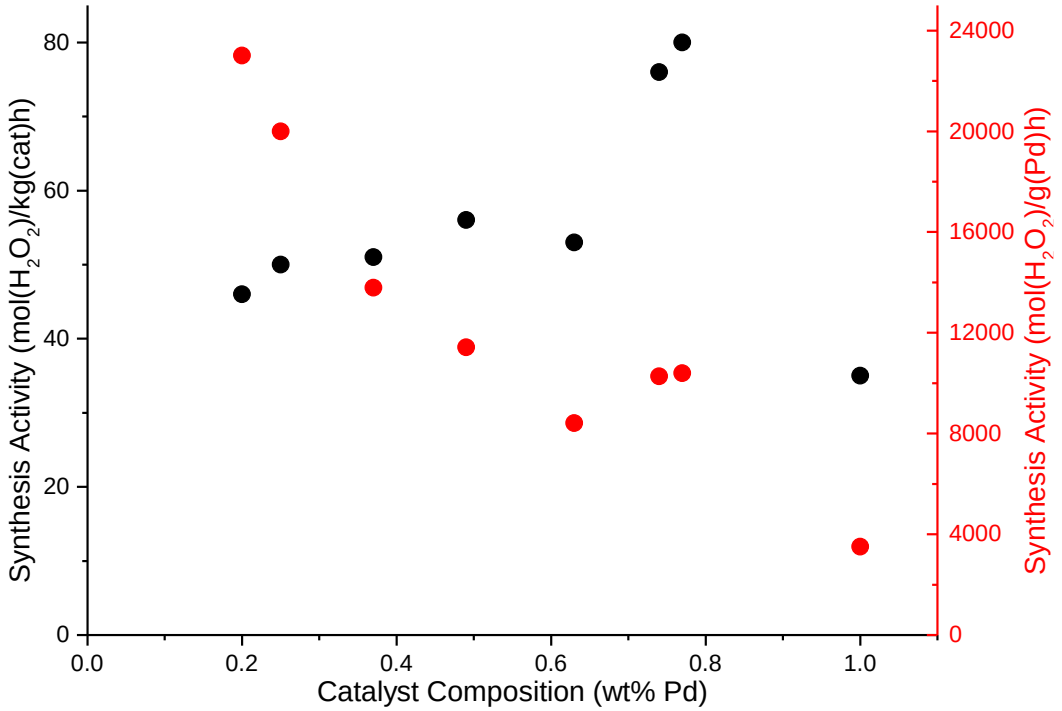


**Figure 3-2 - Hydrogen peroxide synthesis activity of 1 wt% PdAu/$TiO_2$ catalysts with varying Pd content expressed as per g catalyst (●) and per g Pd (●)**

**Reaction Conditions – 5 % $H_2/CO_2$ (2.9 MPa) and 25 % $O_2/CO_2$ (1.1 MPa), 8.5 g solvent (2.9 g $H_2O$, 5.6 g MeOH) 0.01 g catalyst, 2 °C, 1200 rpm, 30 min.**

0.8 wt% Pd0.2 wt% Au/$TiO_2$ is clearly most active on a catalyst mass basis, however the Pd poor catalysts are disproportionally active per mass of palladium, and therefore most active on a metal basis.

Owing to the modest increase in catalyst activity between 0.2 wt% Pd 0.8 wt% Au/$TiO_2$ and 0.66 wt% Pd 0.33 wt% Au/$TiO_2$, on a catalyst mass basis, hydrogen peroxide synthesis activity by Pd content decreases steadily from 23,000 to 8,400 mol$H_2O_2$/h/$g_{Pd}$. 0.75 wt% Pd 0.25 wt% Au/$TiO_2$ and 0.8 wt% Pd 0.25 wt% Au/$TiO_2$ both exhibit similar activities of 10250 and 10400 mol$H_2O_2$/h/$g_{Pd}$. Nonetheless, the hydrogen peroxide synthesis activity per Pd basis is considerably higher for all bimetallic materials when compared to the monometallic 1 wt% Pd/$TiO_2$ catalyst, indicating that, irrespective of composition, the incorporation of Au is beneficial in improving Pd economy.

### *3.2.1.3. The Effect of Heating Method*

To determine the necessity of microwave assisted heating, catalysts of varying composition were also prepared using conventional thermal heating. The hydrogen peroxide synthesis activity of $PdAu/TiO_2$ catalysts prepared by microwave assisted and conventionally heated approaches are shown in Figure 3-3.

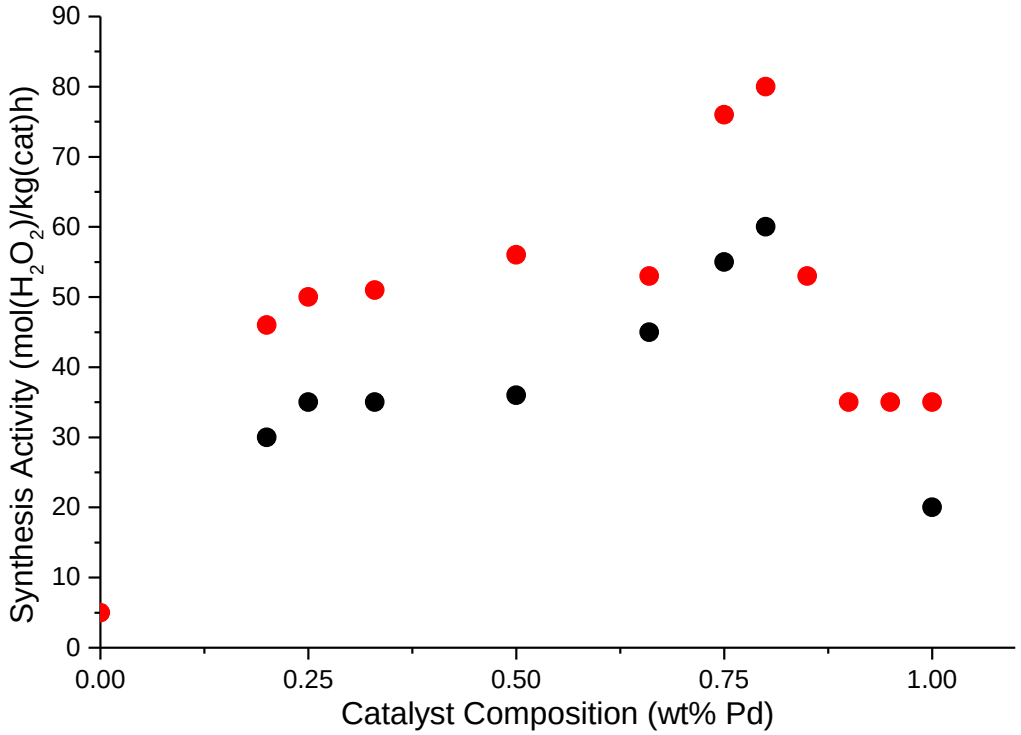


**Figure 3-3 - Hydrogen peroxide synthesis activity of catalysts of varying composition prepared by microwave-assisted (•) and conventional heating (•)**

**Reaction Conditions – 5 % $H_2/CO_2$ (2.9 MPa) and 25 % $O_2/CO_2$ (1.1 MPa), 8.5 g solvent (2.9 g $H_2O$, 5.6 g MeOH) 0.01 g catalyst, 2 °C, 1200 rpm, 30 min.**

Generally, catalysts prepared by conventional heating are less active than the analogous microwave assisted counterparts. Nonetheless, the variation between the two preparation methods differed dependent upon composition. The 0.66 wt% Pd 0.33 wt% $Au/TiO_2$ catalysts have the smallest difference between conventional and microwave assisted preparation, with activities of 45 and 53 $molH_2O_2/h/kg_{cat}$ respectively. The activity difference of the two methods varied by 15-20 $molH_2O_2/h/kg_{cat}$ for all other compositions, which represents approximately a 50 % increase in activity.

The conventionally heated 0.5 wt% Pd 0.5 wt% $Au/TiO_2$ catalyst was also evaluated for hydrogen peroxide hydrogenation activity, with the results displayed in Table 3-1. The hydrogenation activity of the conventionally heated catalyst is 150 $molH_2O_2/h/kg_{cat}$,

marginally higher than the microwave heated sample with an activity of 130 mol$H_2O_2$/h/$kg_{cat}$. Although these results indicate that the conventionally heated catalyst is less selective, it is unlikely that such a small increase in hydrogenation activity is solely responsible for the decrease in synthesis activity. The difference in synthesis activity could be a result of differing nanoparticle structure or composition.

**Table 3-1 - Hydrogen peroxide synthesis and hydrogenation activities of 0.5 wt% Pd 0.5 wt% Au/$TiO_2$ catalyst prepared using conventional and microwave-assisted heating**

| Heating Method | Productivity (mol/kg(**cat**)hr) | Hydrogenation Activity (mol/kg(**cat**)hr) |
|---|---|---|
| Conventional | 36 | 150 |
| Microwave Assisted | 56 | 130 |

**Reaction Conditions – Hydrogen peroxide synthesis: 5 % $H_2/CO_2$ (2.9 MPa) and 25 % $O_2/CO_2$ (1.1 MPa), 8.5 g solvent (2.9 g $H_2O$, 5.6 g MeOH) 0.01 g catalyst, 2 °C, 1200 rpm, 30 min. Hydrogen peroxide hydrogenation: 5% $H_2/CO_2$ (2.9 MPa), 8.5 g solvent (2.22 g $H_2O$, 5.6 g MeOH and 0.68 g 50 wt% $H_2O_2$), 0.01 g catalyst, 2 °C, 1200 rpm, 30 min.**

Humphrey and co-workers previously investigated the beneficial effects of microwave versus conventional heating for solvothermal precious metal nanoparticle synthesis, and observed that microwave assisted heating improved the crystallinity of the prepared nanoparticles and resulted in the formation of highly faceted nanostructures.[20] The authors also showed that metal precursor decomposition occurs much more rapidly under microwave irradiation, even if the solvent was pre-heated to account for slower temperature ramp when using conventional heating. Indeed, comparable observations were made in the preparation of the microwave and conventionally heated catalysts presented in this work. In the preparation of the conventionally heated catalysts, the preparation mixture needed to be heated for at least two hours to ensure complete decomposition of the metal precursors. In the case of microwave-assisted preparation, complete reduction was observed in only 5 min.

### *3.2.1.4.The Effect of Varying Preparation Solvent*

Further work was carried out to determine the effect of various solvents on catalyst preparation. Solvothermal metal nanoparticle synthesis is commonly carried out in alcohols, so much so that the term 'polyol method' has become synonymous with the preparation method.[12] Nonetheless, other solvents have been reported to be suitable for solvothermal synthesis, such as N,N-dimethylformamide (DMF), which has similar physical and redox properties to polyols.[18] To better understand solvent effects during catalyst preparation, 0.5 wt% Pd 0.5 wt% $Au/TiO_2$ catalysts were prepared in the presence of a range of organic solvents, with the hydrogen peroxide synthesis activities of the corresponding catalysts presented in Figure 3-4.

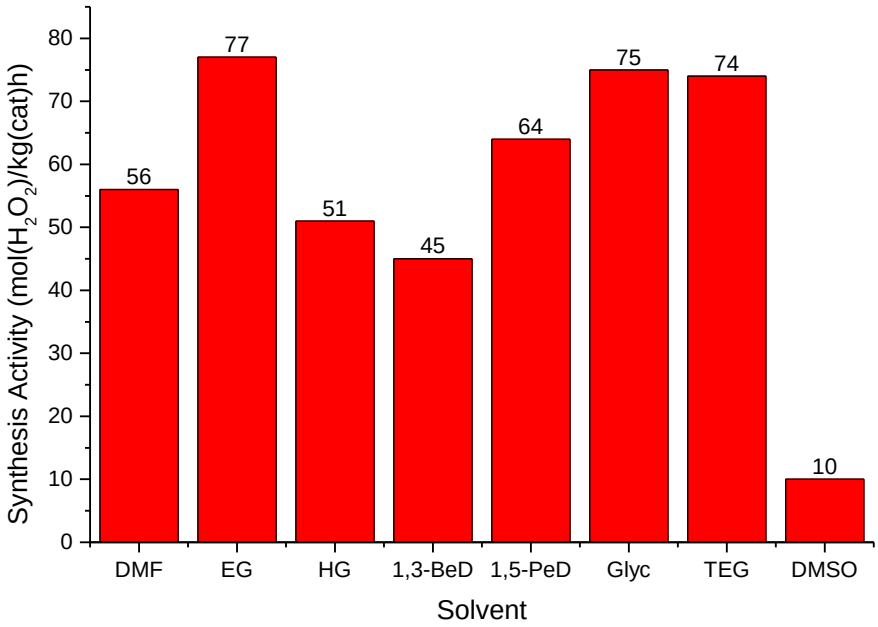


**Figure 3-4 - Hydrogen peroxide synthesis activity of 0.5wt% Pd 0.5 wt% $Au/TiO_2$ catalysts prepared by microwave solvothermal synthesis in a range of solvents**

**Reaction Conditions – 5 % $H_2/CO_2$ (2.9 MPa) and 25 % $O_2/CO_2$ (1.1 MPa), 8.5 g solvent (2.9 g $H_2O$, 5.6 g MeOH) 0.01 g catalyst, 2 °C, 1200 rpm, 30 min.**

The best performing catalysts were prepared in ethylene glycol, glycerol and tetraethylene glycol with hydrogen peroxide synthesis activities of 77, 75 and 74 $molH_2O_2/h/kg_{cat}$ respectively. The performance of these catalysts equates to roughly a 25 % increase in synthesis activity versus a catalyst with the same loading prepared in the benchmark solvent DMF. The worst performing catalyst was prepared in DMSO, which exhibits an activity of 10 $molH_2O_2/h/kg_{cat}$. Catalysts prepared in hexylene glycol or 1,3-butanediol also perform poorly when compared to either DMF or other polyols, which suggests that the structure of the solvent influences the activity of the final catalyst. Ethylene glycol, glycerol and tetraethylene

glycol all contain primary alcohols groups, whereas 1,3-butanediol contains one primary and one secondary, and hexylene glycol, one secondary and one tertiary alcohol. It is well known that the reduction of metal precursors is accompanied by the oxidation of the diol, to yield an aldehyde in the case of primary alcohols.[30,31] The oxidation of the secondary alcohol to a ketone is more difficult and, as a result, may influence reduction kinetics and therefore final nanoparticle structure. Similarly, tertiary alcohols cannot be oxidised through an analogous mechanism and, therefore, do not contribute to reductive nanoparticle formation. DMSO has been previously reported to be particularly useful for the solvothermal preparation of supported metal sulphides and metal oxides.[32–35] The poor activity of the DMSO prepared catalyst in this work could be a result of poisoning of the active metal surface by sulfur containing oxidation products.

### *3.2.1.5. The Effect of Addition of Stabilisers to Catalyst Preparation*

Catalysts were also prepared in the presence of polymeric stabilisers to determine their effect on catalyst activity, the activity of the stabilised catalysts shown in Figure 3-5. Previous work shows that the addition of stabilisers during solvothermal nanoparticle formation results in decreased average particle sizes and therefore improved catalytic activity.[36–39]

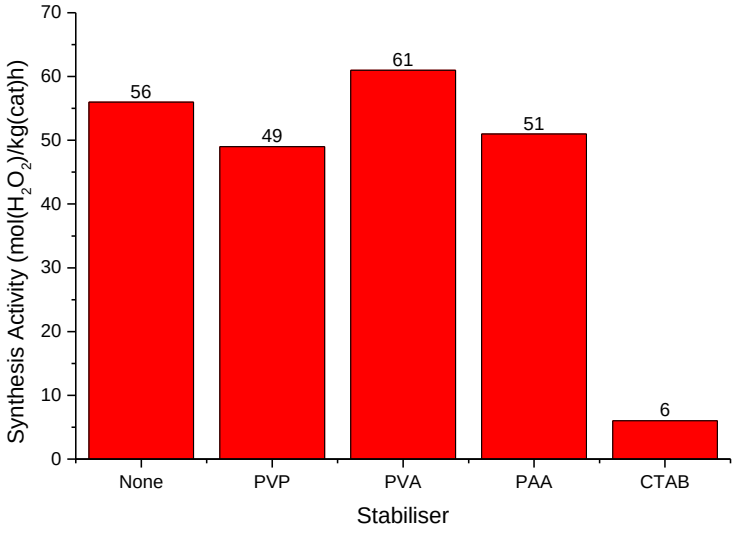


**Figure 3-5 - Hydrogen peroxide synthesis activity of 0.5 wt% Pd 0.5 wt% Au/$TiO_2$ prepared in the presence of polymeric stabilisers**

**Reaction Conditions – 5 % $H_2/CO_2$ (2.9 MPa) and 25 % $O_2/CO_2$ (1.1 MPa), 8.5 g solvent (2.9 g $H_2O$, 5.6 g MeOH) 0.01 g catalyst, 2 °C, 1200 rpm, 30 min.**

As seen in Figure 3-5 the use of stabilisers during catalyst preparation results in a small change in catalyst activity, less than 10 %. The addition of 1 eq PVA results in a modest increase in synthesis activity from 56 to 61 mol$H_2O_2$/h/$kg_{cat}$. The addition of either PVP or

PAA results in a decrease of synthesis activity relative to the stabiliser free catalyst, to 49 and 51 mol$H_2O_2$/h/$kg_{cat}$ respectively. For comparison, cetyltrimethylammonium bromide (CTAB) was also investigated as a potential stabiliser. CTAB is a commonly used surfactant that has previously been used as a stabiliser and structure directing agent during metal nanoparticle synthesis.[40] The CTAB stabilised PdAu/$TiO_2$ catalyst performed very poorly in comparison to either the stabiliser free or polymer stabilised catalyst, yielded a catalyst with an activity of only 6 mol$H_2O_2$/h/$kg_{cat}$.

### *3.2.1.6. The Effect of Varying Total Metal Loading*

Catalysts were prepared with a constant Pd:Au ratio of 1 and varied total metal loading in order to assess the relative dispersion of the metals. The hydrogen peroxide synthesis activities of the catalysts of variable total metal loading are presented in Figure 3-6.

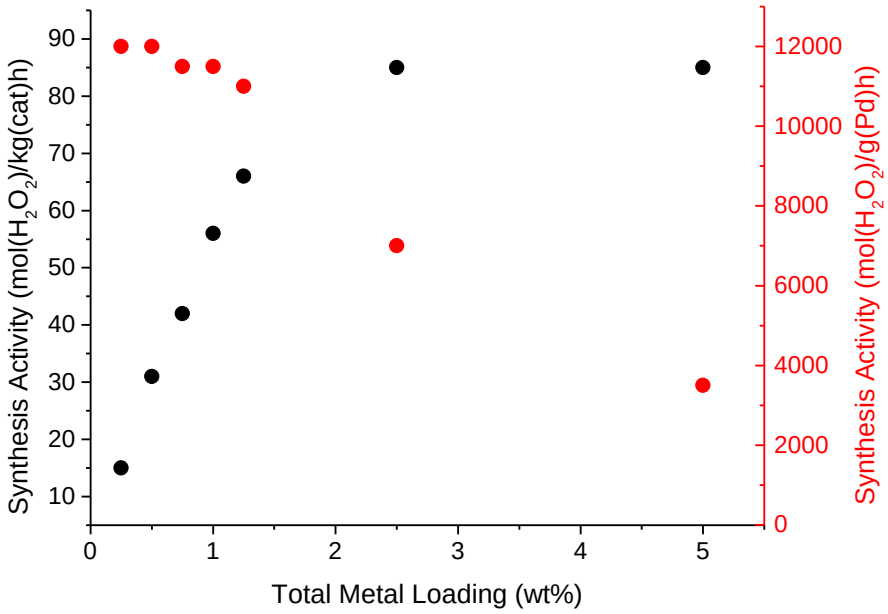


**Figure 3-6 - Hydrogen peroxide synthesis activity of $TiO_2$ supported PdAu catalysts of variable total metal loading, 1:1 Pd:Au mass ratio**

**Reaction Conditions – 5 % $H_2/CO_2$ (2.9 MPa) and 25 % $O_2/CO_2$ (1.1 MPa), 8.5 g solvent (2.9 g $H_2O$, 5.6 g MeOH) 0.01 g catalyst, 2 °C, 1200 rpm, 30 min.**

Increasing the total metal loading from 0.25 to 1 wt% results in the hydrogen peroxide synthesis activity proportionally increasing, and therefore the activity by Pd content remains roughly equal at 11500 mol$H_2O_2$/h/$g_{Pd}$. A further increase to 1.25 wt% results in an increase in activity by catalyst mass to 66 mol$H_2O_2$/h/$kg_{cat}$, but a minor decrease in activity by metal content. This suggests that, at low loadings, the addition of more metal precursors results in

the formation of more nanoparticles, rather than structural changes, such as an increase in particle size or change in particle composition.

Increasing the metal loading further to 2.5 wt% results in an increase in activity by catalyst mass to 85 mol$H_2O_2$/h/$kg_{cat}$; however, this increase was disproportional to the metal content and, as a result, synthesis activity by metal content decreases. Interestingly, further addition of metal resulted in no change in synthesis activity, up to a total loading of 5 wt%. Increased metal precursor concentration during catalyst preparation could result in the formation of larger particles, which have reduced surface area-volume ratio. As a result, more metal forms the catalytically inactive core of ever larger particles at higher loadings. It is of particular importance in precious metal catalysis to utilise the metal as efficiently as possible; increasing metal loading above 1.25 wt% results in decreased activity when normalised for palladium content, and therefore the catalysts are less efficient.

### *3.2.1.7. Catalyst Reuse*

Catalyst reusability is a critical parameter in precious metal catalysis. In hydrogen peroxide synthesis, deactivation of the catalyst is typically associated with metal leaching, and the resultant homogeneous species are often highly active for hydrogen peroxide decomposition.[41] To investigate catalyst stability, 0.5 wt% Pd 0.5 wt% Au/$TiO_2$ was recovered after reaction and subjected to further catalytic testing. Figure 3-7 illustrates the synthesis activity of the catalyst over four consecutive reactions.

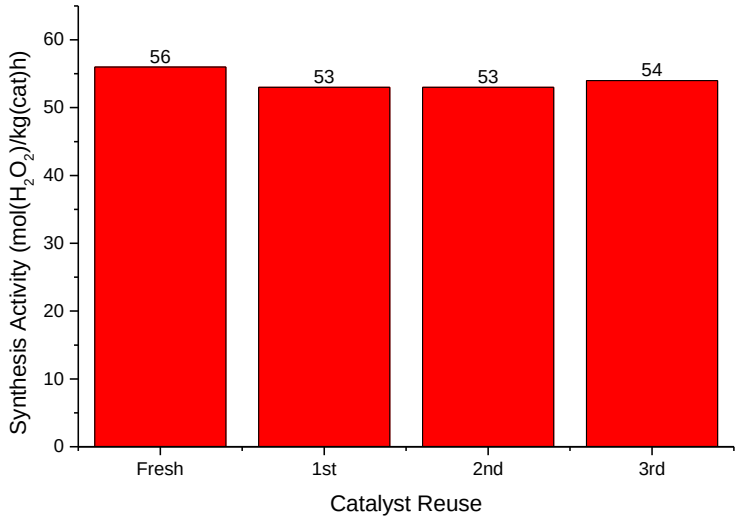


**Figure 3-7 - Hydrogen peroxide synthesis activity of 0.5 wt% Pd 0.5 wt% Au/$TiO_2$ over four consecutive reactions**

**Reaction Conditions – 5 % $H_2/CO_2$ (2.9 MPa) and 25 % $O_2/CO_2$ (1.1 MPa), 8.5 g solvent (2.9 g $H_2O$, 5.6 g MeOH) 0.01 g catalyst, 2 °C, 1200 rpm, 30 min.**

The activity of the catalyst decreases negligibly across the four reactions, suggesting that the catalyst is stable as prepared. Typically, prepared catalysts require heat treatment to afford stability, which introduces further complexity and cost in catalyst preparation. Lopez-Sanchez *et al.* found that, in the case of PdAu catalysts prepared by sol immobilisation, extensive heat treatment slowed catalyst deactivation but a catalytic steady state could not be reached over multiple catalyst reuses.[42] Likewise, heat treatment regimes are prerequisite in the formation of stable catalysts by wet impregnation at considerably higher temperatures than those used during solvothermal catalyst preparation.[5]

### *3.2.1.8. Catalyst Reproducibility*

To better understand the reliability of microwave assisted solvothermal catalyst preparation, a selection of catalysts was prepared in duplicate and their hydrogen peroxide hydrogenation and synthesis activity evaluated. Given the effect of solvent on catalyst activity shown in Section 3.2.1.4, catalyst batches were prepared using freshly sourced solvent and metal precursors, to eliminate any variation due to the presence of impurities. Likewise, catalysts containing low, intermediate and high Pd loadings were prepared to ensure that the reproducibility of the protocol is consistent across various compositions. The hydrogen peroxide synthesis and hydrogenation activities of the catalysts are presented in Table 3-2.

**Table 3-2 - Hydrogen peroxide synthesis and hydrogenation activities of three batches of 0.5 wt% Pd 0.5 wt% Au/$TiO_2$ prepared by microwave assisted solvothermal preparation. (*) Catalyst prepared by Dr J. Edwards under identical conditions in February 2015.**

| Catalyst Batch | Catalyst Loading | Productivity (mol/kg(cat)hr) | Hydrogenation (mol/kg(cat)hr) |
|---|---|---|---|
| 1 | 0.2 wt% Pd 0.8wt% Au | 46 | 101 |
| 2 | 0.2 wt% Pd 0.8 wt% Au | 46 | 95 |
| 1 | 0.5 wt% Pd 0.5 wt% Au | 56 | 130 |
| 2 | 0.5 wt% Pd 0.5 wt% Au | 53 | 150 |
| 3* | 0.5 wt% Pd 0.5 wt% Au | 58 | 120 |
| 1 | 0.8 wt% Pd 0.2 wt% Au | 80 | 165 |
| 2 | 0.8 wt% Pd 0.2 wt% Au | 77 | 170 |

**Reaction Conditions – Hydrogen peroxide synthesis: 5 % $H_2/CO_2$ (2.9 MPa) and 25 % $O_2/CO_2$ (1.1 MPa), 8.5 g solvent (2.9 g $H_2O$, 5.6 g MeOH) 0.01 g catalyst, 2 °C, 1200 rpm, 30 min. Hydrogen peroxide hydrogenation: 5% $H_2/CO_2$ (2.9 MPa), 8.5 g solvent (2.22 g $H_2O$, 5.6 g MeOH and 0.68 g 50 wt% $H_2O_2$), 0.01 g catalyst, 2 °C, 1200 rpm, 30 min.**

The two batches of the Pd lean catalyst 0.2 wt% Pd 0.8 wt% $Au/TiO_2$ are consistently active for direct synthesis, with activities of 46 mol$H_2O_2$/h/$kg_{cat}$. Similarly, the hydrogenation activities of the catalysts are consistent, with hydrogenation activity varying by less than 6 % between batches. The analogous 0.5 wt% Pd 0.5 wt% $Au/TiO_2$ catalyst has a variation of 5 mol$H_2O_2$/h/$kg_{cat}$ with respect to hydrogen peroxide synthesis activity and 30 mol$H_2O_2$/h/$kg_{cat}$ for hydrogenation activity. Whilst this variation in hydrogenation activity corresponds to a range of around 20 % in hydrogenation activity, this variation may in part be attributed to the error associated with the determination of hydrogen peroxide concentration by titration, which scales with decreasing hydrogenation activity. A 0.5 wt% Pd 0.5 wt% $Au/TiO_2$ catalyst prepared by Dr J. Edwards was also tested for comparison. This catalyst was prepared under identical conditions, albeit in a different laboratory, several years prior to the preparation of the catalysts reported in this thesis. The activity of 0.5 wt% Pd 0.5 wt% Au catalyst is comparable to the activity prepared by the author of this thesis, suggesting that the preparation procedure tolerates experimental factors such as the use of differing microwave reactors and the sourcing of reagents. The hydrogen peroxide synthesis and hydrogenation activity of the freshly prepared and aged 0.5 wt% Pd 0.5 wt% $Au/TiO_2$ are comparable, indicating that the catalyst is stable for many years at ambient conditions, and can be used after extensive periods of storage without any reactivation treatment.

The Pd rich catalyst 0.8 wt% Pd 0.2 wt% $Au/TiO_2$ was also prepared in duplicate, with the two batches varying in hydrogen peroxide synthesis and hydrogenation activities minimally, 4 % in the former and 3 % in the latter.

#### *3.2.1.9. Catalyst Support*

Alternative catalyst supports were also briefly explored for catalysts prepared by microwave assisted solvothermal synthesis. 0.5 wt% Pd 0.5 wt% Au catalysts were prepared using ethylene glycol in the presence of three supports, P25 $TiO_2$, commercial XC72R carbon and graphene nanoplatelets. The hydrogen peroxide synthesis activity and BET surface area of the catalysts are presented in Figure 3-8. As a one pot preparation method, the thermal decomposition of the metal precursors occurs in the presence of the support material. Therefore, the surface area of the material could be considered an important factor in

determining the particle size distribution/metal dispersion of the final catalyst, which will influence catalyst activity.

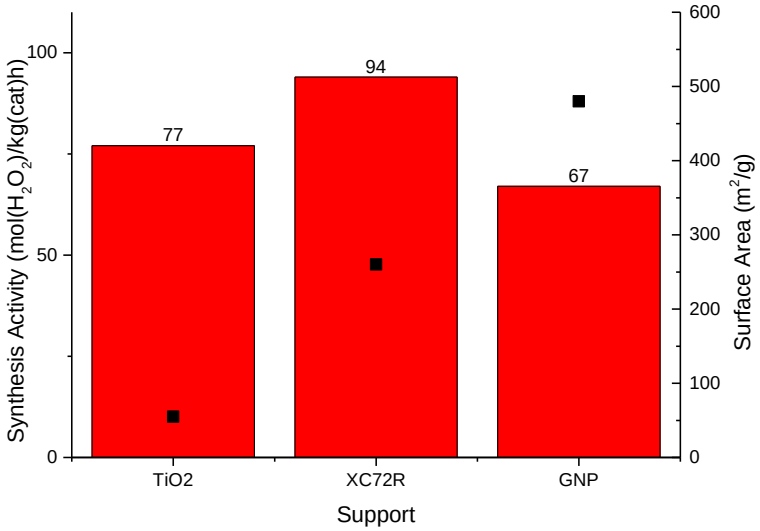


**Figure 3-8 - Hydrogen peroxide synthesis activity (left) and catalyst BET surface area (right) of 0.5 wt% Pd 0.5 wt% Au catalysts**

**Reaction Conditions – 5 % $H_2/CO_2$ (2.9 MPa) and 25 % $O_2/CO_2$ (1.1 MPa), 8.5 g solvent (2.9 g $H_2O$, 5.6 g MeOH) 0.01 g catalyst, 2 °C, 1200 rpm, 30 min.**

The XC72R supported PdAu catalyst is the most active catalyst (94 mol$H_2O_2$/h/$kg_{cat}$). The graphene nanoplatelet catalyst was the least active, with an activity of 67 mol$H_2O_2$/h/$kg_{cat}$. Figure 3-8 shows the relationship between catalyst activity and support surface area, illustrating that the activity of these catalysts is independent of support surface area. The specific surface area of the GNP supported catalyst is nearly an order of magnitude greater than that of the titania supported catalyst (55 and 480 $m^2$/g, respectively) and yet the former exhibits poorer synthesis activity. Likewise, the surface area of the XC72R supported catalyst was roughly half that of the GNP supported analogue, at 260 $m^2$/g, yet the former is 40 % more active for hydrogen peroxide synthesis than the latter . The variation in activity of the catalysts supported on different materials suggests that the surface area of the support is not the dominant factor in determining the activity of catalysts prepared using the microwave assisted polyol method.

*3.2.1.10.STEM-HAADF*

A number of catalysts were interrogated by high angle angular dark field scanning transmission electron microscopy (STEM-HAADF) in order to investigate the microstructure of the catalyst. STEM has previously been utilised to identify bimetallic nanoparticle structure, both alloyed and core-shell materials. High angle angular dark field (HAADF) detectors provide atomic weight contrast during imaging and therefore Au, Pd and Ti are easily distinguished by their varying intensity.[11,43] Representative STEM-HAADF images of the monometallic 1 wt% $Pd/TiO_2$ and 0.5 wt% Pd 0.5 wt% $Au/TiO_2$ catalysts are presented in Figure 3-9. Images (a) and (c) show that both the mono- and bimetallic catalysts contain particles that are approximately 10-20 nm in diameter.

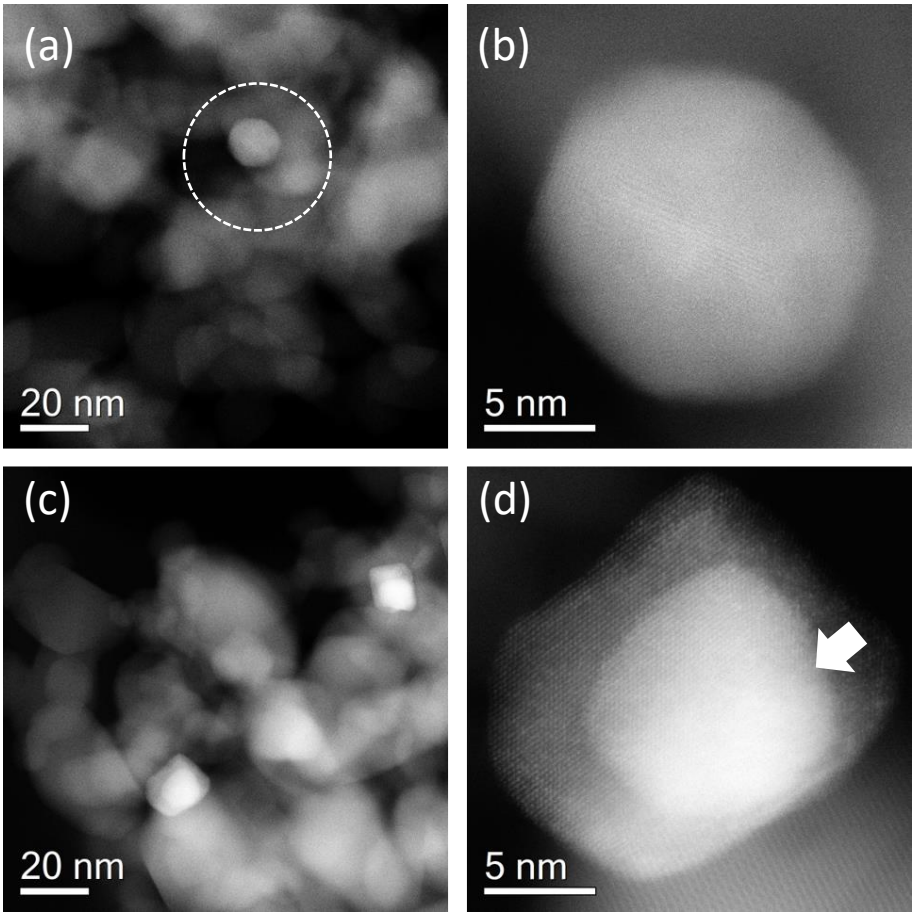


**Figure 3-9 - STEM-HAADF images of 1 wt% $Pd/TiO_2$ (a,b) and 0.5 wt% Pd 0.5 wt% $Au/TiO_2$ (c,d). The circled feature in (a) is a metallic particle, as distinguished from the $TiO_2$ support by their contrast. The core-shell structure of the PdAu catalyst is highlighted in (d).[44]**

Owing to the relatively low loading and large particles observed, determining a statistically relevant particle size distribution was not possible. The $Pd/TiO_2$ and $PdAu/TiO_2$ catalysts shown in Figure 3-9 contain particles larger than those observed in catalysts prepared by

other commonly used preparation methods. For instance, Kiely and co-workers previously found that a 0.5 wt% Pd 0.5 wt% $Au/TiO_2$ catalyst prepared by sol immobilisation had an average particle size of 3.5 nm, which rose to 7.1 nm upon heat treatment.[11] Curiously, the hydrogen synthesis activity of the sol immobilisation catalyst was considerably lower than the analogous solvothermally prepared catalyst presented in this work, 25 vs 56 $molH_2O_2/h/kg_{cat}$. Likewise, the authors reported that the hydrogen peroxide hydrogenation activity of the sol immobilisation catalyst was considerably higher than the analogous catalyst presented in this work, 371 versus 130 $molH_2O_2/h/kg_{cat}$, indicating that sol immobilisation catalyst is considerably less selective. This is contrary to previously reported work by Tian *et al.*, who observed that, for monometallic Pd catalysts, selectivity towards hydrogen peroxide increased with decreasing particle size.[45] The fact that the $PdAu/TiO_2$ catalyst presented in this work exhibits a lower hydrogenation activity than the previously reported sol immobilisation catalyst, despite having larger particles, suggests that factors other than metal surface area are influencing catalyst activity.

Further magnified images of the 1 wt% $Pd/TiO_2$ (b) and 0.5 wt% Pd 0.5 wt% $Au/TiO_2$ (d) catalysts, shown in Figure 3-9, reveal more structural differences between the two. The bimetallic catalyst exhibits a core-shell morphology, with the bright intensity of the core suggesting a palladium shell and gold core structure. Slight variations in the intensity of the signal originating from the shell, however, suggest that that neither the core nor the shell are likely to be perfectly monometallic, as indicated by the arrow in Figure 3-9(d).

The core-shell PdAu catalyst was further investigated by STEM-EDX. Figure 3-10 illustrates the STEM image, Au and Pd EDX maps, and point EDX spectra of the core and shell of a representative particle. The Pd and Au EDX maps (in red and green respectively) agree with the interpretation of the STEM-HAADF image, in that the core is predominantly composed of Au and the shell is Pd. Point spectra of the core (B) and shell (A) in Figure 3-10 show the relative ratios of the Au M and Pd L edges, with the shell being composed primarily of Pd and the core of Au.

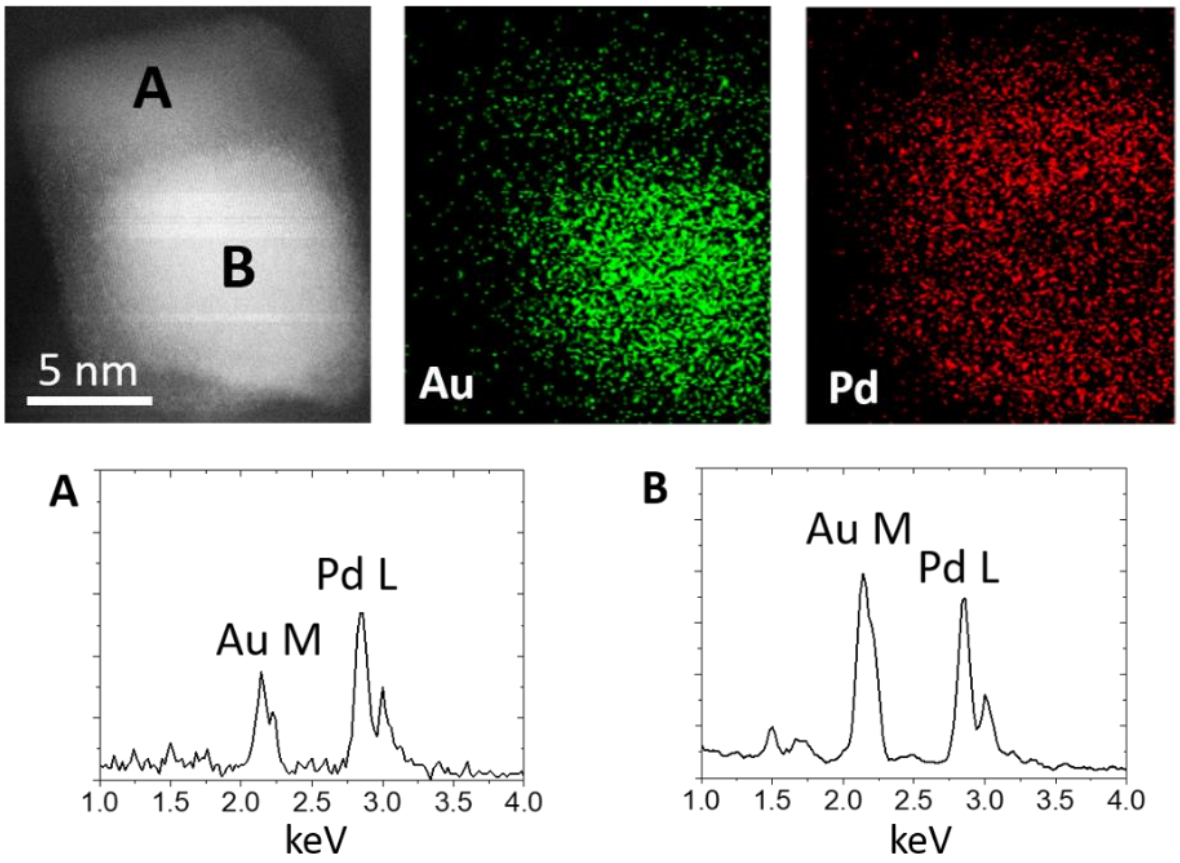


**Figure 3-10 - STEM-HAADF image (top left) of representative core-shell PdAu particle and EDX maps of Pd (red) and Au (green), confirming the bimetallic nature of both the core and shell. The point spectra of positions A and B (below) further confirm the structure of the particle[44]**

The structure of the palladium rich catalyst 0.8 wt% Pd 0.2 wt% Au/$TiO_2$ was also investigated by STEM-HAADF, shown in Figure 3-11. It is observed that Au core-Pd shell structures also form at higher Pd:Au ratios. Further increase in the compositional ratio above 0.5 wt% Pd 0.5 wt% Au results in increasingly thick shells, which are composed of predominantly Pd. The nanoparticle shell is also highly faceted, which is thought to be a consequence of the relatively slow nanoparticle growth kinetics observed in solvothermal preparation methods. Dahal *et al.* previously presented a comparison of conventional and microwave heating regimes, finding that microwave assisted heating considerably altered the kinetics of nanoparticle formation resulting in the controlled formation of faceted nanoparticles.[20]

The structure of the PdAu/$TiO_2$ catalysts as shown by STEM is consistent with the unusual composition-activity relationship found in Figure 3-1. Increasing the palladium content from 0.25 to 0.75 wt% results in minimal increase in hydrogen peroxide synthesis and

hydrogenation activity. As the Pd content of the catalysts increases, the surface composition of the resultant nanoparticles remains roughly constant, with the Pd rich shell becoming increasingly thick in comparison to the Au core. Similarly, 0.85 wt% Pd 0.15 wt% Au/$TiO_2$ and 0.9 wt% Pd 0.1 wt% Au/$TiO_2$ catalysts with even greater Pd content have synthesis and hydrogenation activities comparable to that of the monometallic Pd catalyst. At such high Pd loadings it could be considered that the amount of Au present is insufficient to provide a bimetallic shell, and therefore the activity of the catalyst is essentially dominated by the Pd surface.

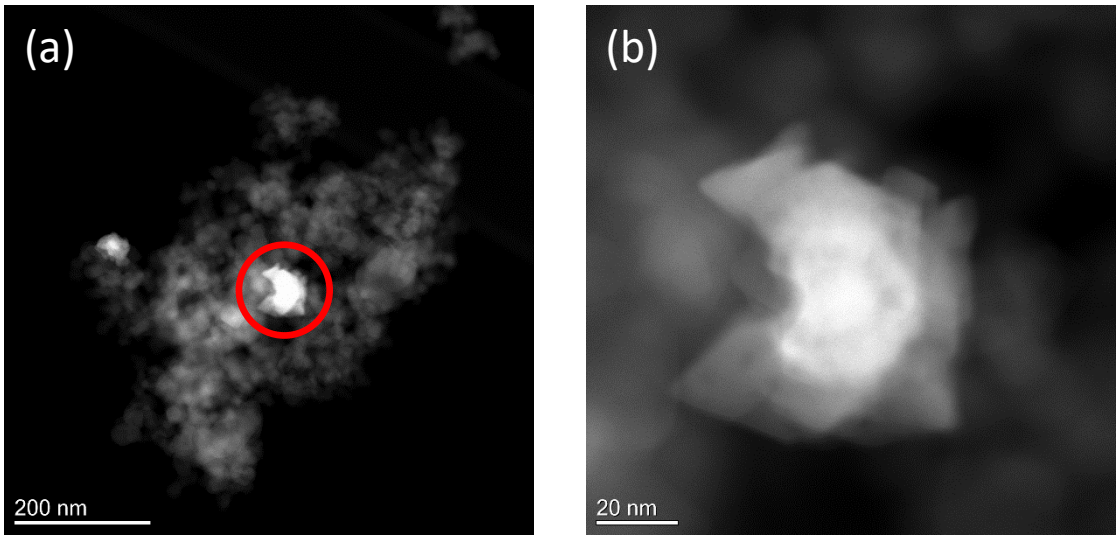


**Figure 3-11 - Representative STEM-HAADF images of 0.8 wt% Pd 0.2 wt% Au/$TiO_2$ catalyst at low (a) and high (b) magnification.**

PdAu core-shell structures have been previously observed in catalysts prepared by both sol immobilisation and wet impregnation.[11,46] In the case of wet impregnation, core-shell structures were found for $Al_2O_3$ and $TiO_2$ supported catalysts, and are thought to form during heat treatment as Pd diffuses through the nanoparticle to form surface oxides. For sol immobilisation, the addition of a reductant to Pd and Au precursors results in the formation of homogeneously alloyed nanoparticles. Sequential addition and reduction of metal precursors instead results in the formation of Pd core-Au shell or Au shell-Pd core nanoparticles.

The formation of Au core-PdAu shell nanoparticles in the 0.5 wt% Pd 0.5 wt% Au/$TiO_2$ and 0.8 wt% Pd 0.2 wt% Au/$TiO_2$ catalysts in this work are likely a result of the difference in reduction kinetics between the Pd and Au metal precursors, $PdCl_2$ and $HAuCl_4$. The structure of the nanoparticles suggest that the Au precursor reduces more rapidly and that the Pd precursor subsequently crystallises around the already formed Au nanoparticles. The

presence of Au in the shell could indicate that the difference between these rates are relatively minor, but sufficiently large that alloyed nanoparticles do not form. In an extreme case where the rate of Au precursor decomposition is considerably faster than for Pd precursors, one would reasonably expect the two regions to be largely monometallic, but such results have not been observed for these catalysts. The suggested relation between nanoparticle structure and precursor decomposition rates is consistent with previous work by Marzan and co-workers, who found that Au(III) salts reduce readily to Au(I), and subsequently Au(0), in DMF, at temperatures as low as 25°C.[18] A study of the solvothermal preparation of Pd nanoparticles in glycerol has also found that the resultant nanoparticles are of varying morphology and highly anisotropic, an indicator of slower reduction kinetics in comparison to Au.[47]

*3.2.1.11.X-ray Photoelectron Spectroscopy*

The nature of the PdAu bimetallic catalysts was further investigated with interrogation of the 0.2 wt% Pd 0.8 wt% $Au/TiO_2$, 0.5 wt% Pd 0.5 wt% $Au/TiO_2$, 0.8wt% Pd 0.2 wt% $Au/TiO_2$ and 1%$Pd/TiO_2$ materials by X-ray photoelectron spectroscopy, the Pd(3d) and Au(4f) narrow scans presented in Figure 3-12.

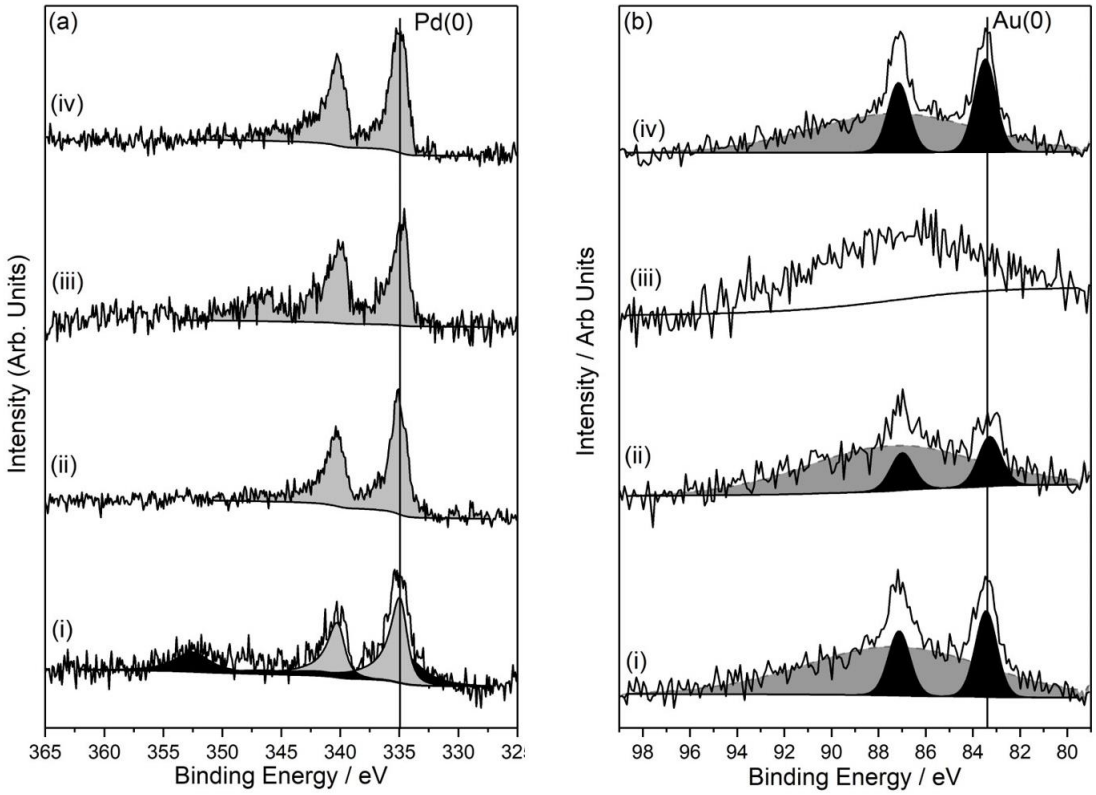


**Figure 3-12 – (a) Pd (3d) spectra of (a)(i)0.2 wt% Pd 0.8 wt% $Au/TiO_2$, (a)(ii)0.5 wt% Pd 0.5 wt% $Au/TiO_2$ , (a)(iii)0.8 wt% Pd 0.2 wt% $Au/TiO_2$and (a)(iv)1 wt% $Pd/TiO_2$. (b) Au(4f) spectra of (b)(i)0.2 wt% Pd 0.8 wt% $Au/TiO_2$, (b)(ii)0.5 wt% Pd 0.5 wt% $Au/TiO_2$, (b)(iii)0.8 wt% Pd 0.2 wt% $Au/TiO_2$ and (b)(iv)1 wt% $Pd/TiO_2$**

In all cases, the binding energies of Au(4f7/2) and Pd(3d5/2) were observed to be 83.4 and 334.9 eV, respectively. These energies are consistent with Au(0) and Pd(0) and therefore confirm that the metal precursors are decomposed entirely into metallic nanoparticles under the given preparation conditions, with no observed oxidation. The Au(0) peak (83.4 eV) is lower than the previously reported binding energy of Au(0) foil of 84.0 eV.[48] A number of factors are likely responsible for this shift. Radnik *et al.* have previously investigated metal oxide supported Au catalysts prepared by various methods and subjected to a range of heat treatment regimes.[49] They found that the choice of support resulted in shifting of the Au(0) binding energy by as much as 1.4eV. The variation in binding energy is attributed to electron transfer between the metal and support, or the presence of low coordination Au species.

Reduced $Au/TiO_2$ catalysts were found to have a binding energy of 83.0-83.4eV depending on preparation method, which aligns with the energy reported in this work. A similar disparity is observed between the reference and actual Pd(0) peak positions. Palladium film has a binding energy of 335.0 eV, versus 334.9 eV observed here. Again the binding energy depression is a consequence of metal-support interaction consistent with previous work on supported Pd catalysts.[50]

High resolution scans of the Pd(3d) and Au(4f) regions are presented in Figure 3-12. The Au(4f) signal intensity decreases with increasing Pd content, consistent with the core-shell structure observed by STEM. XPS is a surface technique, with the depth of material sampled dependent upon the inelastic mean free path (IMFP) of the electrons. The IMFP of an electron varies with energy and is therefore different for Pd(3d) and Au(4f) electrons. In both cases the IMFP is between 4 and 5 nm, and as a result the Au signal features contributions of both the core and shell. The PdAu composition of the shell therefore cannot be determined using XPS, as the nanoparticle shell is not sufficiently thick for the signal to originate from the shell alone.

Using the relative intensity of the Pd(3d) and Au(4f) peaks, the relative surface concentration of Pd and Au were determined presented in Table 3-3. Even when accounting for the contribution of Au core, the Pd/Au surface ratio increases disproportionally upon the further incorporation of Pd into the catalyst which further strengthens the agreement between microscopy and XPS of the Pd rich nature of the nanoparticle shell.

**Table 3-3 - Surface elemental atomic concentrations (at%) of Pd, Au, Ti, O and C for 1 wt% $PdAu/TiO_2$ catalysts of varying composition. n/d – not determinable**

| Catalyst | XPS derived concentration at% | | | | | Pd/Au ratio (XPS) |
|---|---|---|---|---|---|---|
| | Pd | Au | Ti | O | C | |
| 0.2 wt% Pd 0.8 wt% $Au/TiO_2$ | 0.12 | 0.05 | 28.7 | 68.2 | 2.9 | 2.4 |
| 0.5 wt% Pd 0.5 wt% $Au/TiO_2$ | 0.21 | 0.03 | 29.3 | 67.4 | 3.1 | 7 |
| 0.8 wt% Pd 0.2 wt% $Au/TiO_2$ | 0.14 | n/d | 28.8 | 67.0 | 4.0 | n/d |

*3.2.1.12.MP-AES*

The bulk composition of the $PdAu/TiO_2$ catalysts was also determined to ensure that the observed surface Pd enrichment was not a consequence of improper catalyst preparation. The catalysts were digested in aqua regia and the supernatant liquor analysed by microwave plasma atomic emission spectroscopy (MP-AES). The theoretical and experimentally determined catalyst metal loadings are shown in Table 3-4 - Theoretical and experimental

catalyst Pd and Au loadings determined by MP-AES. The actual catalyst loadings are in good agreement with the specific Au and Pd loadings, within 5 % of the target loadings. Likewise, the total metal loading is consistent and deviates from the target loading by 6 % at most.

**Table 3-4 - Theoretical and experimental catalyst Pd and Au loadings determined by MP-AES**

| Au : Pd ratio | Theoretical loading | | Experimental loading | | |
|---|---|---|---|---|---|
| | Au (wt%) | Pd (wt%) | Au (wt%) | Pd (wt%) | Total Loading (wt%) |
| 4 : 1 | 0.8 | 0.2 | 0.77% | 0.20% | 0.97% |
| 3 : 1 | 0.75 | 0.25 | 0.74% | 0.25% | 0.99% |
| 2 : 1 | 0.66 | 0.33 | 0.69% | 0.37% | 1.06% |
| 1 : 1 | 0.5 | 0.5 | 0.51% | 0.49% | 1.00% |
| 1 : 2 | 0.33 | 0.66 | 0.31% | 0.63% | 0.94% |
| 1 : 3 | 0.25 | 0.75 | 0.27% | 0.74% | 1.01% |
| 1 : 4 | 0.2 | 0.8 | 0.18% | 0.77% | 0.95% |

### *3.2.2. Exploration of Alternative Secondary Metals for Hydrogen Peroxide Synthesis*

Given the high cost of Au and Pd, it is of great interest to replace either element in preparing catalysts active for the direct synthesis of hydrogen peroxide. Critical to this is maintaining high selectivity, such that the performance of any new bimetallic catalyst is superior to the monometallic Pd analogue. Recent work shows that Au can be effectively replaced with several elements to yield highly active catalysts for hydrogen peroxide synthesis. For instance, Hutchings and co-workers found that $PdSn/TiO_2$ catalysts prepared by co-impregnation exhibit favourable characteristics for direct synthesis, most notably selectivity in excess of 95 %.[51] The activity of 3 wt% Pd 2 wt% $Sn/TiO_2$ was found to be comparable to the previously reported 2.5 wt% Pd 2.5 wt% $Au/TiO_2$, 61 versus 64 $molH_2O_2/h/kg_{cat}$. The activity of these PdSn catalysts is however significantly lower than PdAu catalysts prepared by sol immobilisation, reported elsewhere.[28] More recently, Li *et al.* investigated $PdSn/TiO_2$ catalysts prepared by a conventionally heated solvothermal method.[52] The formed nanoparticles consist of hollow spheres of differing composition based upon the initial Pd:Sn ratio. Immobilisation of these nanocrystals on metal oxide support materials yielded a $PdSn/TiO_2$ catalyst with synthesis activity of 82 $molH_2O_2/h/kg_{cat}$. The catalyst however exhibited very poor selectivity, with hydrogen peroxide hydrogenation activity in excess of 2000 $molH_2O_2/h/kg_{cat}$.

Based on this data, work was undertaken to investigate the effect of incorporating different secondary metals into the microwave-assisted solvothermal catalyst preparation, and their effects on hydrogen peroxide synthesis and hydrogenation activity were then considered. 0.5 wt% Pd 0.5 wt% $X/TiO_2$ catalysts, where X is a second metal, were prepared by solvothermal reduction of the requisite precursors, using ethylene glycol, in the presence of P25 titania. The hydrogen peroxide synthesis activities of the catalysts are shown in Figure 3-13.

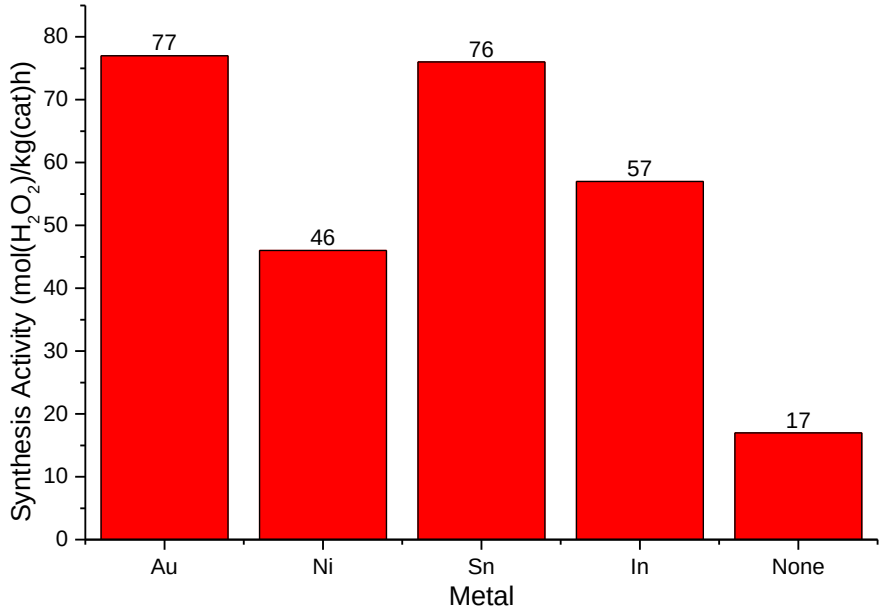


**Figure 3-13 - Hydrogen peroxide synthesis activity of 0.5 wt% Pd 0.5 wt% X/$TiO_2$ catalysts prepared by microwave-assisted solvothermal synthesis, X = Au, Ni, Sn, In**

**Reaction Conditions – 5 % $H_2/CO_2$ (2.9 MPa) and 25 % $O_2/CO_2$ (1.1 MPa), 8.5 g solvent (2.9 g $H_2O$, 5.6 g MeOH) 0.01 g catalyst, 2 °C, 1200 rpm, 30 min.**

0.5 wt% Pd 0.5 wt% Au/$TiO_2$ is the most active catalyst, at 77 mol$H_2O_2$/h/$kg_{cat}$. The incorporation of Ni, Sn or In is however favourable in comparison to the monometallic 0.5 wt% Pd/$TiO_2$ catalyst, which has a synthesis activity of 17 mol$H_2O_2$/h/$kg_{cat}$. In agreement with previous work on PdSn/$TiO_2$ catalysts prepared by wet impregnation, the solvothermally prepared PdSn/$TiO_2$ catalyst is comparable to that of the PdAu analogue presented in Figure 3-4, with an activity of 76 mol$H_2O_2$/h/$kg_{cat}$.

For comparison, titania supported 0.5 wt% monometallic catalysts of the selected secondary metals were also prepared. The hydrogen peroxide synthesis activities of these catalysts are presented in Table 3-5. 0.5 wt% Au/$TiO_2$ is the only active monometallic catalyst, consistent with previous reports that monometallic Au catalysts are active for direct synthesis, although considerably less so than palladium.[53]

**Table 3-5 - Hydrogen peroxide synthesis activity of monometallic 0.5 wt% catalysts supported on titania**

| Metal | Productivity (mol/kg(**cat**)hr) |
|---|---|
| Au | 2 |
| Ni | 0 |
| Sn | 0 |
| In | 0 |

**Reaction Conditions – 5 % $H_2/CO_2$ (2.9 MPa) and 25 % $O_2/CO_2$ (1.1 MPa), 8.5 g solvent (2.9 g $H_2O$, 5.6 g MeOH) 0.01 g catalyst, 2 °C, 1200 rpm, 30 min.**

Table 3-6 illustrates the current market price of the secondary metals used in this study. Considering the similar catalytic performance of the PdAu and PdSn bimetallic catalysts for the direct synthesis of hydrogen peroxide, it follows that the replacement of Au with Sn is an economically viable improvement, with Sn costing 0.05 % of the price of Au on a mass basis.

**Table 3-6 - Table of Metal Spot Prices, Correct As Of 07/2018 [54]**

| **Metal** | Price ($/kg) |
|---|---|
| Au | $40000 |
| Ni | $14 |
| Sn | $20 |
| In | $365 |

### *3.2.3. SnPd Bimetallic Catalysts for Hydrogen Peroxide Synthesis*

Given the high activity of 0.5 wt% Pd 0.5 wt% $Sn/TiO_2$ prepared by solvothermal synthesis, further work was undertaken to optimise the catalyst with a view to maximising activity.

#### *3.2.3.1. The Effect of Catalyst Composition on Hydrogen Peroxide Synthesis Activity*

Following the evaluation of differing secondary metals (X) for the PdX bimetallic catalysts, a series of $PdSn/TiO_2$ catalysts were prepared with varying Pd/Sn ratios to determine the effect of compositional variation on activity. As seen in Figure 3-14, increased Pd content results in increased activity, up to a maximum of 77 $molH_2O_2/h/kg_{cat}$ for 0.5 wt% Pd 0.5 wt% $Sn/TiO_2$. Further increase in Pd content results in a decrease in hydrogen peroxide synthesis activity, presumably accompanied with an increase in hydrogenation activity.

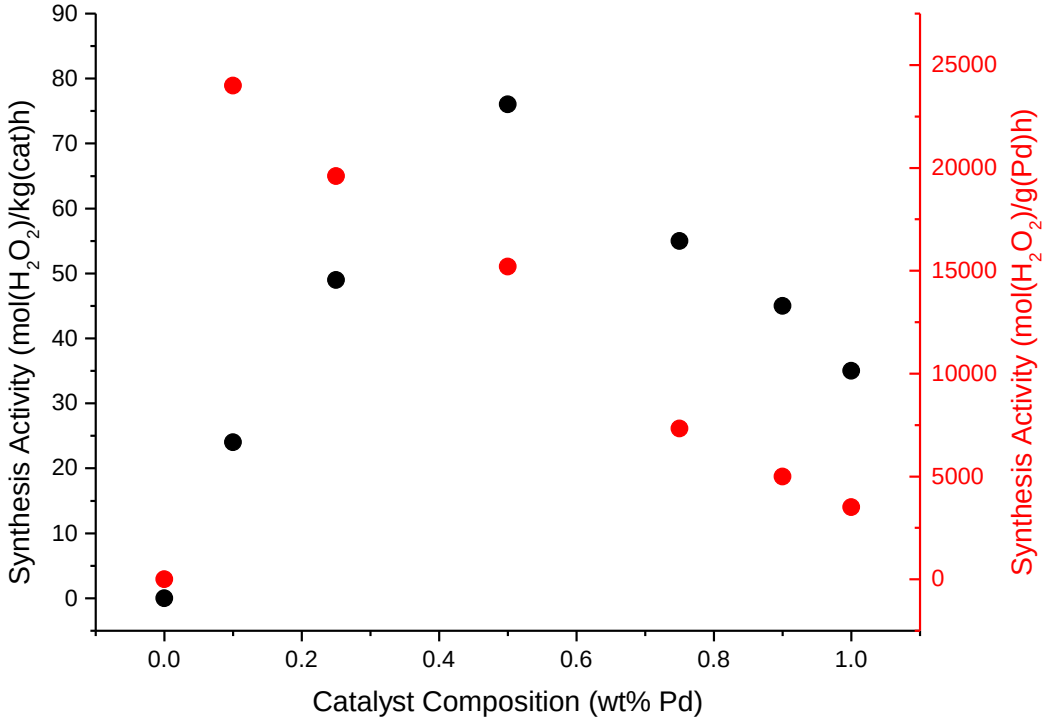


**Figure 3-14 - Hydrogen peroxide synthesis activity of $PdSn/TiO_2$ catalysts of varying composition expressed per g catalyst (●) and per g Pd (●)**

**Reaction Conditions – 5 % $H_2/CO_2$ (2.9 MPa) and 25 % $O_2/CO_2$ (1.1 MPa), 8.5 g solvent (2.9 g $H_2O$, 5.6 g MeOH) 0.01 g catalyst, 2 °C, 1200 rpm, 30 min**

Given that Sn alone is inactive for hydrogen peroxide synthesis, it is useful to also express catalytic activity in terms of catalyst palladium content. In this respect, 0.2 wt% Pd 0.8 wt% $Sn/TiO_2$ is most active, at 24,000 $molH_2O_2/h/g_{Pd}$, due to the combination of high activity and low Pd content. The high activity of the 0.2 wt% Pd 0.8 wt% $Sn/TiO_2$ catalyst suggests it may be possible to improve overall activity by preparing catalysts of higher total metal loading whilst maintaining the palladium lean composition. The activity of these catalysts on a Pd

basis are however significantly higher than $PdSn/TiO_2$ catalysts prepared by co-impregnation by Freakley *et al.*, which required 5wt% total metal loading to produce an activity of 60 $molH_2O_2/h/kg_{cat}$.[51]

*3.2.3.2.The Effect of Varying Preparation Solvent*

Figure 3-4 showed that the choice of solvent played a critical role in determining overall activity for $PdAu/TiO_2$ catalysts prepared by solvothermal synthesis. Given the maximum overall activity of 0.5 wt% Pd 0.5 wt% $Sn/TiO_2$, a series of catalysts were prepared in differing solvents to evaluate the relationship between preparation solvent and catalyst activity, with the results shown in Figure 3-15.

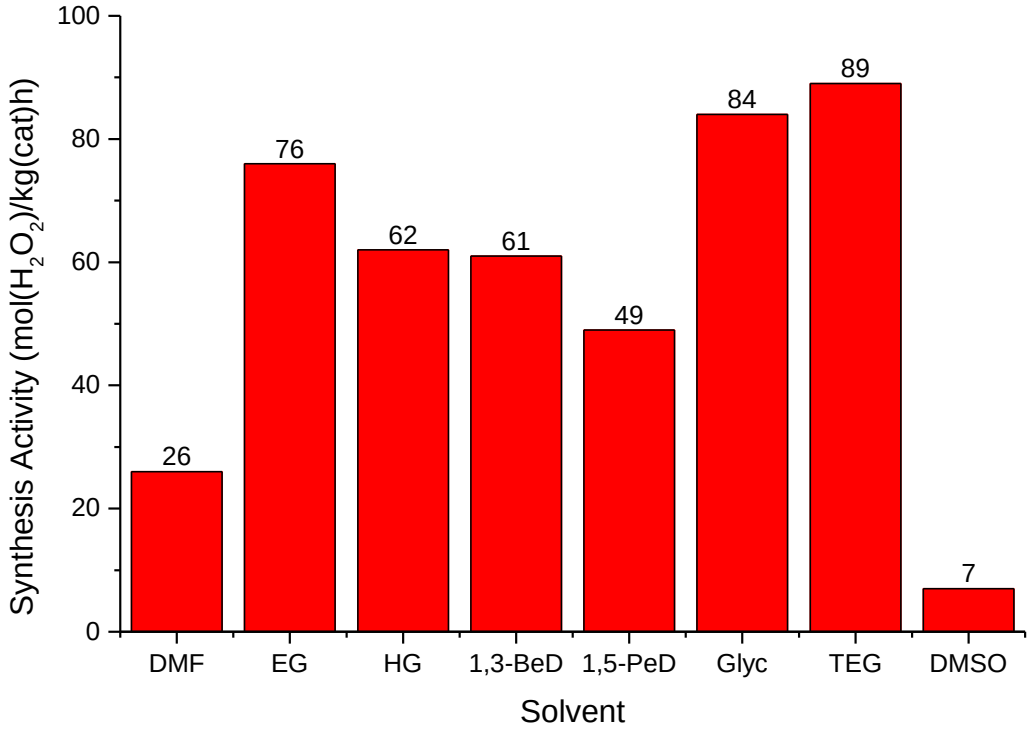


**Figure 3-15 - Hydrogen peroxide synthesis activity of 0.5 wt% Pd 0.5 wt% $Sn/TiO_2$ catalysts prepared by microwave solvothermal synthesis in a range of solvents**

**Reaction Conditions – 5 % $H_2/CO_2$ (2.9 MPa) and 25 % $O_2/CO_2$ (1.1 MPa), 8.5 g solvent (2.9 g $H_2O$, 5.6 g MeOH) 0.01 g catalyst, 2 °C, 1200 rpm, 30 min**

In agreement with the data on $PdAu/TiO_2$ catalysts, preparation of catalysts in secondary or tertiary diols such as HG or 1,3-BeD yields significantly less active catalysts than EG or glycerol. The catalyst prepared in 1,5-PeD is less active than that prepared in EG, 49 vs 76 $molH_2O_2/h/kg_{cat}$, which is likely to be a consequence of different reduction kinetics or solvent-nanoparticle stabilisation effects. Park *et al.* previously investigated the effect of increasing solvent alkyl chain length on the formation of Ag nanoparticles, showing that

increased chain length results in a decrease in nanoparticle diameter, from 144 nm in EG to 30 nm in 1,5-PeD.[55] This was attributed to the increased viscosity of longer chain diols, which results in slower precursor diffusion and therefore increased nucleation of small particles versus the ripening of preformed nanoparticles by diffusive metal precursor.

The interactions between solvent, precursor and nanoparticle are significantly more complex in the case of bimetallic systems. Lim and co-workers previously reported the preparation of PtSn/C by solvothermal synthesis for methanol electrooxidation, highlighting that manipulation of preparation conditions resulted in the formation of either Pt-$SnO_2$/C or PtSn/C alloyed catalysts, with the alloy catalyst considerably more active.[56] An analogous effect may be responsible for the large variation in catalyst activity presented in this work. As seen in Figure 3-15, the PdSn/$TiO_2$ catalyst prepared in DMF performs extremely poorly relative to the catalysts prepared in other solvents, with a synthesis activity of 24 mol$H_2O_2$/h/$kg_{cat}$. The activity of this catalyst is however superior to the monometallic Pd catalyst of identical loading, which exhibited an activity of 17 mol$H_2O_2$/h/$kg_{cat}$. In agreement with the reported PdAu/$TiO_2$ catalysts, the DMSO prepared PdSn catalyst has very low synthesis activity, also likely a consequence of sulfur containing moieties from the preparation procedure poisoning palladium active sites in the prepared catalyst.

#### *3.2.3.3. The Effect of Addition of Stabilisers to Catalyst Preparation*

Stabilisers were also investigated for their effect on catalyst activity. 0.5 wt% Pd 0.5 wt% Sn/$TiO_2$ catalysts were prepared using EG in the presence of common polymeric stabilisers, as well as the surfactant CTAB. The addition of stabiliser negatively impacts catalyst activity, as seen in Figure 3-16. Nonetheless, the activity of the catalysts is still greater than the 0.5 wt% Pd/$TiO_2$ reference catalyst in Section 3.2.1.2, which had an activity of 17 mol$H_2O_2$/h/$kg_{cat}$. The PAA stabilised PdSn/$TiO_2$ catalyst was an exception to this observation, with a low activity of 15 mol$H_2O_2$/h/$kg_{cat}$. The activity of the stabilised catalysts indicates that synergistic activity improvement of Pd and Au is preserved in the presence of stabilisers, but that the addition of stabiliser is largely detrimental to catalyst activity.

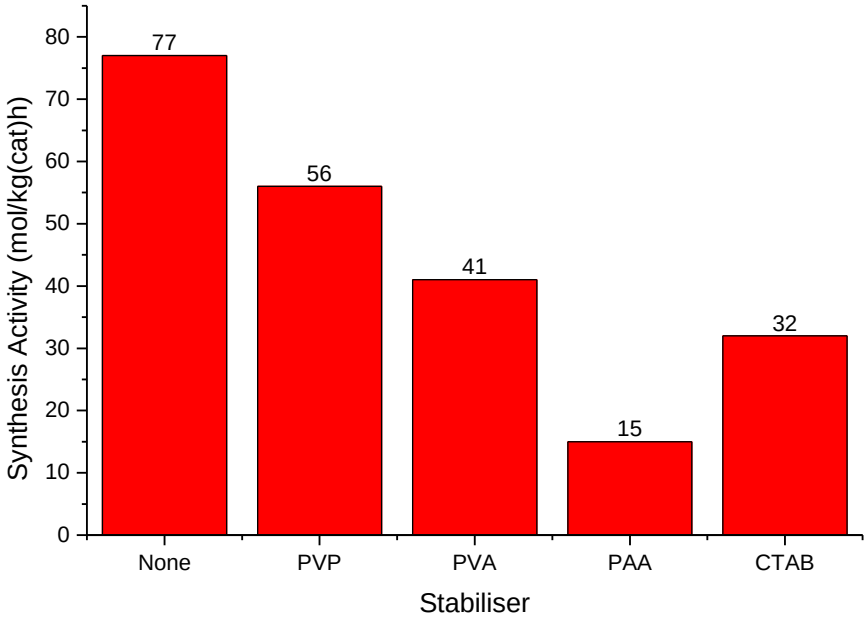


**Figure 3-16 - Hydrogen peroxide synthesis activity of 0.5 wt% Pd 0.5 wt% Sn/$TiO_2$ prepared in the presence of polymeric stabilisers**

**Reaction Conditions – 5 % $H_2/CO_2$ (2.9 MPa) and 25 % $O_2/CO_2$ (1.1 MPa), 8.5 g solvent (2.9 g $H_2O$, 5.6 g MeOH) 0.01 g catalyst, 2 °C, 1200 rpm, 30 min**

Prati and co-workers previously investigated the effect of stabilisers on Au/$TiO_2$ for glycerol oxidation, where they found that stabilisers present during catalyst preparation remain after washing, and the authors attribute coverage of the nanoparticle surface to the activity discrepancy between stabilised and un-stabilised catalyst activity.[57] Lopez-Sanchez *et al.* investigated protocols to remove stabilisers in an effort to improve catalytic activity, finding that refluxing catalysts in organic solvents or water facilitated removal of PVA from the surface of the catalyst, drastically improving activity for benzyl alcohol and CO oxidation.[58] This was preferred to oxidative heat treatment, which removes stabiliser by combustion but also results in nanoparticle agglomeration and therefore reduced catalyst activity. Alternative protocols have been suggested by Kiwi-Minsker and co-workers, who found that ozone treatment of Pd/C catalysts had a similar effect, with the treated catalysts more active for acetylene hydrogenation versus untreated catalysts.[59]

Recently Abis *et al.* thoroughly investigated the preparation of AuPd/$TiO_2$ by sol immobilisation in the absence of stabilisers.[60] The authors found that stabiliser free catalysts were more active for glycerol oxidation than those prepared in the presence of PVP or PVA. The stabiliser free catalyst had a larger average particle diameter, 3.9 nm, compared to 3.0 and 3.2 nm for PVP and PVA stabilised nanoparticles respectively. In this case, increased

active surface availability outweighs the decreased metal surface area and, as a result, the stabiliser free catalyst was most active.

Critically, stabilisers are typically added during preparation to improve nanoparticle stability upon formation. In the case of microwave-assisted solvothermal preparation, the activity disparity between the stabiliser free and stabilised catalyst is such that there is no benefit to using stabilisers during preparation.

*3.2.3.4.SEM-EDX of 0.5 wt% Pd 0.5 wt% Sn/$TiO_2$*

The most active PdSn catalyst, 0.5 wt% Pd 0.5 wt% Sn/$TiO_2$ was further investigated by SEM, with low (a) and high (b) magnification images presented in Figure 3-17.

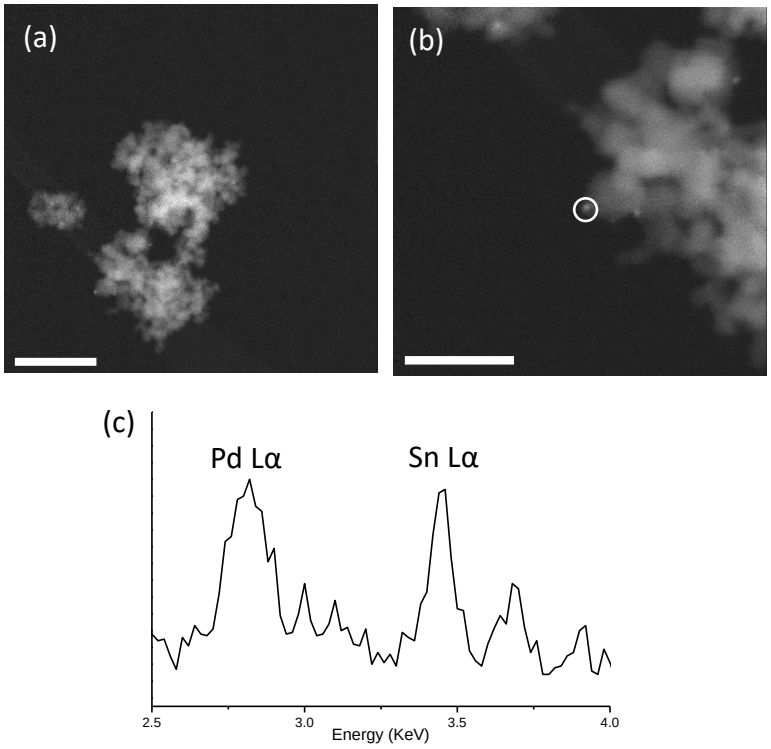


**Figure 3-17 - Low (a) And High (b) magnification SEM-BSE micrographs of 0.5 wt% Pd 0.5 wt% Sn/$TiO_2$. scale bars representative of (a) 200 nm and (b) 100 nm. SEM-EDX spectrum (c) of circled particle from image (b)**

The catalyst contains well dispersed nanoparticles, 5-10 nm in diameter, significantly smaller than the core-shell PdAu catalyst presented in Section 3.2.1.10. EDX of representative PdSn nanoparticles shows the formation of alloyed PdSn nanoparticles. The alloy nanostructure of the 0.5 wt% Pd 0.5 wt% Sn/$TiO_2$ is consistent with the activity of the catalyst in comparison to the 0.5 wt% Pd 0.5 wt% Au/$TiO_2$ prepared using DMF, which exhibits a core-shell structure. Previous work by Tiruvalam *et al.* showed that alloyed bimetallic PdAu/$TiO_2$ catalysts prepared by sol immobilisation are more active than analogous core-shell

catalysts.[11] The exceptional activity of the 0.5 wt% Pd 0.5 wt% Sn/$TiO_2$ catalyst relative to the previously presented PdAu and monometallic Pd catalyst can therefore be considered a combination of the synergistic effect of the addition of Sn to Pd, and the formation of homogenously alloyed nanoparticles, which are more active for hydrogen peroxide synthesis than core-shell structures.

### *3.2.4. PdNi and PdIn Bimetallic Catalysts for Hydrogen Peroxide Synthesis*

In addition to Sn, the work in Section 3.2.2 shows that Ni and In can be considered as alternatives to Au in bimetallic PdX catalysts, as they also yield highly active bimetallic catalysts. Comparison of the PdAu and PdSn composition data presented in Sections 3.2.1.2 and 3.2.3.1 shows that optimum catalyst metal composition is dependent upon the choice of secondary metal. To further maximise catalytic activity, the composition of PdNi and PdIn catalysts are investigated here.

#### *3.2.4.1. The Effect of PdNi Catalyst Composition on Activity*

A series of PdNi/$TiO_2$ catalysts were prepared in EG in order to evaluate the optimal Pd:Ni ratio, with a view to maximising hydrogen peroxide direct synthesis activity. As shown in Figure 3-18 the 0.5 wt% Pd 0.5 wt% Ni/$TiO_2$ sample displays maximum activity of 46 mol$H_2O_2$/h/$kg_{cat}$, with synthesis activity rising sharply upon incorporation of between 0.2 and 0.5wt% Pd, from 25 to 46 mol$H_2O_2$/h/$kg_{cat}$. Further incorporation of Pd has little effect, with the activity of 0.5 wt% Pd 0.5 wt% Ni/$TiO_2$ and 1 wt% Pd/$TiO_2$ differing by less than 20%. This is surprising as previous work on PdAu/$TiO_2$ catalysts for hydrogen peroxide synthesis, by Pritchard *et al.*, found that, after the optimum composition of 0.5 wt% Pd 0.5 wt% Au, further addition of Pd resulted in a sharp decrease in synthesis activity such that a 'volcano' trend was observed.[28] The authors attributed the activity of the Pd rich catalysts to a sharp increase in hydrogen peroxide hydrogenation activity with increasing Pd content, which suggests that the hydrogenation of formed hydrogen peroxide reduces the concentration of hydrogen peroxide and therefore the overall activity falls. In the case of the PdNi/$TiO_2$ catalysts presented in this work, it is unlikely that the variation in hydrogen peroxide synthesis activity is a consequence of increasing hydrogenation activity, due to the minor variations in overall synthesis activity.

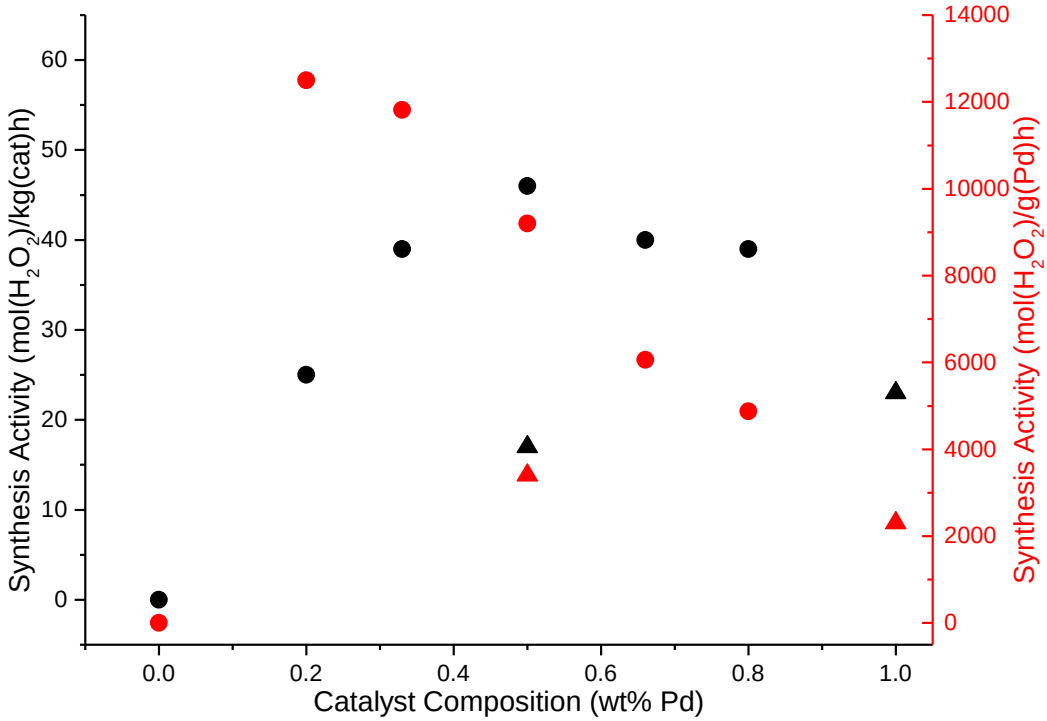


**Figure 3-18 - Hydrogen peroxide synthesis activity of PdNi/$TiO_2$ catalysts expressed as per g catalyst (●) and per g Pd (●). Analogous activity data of Pd/$TiO_2$ displayed as (▲) and (▲).**

**Reaction Conditions – 5 % $H_2/CO_2$ (2.9 MPa) and 25 % $O_2/CO_2$ (1.1 MPa), 8.5 g solvent (2.9 g $H_2O$, 5.6 g MeOH) 0.01 g catalyst, 2 °C, 1200 rpm, 30 min**

It is also useful to consider the activity of the catalysts on a Pd basis, as the monometallic Ni/$TiO_2$ catalyst is inactive for the direct synthesis of hydrogen peroxide. In agreement with the work of Section 3.2.1.2 and 3.2.3.1, the most active catalysts with regards to Pd content is the Ni rich catalyst 0.2 wt% Pd 0.8 wt% Ni/$TiO_2$, which has an activity of 12,500 mol$H_2O_2$/h/$g_{Pd}$. This activity declines with increasing Pd incorporation, to a minimum of 4800 mol$H_2O_2$/h/$g_{Pd}$ for 0.8 wt% Pd 0.2 wt% Ni/$TiO_2$. The low activity of 0.8 wt% Pd 0.2 wt% Ni/$TiO_2$ is still around twice the activity of 1 wt% Pd/$TiO_2$, 2300 mol$H_2O_2$/h/$g_{Pd}$, which suggests that addition of even a small amount of Ni to a Pd catalyst is beneficial for preparing an efficient catalyst.

The synthesis activities of monometallic 0.5 wt% Pd/$TiO_2$ and 1 wt% Pd/$TiO_2$ catalysts are also presented in Figure 3-18. Increased Pd loading from 0.5 wt% to 1 wt% results in a minor increase in synthesis activity from 17 to 23 mol$H_2O_2$/h/$kg_{cat}$, and, as a result, activity by metal mass falls from 3500 to 2300 mol$H_2O_2$/h/$g_{Pd}$. Comparison of the activity of 0.5 wt% Pd/$TiO_2$ and 0.5 wt% Pd 0.5 wt% Ni/$TiO_2$ highlights the synergistic effect observed in the bimetallic catalyst, with activity increasing upon the addition of Ni to 46 versus 17 mol$H_2O_2$/h/$kg_{cat}$ in

the case of the monometallic analogue. Likewise, per Pd content, activity rose from 3500 for the monometallic catalyst to 9200 mol$H_2O_2$/h/$g_{Pd}$ for the Ni containing bimetallic analogue.

*3.2.4.2.The Effect of PdIn Catalyst Composition on Activity*

PdIn/$TiO_2$ catalysts of varying composition were also prepared by microwave-assisted solvothermal synthesis. The relationship between PdIn catalyst composition and hydrogen peroxide synthesis activity is shown in Figure 3-19. Hydrogen peroxide synthesis activity rises steadily from 10 to 58 mol$H_2O_2$/h/$kg_{cat}$ when increasing Pd content from 0.1 wt% Pd 0.9 wt% In to 0.5 wt% Pd 0.5 wt% In. Further increase in Pd content results in a decrease in activity to 33 mol$H_2O_2$/h/$kg_{cat}$.

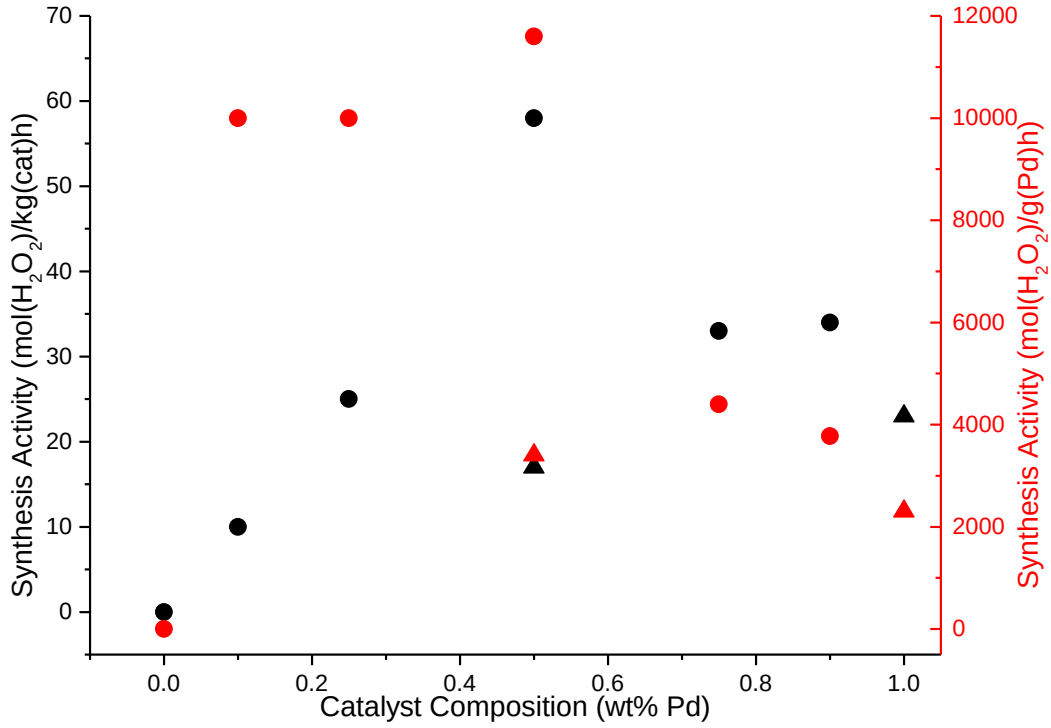


**Figure 3-19 – Hydrogen peroxide synthesis activity of PdIn/$TiO_2$ catalysts expressed as per g catalyst (●) and per g Pd (●). Analogous activity data of Pd/$TiO_2$ displayed as (▲) and (▲).**

**Reaction Conditions – 5 % $H_2/CO_2$ (2.9 MPa) and 25 % $O_2/CO_2$ (1.1 MPa), 8.5 g solvent (2.9 g $H_2O$, 5.6 g MeOH) 0.01 g catalyst, 2 °C, 1200 rpm, 30 min**

Synthesis activity remains roughly constant between 0.75 wt% Pd 0.25 wt% In/$TiO_2$ and 0.9 wt% Pd 0.1 wt% In/$TiO_2$, at 34 mol$H_2O_2$/h/$kg_{cat}$. This is greater than 1 wt% Pd/$TiO_2$, which has a synthesis activity of 23 mol$H_2O_2$/h/$kg_{cat}$. The observed activity trend for Pd rich PdIn catalysts is analogous to that presented in the case of PdAu and PdNi catalysts in Sections 3.2.1.2 and 3.2.4.1, respectively. The addition of a small amount of In to a Pd catalyst results in a disproportionate increase in hydrogen peroxide synthesis activity, with activity by Pd

mass increasing to 3700 mol$H_2O_2$/h/$g_{Pd}$ compared to 2300 mol$H_2O_2$/h/$g_{Pd}$ for the monometallic catalyst. Comparison of 0.5 wt% Pd 0.5 wt% In/$TiO_2$ and 0.5 wt% Pd/$TiO_2$ demonstrates a strong synergistic effect between Pd and In, as activity increases sixfold upon incorporation of In in a 1:1 mass ratio, from 2300 to 11600 mol$H_2O_2$/h/$g_{Pd}$.

*3.2.4.3.SEM of 0.5 wt% Pd 0.5 wt% Ni/$TiO_2$ and 0.5 wt% Pd 0.5 wt% In/$TiO_2$*

The PdNi and PdIn catalysts were interrogated by scanning electron microscopy (SEM) to learn more about catalyst structure and composition. Back-scattered electron (BSE) detection was used to provide atomic weight contrast, allowing for visualisation of the PdNi nanoparticles immobilised on the $TiO_2$ support. SEM-BSE micrographs of 0.5 wt% Pd 0.5 wt% Ni/$TiO_2$ are presented in Figure 3-20. The image of the catalyst contains dispersed particles of varying size, typically 10-100 nm. Previous work for other Pd containing bimetallic catalysts has found that size effects play a critical role in catalyst activity.[61] The PdNi catalysts prepared in this work are inferior to the analogous PdAu, PdSn and PdIn catalysts , consistent with the size variation of the nanoparticles.

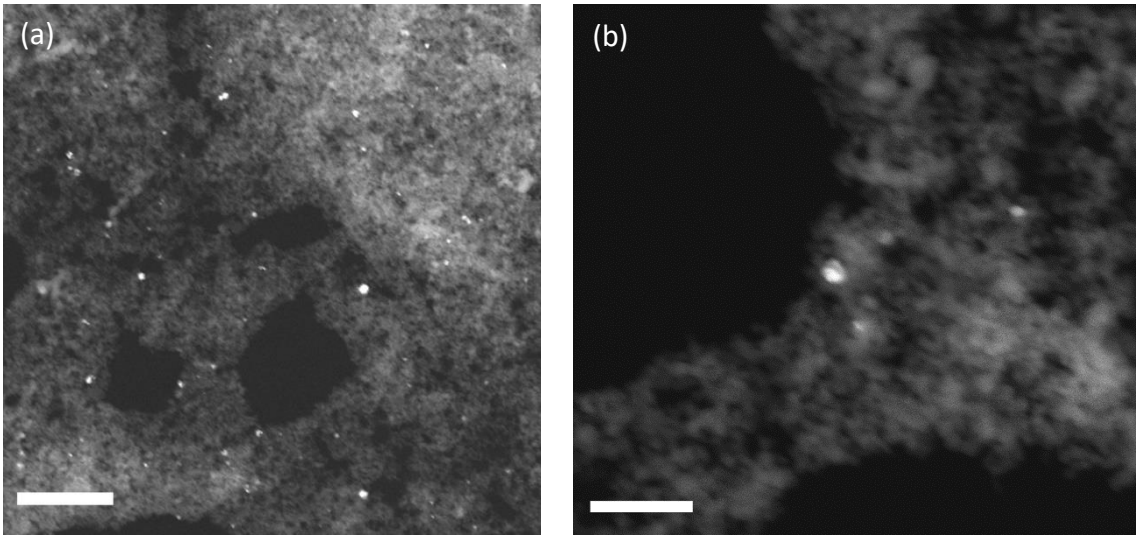


**Figure 3-20 - Low (a) and high (b) magnification SEM-BSE micrographs of 0.5 wt% Pd 0.5 wt% Ni/$TiO_2$. Scale bars representative of (a) 1 µm and (b) 200 nm.**

High and low magnification SEM-BSE images of 0.5%Pd0.5%In/$TiO_2$ are presented in Figure 3-21. In contrast to 0.5 wt% Pd 0.5 wt% Ni/$TiO_2$, the catalyst contains considerably smaller PdIn nanoparticles, <10 nm in diameter, which is reflected in the increased hydrogen peroxide synthesis activity of the catalyst.

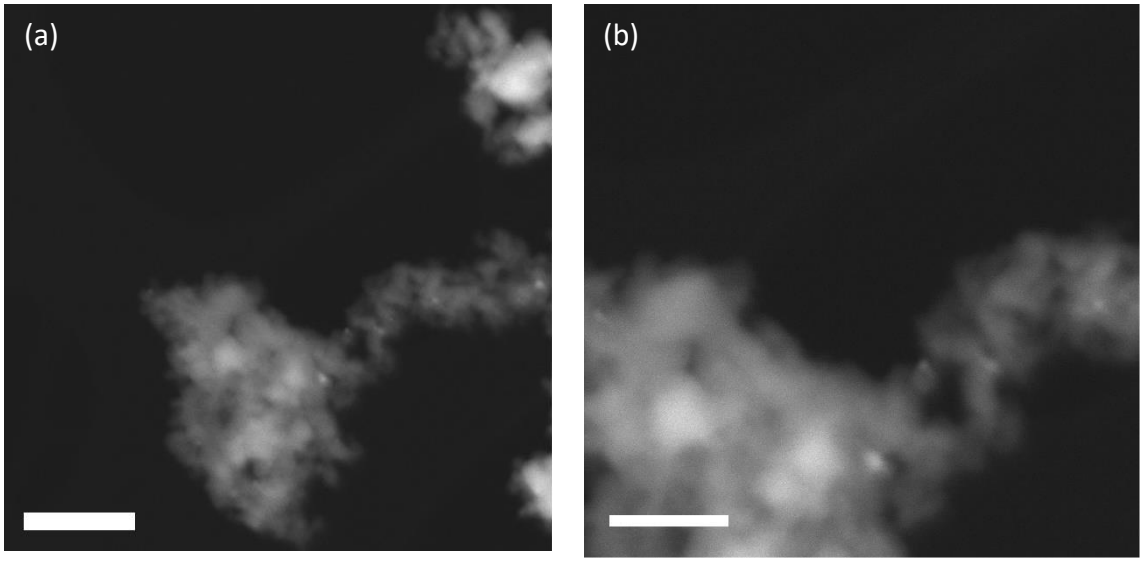


**Figure 3-21 - Low (a) and high (b) magnification SEM-BSE micrographs of 0.5 wt% Pd 0.5 wt% In/$TiO_2$. Scale bars representative of (a) 200 nm and (b) 100 nm.**

### *3.3. Discussion*

Microwave assisted solvothermal catalyst preparation offers several benefits in comparison to techniques previously used to prepare catalysts for hydrogen peroxide synthesis. The most common alternative, wet impregnation, has been explored extensively in preparing active and selective catalysts. The activity of $TiO_2$ supported PdAu catalysts prepared by impregnation by Edwards *et al.* are comparable with those prepared in this work, however the impregnation prepared catalysts contain significantly more active metal.[5] Therefore on a palladium mass basis, PdAu/$TiO_2$ catalysts prepared by solvothermal preparation present a superior alternative. Additionally, the hydrogenation activity of the solvothermally prepared catalysts presented in this work are considerably lower than the analogous impregnation catalysts reported in literature, suggesting that they are more selective towards hydrogen peroxide production.

Stability is also a critical factor in precious metal catalysis. 0.5 wt% Pd0.5 wt% Au/$TiO_2$ prepared by reduction in DMF are stable across four reactions, which is unusual given the lack of a heat treatment regime during preparation. Catalysts prepared by wet impregnation are highly unstable prior to heat treatment, principally deactivating through metal leaching into the reaction solution.[25] Likewise sol immobilisation catalysts are known to be unstable under reaction conditions even when heat treated.[62]

Preparation solvent has a critical effect on catalysts activity, with the formation of metal nanoparticles proceeding via the reduction of metal precursors and associated oxidation of the

solvent. Structure and size of the nanoparticles is therefore highly dependent upon the oxidation kinetics of the solvent. In the case of catalysts prepared in DMF, core-shell nanoparticles were formed featuring a palladium rich shell and gold rich core. This can be attributed to the relative reduction rate of the $PdCl_2$ and $HAuCl_4$ precursors by DMF. Ethylene glycol is a diol that is very commonly used for solvothermal synthesis, and a range of diols were investigated as potential preparation solvents in this work, with primary alcohols yielding more active catalysts than those including secondary or tertiary alcohols. It is thought that this is a consequence of the rate of oxidation of the solvent – primary alcohols are oxidised more readily to aldehydes than secondary alcohols to ketones, which results in slower metal precursor reduction and less active metal nanostructures.

The structure of the solvothermally prepared $PdAu/TiO_2$ catalysts was interrogated by STEM and XPS. The catalysts exhibit an unusual bimetallic core, bimetallic shell structure, with the core and shell being Au and Pd rich respectively. This is consistent with the unusual composition-activity relationship observed, wherein increasingly Pd rich catalysts result in increased activity. PdAu catalysts prepared by other methods are known to result in distinct 'volcano' trends, with the incorporation of more Pd resulting in increased hydrogenation activity and therefore reduced synthesis activity. In contrast, the catalysts in this work have relatively constant hydrogenation activity regardless of Pd content, which can be attributed to the presence of Au in the shell providing the well explored synergistic effects, regardless of compositional variation. STEM analysis of the Pd rich and lean catalysts 0.8 wt% Pd 0.2 wt% $Au/TiO_2$ and 0.2 wt% Pd 0.8 wt% $Au/TiO_2$ shows that the core-shell structure was preserved even at high Pd/Au ratios, and that increasing or decreasing the compositional ratio results in increased shell or core thickness.

The core-shell structure of the $PdAu/TiO_2$ catalysts presented in this work is consistent with previously reported work by Ferrer *et al.* on solvothermally prepared PdAu nanomaterials, who showed that under certain conditions, three layer nanoparticles form, with an alloy core encapsulated in an Au rich PdAu shell, and then further coated in a Pd rich Au shell.[21] Furthermore, significant compositional particle size effects were observed, with segregation only observed in particles larger than 5 nm diameter.

The versatility of solvothermal preparation is also explored in this work. The incorporation of Sn, Ni or In during preparation results in the formation of bimetallic catalysts that are highly active for hydrogen peroxide synthesis, with PdSn catalysts having comparable activity to the

PdAu analogues. The preparation solvent also has a significant effect on activity of these bimetallic catalysts: the TEG prepared 0.5 wt% Pd 0.5 wt% $Sn/TiO_2$ catalyst is more active than any $PdAu/TiO_2$ catalyst (89 $molH_2O_2/h/kg_{cat}$). The activity of this $PdSn/TiO_2$ catalyst is a consequence of varying reduction kinetics, which are dependent on metal, precursor and solvent selection. Huang and co-workers previously reported solvothermally prepared $TiO_2$ supported PdSn catalysts for the direct synthesis of hydrogen peroxide.[52] In their work, the preparation of the catalysts in ethylgene glycol using conventional heating produced hollow PdSn nanospheres, which in turn yielded catalysts similar in activity to those presented in this work. Their catalysts contained considerably more Pd however, and therefore on a Pd basis, the catalysts presented in this work display superior activity.

The PdNi and PdIn bimetallic catalysts are less active than their PdAu or PdSn counterparts, but more active than the monometallic Pd analogue. In both cases, investigation of catalyst composition reveals that maximum catalyst activity exists at 1:1 Pd:Ni/In mass ratio. SEM analysis of the formed nanoparticles found that catalyst microstructure varied significantly between the two compositions: The PdNi catalysts contain particles of varying size, principally 10-100 nm, whereas 0.5 wt% Pd 0.5 wt% $In/TiO_2$ contains nanoparticles exclusively <10 nm in diameter. This observation is consistent with activity data, in which the PdIn catalysts are ~20% more active than the PdNi analogue of a given composition. Comparison of the structure of analogous $PdSn/TiO_2$ and $PdIn/TiO_2$ catalysts by SEM suggests that the synergistic effect between Pd and secondary metal also plays a significant role in determining catalyst activity. 0.5 wt% Pd 0.5 wt% $Sn/TiO_2$ and 0.5 wt% Pd 0.5 wt% $In/TiO_2$ catalysts both contain comparatively small nanoparticles, <10 nm in diameter, and yet the Sn containing catalyst is 30% more active than the In containing counterpart.

### *3.4. Conclusion*

It has been demonstrated that microwave assisted solvothermal methods can be effectively used to prepare supported PdAu, PdSn, PdNi and PdIn catalysts active for the direct synthesis of hydrogen peroxide. A range of catalyst preparation parameters have been investigated including catalyst composition, preparation solvent and the presence of stabilisers. Solvent effects are significant in the formation of active bimetallic catalysts, with the use of high molecular weight polyols and glycerol resulting in improved activity. In comparison, DMSO prepared catalysts performed very poorly, likely a consequence of catalyst poisoning by sulfur containing species.

$TiO_2$ supported PdAu catalysts have been characterised by STEM, XPS and MP-AES. It has been found that the unusual bimetallic core-shell structure is responsible the composition-activity relationship. The activity of the catalysts varied minimally with increasing Pd content, due to the formation of PdAu shells in all catalysts. Variation of the Pd/Au ratio results in varying core diameter and shell thickness, with the composition of the shell remaining roughly constant regardless of overall Pd/Au composition.

PdSn, PdNi and PdIn derived catalysts have also been shown as active for hydrogen peroxide synthesis, demonstrating the versatility of microwave assisted solvothermal catalyst preparation. $PdSn/TiO_2$ catalysts are comparably active to PdAu analogues, and therefore offer a lower-cost greener alternative.

## *3.5. References*

1 N. Dimitratos, A. Villa, D. Wang, F. Porta, D. Su and L. Prati, *J. Catal.*, 2006, **244**, 113–121.
2 B. Katryniok, H. Kimura, E. Skrzyńska, J.-S. Girardon, P. Fongarland, M. Capron, R. Ducoulombier, N. Mimura, S. Paul and F. Dumeignil, *Green Chem.*, 2011, **13**, 1960.
3 N. Dimitratos, F. Porta, L. Prati and A. Villa, *Catal. Letters*, 2005, **99**, 181–185.
4 Y. Mizukoshi, T. Fujimoto, Y. Nagata, R. Oshima and Y. Maeda, *J. Phys. Chem. B*, 2000, **104**, 6028–6032.
5 J. Edwards, B. Solsona, P. Landon, A. Carley, A. Herzing, C. Kiely and G. Hutchings, *J. Catal.*, 2005, **236**, 69–79.
6 J. K. Edwards, A. F. Carley, A. A. Herzing, C. J. Kiely and G. J. Hutchings, *Faraday Discuss.*, 2008, **138**, 225–239.
7 P. J. Miedziak, Q. He, J. K. Edwards, S. H. Taylor, D. W. Knight, B. Tarbit, C. J. Kiely and G. J. Hutchings, *Catal. Today*, 2011, **163**, 47–54.
8 F. Moreau, G. Bond and A. Taylor, *J. Catal.*, 2005, **231**, 105–114.
9 N. Dimitratos, F. Porta and L. Prati, *Appl. Catal. A Gen.*, 2005, **291**, 210–214.
10 J. A. Lopez-Sanchez, N. Dimitratos, P. Miedziak, E. Ntainjua, J. K. Edwards, D. Morgan, A. F. Carley, R. Tiruvalam, C. J. Kiely and G. J. Hutchings, *Phys. Chem. Chem. Phys.*, 2008, **10**, 1921.
11 R. C. Tiruvalam, J. C. Pritchard, N. Dimitratos, J. A. Lopez-Sanchez, J. K. Edwards, A. F. Carley, G. J. Hutchings and C. J. Kiely, *Faraday Discuss.*, 2011, **152**, 63.
12 H. Dong, Y.-C. Chen and C. Feldmann, *Green Chem.*, 2015, **17**, 4107–4132.
13 L. K. Kurihara, G. M. Chow and P. E. Schoen, *Nanostructured Mater.*, 1995, **5**, 607–613.
14 L. C. Varanda and M. Jafelicci, *J. Am. Chem. Soc.*, 2006, **128**, 11062–11066.
15 G. Viau, F. Fiévet-Vincent and F. Fiévet, *Solid State Ionics*, 1996, **84**, 259–270.
16 Y. Sun, Y. Yin, B. T. Mayers, T. Herricks and Y. Xia, *Chem. Mater.*, 2002, **14**, 4736–4745.
17 I. Pastoriza-Santos and L. M. Liz-Marzán, *Nano Lett.*, 2002, **2**, 903–905.
18 I. Pastoriza-Santos and L. M. Liz-Marzán, *Adv. Funct. Mater.*, 2009, **19**, 679–688.
19 I. Pastoriza-Santos and L. M. Liz-Marzán, *Langmuir*, 2002, **18**, 2888–2894.
20 N. Dahal, S. García, J. Zhou and S. M. Humphrey, *ACS Nano*, 2012, **6**, 9433–9446.
21 D. Ferrer, A. Torres-Castro, X. Gao, S. Sepúlveda-Guzmán, U. Ortiz-Méndez and M. José-Yacamán, *Nano Lett.*, 2007, **7**, 1701–1705.
22 K. Patel, S. Kapoor, D. P. Dave and T. Mukherjee, *Res. Chem. Intermed.*, 2006, **32**, 103–113.
23 A. R. Vaino, *J. Org. Chem.*, 2000, **65**, 4210–4212.
24 D. G. Lee and U. A. Spitzer, *J. Org. Chem.*, 1970, **35**, 3589–3590.
25 J. C. Pritchard, Q. He, E. N. Ntainjua, M. Piccinini, J. K. Edwards, A. A. Herzing, A. F. Carley, J. A. Moulijn, C. J. Kiely and G. J. Hutchings, *Green Chem.*, 2010, **12**, 915.
26 D. Ferrer, A. Torres-Castro, X. Gao, S. Sepúlveda-Guzmán, U. Ortiz-Méndez and M. José-Yacamán, *Nano Lett.*, 2007, **7**, 1701–1705.

27 M. Tsuji, K. Ikedo, M. Matsunaga and K. Uto, *CrystEngComm*, 2012, **14**, 3411.
28 J. Pritchard, L. Kesavan, M. Piccinini, Q. He, R. Tiruvalam, N. Dimitratos, J. A. Lopez-Sanchez, A. F. Carley, J. K. Edwards, C. J. Kiely and G. J. Hutchings, *Langmuir*, 2010, **26**, 16568–16577.
29 J. K. Edwards, B. Solsona, E. N. N, A. F. Carley, A. A. Herzing, C. J. Kiely and G. J. Hutchings, *Science*, 2009, **323**, 1037–1041.
30 J. Yang, T. C. Deivaraj, H. P. Too and J. Y. Lee, *Langmuir*, 2004, **20**, 4241–4245.
31 S. Horiuchi, T. Fujita, T. Hayakawa and Y. Nakao, *Langmuir*, 2003, **19**, 2963–2973.
32 Y. Li, Y. Liu, W. Shen, Y. Yang, Y. Wen and M. Wang, *Mater. Lett.*, 2011, **65**, 2518–2521.
33 A. Cao, Z. Liu, S. Chu, M. Wu, Z. Ye, Z. Cai, Y. Chang, S. Wang, Q. Gong and Y. Liu, *Adv. Mater.*, 2010, **22**, 103–106.
34 R. Song, S. Feng, H. Wang and C. Hou, *J. Solid State Chem.*, 2013, **202**, 57–60.
35 X. Huang, X. Zhou, L. Zhou, K. Qian, Y. Wang, Z. Liu and C. Yu, *ChemPhysChem*, 2011, **12**, 278–281.
36 F. Bonet, K. Tekaia-Elhsissen and K. Vijaya Sarathy, *Bull. Mater. Sci.*, 2000, **23**, 165–168.
37 D. Chen and L. Gao, *J. Cryst. Growth*, 2004, **264**, 216–222.
38 X. Yan, H. Liu and Kong Yong Liew, *J. Mater. Chem.*, 2001, **11**, 3387–3391.
39 M. Tsuji, D. Yamaguchi, M. Matsunaga and M. J. Alam, *Cryst. Growth Des.*, 2010, **10**, 5129–5135.
40 S. H. Wu and D. H. Chen, *J. Colloid Interface Sci.*, 2004, **273**, 165–169.
41 D. P. Dissanayake and J. H. Lunsford, *J. Catal.*, 2002, **206**, 173–176.
42 J. A. Lopez-Sanchez, N. Dimitratos, N. Glanville, L. Kesavan, C. Hammond, J. K. Edwards, A. F. Carley, C. J. Kiely and G. J. Hutchings, *Appl. Catal. A Gen.*, 2011, **391**, 400–406.
43 J. K. Edwards, B. Solsona, P. Landon, A. F. Carley, A. Herzing, M. Watanabe, C. J. Kiely and G. J. Hutchings, *J. Mater. Chem.*, 2005, **15**, 4595.
44 A. Howe, P. Miedziak, D. J. Morgan, Q. He, P. Strasser and J. Edwards, *Faraday Discuss.*, 2018.
45 P. Tian, L. Ouyang, X. Xu, C. Ao, X. Xu, R. Si, X. Shen, M. Lin, J. Xu and Y.-F. Han, *J. Catal.*, 2017, **349**, 30–40.
46 J. K. Edwards, A. F. Carley, A. A. Herzing, C. J. Kiely and G. J. Hutchings, *Faraday Discuss.*, 2008, **138**, 225–239.
47 A. Nirmala Grace and K. Pandian, *Mater. Chem. Phys.*, 2007, **104**, 191–198.
48 M. P. Casaletto, A. Longo, A. Martorana, A. Prestianni and A. M. Venezia, *Surf. Interface Anal.*, 2006, **38**, 215–218.
49 J. Radnik, C. Mohr and P. Claus, *Phys. Chem. Chem. Phys.*, 2003, **5**, 172–177.
50 A. Fischer, A. Krozer and L. Schlapbach, *Surf. Sci.*, 1992, **269**–**270**, 737–742.
51 S. J. Freakley, Q. He, J. H. Harrhy, L. Lu, D. A. Crole, D. J. Morgan, E. N. Ntainjua, J. K. Edwards, A. F. Carley, A. Y. Borisevich, C. J. Kiely and G. J. Hutchings, *Science*, 2016, **351**, 965–968.
52 F. Li, Q. Shao, M. Hu, Y. Chen and X. Huang, *ACS Catal.*, 2018, 3418–3423.

53 P. Landon, P. J. Collier, A. J. Papworth, J. Kiely, J. Graham, C. J. Kiely and G. J. Hutchings, *Chem. Commun.*, 2002, 2058–2059.
54 InvestmentMine, http://www.infomine.com/investment/metal-prices, (accessed 23 July 2018).
55 K. H. Park, S. H. Im and O. O. Park, *Nanotechnology*, 2011, **22**.
56 Z. Liu, B. Guo, L. Hong and T. H. Lim, *Electrochem. commun.*, 2006, **8**, 83–90.
57 A. Villa, D. Wang, G. M. Veith, F. Vindigni and L. Prati, *Catal. Sci. Technol.*, 2013, **3**, 3036.
58 J. A. Lopez-Sanchez, N. Dimitratos, C. Hammond, G. L. Brett, L. Kesavan, S. White, P. Miedziak, R. Tiruvalam, R. L. Jenkins, A. F. Carley, D. Knight, C. J. Kiely and G. J. Hutchings, *Nat. Chem.*, 2011, **3**, 551–556.
59 M. Crespo-Quesada, J. M. Andanson, A. Yarulin, B. Lim, Y. Xia and L. Kiwi-Minsker, *Langmuir*, 2011, **27**, 7909–7916.
60 L. Abis, S. J. Freakley, G. Dodekatos, D. J. Morgan, M. Sankar, N. Dimitratos, Q. He, C. J. Kiely and G. J. Hutchings, *ChemCatChem*, 2017, **9**, 2914–2918.
61 F. Menegazzo, M. Signoretto, M. Manzoli, F. Boccuzzi, G. Cruciani, F. Pinna and G. Strukul, *J. Catal.*, 2009, **268**, 122–130.
62 J. Pritchard, M. Piccinini, R. Tiruvalam, Q. He, N. Dimitratos, J. A. Lopez-Sanchez, D. J. Morgan, A. F. Carley, J. K. Edwards, C. J. Kiely and G. J. Hutchings, *Catal. Sci. Technol.*, 2013, **3**, 308–317.

# 4. Catalysts Prepared by Modified Sol Immobilisation for Direct Hydrogen Peroxide Synthesis

## 4.1. Introduction

The catalytic activity of supported metal nanoparticles has long been known to be highly dependent on the structure of the catalytically active material.[1] A wide range of parameters have been found to be critical in maximising catalyst activity and selectivity for a variety of reactions such as the choice of catalytically active metal, support material, textural/chemical properties of support and catalyst preparation method to name a few.[2,3,4] Indeed the effect of these factors have been known in excess of 80 years, although the development of understanding remains an essential undertaking in part due to the tremendous difficulty of interrogating catalytically active materials under working conditions.[5,6]

Significant work has been undertaken on developing selective precious metal catalysts for the direct synthesis of hydrogen peroxide from molecular hydrogen and oxygen.[7] Hutchings and co-workers have studied PdAu bimetallic catalysts prepared by conventional impregnation exhaustively, investigating factors such as metal precursor, weight loadings, heat treatment regimes and choice of support material.[8,9,10] In wet impregnation, metal precursors are deposited on a support material typically by evaporation. This resultant material is then heat treated to decompose the precursors, which yields supported metal nanoparticles. The principle benefit of wet impregnation is its relative simplicity and scalability to industrial quantities. Unfortunately the lack of control in this method results in catalysts with large metal nanoparticle size distributions, which often results in poor selectivity.[11]

Sol immobilisation is an alternative preparation method in which active metal nanoparticles are formed and subsequently immobilised on an appropriate support.[12] The formation of colloidal metal nanoparticles can be more closely controlled than in wet impregnation, and as a result the size and structure of the nanoparticles can be directed to afford the desired selectivity or activity.[13] Sol immobilisation prepared PdAu bimetallic catalysts have been found to be highly active for hydrogen peroxide direct synthesis.[14] In a typical preparation of colloidal bimetallic PdAu catalysts, metal precursors are first reduced with sodium borohydride ($NaBH_4$) in the presence of polymeric stabilisers such as polyvinylpyrrolidone (PVP) or polyvinylalcohol (PVA).[15] The resultant colloids are supported then on metal oxides such as $TiO_2$ or carbon.[16] A number of challenges remain in the preparation of PdAu catalysts

by sol immobilisation. The preparation of colloidal metal nanoparticles coupled with the nanoparticle-stabiliser interaction in solution often results in poor adsorption between the metal and support materials. As a result, catalysts are often highly unstable with catalytic activity rapidly decaying over a number of subsequent reactions. The use of sodium borohydride as a reductant is synonymous with colloidal metal nanoparticle preparation. This is in part due to the physical and chemical properties of sodium borohydride; it is a stable solid under atmospheric conditions at room temperature, produced industrially in large quantities (and therefore relatively cheap), has a sufficiently large oxidation potential to reduce a wide range of precursors, and said reductions proceed rapidly allowing for fast screening of catalysts of varying composition.[17] Although the use of sodium borohydride is convenient, previous work has found that the choice of reductant can have profound effects on the size and structure of the resultant nanoparticles. Mucalo and co-workers previously investigated the formation of palladium and rhodium colloids using several different reductants.[18] It was found in the case of PVP stabilised palladium colloids that reduction using sodium borohydride yielded nanoparticles of 4.4 nm average diameter. In comparison, the colloid prepared under analogous conditions using hydrazine yielded nanoparticles 2.5 nm in diameter. Similar trends were observed in the presence of other stabilisers. Reduction using sodium borohydride in the presence of arginine yielded nanoparticles of 2.5 nm average diameter, versus 2.0 nm in the case of hydrazine. Such comparisons are seldom reported in literature and as a result the design of appropriate preparation conditions remains underutilised in catalytic literature.

The aim of this work is therefore to prepare catalytically active materials by sol immobilisation, with careful control of preparation parameters. The preparation method used in this work can be considered a modified sol immobilisation method, in that parameters such as choice and relative concentration of stabiliser, reductant and preparation temperature vary considerably from the principles fundamentally established in the state of the art. The evaluation of these materials for the direct hydrogen peroxide synthesis should allow for further refinement in producing more active and selective catalysts as well as further develop understanding of catalyst structure-activity relationship.

## *4.2. Results*

### *4.3. PVP Stabilised PdAu Catalysts for The Direct Synthesis Of Hydrogen Peroxide*

Polyvinylpyrrolidone (PVP) is a commonly used stabiliser that has been previously used to prepare metal colloids with activity for a range of reactions including glycerol oxidation, methane oxidation and acetylene hydrogenation.[19,20,21] Given the plethora of preparation parameters potentially influencing the activity of catalysts prepared by sol immobilisation, work was undertaken to investigate the effect of preparation variables on the activity of PVP stabilised catalysts prepared by sol immobilisation.

#### *4.3.1. The Effect of Au Incorporation on The Activity of 0.5 wt% Pd/$TiO_2$ Catalysts For $H_2O_2$ Direct Synthesis*

Previous work by Hutching and co-workers has found that for catalysts prepared by both wet impregnation and sol immobilisation, the addition of Au to a Pd monometallic catalyst displays a synergistic effect wherein hydrogen peroxide synthesis activity increased and hydrogenation activity depressed.[22] Monometallic 0.5 wt% Pd/$TiO_2$ and 0.5 wt% Au/$TiO_2$ catalysts and their 0.5 wt% Pd 0.5 wt% Au/$TiO_2$ analogue, prepared by a modified sol immobilisation procedure, were evaluated for both hydrogen peroxide synthesis and hydrogenation, the activity data presented in Figure 4-1.

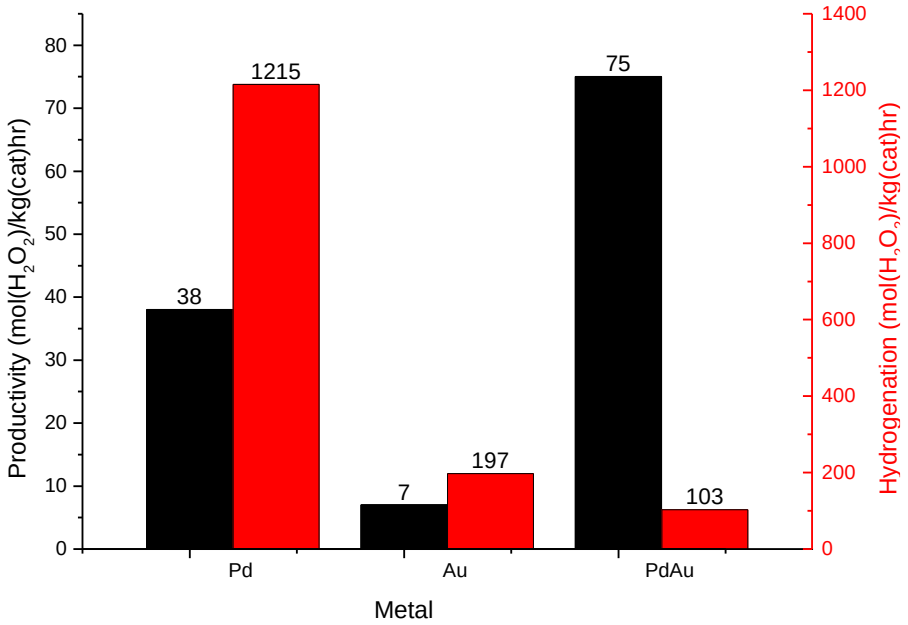


**Figure 4-1 - Hydrogen peroxide synthesis and hydrogenation activity of 1 wt% Pd, 1 wt% Au and 0.5 wt% Pd 0.5 wt% Au/$TiO_2$ catalysts prepared by sol immobilisation**

**Reaction Conditions – Hydrogen peroxide synthesis: 5 wt% $H_2/CO_2$ (2.9 MPa) and 25 wt% $O_2/CO_2$ (1.1 MPa), 8.5 g solvent (2.9 g $H_2O$, 5.6 g MeOH) 0.01 g catalyst, 2 °C, 1200 rpm, 30 min. Hydrogen peroxide hydrogenation: 5 wt% $H_2/CO_2$ (2.9 MPa), 8.5 g solvent (2.22 g $H_2O$, 5.6 g MeOH and 0.68 g 50 wt% $H_2O_2$), 0.01 g catalyst, 2 °C, 1200 rpm, 30 min.**

In agreement with previously published data, the bimetallic catalyst 0.5 wt% Pd 0.5 wt% $Au/TiO_2$ is considerably more active than either the Pd or Au monometallic catalysts, with a hydrogen peroxide synthesis activity of 75 mol$H_2O_2$/h/$kg_{cat}$. The monometallic Pd catalyst performs reasonably with an activity of 38 mol$H_2O_2$/h/$kg_{cat}$, which is greater than a 5 wt% $Pd/TiO_2$ prepared by wet impregnation previously reported by Edwards *et al.*, which was found to have an activity of 38 mol$H_2O_2$/h/$kg_{cat}$.[23] This suggests that sol immobilisation is a superior technique in preparing highly active catalysts, disregarding other factors such as catalyst stability. Likewise, the $Au/TiO_2$ catalyst has a synthesis activity of 7 mol$H_2O_2$/h/$kg_{cat}$ comparable to a 5 wt% $Au/TiO_2$ sample prepared by impregnation previously reported, which also had a hydrogen peroxide synthesis activity of 7 mol$H_2O_2$/h/$kg_{cat}$, despite containing ten times more Au by mass.[24]

The synergistic effect of Pd and Au was also observed for hydrogen peroxide hydrogenation activity, consistent with previous work on PdAu bimetallic catalysts prepared by wet impregnation and conventional sol immobilisation.[25,13] The hydrogenation activity of the monometallic Pd and Au catalysts are 1215 and 197 mol$H_2O_2$/h/$kg_{cat}$, and the PdAu catalyst exhibiting a hydrogenation activity of only 103 mol$H_2O_2$/h/$kg_{cat}$. Under batch conditions, hydrogenation of in-situ formed hydrogen peroxide is the dominant pathway governing hydrogen selectivity towards hydrogen peroxide. A lower hydrogenation activity means that less hydrogen peroxide will be consumed over the course of a reaction; therefore, the hydrogen peroxide synthesis activity, which is representative of the sum of all the productive and destructive reaction rates, will increase with decreasing hydrogenation activity

### *4.3.2. The Effect of Varying Reductant on PdAu/$TiO_2$ Activity For $H_2O_2$ Direct Synthesis*

0.5 wt% Pd 0.5 wt% $Au/TiO_2$ catalysts were prepared from PVP stabilised colloids using three reductants, sodium borohydride ($NaBH_4$), ammonia borane ($NH_3BH_3$) and hydrazine ($N_2H_4$) to investigate the effect on catalyst activity towards the direct synthesis and subsequent hydrogenation of hydrogen peroxide. The hydrogen peroxide synthesis and hydrogenation activities of the catalysts are presented in Figure 4-2. Regardless of choice of reductant, the resulting catalysts have a synthesis activity of 75 mol$H_2O_2$/h/$kg_{cat}$. Previous work by Tiruvalam *et al.* found that a PVA stabilised 0.5 wt% Pd 0.5 wt% $Au/TiO_2$ catalyst,

prepared by sol immobilisation using $NaBH_4$, had a hydrogen peroxide synthesis activity of 31 mol$H_2O_2$/h/$kg_{cat}$.[13] The PVP stabilised catalysts presented in Figure 4-2 are over twice as active, indicating that the choice of stabiliser has a significant effect on catalyst activity.

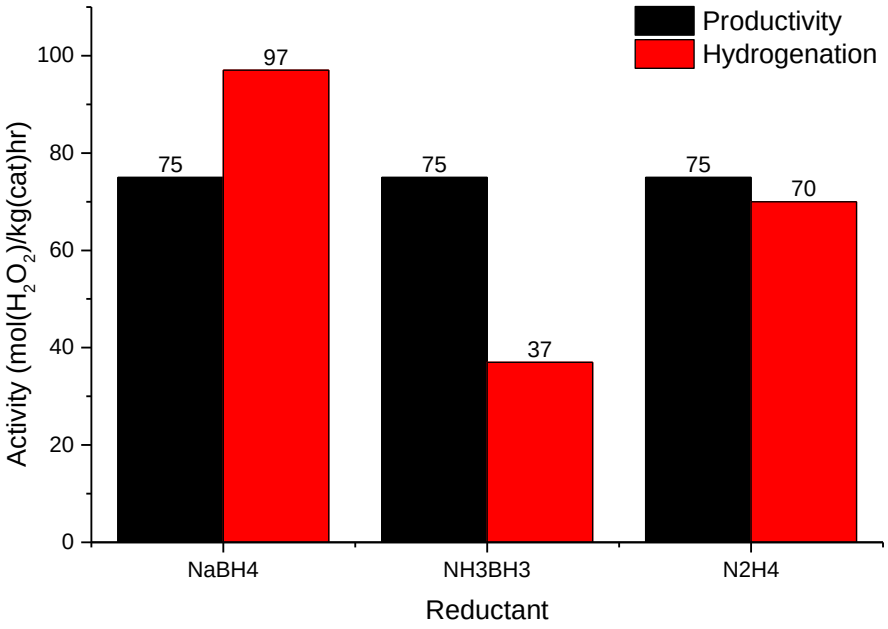


**Figure 4-2 - Hydrogen peroxide synthesis and hydrogenation activity 0.5 wt% Pd 0.5 wt% Au/$TiO_2$ catalysts prepared by sol immobilisation using various reductants**
**Reaction Conditions – Hydrogen peroxide synthesis: 5 % $H_2/CO_2$ (2.9 MPa) and 25 % $O_2/CO_2$ (1.1 MPa), 8.5 g solvent (2.9 g $H_2O$, 5.6 g MeOH) 0.01 g catalyst, 2 °C, 1200 rpm, 30 min. Hydrogen peroxide hydrogenation: 5 % $H_2/CO_2$ (2.9 MPa), 8.5 g solvent (2.22 g $H_2O$, 5.6 g MeOH and 0.68 g 50 wt% $H_2O_2$), 0.01 g catalyst, 2 °C, 1200 rpm, 30 min.**

The catalysts were also evaluated for hydrogen peroxide hydrogenation activity. Curiously the hydrogenation activity of the catalysts varies considerably with differing reductants despite having identical synthesis activities. The $NaBH_4$ reduced catalyst is most active for hydrogenation with an activity of 97 mol$H_2O_2$/h/$kg_{cat}$. For comparison, the PVA stabilised catalyst previously reported by Pritchard *et al.* had a hydrogenation activity of 384 mol$H_2O_2$/h/$kg_{cat}$. This suggests that the improvement in synthesis activity between the previous and current catalysts is likely due to the decrease in the hydrogenation of formed hydrogen peroxide.

The hydrogenation activity cannot however be the only factor influencing catalyst synthesis activity. If this were the case, it would be reasonable to expect that the catalyst with the lowest hydrogenation activity would exhibit the greatest synthesis activity, which is not observed in the catalyst activity data presented in Figure 4-2. Nonetheless, preparation of 0.5 wt% Pd 0.5 wt% Au/$TiO_2$ using $NH_3BH_3$ or $N_2H_4$ results in a 60 and 20 % reduction on

hydrogenation activity when compared to their $NaBH_4$ reduced counterpart, suggesting that they are more selective towards the formation of hydrogen peroxide and therefore superior performing catalysts.

### *4.3.3. The Effect of Varying Preparation Temperature on PdAu/$TiO_2$ Activity For $H_2O_2$ Direct Synthesis*

To further explore catalyst preparation parameters, preparation temperature was varied during the sol immobilisation preparation of 0.5 wt% Pd 0.5 wt% Au/$TiO_2$ catalysts. Previous work by Peng *et al.* found that temperature changes are highly effective in influencing the kinetic formation of metallic nanostructures from colloidal nanoparticles, resulting in improved control of the resultant nanoparticle structure[26] The hydrogen peroxide synthesis and hydrogenation activities of 0.5 wt% Pd 0.5 wt% Au/$TiO_2$ catalysts prepared using $NaBH_4$, $NH_3BH_3$ and $N_2H_4$ at 0, 25 and 60°C are shown in Figure 4-3.

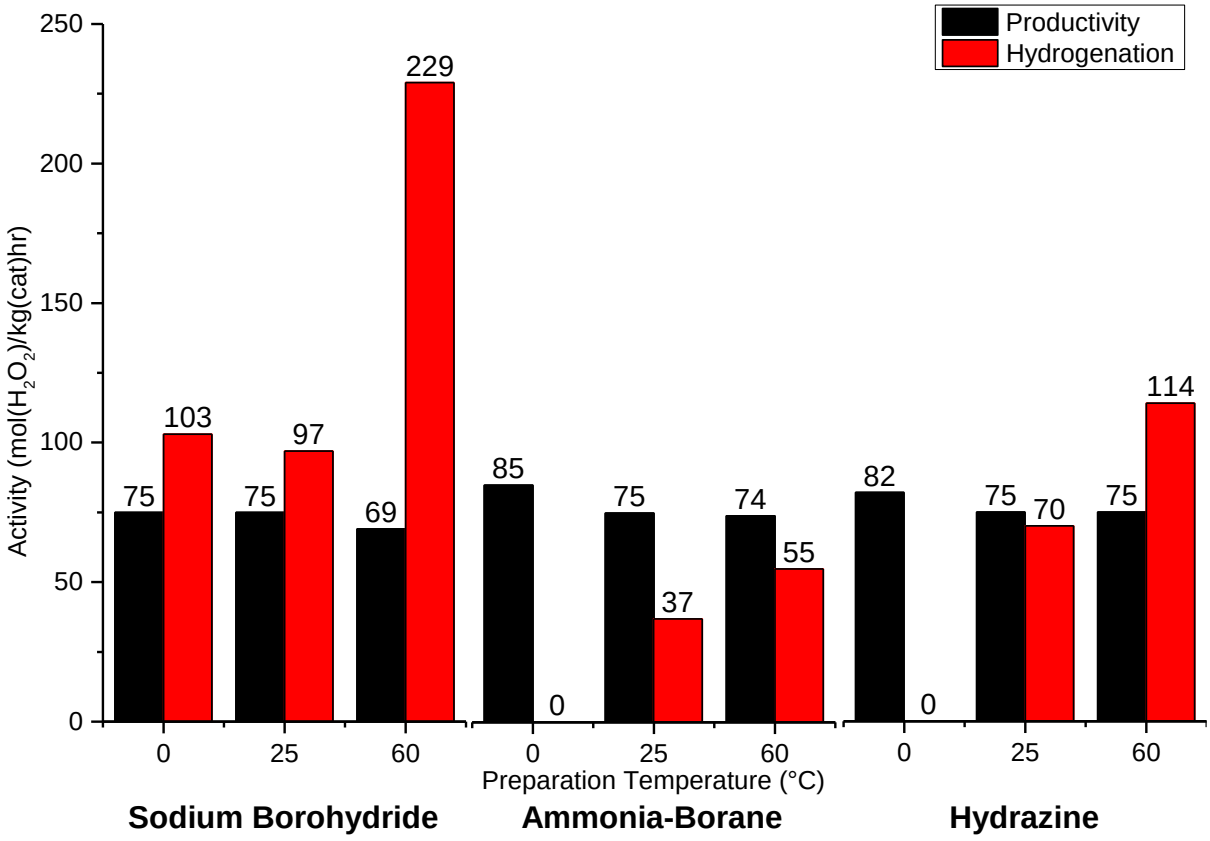


**Figure 4-3 - Hydrogen peroxide synthesis and hydrogenation activity of 0.5 wt% Pd 0.5 wt% Au/$TiO_2$ catalysts prepared by sol immobilisation using $NaBH_4$, $NH_3BH_3$ and $N_2H_4$ at 0, 25 and 60 °C**

**Reaction Conditions – Hydrogen peroxide synthesis: 5 % $H_2/CO_2$ (2.9 MPa) and 25 % $O_2/CO_2$ (1.1 MPa), 8.5 g solvent (2.9 g $H_2O$, 5.6 g MeOH) 0.01 g catalyst, 2 °C, 1200 rpm, 30 min. Hydrogen peroxide hydrogenation: 5 % $H_2/CO_2$ (2.9 MPa), 8.5 g solvent (2.22 g $H_2O$, 5.6 g MeOH and 0.68 g 50 wt% $H_2O_2$), 0.01 g catalyst, 2 °C, 1200 rpm, 30 min.**

In the case of $NaBH_4$ reduced catalysts, the hydrogen peroxide synthesis activity remains constant for catalysts prepared at 0 and 25°C, 75 mol$H_2O_2$/h/$kg_{cat}$. Increasing the preparation temperature to 60°C results in a decrease of synthesis activity, to 69 mol$H_2O_2$/h/$kg_{cat}$. The hydrogenation activities of the catalysts are consistent with this data, as the hydrogenation activity remains roughly constant for catalysts prepared at 0 and 25°C, 103 vs 97 mol$H_2O_2$/h/$kg_{cat}$, but rises sharply upon preparation at 60°C, to 229 mol$H_2O_2$/h/$kg_{cat}$. This indicates that increasing preparation temperature yields catalysts with greater hydrogenation activity and therefore low temperature preparation would be beneficial in preparing more selective, low hydrogenation activity catalysts.

Similar trends are observed in the case of $NH_3BH_3$ and $N_2H_4$ reduced catalysts, that as preparation temperature increases, hydrogen peroxide synthesis activity decreases and hydrogenation activity increases. Unlike the $NaBH_4$ reduced catalysts, those prepared using $N_2H_4$ or $NH_3BH_3$ as reductants offered no activity towards hydrogen peroxide hydrogenation when prepared at 0 °C. For the $NH_3BH_3$ reduced catalysts, reduction of the preparation temperature from 60 to 0°C results in an increase in hydrogen peroxide synthesis activity from 74 to 85 mol$H_2O_2$/h/$kg_{cat}$. At the same time; the hydrogenation activity decreases from 55 to 0 mol$H_2O_2$/h/$kg_{cat}$. The combination of increased hydrogen peroxide synthesis and decreased hydrogenation activities of this catalyst indicates that the improvement in synthesis activity when decreasing preparation temperature is most probably a consequence of decreased hydrogenation activity. The hydrogenation activity of $NH_3BH_3$ reduced catalysts is lower than the $NaBH_4$ reduced analogues at all temperatures, indicating that they yield more selective catalysts.

Critically, the $NH_3BH_3$ reduced catalyst prepared at 0°C has a hydrogenation activity of 0 mol$H_2O_2$/h/$kg_{cat}$. This suggests the catalyst has no activity towards the hydrogenation of hydrogen peroxide formed during reaction, and therefore is completely selective towards hydrogen peroxide under the standard reaction conditions used in this work.

The hydrogen peroxide synthesis and hydrogenation activities of the $N_2H_4$ reduced catalysts are consistent with catalysts reduced by the other species. Decreasing preparation temperature from 60 to 0 °C results in an increase in synthesis activity, from 75 to 82 mol$H_2O_2$/h/$kg_{cat}$, and hydrogenation activity decreases from 114 to 0 mol$H_2O_2$/h/$kg_{cat}$. The hydrogenation rates of the $N_2H_4$ reduced catalysts are lower than those prepared using $NaBH_4$, but greater than the $NH_3BH_3$ reduced analogues. The synthesis activities of the catalysts are congruent with

the hydrogenation activities as they follow the trend $NH_3BH_3$ > $N_2H_4$ > $NaBH_4$ for catalysts prepared at any given temperature.

Although the hydrogen peroxide synthesis, hydrogenation and decomposition activities of a catalyst are quantitatively related to the relative rates of the three processes, the reaction conditions used in this work do not allow for direct calculation of the hydrogen selectivity from the requisite reaction rates. As outlined in Chapter 2, the hydrogenation activity of the catalysts is determined by the decomposition of a 4 wt% hydrogen peroxide solution in the presence of the catalyst. This corresponds to approximately 25 times the concentration of hydrogen peroxide resulting from the direct synthesis reactions, and therefore a catalyst that is inactive at the comparatively harsh hydrogenation reaction conditions can be considered inactive for hydrogenation and decomposition under the direct synthesis reaction conditions.

### *4.3.4. The Effect of Varying PVP-Metal Ratio on PdAu/$TiO_2$ Activity For $H_2O_2$ Direct Synthesis*

Given the effect of varying reductant and preparation temperature, work was also undertaken to investigate the effect of the stabiliser-metal precursor ratio during the preparation of 0.5 wt% Pd 0.5 wt% Au/$TiO_2$ catalysts. Most typically, stoichiometric or superstoichiometric amounts of stabiliser are used on a monomer basis, under the assumption that this is sufficient to completely cover the surface of the nanoparticles upon formation and avoid agglomeration and colloid decomposition, thus preventing the formation of larger, less catalytically active nanostructures.[27,28]

0.5 wt% Pd 0.5 wt% Au/$TiO_2$ catalysts were prepared using $NH_3BH_3$ at 0°C with varying PVP-metal ratio. The hydrogen peroxide synthesis and hydrogenation activities of these catalysts are shown in Figure 4-4.

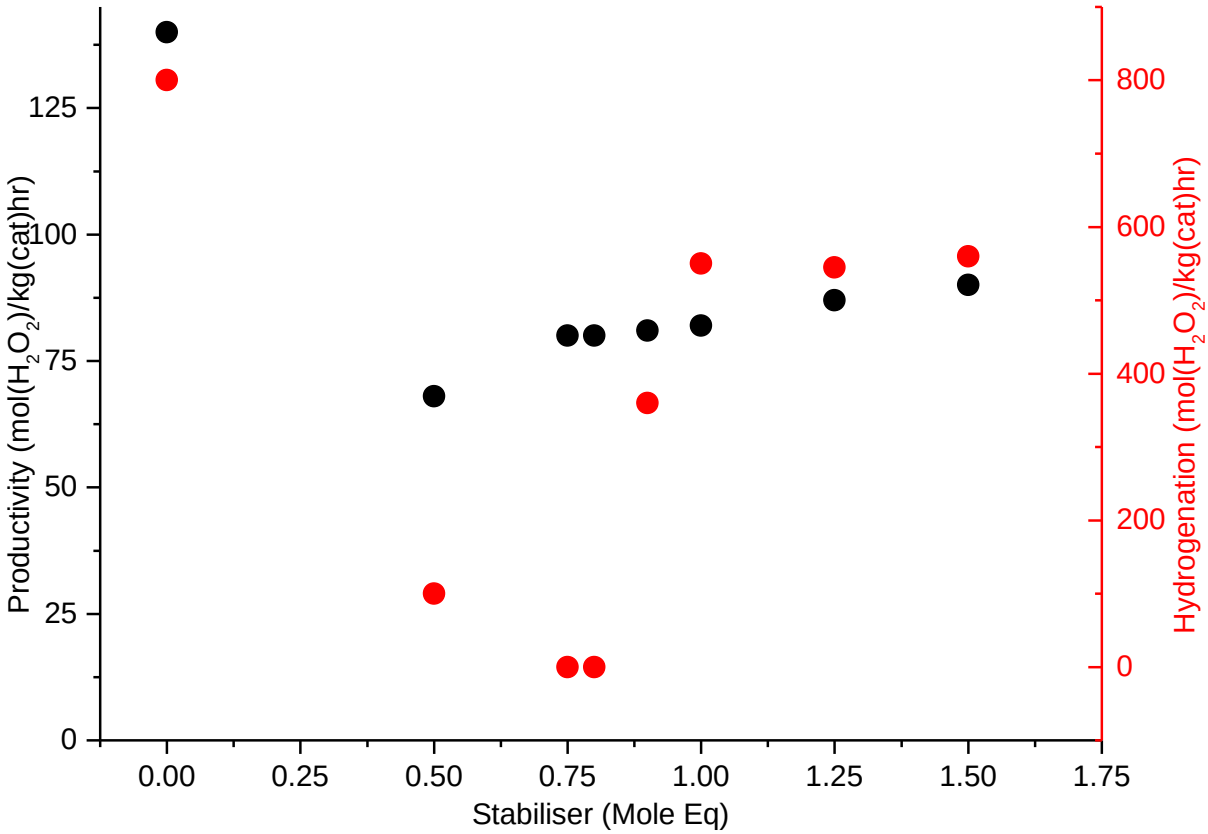


**Figure 4-4 - Hydrogen peroxide synthesis (●) and hydrogenation activity (●) of 0.5 wt% Pd 0.5 wt% Au/$TiO_2$ prepared PVP stabilised sol immobilisation with varying PVP-metal ratio**

**Reaction Conditions – Hydrogen peroxide synthesis: 5 % $H_2/CO_2$ (2.9 MPa) and 25 % $O_2/CO_2$ (1.1 MPa), 8.5 g solvent (2.9 g $H_2O$, 5.6 g MeOH) 0.01 g catalyst, 2 °C, 1200 rpm, 30 min. Hydrogen peroxide hydrogenation: 5 % $H_2/CO_2$ (2.9 MPa), 8.5 g solvent (2.22 g $H_2O$, 5.6 g MeOH and 0.68 g 50 wt% $H_2O_2$), 0.01 g catalyst, 2 °C, 1200 rpm, 30 min.**

The catalyst prepared in the absence of stabiliser has the greatest synthesis activity, 140 mol$H_2O_2$/h/$kg_{cat}$, which is consistent with previous work by Abis *et al.*, who found that PdAu/$TiO_2$ catalysts prepared in the absence of stabilisers were more active for glycerol oxidation than those in the presence of PVP or PVA.[20] Likewise, Hutchings and co-workers found that by refluxing formed catalysts in water or organic solvents, remaining PVA stabiliser could be removed from a 0.5 wt% Pd 0.5 wt% Au/$TiO_2$ catalyst, increasing active metal surface area and therefore activity for CO oxidation.[29] The authors also observed that the decrease in hydrogen peroxide synthesis activity in the presence of stabiliser was accompanied by a decrease in hydrogenation activity. In the case of the modified sol immobilisation catalysts presented in this work, incorporation of a relatively small amount of PVP (0.5 mole eq) results in a decrease in hydrogenation activity of more than 85 %, from

800 to 100 mol$H_2O_2$/h/$kg_{cat}$ but only 50 % decrease in synthesis activity, indicating a net selectivity improvement towards hydrogen peroxide formation.

Further increasing the PVP-metal ratio from 0.5 to 1.5 equivalents results in an increase in hydrogen peroxide synthesis activity from 68 to 90 mol$H_2O_2$/h/$kg_{cat}$. Additionally, the hydrogen peroxide hydrogenation activity varies considerably with increasing stabiliser content, with hydrogenation activity tending to a minimum at 0.75-0.8eq PVP of 0 mol$H_2O_2$/h/$kg_{cat}$; at either 0.5 or 0.9 eq PVP, the hydrogenation activity rises rapidly to 100 and 360 mol$H_2O_2$/h/$kg_{cat}$ respectively. This suggests that the catalyst structure, and therefore activity, is highly sensitive to the amount of stabiliser present during catalyst preparation. Increasing the PVP-metal ratio from 0.9 to 1 eq results in an increase from 360 to 550 mol$H_2O_2$/h/$kg_{cat}$, though further increases to 1.25 or 1.5 eq results in no further change in activity. Miyake and co-workers previously investigated the effect of increasing PVP content on the particle size distribution of Pd colloids.[30] They reported that the addition of superstoichiometric amounts of PVP resulted in no further decrease in average particle diameter. Such an effect could be responsible for the observed hydrogen peroxide synthesis and hydrogenation activity observed here between 1-1.5 eq PVP, where the catalyst activity varies only marginally.

### *4.3.5. The Effect of Varying Pd-Au Ratio on PdAu/$TiO_2$ Activity For $H_2O_2$ Direct Synthesis*

In the preceding sections it has been established that reductant, stabiliser content, and preparation temperature all influence the activity of a 0.5 wt% Pd 0.5 wt% Au/$TiO_2$ catalyst for the direct synthesis of hydrogen peroxide. To further assess the applicability and scope of the modified sol immobilisation protocol introduced in this work, a series of catalysts were prepared with variable Pd-Au ratio at 0 °C using $NH_3BH_3$ as the reductant. The hydrogen peroxide synthesis and hydrogenation activities of these catalysts are presented in Figure 4-5. The monometallic Pd catalyst, 1 wt% Pd/$TiO_2$, is less active for hydrogen peroxide direct synthesis and more active for hydrogenation relative to the bimetallic catalysts, with a synthesis activity of 15 and hydrogenation activity of 750 mol$H_2O_2$/h/$kg_{cat}$ respectively. Likewise, the analogous monometallic Au catalyst exhibits low synthesis and hydrogenation activities of 8 and 110 mol$H_2O_2$/h/$kg_{cat}$. Incorporation of a small amount of Pd into the preparation to yield a catalyst of composition 0.2 wt% Pd 0.8 wt% Au results in a significant increase in synthesis activity to 50 mol$H_2O_2$/h/$kg_{cat}$. Addition of increasing amounts of Pd to 0.35 wt%, 0.5 wt% and 0.65 wt% Pd (remainder Au) resulted in an increase in hydrogen

peroxide synthesis activity to a maximum 90 mol$H_2O_2$/h/$kg_{cat}$ in the case of the 0.65 wt % Pd 0.35 wt% Au/$TiO_2$ catalyst.

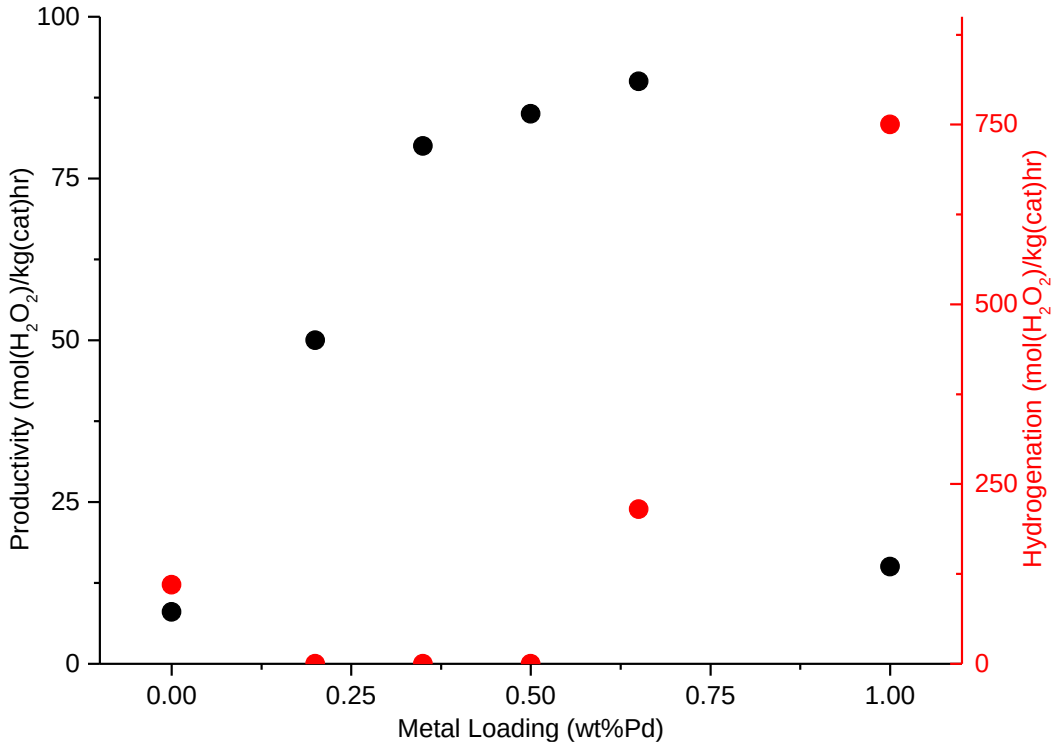


**Figure 4-5 - Hydrogen peroxide synthesis (●) and hydrogenation activity (●) of 1 wt% PdAu/$TiO_2$ catalysts of variable Pd-Au composition prepared by sol immobilisation**
**Reaction Conditions – Hydrogen peroxide synthesis: 5 % $H_2/CO_2$ (2.9 MPa) and 25 % $O_2/CO_2$ (1.1 MPa), 8.5 g solvent (2.9 g $H_2O$, 5.6 g MeOH) 0.01 g catalyst, 2 °C, 1200 rpm, 30 min. Hydrogen peroxide hydrogenation: 5% $H_2/CO_2$ (2.9 MPa), 8.5 g solvent (2.22 g $H_2O$, 5.6 g MeOH and 0.68 g 50 wt% $H_2O_2$), 0.01 g catalyst, 2 °C, 1200 rpm, 30 min.**

In Section 4.3.3, it was shown that 0.5 wt% Pd 0.5 wt% Au/$TiO_2$ catalysts prepared using $NH_3BH_3$ at 0°C was entirely selective towards the synthesis of hydrogen peroxide and exhibited a hydrogenation activity of 0 mol$H_2O_2$/h/$kg_{cat}$. The 0.35 wt% Pd 0.65 wt% Au/$TiO_2$ and 0.2 wt% Pd 0.8 wt% Au/$TiO_2$ catalysts also have similar activity to the 0.5 wt% Pd 0.5wt% Au/$TiO_2$ catalyst in that they exhibit good hydrogen peroxide synthesis activity but a hydrogenation value of nil. Further increases in Pd loading to 0.65 wt% Pd 0.35 wt% Au/$TiO_2$ result in an increase in hydrogenation activity to 215 mol$H_2O_2$/h/$kg_{cat}$, which continues to increase with incorporation of Pd up to a monometallic catalyst composition.

Tian *et al.* recently investigated size effects in impregnation prepared monometallic Pd catalysts for direct synthesis of hydrogen peroxide, reporting that sub-nanometre nanoparticles exhibited an $H_2O_2$ selectivity of 94 % versus 42 % and below for nanoparticles

larger than 2.5 nm.[31] The selectivity of the Pd nanocluster catalyst is comparable to that of optimised PdAu catalysts reported elsewhere, however this is likely due to the use of highly acidified reaction mixtures in this work, as strong acids are known to supress hydrogen peroxide hydrogenation activity. The authors also showed that a single site Pd catalyst was inactive for the direct synthesis of hydrogen peroxide. Other work by Schiffrin and co-workers on PdAu bimetallic catalysts has suggested that Au acts to minimise Pd domain size, which minimises the catalyst decomposition of hydrogen peroxide on the catalyst surface and therefore improves selectivity.[32] The onset of hydrogenation activity at 0.65 wt% Pd 0.35 wt% Au/$TiO_2$ could be a consequence of this effect, with increased Pd content resulting in larger Pd domains. The increase in hydrogenation activity could also be attributed to monometallic Pd species, however previous work on PdAu catalysts, prepared by sol immbolisation, found that the co-reduction of Pd and Au precursors results in homogeneously alloyed nanoparticles.[13]

### *4.3.6. The Effect of Varying Total Metal Loading on PdAu/$TiO_2$ Activity For $H_2O_2$ Direct Synthesis*

In Section 4.3.5, the catalyst of composition 0.5 wt% Pd 0.5 wt% Au exhibited maximum synthesis activity whilst minimising hydrogenation activity. In adhereing to the principles of green chemistry, with a view to reducing usage of high cost precious metals a series of catalysts were prepared with a 1:1 Pd:Au weight ratio with variable total metal loading, at 0 °C using $NH_3BH_3$ as the reductant. The hydrogen peroxide synthesis of catalysts of variable total loading are presented in Figure 4-6.

Like the 0.5 wt% Pd 0.5 wt% Au/$TiO_2$ catalyst, the lower loaded catalysts also exhibited no hydrogenation activity. This is consistent with previous work reported using catalysts prepared by sol immobilisation, in which preformed colloids are immobilised onto an appropriate support material.[14] In the preceding sections of this work, the selective nature of the catalyst has been shown to be highly dependent upon the conditions utilised during colloid preparation, and therefore variations in the quantities of metal colloid or support (yielding catalysts of differing total loading) has little effect on the selectivity of the catalyst. This is consistent with the activity of the catalysts of variable total loading, as decreasing total metal loading from 1 to 0.25 wt% resulted in a regular decrease in synthesis activity, consistent with reduced Pd content.

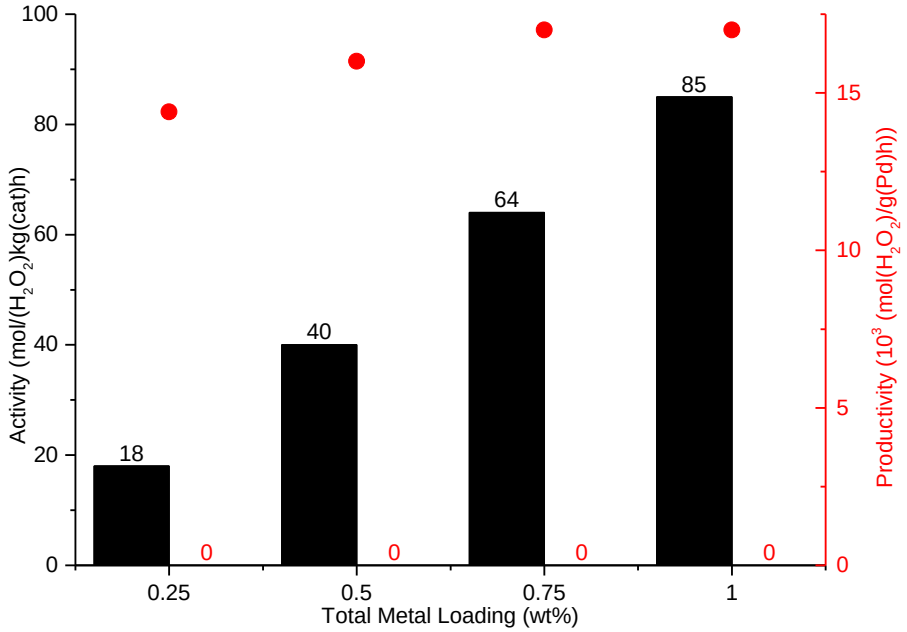


**Figure 4-6 - Hydrogen peroxide synthesis (left) and hydrogenation activity (right) of PdAu/$TiO_2$ (1:1 wt ratio) catalysts of variable total metal loading prepared by sol immobilisation. hydrogen peroxide synthesis activities also presented per metal basis (●)**
**Reaction Conditions – Hydrogen peroxide synthesis: 5 % $H_2/CO_2$ (2.9 MPa) and 25 % $O_2/CO_2$ (1.1 MPa), 8.5 g solvent (2.9 g $H_2O$, 5.6 g MeOH) 0.01 g catalyst, 2 °C, 1200 rpm, 30 min. Hydrogen peroxide hydrogenation: 5 % $H_2/CO_2$ (2.9 MPa), 8.5 g solvent (2.22 g $H_2O$, 5.6 g MeOH and 0.68 g 50 % $H_2O_2$), 0.01 g catalyst, 2 °C, 1200 rpm, 30 min.**

The hydrogen peroxide synthesis activities of the catalysts are also presented based on a Pd mass basis in Figure 4-6. The activity remains roughly constant between 1 and 0.5 wt% loading, decreasing from 17000 to 16000 mol$H_2O_2$/h/$g_{Pd}$. Further decrease in loading results in a decrease of synthesis activity to 14500 mol$H_2O_2$/h/$g_{Pd}$, a decrease of less than 15% in relation to the 1 wt% catalyst despite a fourfold decrease in catalyst Pd mass.

### *4.3.7. Reproducibility of Optimised 0.5 wt% Pd 0.5 wt% Au Catalyst*

Given the unusual activity of the $TiO_2$ and carbon supported 0.5 wt% Pd 0.5 wt% Au catalysts, a reproducibility study was carried out to determine the reliability of the preparation method. The hydrogen peroxide synthesis and hydrogenation activities of three independent batches of $TiO_2$ and carbon supported PdAu catalysts are presented in Figure 4-7.

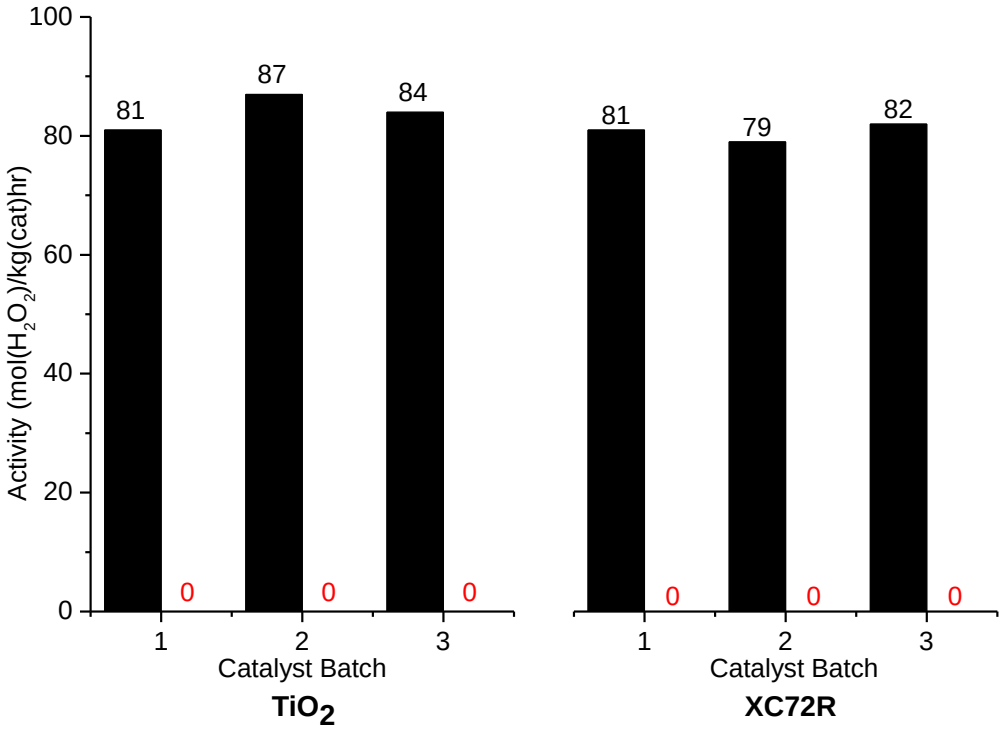


**Figure 4-7 - Hydrogen peroxide synthesis (left) and hydrogenation (right) activities of three batches of $TiO_2$ and XC72R carbon supported PdAu catalysts**

**Reaction Conditions – Hydrogen peroxide synthesis: 5 % $H_2/CO_2$ (2.9 MPa) and 25 % $O_2/CO_2$ (1.1 MPa), 8.5 g solvent (2.9 g $H_2O$, 5.6 g MeOH) 0.01 g catalyst, 2 °C, 1200 rpm, 30 min. Hydrogen peroxide hydrogenation: 5 % $H_2/CO_2$ (2.9 MPa), 8.5 g solvent (2.22 g $H_2O$, 5.6 g MeOH and 0.68 g 50 wt% $H_2O_2$), 0.01 g catalyst, 2 °C, 1200 rpm, 30 min.**

The synthesis activity of the 0.5 wt% Pd 0.5 wt% $Au/TiO_2$ catalyst varies between 81 and 87 $molH_2O_2/h/kg_{cat}$ by batch, representing a 7 % range in activity. In comparison, the XC72R supported analogue was more consistent, hydrogen peroxide synthesis activity varying by only 3.5 %.

The hydrogen peroxide hydrogenation activity of the catalysts remains consistent across all the batches, with the catalysts being completely inactive towards the hydrogenation pathway. The marginal variation between the activity of catalyst batches indicates that this preparation method is highly reproducible and therefore that the modified sol immobilisation method reliably yields consistent catalysts.

### *4.3.8. Reuse of 0.5 wt% Pd 0.5 wt% Au/$TiO_2$ and 0.5 wt% Pd 0.5 wt% Au/C Catalysts For $H_2O_2$ Direct Synthesis*

Catalyst reuse is a critical parameter in the industrial applicability of precious metal catalysis. Previous work on sol immobilisation prepared catalysts has demonstrated that catalysts prepared by this technique are seldom stable, primarily due to the inhibitory nature of the stabiliser in weakening metal-support interaction.[33,34,35] As a result, active metals are known to readily leach into solution and as a result catalyst activity rapidly decays over subsequent reactions. 0.5 wt% Pd 0.5 wt% Au/$TiO_2$ and 0.5 wt% Pd 0.5 wt% Au/C catalysts were prepared using optimum (zero hydrogenation activity) conditions, and then filtered, washed and dried after the initial reaction and tested for subsequent reuse. The hydrogen peroxide synthesis and hydrogenation activities of the fresh and used catalysts are shown in Figure 4-8.

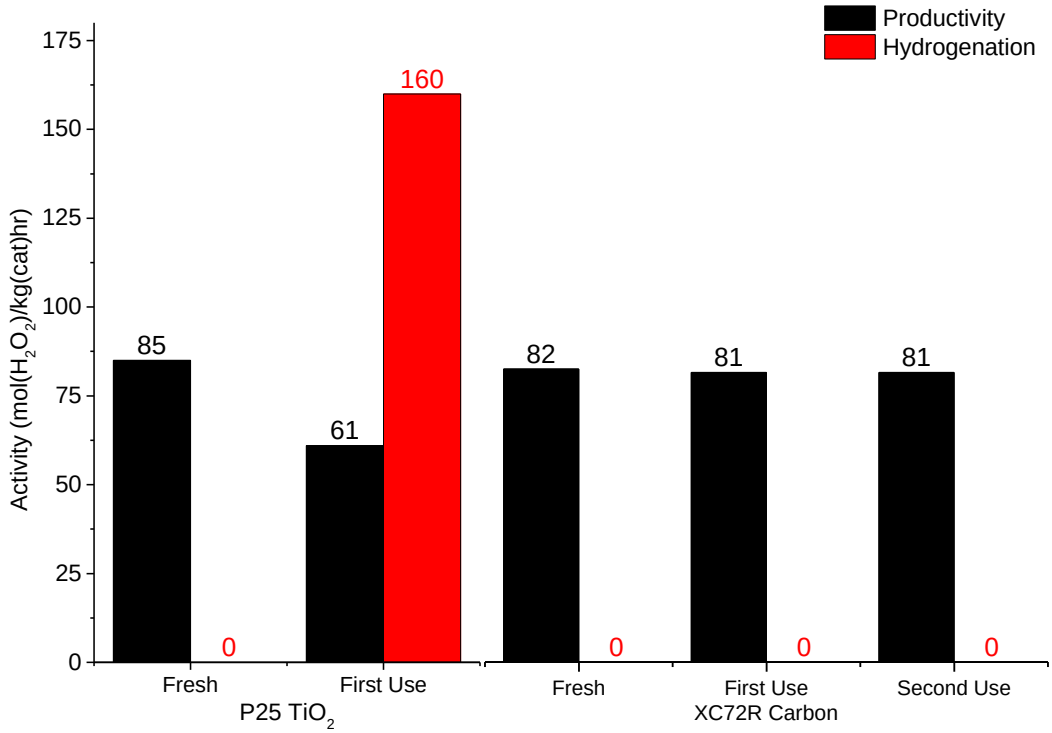


**Figure 4-8 - Hydrogen peroxide synthesis and hydrogenation activity of 0.5 wt% Pd 0.5 wt% Au catalysts supported On $TiO_2$ and carbon before and after reuse**

**Reaction Conditions – Hydrogen peroxide synthesis: 5 % $H_2/CO_2$ (2.9 MPa) and 25 % $O_2/CO_2$ (1.1 MPa), 8.5 g solvent (2.9 g $H_2O$, 5.6 g MeOH) 0.01 g catalyst, 2 °C, 1200 rpm, 30 min. Hydrogen peroxide hydrogenation: 5 % $H_2/CO_2$ (2.9 MPa), 8.5 g solvent (2.22 g $H_2O$, 5.6 g MeOH and 0.68 g 50 wt% $H_2O_2$), 0.01 g catalyst, 2 °C, 1200 rpm, 30 min.**

In the case of the $TiO_2$ supported catalyst, hydrogen peroxide synthesis activity decreases from 85 to 61 mol$H_2O_2$/h/$kg_{cat}$ upon reuse, and a substantial increase in hydrogenation activity occurs, rising from 0 to 160 mol$H_2O_2$/h/$kg_{cat}$. The increase of the hydrogenation

pathway demonstrates a decrease in selectivity and synthesis activity, which is consistent with a change in the catalyst structure or composition from metal leaching.

The XC72R carbon supported catalyst exhibits very similar activity to the $TiO_2$ supported analogue upon first use, both exhibiting zero hydrogenation activity and synthesis activities of 82 and 85 mol$H_2O_2$/h/$kg_{cat}$ respectively, suggesting that the support plays a negligible role in the preparation of the catalyst. The results are consistent with those in Section 4.3.6, which found that catalyst activity is largely independent of support due to the poor metal-support interaction typically present in immobilised colloidal catalysts. Interestingly, subsequent reuse of the carbon supported catalyst resulted in no change in catalyst activity over two further reactions, unlike $TiO_2$ supported catalysts which became active for hydrogen peroxide hydrogenation upon reuse. Especially surprising is the fact that the carbon supported catalyst remains inactive for the hydrogenation of hydrogen peroxide once formed, suggesting that the high selectivity of the catalyst is preserved upon reuse and that such stability is intimately linked to the nature of the support.

### *4.3.9. Electron Microscopy*

To better understand the chemical and physical structure of the catalysts, scanning electron microscopy (SEM), transmission electron microscopy (TEM) and scanning transmission electron microscopy (STEM) were used to interrogate a range of samples.

#### *4.3.9.1. Optimised 0.5 wt% Pd 0.5 wt% Au/$TiO_2$ Catalyst*

In Sections 4.3.3 and 4.3.4, it was shown that, under optimal preparation conditions the hydrogenation activity of 0.5 wt% Pd 0.5 wt% Au/$TiO_2$ catalysts is deactivated such that the catalysts are selective towards hydrogen peroxide. High resolution HAADF-STEM images of the catalyst, prepared by reduction with $NH_3BH_3$ at 0°C, are presented in

Figure 4-9. Unlike sol immobilisation catalysts previously reported by Kiely and co-workers, the resultant particles form agglomerate chain nanostructures of variable length. The constructs have rounded edges perpendicular to the direction of growth, indicating that the chains are formed from the agglomeration of discrete spherical PdAu nanoparticles. Measurement of the width of the chains at several positions along the length indicates that the parent PdAu nanoparticles are 3-5 nm in diameter. The nanochain structures contained considerable branching, suggesting that the structure is a result of disordered self-assembly of spherical PdAu nanoparticles in the colloidal phase during preparation.

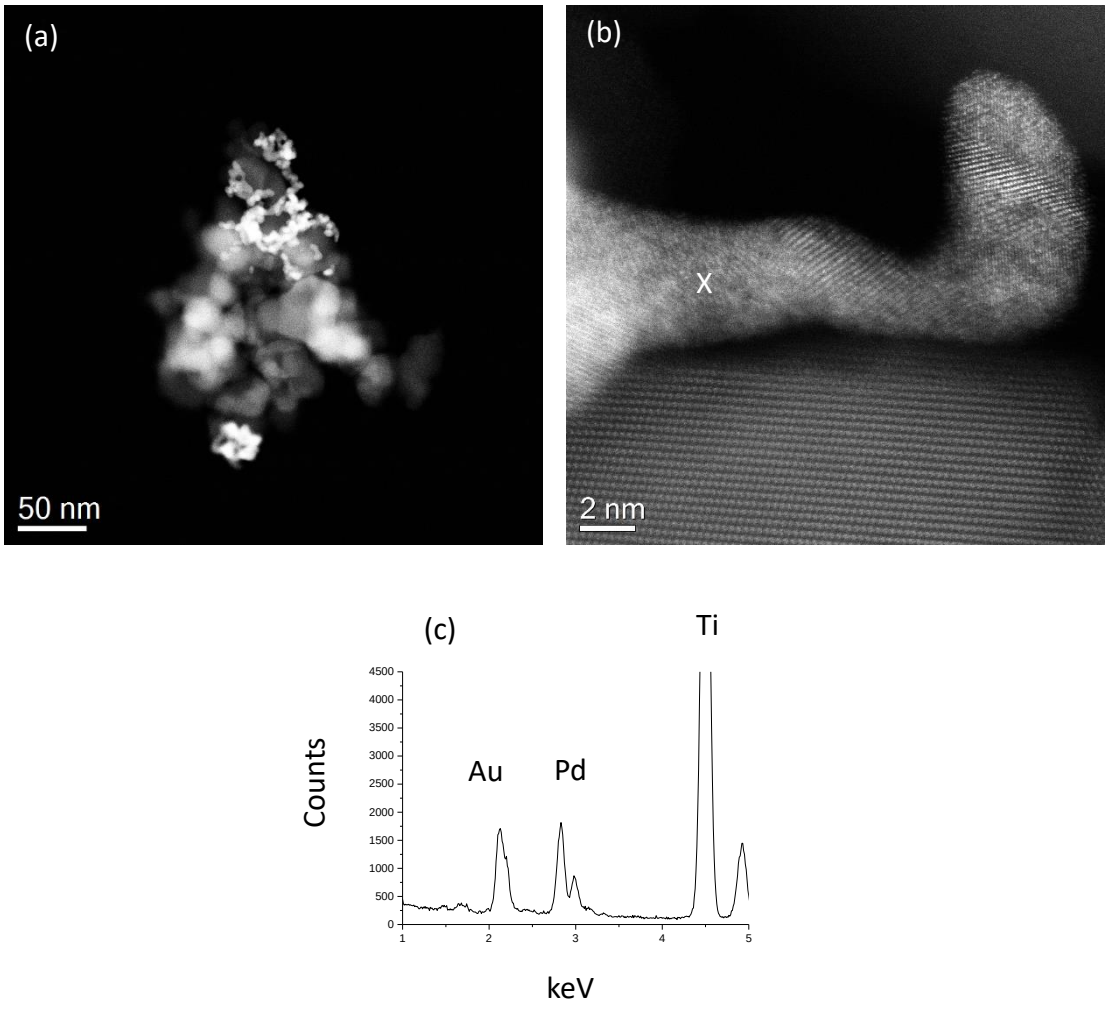


**Figure 4-9 - Representative HAADF-STEM images of optimised 0.5 wt% Pd 0.5 wt% Au/$TiO_2$ catalyst at (a) low and (b) high magnification. Representative EDX spectrum of PdAu nanostructure at point X (c).**

Au nanochains have previously been investigated for their unusual magnetic and optical properties by a number of groups. Kamat *et al.* previously prepared Au nanochains for optical applications using an analogous method to the colloidal preparation used in this work.[36] Similar to this work, the nanoparticles were prepared from the solution phase reduction of the gold precursor $HAuCl_4$ in the presence of polymeric stabiliser and were found to spontaneously self assemble into linear non-branching chain structures. Critically, the preparation yielded Au nanorods rather than spherical particles with the authors suggesting that the linear assembly is a consequence of the stabiliser preferentially wrapping the diameter of the rods, leaving the ends of the rods free to assemble end to end. Fu *et al.* previously prepared monometallic Pd nanochain catalysts with morphology closely resembling the structure of the catalyst presented in

Figure 4-9 in this work.[37] Time-online analysis of the colloidal structure by STEM found that in the first instance oligomeric fragments of 2-5 nanoparticles formed which upon further ageing ultimately yielded micron sized highly branched nanochain networks. This suggests that symmetrical nanoparticles, free from face specific interactions between the stabiliser and nanoparticle surface, are unable to agglomerate to form linear chains, unlike anisotropic particles such as Au nanorods.

In the case of the 0.5 wt% Pd 0.5 wt% Au/$TiO_2$ catalyst presented in

Figure 4-9, the length of the nanostructures also varied considerably; the minimum chain length was 30 nm whilst structures larger than 300 nm were also observed. Owing to the low loading of the catalysts and the variable size of the nanostructures, clean support particles were commonly observed indicating that the composition of the bulk catalyst material varies. In addition, no discrete nanoparticles were observed on the surface of the support indicating that the parent PdAu nanoparticles are entirely incorporated into the metal nanostructure.

STEM-EDX was carried out to determine the composition of the metallic nanostructures. The spherical geometry of the parent PdAu nanoparticles precludes anisotropic effects from being responsible for the formation of the nanochain agglomerate structure in the colloidal phase. The self assembly of the nanoparticles could instead be a compositional effect in which the structures form from the contact of monometallic regions of Au or Pd of two particles to minimise surface energy. The recorded point EDX spectrum of a $TiO_2$ supported PdAu nanochain structure is shown in

Figure 4-9(c) The spectrum shows that the surface composition at the given point is consistent of the 1:1 Pd:Au bulk metal loading. This agrees with previous work by Kiely and co-workers who showed that the simultaneous reduction of Pd and Au precursors used for preparing PdAu/$TiO_2$ catalysts by conventional sol immobilisation results in the formation solely of alloyed PdAu nanoparticles.[13] EDX mapping was also undertaken to determine the homogeneity of PdAu alloy across the surface of a typical metal nanostructure. EDX maps corresponding to the Lα edge of Pd and M edge of Au are presented in Figure 4-10(c) and (d) respectively. The intensity of the Pd and Au signals vary in tandem across the metal structure indicating that the PdAu surface composition of the metal nanostructures is constant and therefore the composition could not be responsible for the self-assembly of the nanoparticles.

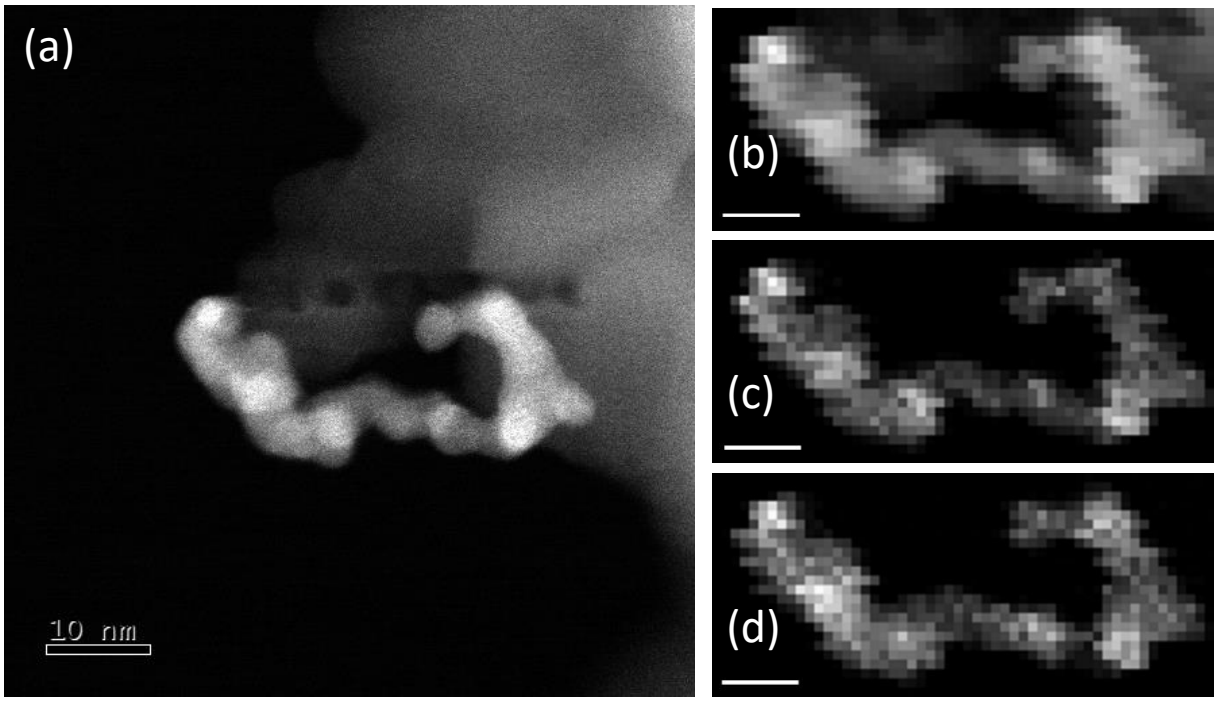


**Figure 4-10 - Representative STEM-HAADF image of 0.5 wt% Pd 0.5 wt% Au/$TiO_2$ $NH_3BH_3$ 0.8eq PVP (a). STEM-HAADF image of EDX acquisition area (b) and EDX maps corresponding to Au M (2.0-2.5eV) (c) and Pd L$\alpha$ edge (2.7-3.2eV) (d). Scale bars representative of 10 nm.**

The nanochain structure of the $NH_3BH_3$ reduced 0.5 wt% Pd 0.5 wt% Au/$TiO_2$ catalyst could be a consequence of the substoichiometric amount of PVP used during preparation. In the absence of sufficient stabiliser, some portion of the surface of the resultant nanoparticles remains uncovered, and the agglomeration of these nanoparticles through these surfaces would represent a favourable reduction in surface energy. Zheng *et al.* previously reported the preparation of structured nanochain Pd catalysts for formic acid electrooxidation.[38] In parallels to the synthetic methodology used in this work the catalysts were prepared through the chemical reduction of palladium chloride using sodium borohydride at 0°C. Rather than using polymeric stabilisers, the preparation utilised the non-ionic surfactant octylphenol ethoxylate, which itself self assembles in aqueous solution to minimise the interfacial energy between the hydrophobic octylphenol group and water. The chain structure of the final catalyst is attributed by the authors to the coordination of the Pd precursor to this surfactant structure, which yields nanostructured agglomerates upon reduction.

Unlike octylphenol ethoxylate, polyvinylpyrollidone, which was used as a nanoparticle stabiliser in this work, does not self assemble in water, and therefore could not provide such a structure for the precursor to interact with and direct the formation of the nanochains. Nonetheless, the activity of the catalysts reported by Zheng *et al.* show many similarities with

the activity data presented in Section 4.3.3. In agreement with the catalysts presented in this work, preparation at higher temperature resulted in more poorly defined nanochain structures which translated into a decrease in catalyst activity. Similarly, preparing the monometallic Pd nanochains using reductants such as hydrazine or ascorbic acid also resulted in varied catalyst performance and metal nanostructuring.

#### *4.3.9.2. Tomographic STEM of Optimised 0.5 wt% Pd 0.5 wt% Au/$TiO_2$*

Inspection of the 0.5 wt% Pd 0.5 wt% Au/$TiO_2$ catalyst presented in

Figure 4-9 by STEM-HAADF found that in many cases significant portions of the nanochains were free of contact with the support, instead being held in place through contact with neighbouring particles on the chain structure. The catalyst was further investigated using tomographic STEM to evaluate the frequency and extent of tethered, unsupported nanochains on the catalyst support. STEM-HAADF images of a representative nanochain at various angles are presented in Figure 4-11.

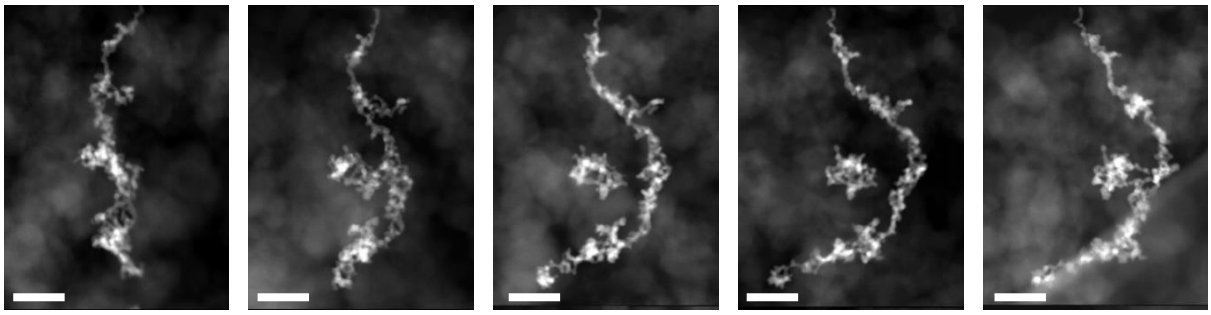

**Figure 4-11 - Tomographic STEM-HAADF images of 0.5 wt% Pd 0.5 wt% Au/$TiO_2$ $NH_3BH_3$ 0.8eq PVP. Scale bars representative of 100 nm.**

Upon rotation, the image is comprised of two agglomerate structures that overlap in the plane of the original image. Furthermore, one of the agglomerate structures is in the form of a 'collapsed chain' – in which the chain folds up upon itself such that the centre of the structure is partially hollow. Importantly, 100 nm lengths of the nanochain structure are bound only to neighbouring parent nanoparticles and free from metal-support interaction. It may be that the unsupported lengths of PdAu nanochains are responsible for the high selectivity of the catalysts prepared by modified sol immobilisation in comparison to well dispersed PdAu catalysts previously reported by Hutchings and co-workers.[15]

*4.3.9.3.0.5 wt% Pd 0.5wt% Au/$TiO_2$ Catalysts Prepared with Varying Stabiliser Equivalents*

The 0.5 wt% Pd 0.5 wt% Au/$TiO_2$ catalyst prepared in the presence of superstoiciometric quantities of PVP was also investigated by STEM-HAADF to determine whether the formation of nanochains was a result of PVP concentration. The catalyst prepared in the presence of 1.5 equivalents of PVP also forms chain nanostructures, however in comparison to the optimised catalyst, minimum chain length was supressed as indicated in Figure 4-12.

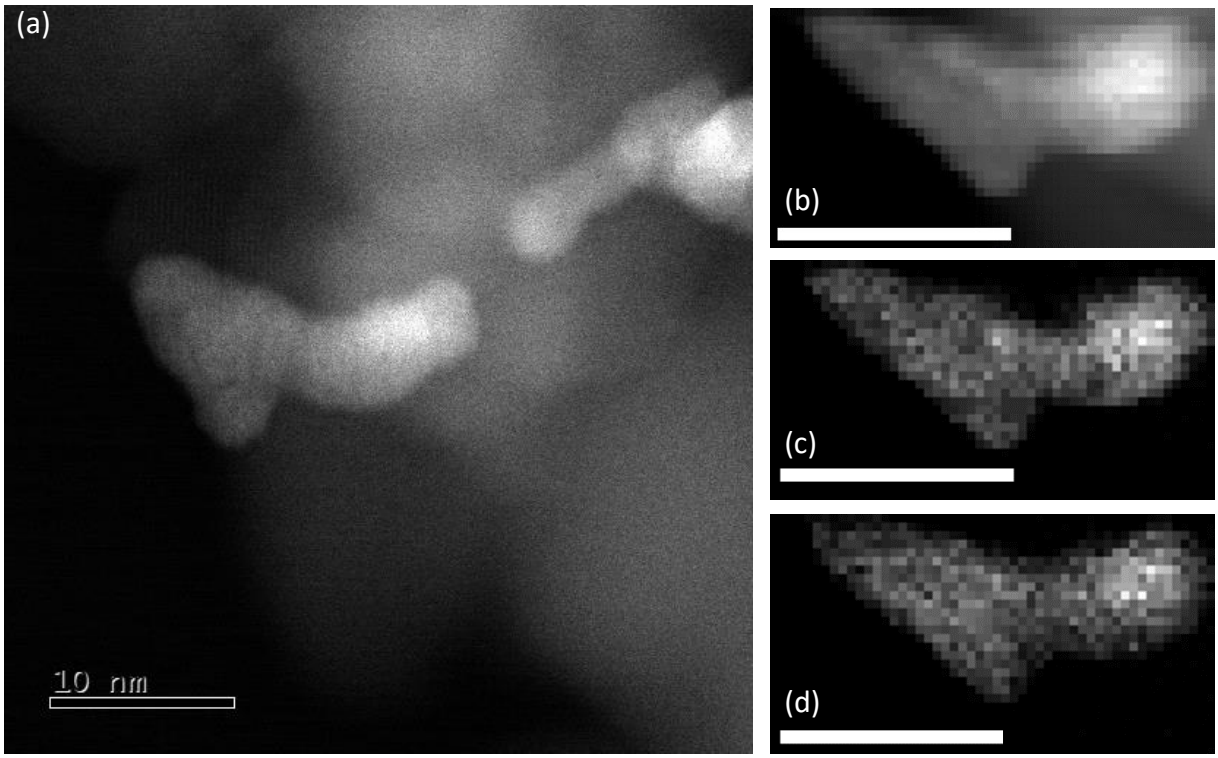


**Figure 4-12 - Representative STEM-HAADF image of metal nanostructuring present in 0.5 wt% Pd 0.5 wt% Au/$TiO_2$ $NH_3BH_3$ 1.5eq PVP(a). STEM-HAADF image of edx acquisition area (b) and EDX maps corresponding to Au Lα (2.0-2.5eV) (c) and Pd Lα Edge (2.7-3.2eV) (d). Scale bars representative of 10 nm.**

Chains as short as 10 nm were observed, corresponding to the agglomeration of a small number of particles. The formation of chain agglomerates in the presence of sufficient stabiliser to fully encapsulate the spherical parent PdAu nanoparticles indicates that stabiliser concentration alone is not responsible for the formation of the nanochain agglomerates. Agarwal *et al.* previously reported the preparation of PVP stabilised PdAu colloids for methane oxidation.[39] Similar to the optimised 0.5 wt% Pd 0.5 wt% Au/$TiO_2$ presented in this work, the author's catalysts were prepared by sol immobilisation using substoichiometric quantities of PVP, albeit using sodium borohydride rather than hydrazine. Interestingly, Argawal *et al.* found that the resultant catalysts contained well dispersed PdAu nanoparticles

of 3.7 nm average diameter. This suggests that the formation of structured agglomerates in the catalysts presented in this work is dependent on the nature of the reductant rather than the concentration of stabiliser.

The 0.5 wt% Pd 0.5 wt% Au/$TiO_2$ catalyst prepared in the presence of high concentration of PVP was also analysed using EDX mapping. Pd and Au were homogenously dispersed across the surface of the metal nanostructure, consistent with the optimised PdAu catalyst prepared using lower concentrations of PVP, indicating that the surface composition of the two catalysts is comparable, despite showing different activities for hydrogen peroxide synthesis and hydrogenation.

#### *4.3.10.X-Ray Photoelectron Spectroscopy (XPS) of PVP Stabilised PdAu Catalysts Prepared by Modified Sol Immobilisation*

The PVP stabilised PdAu catalysts prepared by modified sol immobilisation were also interrogated by x-ray photoelectron spectroscopy (XPS). XPS can be used to determine the surface elemental composition and oxidation state of a catalyst surface. The electron microscopy data presented in Section 4.3.9 indicates that for the optimised PdAu catalyst, the nanostructure is homogenously alloyed. The variation in activity of the catalysts prepared using different reductants at different temperatures could however be due to variations in Pd/Au surface composition, which can be accurately measured using XPS.

##### *4.3.10.1.0.5 wt% Pd 0.5 wt% Au/$TiO_2$ Catalysts Prepared Using Different Reductants At 0, 25 and 60 °C*

The chemical composition of the PVP stabilised catalysts was investigated by x-ray photoelectron spectroscopy (XPS). The 0.5 wt% Pd 0.5 wt% Au/$TiO_2$ catalysts (Section 4.3.3), prepared using varying reductants at various temperatures, were interrogated by XPS to determine whether the hydrogenation activity, and therefore selectivity, was a consequence of variations in the surface composition of the materials. Detailed scans of the Au(4f) and Pd(3d) regions are shown in Figure 4-13 and Figure 4-14 respectively.

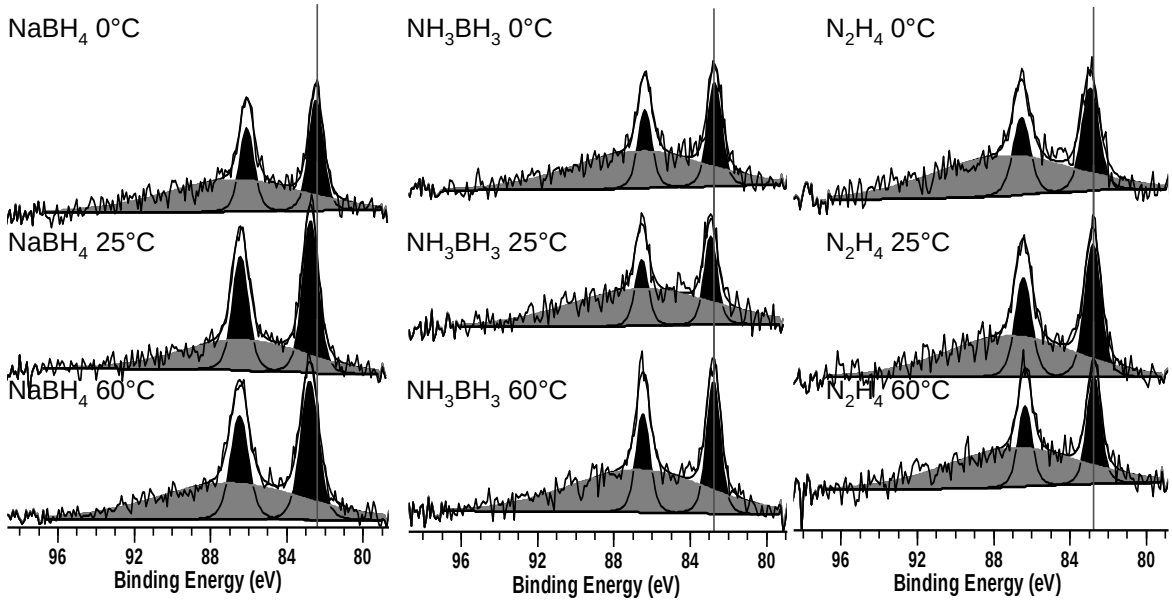


**Figure 4-13 - Au(4f) XPS spectra of 0.5 wt% Pd 0.5 wt% Au/TiO prepared using $NaBH_4$, $NH_3BH_3$ and $N_2H_4$ At 0, 25 and 60°C. Grey shading indicative of Ti loss structure, black shading Au(4f) signal.**

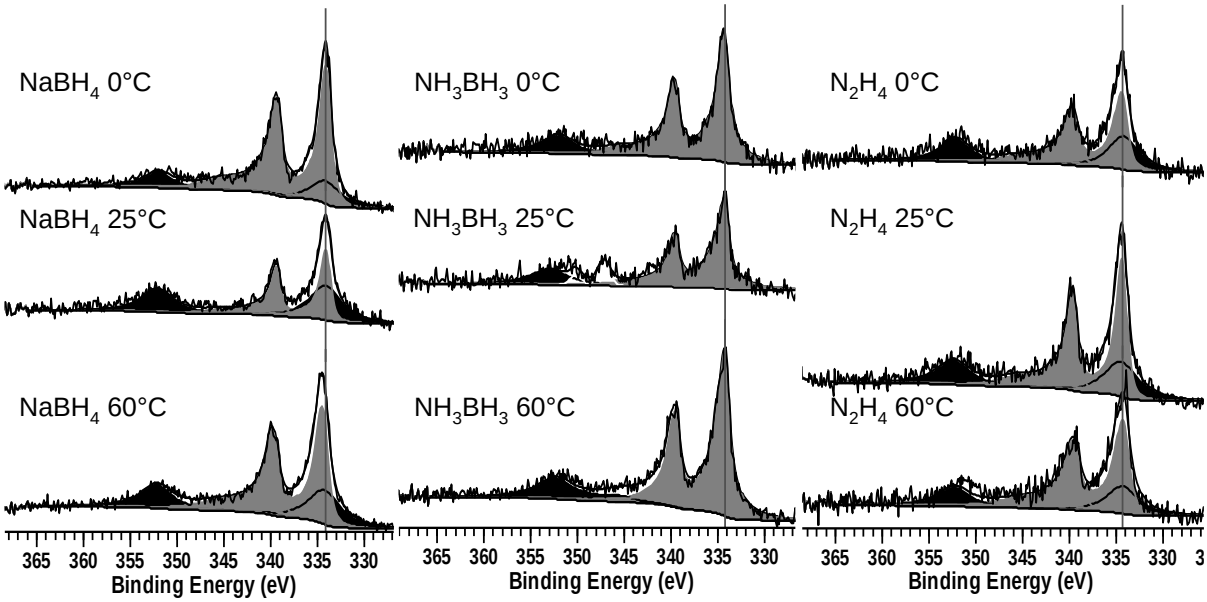


**Figure 4-14 - Pd(3d) XPS spectra of 0.5 wt% Pd 0.5 wt% Au/TiO prepared using $NaBH_4$, $NH_3BH_3$ and $N_2H_4$ At 0, 25 and 60°C. Grey and black shading representative of Pd(3d) and Au(4d) components.**

The Pd(3d) binding energy varies between 339.4 and 334.5 eV, consistent with Pd(0) binding energies previously reported for PdAu/$TiO_2$ catalysts.[40] Pd(II) was not detected in any catalyst, indicating that the Pd precursor was fully reduced during preparation and that the catalyst was resistant to re-oxidation between preparation and characterisation. Au(4f) binding energies vary between 82.4 and 83.0 eV, comparable to previously reported binding energies for Au(0) found in PdAu/$TiO_2$ bimetallic catalysts.[3] These values are lower than that of Au(0) foil, which has previously been attributed to charge transfer between Au and the $TiO_2$ surface in the case of supported Au containing nanoparticles.[41]

Binding energy shifts are typically associated with a change in electronic structure or coordination environment. The similarity of both the Pd(3d) and Au(4f) binding energies between catalysts suggest that there are minimal differences in Pd surface oxidation and coordination state and therefore this cannot be responsible for the activity improvement observed in catalysts prepared at lower temperatures. Indeed, no discernible trend in binding energy can be deduced based on either reductant or temperature, suggesting that preparation conditions have little effect on final Pd or Au oxidation state.

The surface composition and PdAu ratios of the catalysts were also determined using XPS, and the results are presented in Table 4-1. The Pd and Au surface concentrations varied wildly between catalysts, with Pd surface concentration between 0.12 and 0.44 at%, whilst Au concentration is between 0.07 and 0.15 at%. In Section 4.3.9.1 it was shown by STEM that the optimised 0.5 wt% Pd 0.5 wt% Au/$TiO_2$ catalysts form chain-like agglomerate nanostructures, and that due to size of the agglomerates and low metal loading of the catalysts, naked support particles were commonly observed. The poor dispersion of the metal nanostructure accounts for the large variation in XPS derived Pd and Au surface concentrations, due to the static collection of the XPS spectra from 400 µm spots on each catalyst sample. It can therefore be suggested that the inhomogeneity of the supported catalysts results in sampling from metal-rich and metal-poor surfaces during XPS data collection, causing changes in the relative Pd and Au surface concentrations.

**Table 4-1 - Tabulated XPS derived surface concentrations of Pd, Au, Ti, O and C of 0.5 wt% Pd 0.5 wt% Au/$TiO_2$ Catalysts Prepared Using $NH_3BH_3$, $NaBH_4$ and $N_2H_4$ At 0, 25 and 60 °C.**

| Catalyst | | XPS Derived Concentration (at%) | | | | | Pd/Au Ratio |
|---|---|---|---|---|---|---|---|
| Reductant | Temperature (0°C) | Pd | Au | Ti | O | C | |
| $NH_3BH_3$ | 0 | 0.3 | 0.1 | 28.23 | 65.67 | 5.7 | 3 |
| | 25 | 0.23 | 0.07 | 27.52 | 64.03 | 8.22 | 2.4 |
| | 60 | 0.19 | 0.07 | 27.69 | 65.56 | 6.48 | 2.7 |
| $NaBH_4$ | 0 | 0.37 | 0.15 | 26.81 | 64.08 | 8.61 | 2.5 |
| | 25 | 0.16 | 0.13 | 28.08 | 65.11 | 6.53 | 1.2 |
| | 60 | 0.44 | 0.1 | 27.62 | 65.18 | 6.67 | 4.4 |
| $N_2H_4$ | 0 | 0.17 | 0.05 | 28.04 | 65.86 | 5.88 | 3.4 |
| | 25 | 0.2 | 0.09 | 27.74 | 65.18 | 6.78 | 2.2 |
| | 60 | 0.12 | 0.07 | 28.43 | 65.64 | 5.74 | 1.7 |

The XPS derived Pd/Au surface ratio varies considerably between 1.2 for the $NaBH_4$-20 °C and 4.4 for the $NaBH_4$-60 °C samples. In the case of either $NH_3BH_3$ or $NaBH_4$ reduced catalysts, increasing the preparation temperature from 0 to 25 °C resulted in a decrease in Pd/Au surface ratio and therefore more Au rich surfaces. Further increase in temperature to 60 °C however resulted in an increase, which cannot be entirely explained. In comparison, the $N_2H_4$ reduced catalysts have decreased Pd/Au surface ratio with increasing preparation temperature, falling from 3.4 at 0 °C to 1.7 at 60 °C. The inverse relationship between the Pd/Au surface ratio and preparation temperature observed for the $N_2H_4$ reduced catalysts indicates that preparation at low temperatures results in Pd enrichment of the active metal surface.

The nature of the Pd active site for hydrogen peroxide synthesis has been previously thoroughly explored, in particular the role of Au in bimetallic catalysts. Menegazzo *et al.* prepared PdAu/$ZrO_2$ catalysts of varying composition by deposition-precipitation and wet impregnation for the direct synthesis of hydrogen peroxide, and found that the Pd/Au ratio varied significantly by particle size.[42] Alteration of the bulk Pd/Au ratio resulted in shifting of the compositional surface ratios with smaller particles being Pd rich and larger particles Pd lean. The catalyst with a 2:1 Pd:Au mole ratio was most active and selective for hydrogen peroxide synthesis, with 1:2 Pd:Au and 1:1 Pd:Au catalysts performing poorly in comparison.

In Section 4.3.9.1, it was observed by STEM-EDX that Pd and Au are evenly distributed throughout the bimetallic nanostructuring of the PVP stabilised catalysts. As a result, it should be considered that, although the concentrations of Au and Pd may not be indicative of their bulk concentration, the ratio between them remains constant between the bulk and the surface. The low catalyst loading however makes the uncertainty in these values particularly large due to the overlap of the Pd(3d) and Au(4d) peaks and low signal to noise ratio.

#### *4.3.10.2.Reuse of $TiO_2$ and C supported PdAu Catalysts Prepared by Modified Sol Immobilisation*

In Section 4.3.8, it was presented that the $TiO_2$ supported catalyst deactivate upon reuse with hydrogen peroxide synthesis activity decreasing from 80 to 61 mol$H_2O_2$/h/$kg_{cat}$. This was accompanied with an increase in hydrogenation activity from 0 to 160 mol$H_2O_2$/h/$kg_{cat}$, indicating that the selectivity of the catalyst decreases upon reuse. In comparison the XC72R carbon supported catalyst was stable over two reuses with synthesis activity falling from 82 to 81 mol$H_2O_2$/h/$kg_{cat}$, and hydrogenation activity remaining at 0 mol$H_2O_2$/h/$kg_{cat}$. The fresh and used $TiO_2$ and XC72R supported catalysts were examined by XPS to determine whether catalyst deactivation was a result of changing in surface composition or the stabilising effect of the support. Au(4f) and Pd(3d) XPS scans of fresh and used 0.5 wt% Pd 0.5 wt% Au/$TiO_2$ are presented in Figure 4-15. The Pd(3d) binding energy of the fresh and used catalyst are 334.4 and 334.0 eV and the Au(4f) signals 82.6 and 82.7 eV, respectively. These values are consistent with binding energies previously reported by Pritchard *et al.* for PdAu/$TiO_2$ catalysts prepared by conventional sol immobilisation prior to use.[15] These binding energies are indicative of Pd(0) and Au(0) species, suggesting that the active metal surface resists oxidation during reaction.

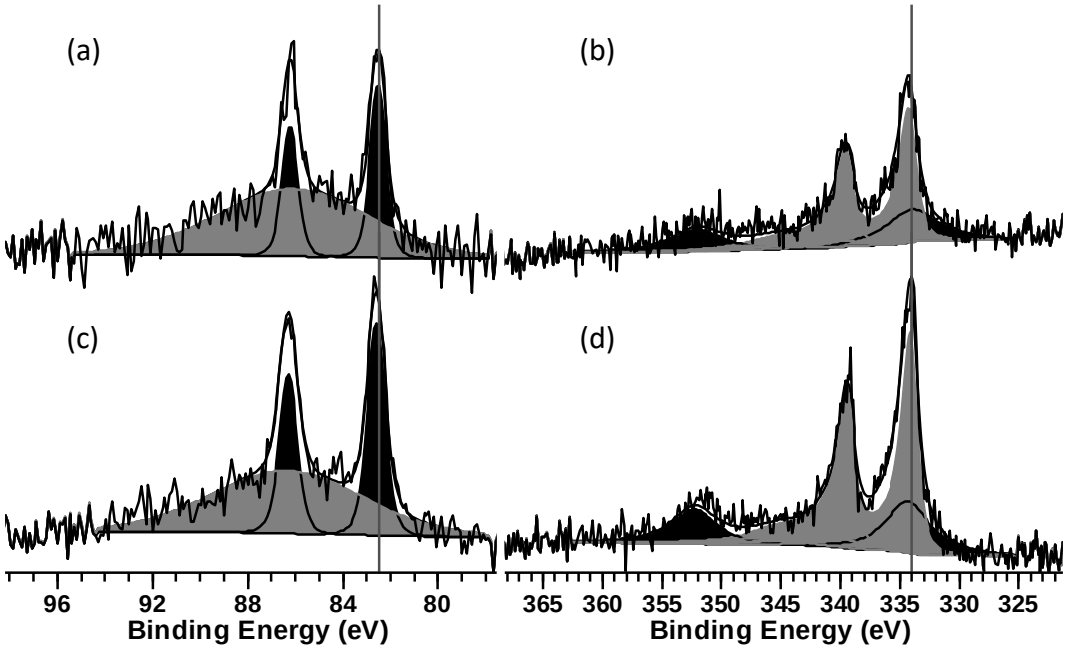


**Figure 4-15 - Au(4f) XPS spectra of fresh (a) and used (c) 0.5 wt% Pd 0.5 wt% Au/$TiO_2$. Grey shading indicative of Ti loss structure. Pd(3d) XPS Spectra of fresh (b) and used (d) 0.5 wt% Pd 0.5 wt% Au/$TiO_2$. Grey and black shading representative of Au(4f) and Pd(3d) components respectively.**

The effective elemental surface concentrations of the fresh and used catalysts are presented in Table 4-2. In the case of the $TiO_2$ supported catalyst, the surface concentration of Pd fell from 0.24 to 0.16 at% upon reuse. Similarly, Au concentration fell from 0.09 to 0.06 at%. Catalysts prepared by sol immobilisation are known to typically deactivate through leaching of soluble Au and Pd species into the reaction mixture. The decrease in metal surface concentration upon reuse of the catalysts is consistent with this scenario.[12] Leaching of the active metal species may be further exacerbated by reaction conditions. Panpranot and co-workers found that deactivation of a Pd/$SiO_2$ catalyst was worsened considerably in reactions undertaken in pressurised $CO_2$. The authors consider that the deactivation of the Pd/$SiO_2$ is a result of increased metal leaching is due to the equilibrium between $CO_2$ and carbonic acid resulting in acidification of the reaction mixture hastens Pd dissolution[43] Similar conditions are used in this work, as $CO_2$ was used as a diluent gas to safely mix hydrogen and oxygen outside the explosive limit. This indicates that the stability of these catalysts could be improved through the use inert gasses such as nitrogen or argon as the diluent which would not alter the pH of the reaction mixture and therefore minimise metal leaching.

In Section 4.3.8, it was shown that the hydrogenation activity of the optimised 0.5 wt% Pd 0.5 wt% Au/$TiO_2$ catalyst increased upon reuse. It would be considered conventionally that deactivation through leaching would result in a decrease in activity for all reactions, especially in the case of a single site catalyst. Given the interrelation between the hydrogen peroxide synthesis and hydrogenation pathways, the fall in synthesis activity could in fact be considered a 'reactivation' of the hydrogenation pathway. As a result, the catalyst is no longer stable to formed hydrogen peroxide and decomposes the product over the course of the reaction. The increase in hydrogenation activity of the $TiO_2$ supported catalyst upon reuse may be attributed to the leaching of the metal surface revealing a fresh metal surface which is active for hydrogenation. The Pd/Au surface ratio of the $TiO_2$ supported catalyst remains the same before and after reuse, which indicates that the reactivation of the hydrogenation pathway in the used catalyst is not due to changes in metal surface composition. Alternatively, reprecipitation of leached Pd and Au onto the surface of the support, creating sites active for hydrogenation. Pd and Au were both found to have a similar affinity to be leached, as their surface concentrations were found to both fall by 30 %. Therefore, it could be considered that, although the bulk metal composition remains constant, the increase in hydrogenation activity is a result of local imbalances in Pd/Au ratio, forming Pd rich sites that are highly active for hydrogen peroxide hydrogenation.

**Table 4-2 - Tabulated XPS derived surface concentrations of Pd, Au, Ti, O and C of $TiO_2$ and XC72R carbon supported 0.5 wt% Pd 0.5 wt%Au catalysts before and after reuse**

| Support | Use | XPS Derived Concentration (at%) | | | | | Pd/Au Ratio | Pd Oxidation State (%) | |
|---|---|---|---|---|---|---|---|---|---|
| | | Pd | Au | Ti | O | C | | Pd(0) | Pd(II) |
| $TiO_2$ | Fresh | 0.24 | 0.09 | 23.01 | 55.73 | 20.85 | 2.7 | 100 | 0 |
| | First | 0.16 | 0.06 | 15.99 | 45.41 | 38.22 | 2.7 | 100 | 0 |
| XC72R | Fresh | 0.08 | 0.03 | - | 5.47 | 94.4 | 2.7 | 75 | 25 |
| | First | 0.09 | 0.03 | - | 4.25 | 95.61 | 2.5 | 80 | 20 |
| | Second | 0.08 | 0.03 | - | 7.24 | 92.64 | 2.7 | 78 | 22 |

The stable XC72R supported PdAu catalysts were also investigated by XPS. The Pd(3d) and Au(4f) scans are presented in Figure 4-16. The Pd(3d) binding energy remains roughly constant upon reuse with a binding energy of 334.6 eV, versus 334.8 eV for the fresh sample. Likewise, the Au(4f) binding energy was found to decrease negligibly from 83.4 to 83.3 after reuse. This suggests that the oxidation and coordination state of the Pd and Au environments

remains constant across multiple reactions. In contrast to the $TiO_2$ supported catalyst, the atomic surface concentrations of Pd and Au for the XC72R supported catalyst, and therefore Pd/Au ratio, remained unchanged after reuse, suggesting that the catalyst is resistant to leaching.

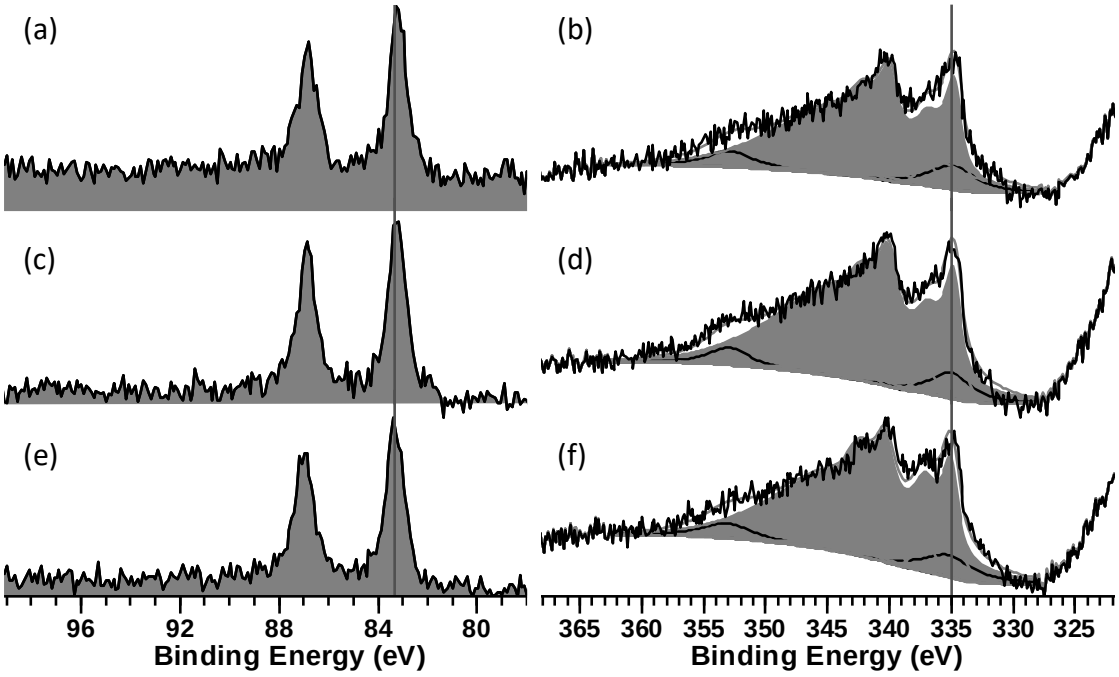


**Figure 4-16 Au(4f) and Pd(3d) XPS spectra of 0.5 wt% Pd 0.5 wt% Au/C fresh (a, b) and after first (c, d) and second (e, f) reuse. Au(4d) component represented in Pd(3d) scans by black line.**

Interestingly, the XC72R supported PdAu catalyst contains both Pd(0) and Pd(II) in an approximately 4:1 ratio. In contrast, all the $TiO_2$ supported PdAu catalysts presented in this work contain Pd and Au exclusively in the metallic state. Furthermore, the Pd(0)/Pd(II) ratio remains roughly constant across two reuses. This provides possible explanations for the catalysts' unusual activity and stability. Pd(II) sites are known to be considerably less active for hydrogen peroxide hydrogenation than monometallic Pd(0) species, and therefore more selective towards hydrogen peroxide synthesis.[44] Centomo *et al.* have previously examined resin supported Pd catalysts using in-situ XAFS for direct hydrogen peroxide synthesis, and found that mixed Pd(0)/Pd(II) catalysts were considerably more stable towards leaching than those containing pure Pd(0) phases; such an effect could be responsible for the improved stability found in our work.[45]

The presence of Pd(II) in PdAu bimetallic catalysts has also previously been attributed to the formation of monometallic PdO species.[46,47] The formation of PdO phases is inconsistent with

the STEM data presented in Section 4.3.9, which found that for in all cases, Pd and Au were observed to be homogenously alloyed across the surface of the metallic nanostructure. Furthermore, supported PdO nanoparticles are known to be more active for hydrogen peroxide hydrogenation than PdAu bimetallic nanoparticles, whilst in this work the only Pd(II) containing catalyst is shown to be inactive towards hydrogen peroxide hydrogenation.[48]

## *4.4. Alternative Stabilisers for Modified Sol Immobilisation PdAu Catalysts For The Direct Synthesis Of Hydrogen Peroxide*

### *4.4.1. The Effect of Varying Stabiliser on Supported PdAu Catalysts*

Given the large variation in hydrogen peroxide synthesis and hydrogenation activity of the PVP stabilised PdAu catalysts, $TiO_2$ supported catalysts were prepared using PVA and PAA to determine whether the activity of the catalysts is dependent upon the nature of the colloidal stabiliser.

### *4.4.2. PAA Stabilised PdAu/$TiO_2$ Catalysts*

0.5 wt% Pd 0.5 wt% Au/$TiO_2$ catalysts were prepared with varying metal precursor-PAA ratio using the optimal conditions identified previously in Section 4.3.3 for the preparation of PVP stabilised catalysts (0°C, $NH_3BH_3$ as reductant). The hydrogen peroxide synthesis and hydrogenation activities of these catalysts are shown in Figure 4-17. The stabiliser free catalyst is the most active catalyst for hydrogen peroxide synthesis and hydrogenation, 140 and 800 mol$H_2O_2$/h/$kg_{cat}$ respectively. Consistent with the trend observed for PVP stabilised catalysts in Section 4.3.4, the addition of increasing stabiliser concentrations during preparation results in catalysts that are less active for both the direct synthesis and hydrogenation reactions.

The hydrogen peroxide synthesis activity of the stabilised catalyst increases with increasing PAA content, from 78 in the presence of 0.5 eq PAA to 130 for 1.2 eq PAA. Conversely, the hydrogenation activity also decreases regularly with increasing PAA content, from 400 to 0 mol$H_2O_2$/h/$kg_{cat}$. This is especially surprising given that PAA is known to be a highly effective stabiliser for colloidal preparation and typically yields smaller nanoparticles than either PVP or PVA.[18] If size effects were responsible for the activity of these catalysts, as proposed by Tian *et al.*, it follows that increasing PAA content should result in increased hydrogenation activity also due to the presence of smaller, more active nanoparticles.

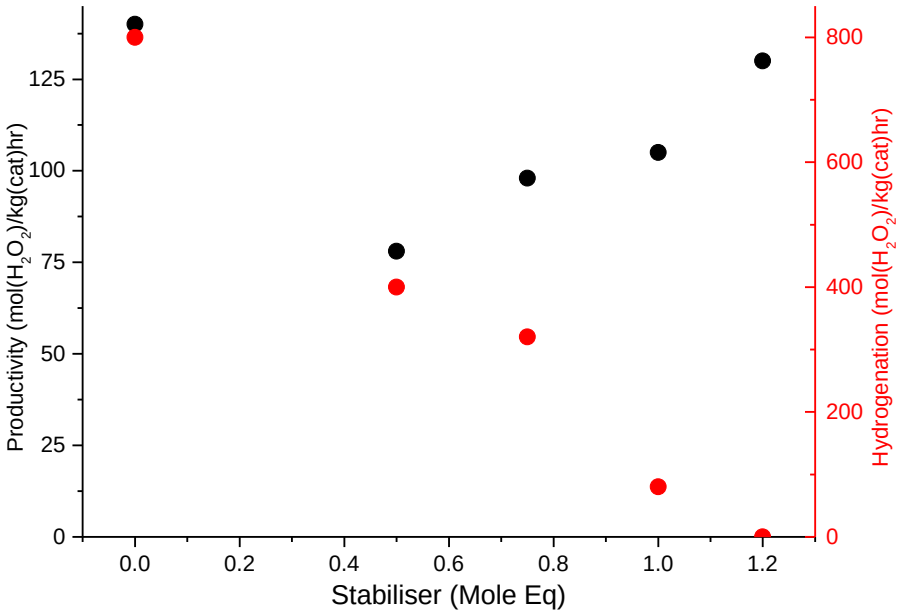


**Figure 4-17 - Hydrogen Peroxide Synthesis (●) And Hydrogenation Activity (●) of 0.5 wt% Pd 0.5 wt% Au/$TiO_2$ Prepared With Varying PAA-Metal Ratio.**

**Reaction Conditions – Hydrogen peroxide synthesis: 5 % $H_2/CO_2$ (2.9 MPa) and 25 % $O_2/CO_2$ (1.1 MPa), 8.5 g solvent (2.9 g $H_2O$, 5.6 g MeOH) 0.01 g catalyst, 2 °C, 1200 rpm, 30 min. Hydrogen peroxide hydrogenation: 5 % $H_2/CO_2$ (2.9 MPa), 8.5 g solvent (2.22 g $H_2O$, 5.6 g MeOH and 0.68 g 50 wt% $H_2O_2$), 0.01 g catalyst, 2 °C, 1200 rpm, 30 min.**

Previously, the presence of acid in reaction has been shown to greatly influence hydrogen peroxide hydrogenation activity. It has been found that the presence of solution phase acids greatly reduces the hydrogen peroxide hydrogenation activity of supported catalysts and this effect has been further extended to the surface functionalisation of heterogeneous materials.[49,50] It is therefore reasonable to suggest that owing to the weakly acidic nature of PAA, the presence of increasing amounts of PAA after preparation results in decreased hydrogenation activity through interaction with the active metal surface of the catalyst.

To investigate this, reactions were undertaken using a 0.5 wt% Pd 0.5 wt% Au/$TiO_2$ catalyst prepared by conventional impregnation with the addition of extra PAA in the reaction solution. The hydrogen peroxide synthesis and hydrogenation activity of the catalyst in the presence of 0-5 metal equivalents of PAA are shown in Figure 4-18. The catalyst exhibits synthesis and hydrogenation activities of 80 and 400 mol$H_2O_2$/h/$kg_{cat}$ in the absence of PAA and, upon addition of 1 eq PAA, synthesis activity drops marginally to 72 whilst hydrogenation activity decreases considerably to 215 mol$H_2O_2$/h/$kg_{cat}$. Addition of two equivalents of PAA results in a further decrease in synthesis activity to 65 mol$H_2O_2$/h/$kg_{cat}$, which was accompanied by a deactivation of the hydrogenation pathway.

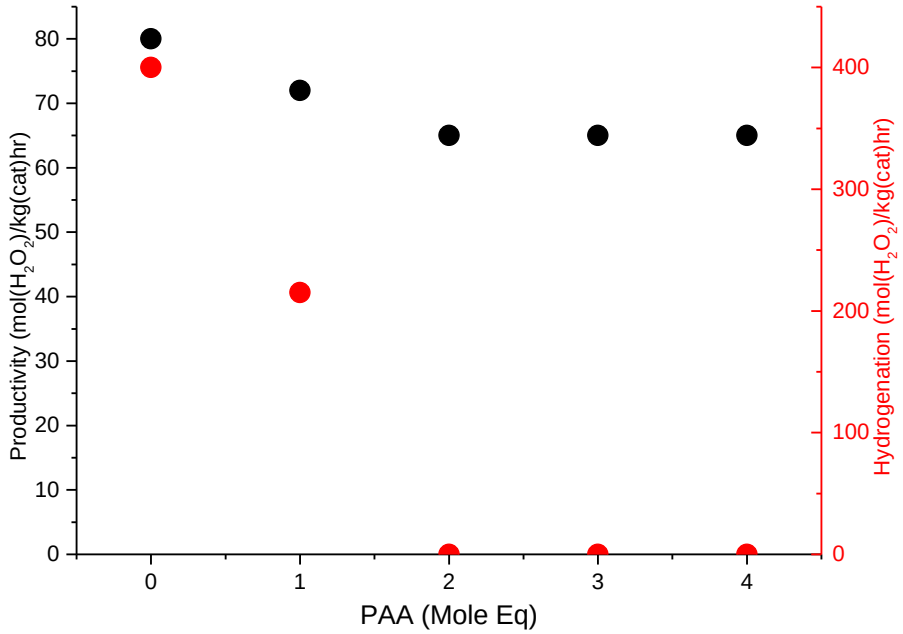


**Figure 4-18 – Hydrogen peroxide synthesis (●) and hydrogenation activity (●) of 0.5 wt% Pd 0.5 wt%Au/$TiO_2$ in the presence of additional solution phase PAA.**
**Reaction Conditions – Hydrogen peroxide synthesis: 5 % $H_2/CO_2$ (2.9 MPa) and 25 % $O_2/CO_2$ (1.1 MPa), 8.5 g solvent (2.9 g $H_2O$, 5.6 g MeOH) 0.01 g catalyst, 2 °C, 1200 rpm, 30 min. Hydrogen peroxide hydrogenation: 5 % $H_2/CO_2$ (2.9 MPa), 8.5 g solvent (2.22 g $H_2O$, 5.6 g MeOH and 0.68 g 50 wt% $H_2O_2$), 0.01 g catalyst, 2 °C, 1200 rpm, 30 min.**

The addition of increasingly large amounts of PAA, three or four equivalents, results in no further improvement in catalytic activity as synthesis and hydrogenation activity remains constant at 65 and 0 mol$H_2O_2$/h/$kg_{cat}$ respectively.

Consideration of the data presented in Figure 4-17 and Figure 4-18 suggests that multiple factors are responsible for the remarkable activity of the PAA stabilised PdAu/$TiO_2$ catalyst. It is well documented that the amount of stabiliser present during colloid preparation influences average particle size. Li *et al.* investigated the effect of PVP-Pd ratio in the preparation of catalytically active Pd colloids, and found that decreasing the ratio from 20 to 2.5 resulted in an increase in average particle size from 3.0 to 6.2 nm.[51] As such, it would be expected that by increasing the PAA-metal ratio in this work, particle size would decrease and as a result hydrogen peroxide synthesis activity would increase. Such a relationship is observed in Figure 4-17.

The presence of residual stabiliser from catalyst preparation is known to greatly affect catalytic activity, although most exclusively in a negative manner. Prati and co-workers investigated the effect of PVA on Au/$TiO_2$ catalysts for glycerol oxidation, showing that decreasing the amount of PVA from 1 to 0.125 resulted in an increase in average particle size

from 3.5 to 4.1; additionally, they found that discrete nanoparticles readily formed even in the presence of stoichiometric amounts of stabiliser.[52,53] Interestingly, the catalyst prepared using the most sparing amount of PVA in their work was the most active, and this could be attributed to active site deactivation by PVA remaining on the prepared catalyst. The synthesis and hydrogenation activity data presented in Figure 4-18 suggests that a similar effect is present in the PAA stabilised catalysts in this work. Crucially, however, PAA appears to interact more strongly with metal sites active for hydrogenation, as the hydrogenation activity falls disproportionally to the synthesis activity.

Therefore, is the role of PAA could be proposed as twofold in the preparation of catalysts in that (a) increasing amounts of PAA result in smaller particles which are more active overall and (b) increasing amounts of PAA results in more PAA remaining on the prepared catalyst, which in turn selectively poisons hydrogenation sites and therefore improves synthesis activity.

### *4.4.3. PVA Stabilised PdAu/$TiO_2$ Catalysts*

0.5 wt% Pd 0.5 wt% Au/$TiO_2$ catalysts were also prepared using varying amounts of PVA, to determine the effect of the stabiliser on supported catalysts. Figure 4-19 presents the hydrogen peroxide synthesis and hydrogenation activities of these catalysts. In Sections 4.3.4 and 4.4.1 it has been shown that the addition of either PVP or PAA during preparation resulted in a decrease in hydrogen peroxide synthesis and hydrogenation activity relative to the stabiliser free catalyst. In agreement with this observation, the catalyst prepared here in the presence of 0.5 eq PVA had a synthesis activity of 84 mol$H_2O_2$/h/$kg_{cat}$, versus 140 mol$H_2O_2$/h/$kg_{cat}$ for the stabiliser free catalyst. Interestingly, however, hydrogenation activity of the catalyst is comparable to that of the stabiliser free analogue, 780 versus 800 mol$H_2O_2$/h/$kg_{cat}$, which is approximately double that of the PVP and PAA stabilised catalysts prepared under analogous conditions, and indicates that the PVA stabilised catalyst is considerably less selective.

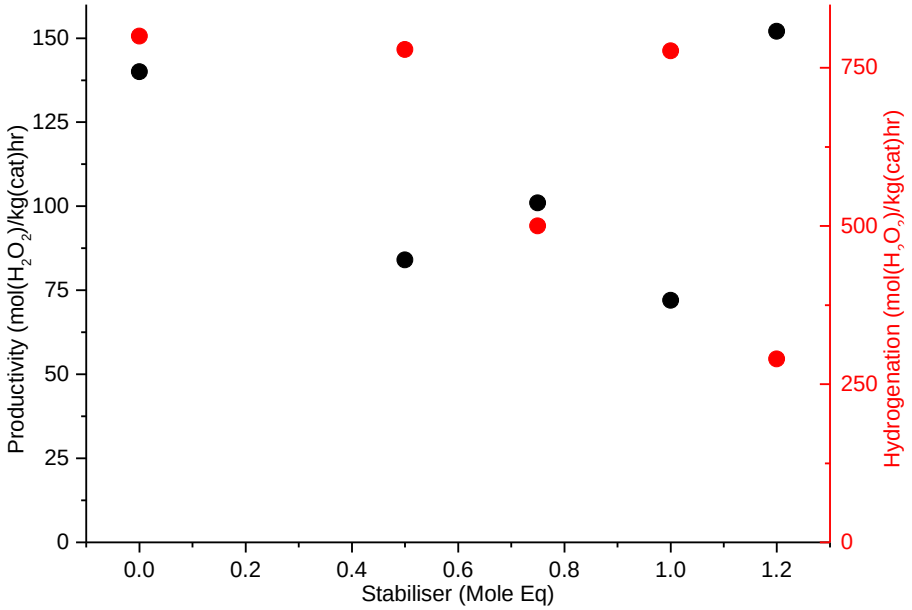


**Figure 4-19 - Hydrogen peroxide synthesis (●) and hydrogenation activity (●) of 0.5 wt% Pd 0.5 wt% Au/$TiO_2$ prepared with varying PVA-metal ratio.**
**Reaction Conditions – Hydrogen peroxide synthesis: 5 % $H_2/CO_2$ (2.9 MPa) and 25 % $O_2/CO_2$ (1.1 MPa), 8.5 g solvent (2.9 g $H_2O$, 5.6 g MeOH) 0.01 g catalyst, 2 °C, 1200 rpm, 30 min. Hydrogen peroxide hydrogenation: 5 % $H_2/CO_2$ (2.9 MPa), 8.5 g solvent (2.22 g $H_2O$, 5.6 g MeOH and 0.68 g 50 wt% $H_2O_2$), 0.01 g catalyst, 2 °C, 1200 rpm, 30 min.**

No discernible trend could be observed when increasing the PVA-metal ratio from 0.5 to 1.2. The increase from 0.5 to 0.75 results in a marginal increase in synthesis activity from 84 to 101 mol$H_2O_2$/h/$kg_{cat}$ and a decrease in hydrogenation activity to 500 mol$H_2O_2$/h/$kg_{cat}$. The catalytic activity of material prepared in the presence of 1 eq PVA was inferior to that of the 0.75 eq PVA stabiliser and comparable to that of the 0.5 eq PVA catalyst. The catalyst prepared in the presence of 1.2 eq PVA was more active for synthesis than any of the supported catalyst presented in this Chapter, with an activity of 152 mol$H_2O_2$/h/$kg_{cat}$ but has a hydrogenation activity of 290 mol$H_2O_2$/h/$kg_{cat}$, and therefore is unstable towards hydrogen peroxide produced by direct synthesis.

### *4.4.4. Stabiliser Free PdAu/$TiO_2$ Catalysts Prepared Using Different Reductants*

The stabiliser free catalyst 0.5 wt% Pd 0.5 wt% Au/$TiO_2$, prepared using ammonia borane, has been shown in Section 4.3.4 to be highly active for hydrogen peroxide synthesis, more so than nearly all the stabilised catalysts presented. To better understand the origin of catalytic activity, additional catalysts were prepared in the absence of stabilisers using sodium borohydride and hydrazine as the reductants.

The hydrogen peroxide synthesis and hydrogenation activity of the resultant catalysts are presented in Figure 4-20. The $NH_3BH_3$ reduced catalyst has a hydrogen peroxide synthesis activity of 140 mol$H_2O_2$/h/$kg_{cat}$, considerably greater than the $NaBH_4$ and $N_2H_4$ prepared catalysts, which themselves exhibit activities of 79 and 41 mol$H_2O_2$/h/$kg_{cat}$ respectively.

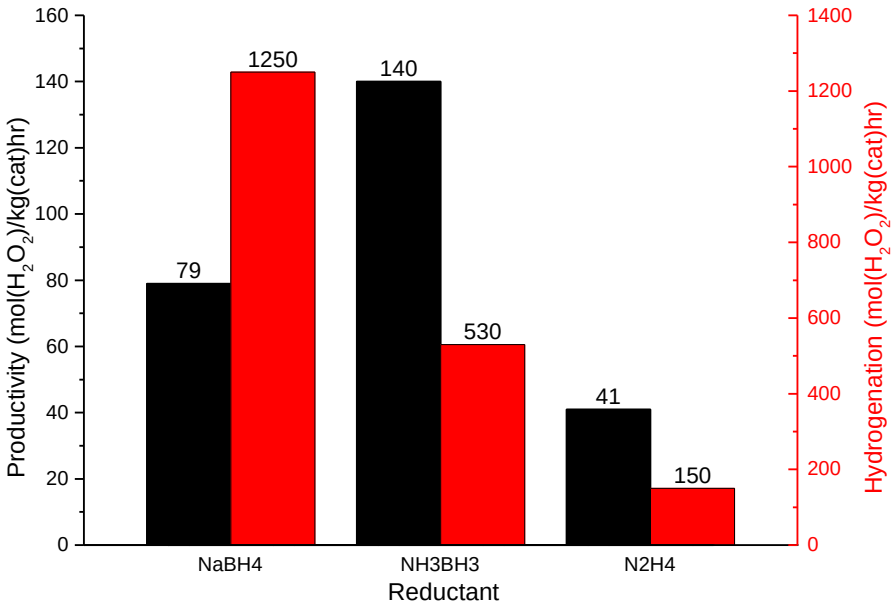


**Figure 4-20 – Hydrogen peroxide synthesis (●) and hydrogenation activity (●) of 0.5 wt% Pd 0.5 wt% Au/$TiO_2$ prepared using $NaBH_4$, $NH_3BH_3$ and $N_2H_4$.**
**Reaction Conditions – Hydrogen peroxide synthesis: 5 % $H_2/CO_2$ (2.9 MPa) and 25 % $O_2/CO_2$ (1.1 MPa), 8.5 g solvent (2.9 g $H_2O$, 5.6 g MeOH) 0.01 g catalyst, 2 °C, 1200 rpm, 30 min. Hydrogen peroxide hydrogenation: 5 % $H_2/CO_2$ (2.9 MPa), 8.5 g solvent (2.22 g $H_2O$, 5.6 g MeOH and 0.68 g 50 wt% $H_2O_2$), 0.01 g catalyst, 2 °C, 1200 rpm, 30 min.**

Hydrogen peroxide hydrogenation activity varied appreciably between catalysts. The $N_2H_4$ prepared catalyst had a synthesis activity that was half of the $NaBH_4$ analogue, but also an order of magnitude lower hydrogenation activity; this suggests that the catalyst prepared using hydrazine is considerably more selective than the sodium borohydride or ammonia-borane reduced analogues. Likewise, the $NH_3BH_3$ reduced catalyst displayed 40 % of the hydrogenation activity relative to the $NaBH_4$ prepared catalyst but nearly double the synthesis activity.

Previous work by Abis *et al.* on stabiliser free catalysts has found that supported discrete PdAu bimetallic nanoparticles of diameter 3.9 nm can be readily prepared providing the colloid is immobilised rapidly before its stability is compromised and the colloid decomposes in metal particulates.[20] However, the data presented in Figure 4-20 suggests that the origin of catalyst activity lies beyond simple particle size effects as, if that were the case, the

hydrogenation and synthesis activity would be negatively correlated such that the catalyst with the greatest hydrogenation activity would have the lowest synthesis activity. Despite the lack of implicit colloidal stabilisers, when using chemical reductants the reduction of metal precursors is accompanied by decomposition of the reducing agent to yield solution phase impurities. As an electron transfer process, the mechanism of metal precursor reduction using reducing agents is closely tied to the corresponding electrochemical reaction which has been extensively studied in the case of all three reductants, as highlighted in Table 4-3 below.[55–59]

**Table 4-3 - Redox equations of $NaBH_4$, $NH_3BH_3$ and $N_2H_4$ undergoing oxidation and hydrolysis.**[55–59]

| Reductant | Process | Equation |
|---|---|---|
| $NaBH_4$ | Oxidation | $NaBH_4 + 8OH^- \rightarrow NaB(OH)_4 + 4H_2O + 8e^-$ |
| | Hydrolysis | $NaBH_4 + 4H_2O \rightarrow NaB(OH)_4 + 4H_2$ |
| $NH_3BH_3$ | Oxidation | $NH_3BH_3 + 6OH^- \rightarrow NaBO_2 + NH_4^+ + 4H_2O + 6e^-$ |
| | Hydrolysis (acid) | $NH_3BH_3 + H^+ + 3H_2O \rightarrow B(OH)_3 + NH_4^+ + 3H_2$ |
| | Hydrolysis | $NH_3BH_3 + 2H_2O \rightarrow BO_2^- + NH_4^+ + 3H_2$ |
| $N_2H_4$ | Oxidation | $N_2H_4 + 4OH^- \rightarrow N_2 + 4H_2O + 4e^-$ |
| | Oxidation (acid) | $N_2H_5^+ \rightarrow N_2 + 5H^+ + 5e^-$ |
| | Catalytic Decomposition | $3N_2H_4 \rightarrow 4NH_3 + N_2$ |

The use of these reductant species depends upon both the thermodynamics and kinetics of their corresponding oxidation processes. The electrochemical oxidation potential of $N_2H_4$ is considerably greater than that of $NH_3BH_3$ or $NaBH_4$, -1.61V versus -1.22 and -1.22V respectively. In the context of this work, the oxidation potentials are largely meaningless as they are greater than the corresponding reduction potentials of the metal precursors, and as a result readily reduce a wide range of metal precursors. The variation in nanoparticle structure and composition are therefore a consequence of the kinetics of the reduction reaction which remains critically underexplored in determining the kinetic formation of nanoparticles using reductants such as those employed in this work. Polte and co-workers investigated the formation of Au nanoparticles using $NaBH_4$ by XAS, and found that a $Au^{3+}$ precursor was completely reduced to $Au^0$ nanoparticles of average diameter 1.6 nm in the first 200ms, after which time aggregation resulted in slow growth of nanoparticle diameter.[17] Such

determination of reduction rates has not been reported for $NH_3BH_3$ or $N_2H_4$, though it has been observed in the preparation of this work, that the formation of metal colloids occurs on a similar indistinguishable time scale. This suggests that factors other than reduction kinetics may be responsible for the large variation in catalyst activity presented here $NaBH_4$ and $NH_3BH_3$ are sensitive to hydrolysis during preparation and therefore are used in excess during the preparation of materials, either colloidal or supported. The hydrolysis of these compounds is effectively catalysed by precious metal catalysts, which further accelerates composition during catalyst preparation. The product of reductant oxidation and hydrolysis in solution are shown in Table 4-3.

The oxidation and hydrolysis of $NaBH_4$ results in the formation of the borate anion $B(OH)_4^-$, and thus borate concentration during nanoparticle formation and subsequent colloid aging is expected to be significant. Oxidation and hydrolysis of $NH_3BH_3$ also results in the formation of boron containing species, in the first instance the metaborate $BO_2^-$ anion and boric acid, $H_3BO_3$. Both species further hydrolyse to also form $B(OH)_4^-$, and in this respect reduction by either $NaBH_4$ or $NH_3BH_3$ both result in the formation of tetrahydroxyborate. Oxidation and hydrolysis of $NH_3BH_3$ results in the formation of the ammonium cation $NH_4^+$, unlike $NaBH_4$ in which $Na^+$ ions are present. Reduction using hydrazine results in the formation of only gaseous nitrogen and water, and therefore represents the case where the preparation mixture remains untainted by decomposition products. However, in the case of catalyst preparation using either sodium borohydride or ammonia-broane complex, it can be suggested that these decomposition products interact with the PdAu nanoparticles upon formation and may influence colloidal stability and ultimately catalyst activity.

### *4.4.5. Reductant Decomposition Products as Colloid Stabilisers*

To further probe the role of reductants in directing catalyst activity, catalysts were prepared in the presence of a range of species indicative of local environment during colloid formation. In Sections 4.3.2. and 4.3.3, we reported that catalysts prepared using ammonia borane are less active towards hydrogen peroxide hydrogenation versus those prepared in sodium borohydride, and therefore more active for synthesis overall. Given the presence of $BO_4^-$ in both preparations, 0.5 wt% Pd 0.5 wt% $Au/TiO_2$ catalysts were prepared in the presence and absence of $NH_4^+$ and PVP as the stabiliser to ascertain whether the presence of ammonium cations during preparation influences final catalyst activity.

The hydrogen peroxide synthesis and hydrogenation activities of the catalysts are presented in Table 4-4. In this case, the reference catalysts were prepared in the absence of any stabiliser, using $NaBH_4$ and $NH_3BH_3$ as the reductants, as previously presented in Section 4.4.1. For these stabiliser free catalysts, the stability of the resultant colloids depends on the stabilising nature of the decomposition products of the reductants; $BO_4^-$ for the $NaBH_4$ prepared catalyst and $BO_4^-$ and $NH_4^+$ for the $NH_3BH_3$ prepared catalyst. The catalyst prepared using $NaBH_4$ in the presence of $NH_4Cl$ alone is significantly less active for both hydrogen peroxide synthesis and hydrogenation, with activities of 34 and 530 mol$H_2O_2$/h/$kg_{cat}$ respectively, in comparison to the $NH_3BH_3$ reduced analogue. This suggests that the presence of ammonium ions from the decomposition of $NH_3BH_3$ is not solely responsible for the activity variation between $NaBH_4$ and $NH_3BH_3$ reduced catalysts.

**Table 4-4 - Hydrogen peroxide synthesis and hydrogenation activity of 0.5 wt% Pd 0.5 wt% Au/$TiO_2$ catalysts prepared in the presence of PVP and $NH_4Cl$.**

| Stabiliser | Reductant | Productivity (mol/kg(**cat**)hr) | Hydrogenation Activity (mol/kg(**cat**)hr) |
|---|---|---|---|
| None | $NaBH_4$ | 79 | 1250 |
| None | $NH_3BH_3$ | 140 | 530 |
| $NH_4Cl$ | $NaBH_4$ | 34 | 200 |
| PVP | $NaBH_4$ | 75 | 100 |
| PVP | $NH_3BH_3$ | 85 | 0 |
| $NH_4Cl$ + PVP | $NaBH_4$ | 85 | 30 |
| $NH_4Cl$ + PVP | $NH_3BH_3$ | 85 | 0 |

**Reaction Conditions – Hydrogen peroxide synthesis: 5 % $H_2/CO_2$ (2.9 MPa) and 25 % $O_2/CO_2$ (1.1 MPa), 8.5 g solvent (2.9 g $H_2O$, 5.6 g MeOH) 0.01 g catalyst, 2 °C, 1200 rpm, 30 min. Hydrogen peroxide hydrogenation: 5 % $H_2/CO_2$ (2.9 MPa), 8.5 g solvent (2.22 g $H_2O$, 5.6 g MeOH and 0.68 g 50 wt% $H_2O_2$), 0.01 g catalyst, 2 °C, 1200 rpm, 30 min.**

Catalyst preparations were also carried out using PVP as the stabiliser and sodium borohydride as the reductant, in the presence and absence of $NH_4Cl$ to closely imitate the solution phase species present during the preparation of catalysts using ammonia-borane complex as the reductant. It is observed that the combination of $NH_4Cl$ and PVP results in an increase in hydrogen peroxide synthesis activity from 75 to 85 mol$H_2O_2$/h/$kg_{cat}$ and a

decrease in hydrogenation activity, from 100 to 30 mol$H_2O_2$/h/$kg_{cat}$, suggesting that the presence of both PVP and $NH_4^+$ during preparation results in improved catalyst performance. Analogous preparations were conducted using $NH_3BH_3$ as the reductant to determine whether the beneficial effect of $NH_4Cl$ during preparation is isolated to the use of sodium borohydride, but in this case, the addition of $NH_4Cl$ during preparation results in no change in catalyst activity. When considered in relation to the other catalysts presented in Table 4-4, the activity variation of the catalysts prepared in the presence of ammonium salts suggests that solution phase species present during preparation play an important role in preparing active and selective catalysts.

### *4.4.6. Electron Microscopy*

#### *4.4.6.1. SEM-BSE Imaging of PAA Stabilised 0.5 wt% Pd 0.5 wt% Au/$TiO_2$ Catalysts*

In Section 4.4.2, it is shown that PAA stabilised PdAu/$TiO_2$ catalysts are active for hydrogen peroxide synthesis and inactive for hydrogenation. Considering the unusual metal nanostructuring observed in the case of PVP stabilised analogues, catalysts prepared in the presence of high and low concentrations of PAA were investigated by SEM-BSE, as shown in Figure 4-21.

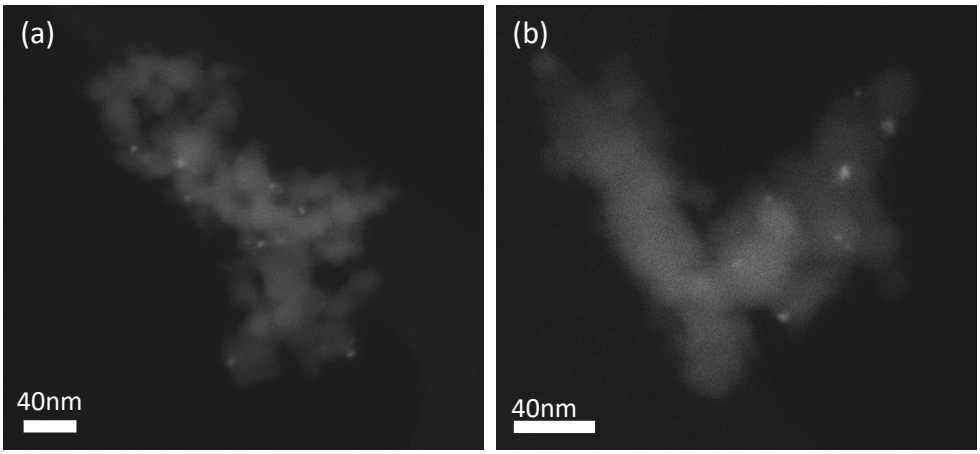


**Figure 4-21 - Representative SEM-BSE images of 0.5 wt% Pd 0.5 wt% Au/$TiO_2$ prepared in the presence of 1.5eq (a) and 0.8eq (b) PAA.**

The catalyst prepared in the presence of high concentrations of PAA contains well dispersed nanoparticles, 3-6 nm in diameter. Likewise, the catalyst prepared in the presence of substoichiometric quantities of PAA also contained dispersed particles, 3-8 nm diameter. The structure and the activity of the PAA stabilised catalysts is surprising considering the nature of the PVP stabilised catalysts presented in the preceding sections. In the case of PVP stabilised catalysts, the formation of agglomerate nanostructures results is partly due to use of sub-stoichiometric quantities of PVP and results in decreased hydrogen peroxide

hydrogenation activity. The disparity between the structure of the PVP and PAA stabilised catalysts prepared under analogous conditions indicates that the structure of the resultant catalyst is dependent upon the nature of stabiliser in addition to its concentration. This is consistent with previous work by Jones *et al.*, who reported that the preparation of 1 wt% Ru/C by sol immobilisation in the presence of only 0.1eq PVA yielded a catalyst containing highly dispersed 2 nm nanoparticles.[33] In addition, it was shown that catalyst hydrogenation activity decreased with increasing stabiliser content, analogous to the trend for the PAA stabilised catalysts presented in Section 4.4.2 of this work.

#### *4.4.6.2. Stabiliser Free 0.5 wt% Pd 0.5 wt% Au/$TiO_2$ Catalysts Prepared Using Varying Reductants*

In the preceding section it is established that the formation of PdAu chain nanostructures is independent of the concentration of stabiliser during preparation. In addition, previous work has found that catalysts prepared under analogous conditions using $NaBH_4$ instead of $NH_3BH_3$ yielded well dispersed PdAu nanoparticles. To determine the effect of choice of reductant on PdAu metal nanostructure, the 0.5 wt% Pd 0.5 wt% Au/$TiO_2$ catalysts prepared in the absence of stabiliser were interrogated by STEM-HAADF.

STEM-HAADF images of the $NH_3BH_3$ reduced PdAu/$TiO_2$ catalyst are shown in Figure 4-22. The catalyst contains highly branched agglomerate nanostructures which are considerably larger than for catalysts prepared in the presence of stabiliser. The minimum agglomerate diameter was found to be 70 nm, approximately 7x and 2x larger than for catalysts prepared in the presence of high and low concentrations of PVP respectively. Furthermore, the diameter of the parent PdAu nanoparticles was also larger in the absence of stabiliser, 5-10 nm versus 2-5 nm in the case of the stabilised catalysts. EDX mapping of the Pd Lα and Au M edges confirms that like the stabilised catalysts, the active metal surface of the stabiliser free catalyst is of constant Pd and Au composition and in agreement with the bulk metal loading.

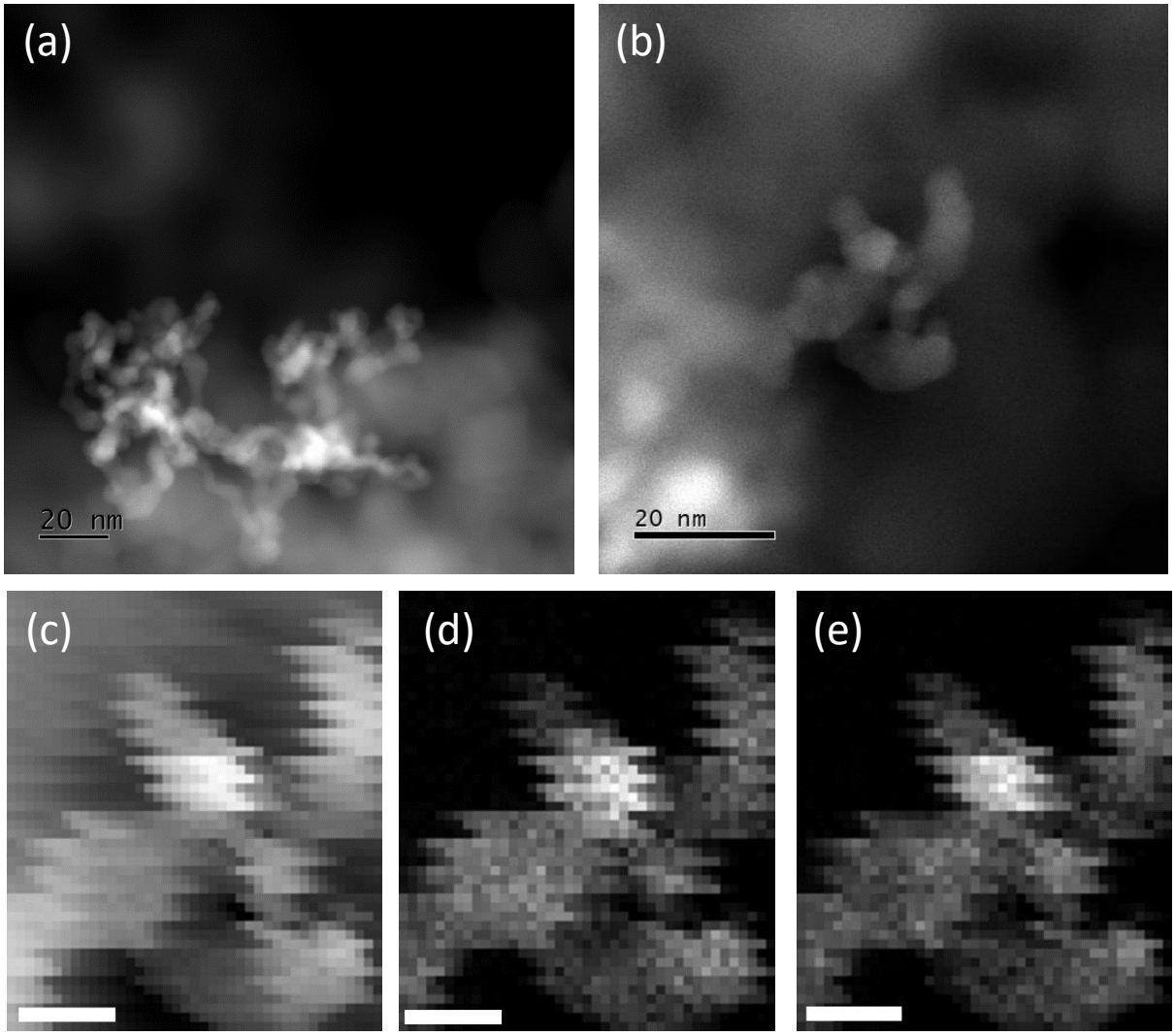


**Figure 4-22 - Representative STEM-HAADF image of metal nanostructuring present in 0.5 wt% Pd 0.5 wt% Au/$TiO_2$ $NH_3BH_3$ reductant, 0 mol eq PVP at low (a) and high (b) magnification. STEM-HAADF image of EDX acquisition area (c) and EDX maps corresponding to Au Lα (2.0-2.5eV) (d) and Pd Lα Edge (2.7-3.2eV) (e). Scale bars representative of 10 nm.**

In Section 4.3.4 it was found that the $NH_3BH_3$ reduced stabiliser free catalyst was exceptionally active for hydrogen peroxide synthesis and hydrogenation in comparison to the analogous catalysts prepared in the presence of stabiliser. The structure and composition of the catalyst determined by STEM indicates that neither composition nor metal surface area is responsible for the high activity of the catalyst. Previous work has found that in the case of PdAu/$TiO_2$ catalysts, increasingly Pd rich PdAu surfaces are more active for hydrogen peroxide hydrogenation and therefore detrimental for hydrogen peroxide synthesis.[62] For modified sol immobilisation catalysts presented in this work however the stabiliser free and stabilised catalysts show regular PdAu surface concentration indicative of homogenous

alloying across the metal surface, and therefore variations in surface composition cannot be responsible for the variation in catalyst activity.

STEM analysis of the $NH_3BH_3$ reduced catalysts also precludes variation in metal surface area as a determinant of catalyst activity. The stabiliser free catalyst contained the largest agglomerates assembled from the largest parent PdAu nanoparticles. Likewise, the catalyst prepared using the highest concentration of PVP show the smallest agglomerates formed from the smallest PdAu nanoparticles. Fundamental appreciation of surface catalysis kinetics would suggest that the PVP stabilised catalyst with high metal surface area should be more active than the stabiliser free, low metal surface area catalyst. The activity data presented in Section 4.3.4 contradicts this assumption; the stabiliser free catalyst is in fact considerably more active for both hydrogen peroxide synthesis and hydrogenation than the stabilised catalyst.

The contradiction between the structure and activity of the $NH_3BH_3$ catalysts can instead be attributed to the presence of latent PVP present on the catalyst after preparation. Prati and co-workers previously investigated the role of stabiliser on the activity of $Au/TiO_2$ catalysts for glycerol oxidation.[53] The authors show that presence of residual stabiliser can hinder flux of reactants and products at the active surface, reducing activity. The same effect was observed by Lopez-Sanchez *et al.* who found that removing stabiliser from the surface of a $Au/TiO_2$ catalyst resulted in a significant increase in CO oxidation activity, resulting in conversion increasing from 0 to 55 wt%.[29] This suggests that in this work, PVP serves to not only direct the structure of the catalyst during preparation but also modulate the activity of the catalyst during reaction.

The $NaBH_4$ reduced stabiliser free catalyst was also investigated by STEM to determine the metal nanostructure of the catalyst. STEM-HAADF micrographs of the $NaBH_4$ reduced stabiliser free are presented in Figure 4-23. Unlike the $NH_3BH_3$ reduced analogue previously presented, the $PdAu/TiO_2$ catalyst contains well dispersed nanoparticles <10 nm in diameter.

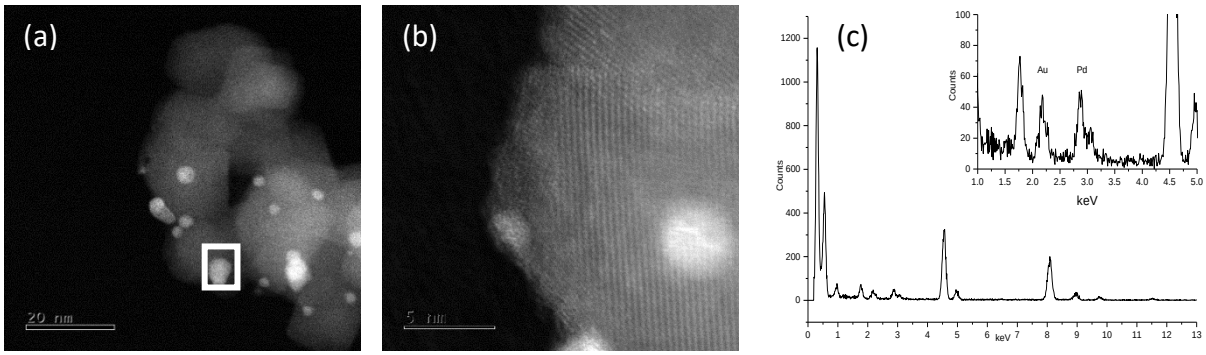


**Figure 4-23 Representative STEM-HAADF image of 0.5 wt% Pd 0.5 wt% Au/$TiO_2$ $NaBH_4$ 0eq PVP at low (a) and high (b) magnification. EDX spectrum of nanoparticle highlighted in image (c) with insert of Au Lα And Pd Lα Region.**

The structure of this catalyst is consistent with work previously reported by Abis *et al.*, who found that PdAu/$TiO_2$ catalysts prepared by a comparable sol immobilisation method yielded discrete nanoparticles with no particle agglomerates being observed.[20] This suggests that the choice of reductant is solely responsible for the chain agglomerate structure of the resultant catalyst. EDX analysis of large and small particles confirms that like the other catalysts presented in this work, the metal surface composition was regular and consistent with the bulk Pd/Au ratio of 1:1 by mass.

The $N_2H_4$ reduced, stabiliser-free 0.5 wt% Pd 0.5 wt% Au/$TiO_2$ catalyst was also interrogated by STEM. In Section 4.3.3 the hydrogenation activity of the catalysts correlates with the reductant used such that $NH_3BH_3$ < $N_2H_4$ < $NaBH_4$ for PVP stabilised catalysts. Likewise, through optimisation of conditions, it was possible to prepare catalysts with either $NH_3BH_3$ or $N_2H_4$ which were inactive for hydrogen peroxide hydrogenation and therefore selective towards hydrogen peroxide synthesis. The hydrazine reduced catalyst, shown in Figure 4-24 exhibited a distinct morphology, different again from the catalysts prepared using $NaBH_4$ or $NH_3BH_3$, with the nanoparticles forming 'collapsed' nanochains, spherical agglomerates 20-40 nm in diameter with internal structure consistent of the coiling of nanochain colloids. EDX mapping of a representative particle confirmed that the Pd/Au composition of the nanostructure was constant, consistent with that of the previously investigated catalysts.

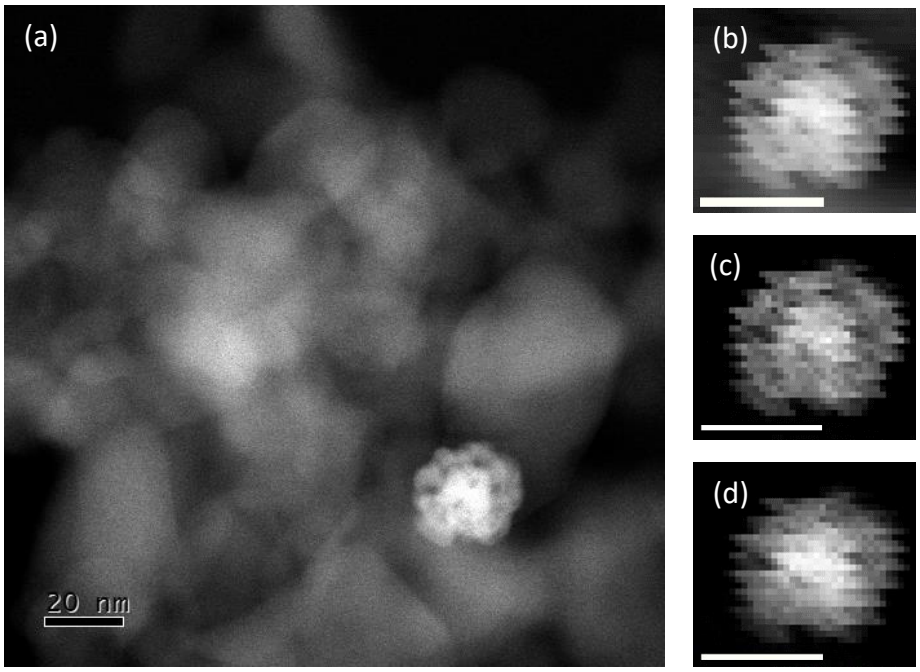


**Figure 4-24 - Representative STEM-HAADF image of metal nanostructuring present in 0.5 wt% Pd 0.5 wt% Au/$TiO_2$ $N_2H_4$ reductant, 0 mol eq PVP(a). STEM-HAADF image of EDX acquisition area (b) and EDX maps corresponding to Au Lα (2.0-2.5eV) (c) and Pd Lα Edge (2.7-3.2eV) (d). Scale bars representative of 20 nm.**

*4.4.6.3.SEM-BSE Images of $NH_4Cl$ Promoted PdAu/$TiO_2$ Catalysts*

It is thought that, as a decomposition product of $NH_3BH_3$ and $N_2H_4$, the presence of ammonium cations during preparation results in morphological changes that in turn improve catalyst selectivity. The effect of ammonium cations on catalyst nanostructure was investigated by preparing catalysts using $NaBH_4$ in the presence and absence of $NH_4^+$. In Section 4.4.5, the addition of $NH_4Cl$ during catalyst preparation using $NaBH_4$ as the reductant yielded catalysts with increased hydrogen peroxide synthesis activity and reduced hydrogenation activity, comparable to the activity of the catalysts prepared using other reductants. The inactivity of the $NH_3BH_3$ and $N_2H_4$ reduced catalysts towards hydrogen peroxide hydrogenation could be a consequence of the PdAu chain nanostructure observed in catalysts prepared using these reductants, shown in Section 4.4.6.2. To verify this, 0.5 wt% Pd 0.5 wt% Au/$TiO_2$ catalysts prepared in the presence of PVP and $NH_4Cl$ using $NaBH_4$ were investigated by SEM-BSE, shown in Figure 4-25(a). For reference, PVP stabilised, $NH_3BH_3$ and $NaBH_4$ reduced catalysts are also presented in Figure 4-25(b) and (c). In agreement with the previously presented STEM data, the $NH_3BH_3$ reduced catalyst contains chain-like nano-assemblies. Interestingly, the ammonium promoted $NaBH_4$ reduced catalysts prepared both in

the presence and absence of PVP also contain chain structures.

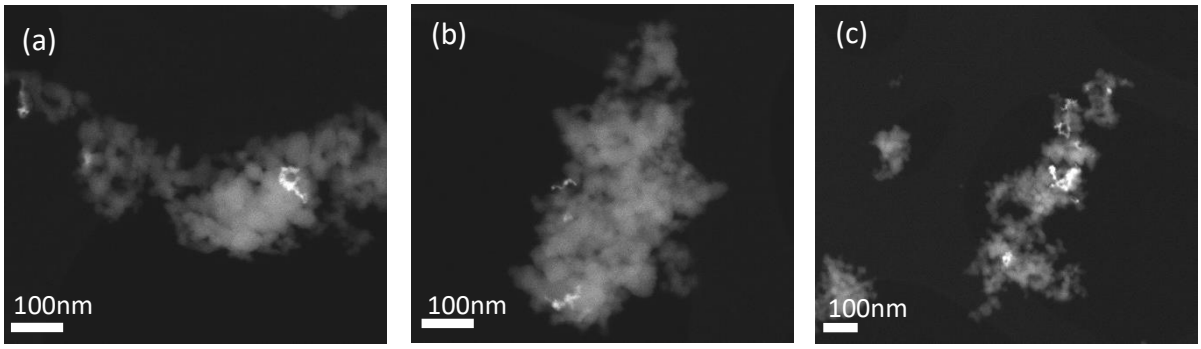


**Figure 4-25 - Representative SEM-BSE images of 0.5 wt% Pd 0.5 wt% Au/$TiO_2$ prepared in the presence of PVP and $NH_4Cl$ using $NH_3BH_3$ (a), $NaBH_4$ (b). Catalyst prepared in the presence of $NH_4Cl$ alone using $NaBH_4$ (c).**

In Section 4.4.5 it is established that for $NaBH_4$ reduced catalysts, the presence of either PVP or $NH_4Cl$ during preparation results in decreased catalyst hydrogenation activity, following the series No stabiliser > $NH_4Cl$ > PVP > $NH_4Cl$ and PVP. Comparison of the activity and structure of the catalysts determined by electron microscopy, indicates that the catalysts containing PdAu chain structures are less active for hydrogen peroxide hydrogenation and therefore more selective towards hydrogen peroxide than the catalyst containing well dispersed nanoparticles. The hydrogenation activity of the $NaBH_4$ reduced catalysts are however non-zero and therefore they are inferior to $NH_3BH_3$ reduced catalysts which are inactive towards hydrogen peroxide hydrogenation. It is therefore difficult to discern conclusively whether the presence of ammonium cations, as the decomposition product of $NH_3BH_3$ and $N_2H_4$, are responsible for the improved performance of the catalysts prepared using these reductants.

### *4.5. Colloidal PdAu Catalysts Prepared Using Varying Stabilisers*

Colloidal catalysts were prepared to determine the effect of metal sol immobilisation on catalyst activity. Catalysts were prepared at the conditions optimised for supported catalyst preparation i.e. at 0°C using $NH_3BH_3$ as the reductant using PVP, and additionally in the presence of PVA and PAA to further understand the role the nanoparticle stabiliser plays in directing catalyst activity and selectivity. The colloidal catalysts were tested such that the amount of metal present in the reaction was the same as for the heterogeneous catalysts of 1 wt% metal loading. The hydrogen peroxide synthesis and hydrogenation activities of the colloidal catalysts are presented in Table 4-5.

**Table 4-5 - Hydrogen peroxide synthesis and hydrogenation activity of PdAu colloids prepared in the presence of varying stabilisers.**

| Stabiliser | Synthesis Activity (mol/kg(**cat**)hr) | Hydrogenation Activity (mol/kg(**cat**)hr) |
|---|---|---|
| PVP | 225 | 0 |
| PVA | 190 | 230 |
| PAA | 103 | 1400 |

**Reaction Conditions – Hydrogen peroxide synthesis: 5 % $H_2/CO_2$ (2.9 MPa) and 25 % $O_2/CO_2$ (1.1 MPa), 8.5 g solvent (2.9 g $H_2O$, 5.6 g MeOH) 0.01 g catalyst, 2 °C, 1200 rpm, 30 min. Hydrogen peroxide hydrogenation: 5 % $H_2/CO_2$ (2.9 MPa), 8.5 g solvent (2.22 g $H_2O$, 5.6 g MeOH and 0.68 g 50 wt% $H_2O_2$), 0.01 g catalyst, 2 °C, 1200 rpm, 30 min.**

The PVP stabilised colloid is considerably more active than either the PVA or PAA stabilised colloid with a hydrogen peroxide synthesis activity of 225 mol$H_2O_2$/h/$kg_{cat}$, which is higher than any previously reported supported metal catalysts. Hutchings and co-workers previously reported a 2.5 wt% Pd 2.5 wt% Au/C catalyst prepared by wet impregnation with a synthesis activity of 175 mol$H_2O_2$/h/$kg_{cat}$ that also exhibit $H_2O_2$ selectivity in excess of 98 % under identical conditions, finding that the selectivity of the catalyst is considerably enhanced by acid pre-treatment of the support .[54] PdAu/C catalysts prepared by sol immobilisation for direct hydrogen peroxide synthesis have previously been explored by Pritchard *et al.*, where a co-reduced 0.5 wt% Pd 0.5 wt% Au/C catalyst had synthesis and hydrogenation activities of 158 and 384 mol$H_2O_2$/h/$kg_{cat}$ respectively.[13] The high hydrogenation rate of the catalyst indicates that although active, it is considerably less selective than either the colloidal or optimised supported catalysts presented here.

In this work, PVA and PAA stabilised colloids are considerably less active for hydrogen peroxide direct synthesis than the PVP stabilised analogue, giving synthesis activities of 190 and 103 mol$H_2O_2$/h/$kg_{cat}$ respectively. In addition, these colloids are active for hydrogen peroxide hydrogenation and as a result are significantly less selective than the PVP analogue. The PAA stabilised colloid is most active for hydrogenation with an activity of 1400 mol$H_2O_2$/h/$kg_{cat}$. The high synthesis activity of the PAA stabilised colloid is most surprising given its hydrogenation activity; The known interrelation between synthesis and hydrogenation activity suggests that high hydrogenation activity is detrimental towards

hydrogen peroxide production under batch conditions and as a result the accompanying synthesis activity should also be low.

Previous work by Jaine and co-workers investigated the effect of a range of polymeric stabilisers on Pd and Rh colloidal catalysts, and they reported that average particle diameter varied with the series PAA < PVA < PVP, independent of the metal or solvent system used during preparation.[18] As discussed in Section 4.3.5, the role of Pd particle size (Pd domain size in bimetallic systems) is well established, experimentally and theoretically, for direct hydrogen peroxide synthesis. This suggests that, in the case of the colloidal catalysts, the formation small, highly active PdAu nanoparticles results in high hydrogenation activity and this ultimately diminishes the synthesis activity under standard reaction conditions. As a result, the PVP stabilised colloid, which has the lowest hydrogenation activity, also has the highest synthesis activity as no hydrogen peroxide was destroyed upon preparation.

*4.5.1.1. TEM Analysis of PVP Stabilised Colloidal PdAu Catalyst*

The PVP stabilised PdAu colloidal catalyst was also investigated using TEM BF imaging, images presented in Figure 4-26. Here, the colloidal catalysts also exhibited chain nanostructured morphology, indicating that the agglomerate nanostructure forms during colloid preparation and not subsequent immobilisation. This is consistent with previous work on monometallic Pd and Au nanochain materials which were found to form the structures regardless of whether they were isolated as bulk samples or immobilised on support materials.[37,38,60,61]

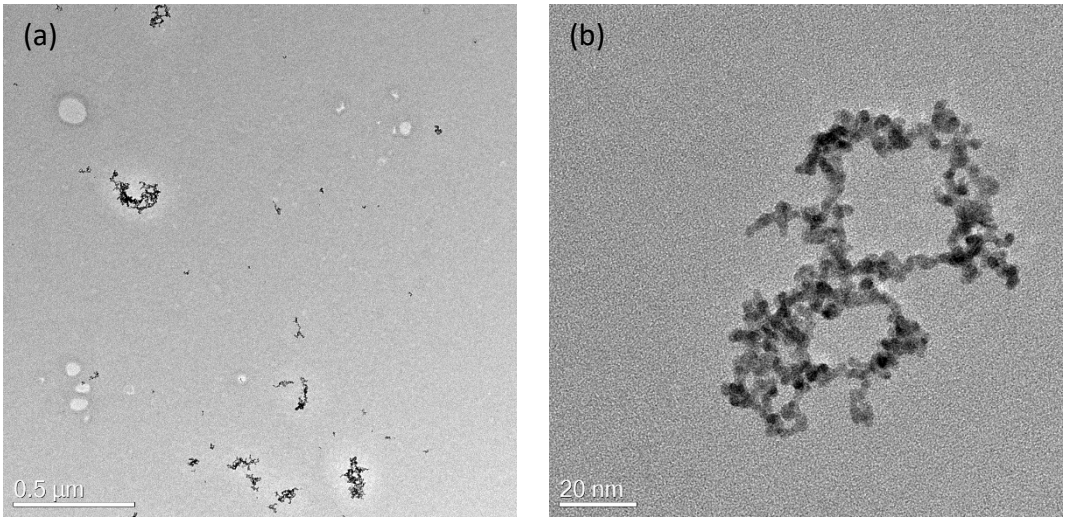


**Figure 4-26 – TEM-BF images of PdAu colloids prepared using $NH_3BH_3$ and 0.8 mol eq PVP at low (a) and high(b) magnifications.**

### *4.6. The Effect of Varying Secondary Metal*

Given the high activity and selectivity of PdAu catalysts prepared by a modified sol immobilisation method, further work was undertaken to explore the activity of other bimetallic catalyst systems. Pd containing bimetallic catalysts have been previously found to be highly active for the direct synthesis of hydrogen peroxide. In an investigation of trimetallic PdPtAu catalysts, Edwards *et al.* found that a PdPt catalyst was significantly more active than a PdAu analogue, the former shown to have hydrogen peroxide synthesis activity of 124 mol$H_2O_2$/h/$kg_{cat}$ and the latter 64 mol$H_2O_2$/h/$kg_{cat}$.[63] Other work has explored the use of cheaper and more abundant secondary metals. Hutching and co-workers reported that PdSn/$TiO_2$ catalysts were highly selective in direct synthesis owing to the formation of a $SnO_2$ metal surface overlayer which isolated monometallic Pd particles highly active for hydrogenation.[64] More recently, Tian and co-workers found that incorporation of tellurium into a Pd/$TiO_2$ catalyst in a 1:100 ratio resulted in a selectivity improvement from 65 to 100 %.[38] Likewise, similar effects have also been observed by Han and co-workers, who found that the addition of Sb to a monometallic Pd/$TiO_2$ catalyst resulted in an increase in selectivity from 54 to 73 %.[65]

This work from the literature suggests that a wide range of Pd alloy forming elements can improve the properties of catalysts for the direct synthesis of hydrogen peroxide. Indeed Xu and co-workers recently undertook a theoretical evaluation of bimetallic Pd containing nanoparticles for direct synthesis.[66] Bimetallic clusters containing Pd and elements of the 4$^{th}$, 5$^{th}$ and 6$^{th}$ row of the periodic table were analysed using DFT calculations for the various fundamental reactions in hydrogen peroxide synthesis, hydrogenation and decomposition. In their work, they observed that Pb, W and Rh derived bimetallic clusters were significantly less active for decomposition pathways versus PdAu clusters, indicating that further exploration of bimetallic catalyst may yield more selective catalysts.

Considering the above, Ni, In and Sn bimetallic Pd catalysts were prepared using the optimised PdAu preparation conditions presented in Section 4.3.3. The hydrogen peroxide synthesis and hydrogenation activities of these catalysts are presented in Figure 4-27. The activity of 0.5 wt% Pd 0.5 wt% Sn/$TiO_2$ is comparable to that of the analogous 0.5 wt% Pd 0.5 wt% Au/$TiO_2$ catalyst, with the former displaying a hydrogen peroxide synthesis activity of 88 mol$H_2O_2$/h/$kg_{cat}$ versus 85 mol$H_2O_2$/h/$kg_{cat}$ for the latter. The PdSn bimetallic catalyst

also had the highest hydrogen peroxide hydrogenation activity, 320 mol$H_2O_2$/h/$kg_{cat}$, indicating that selectivity towards the productive synthesis pathway is poor.

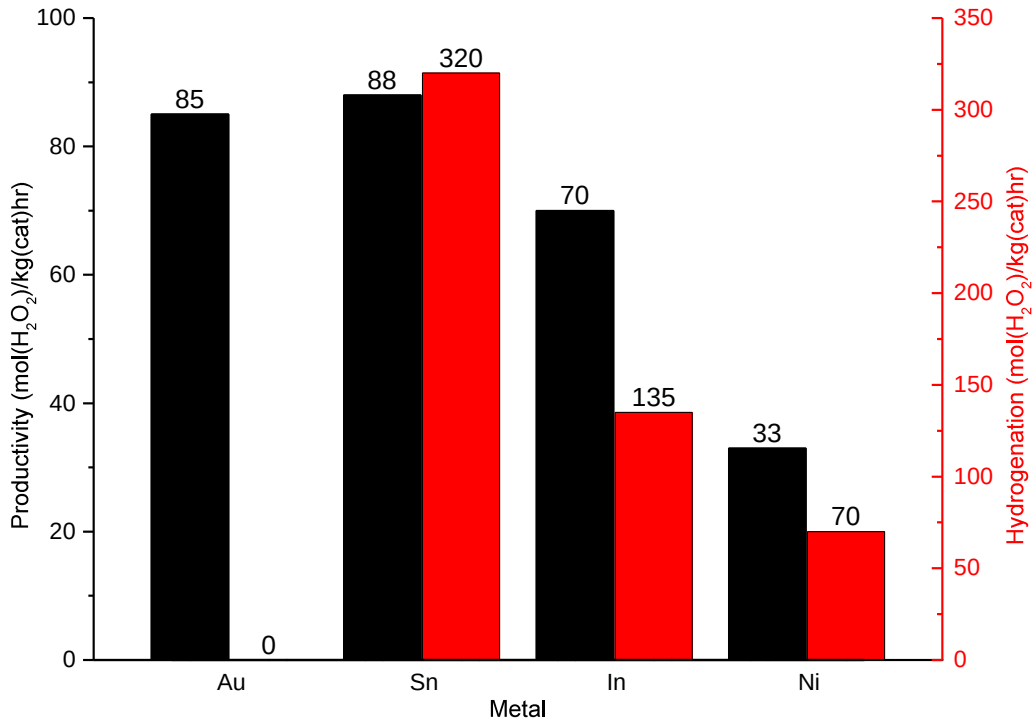


**Figure 4-27 - Hydrogen peroxide synthesis and hydrogenation activities of 0.5 wt% Pd 0.5 wt% X/$TiO_2$ catalysts prepared by modified sol immobilisation**
**Reaction Conditions – Hydrogen peroxide synthesis: 5 % $H_2/CO_2$ (2.9 MPa) and 25 % $O_2/CO_2$ (1.1 MPa), 8.5 g solvent (2.9 g $H_2O$, 5.6 g MeOH) 0.01 g catalyst, 2 °C, 1200 rpm, 30 min. Hydrogen peroxide hydrogenation: 5 % $H_2/CO_2$ (2.9 MPa), 8.5 g solvent (2.22 g $H_2O$, 5.6 g MeOH and 0.68 g 50 % $H_2O_2$), 0.01 g catalyst, 2 °C, 1200 rpm, 30 min.**

The 0.5 wt% Pd 0.5 wt% In/$TiO_2$ catalyst possesses intermediate hydrogen peroxide synthesis and hydrogenation activity. In comparison to the Sn containing analogue, a 20 % reduction in synthesis activity to 70 mol$H_2O_2$/h/$kg_{cat}$ is accompanied by a 68 % reduction in hydrogenation activity, indicating that the catalyst is considerably more selective towards hydrogen peroxide than the 0.5 wt% Pd 0.5 wt% Sn/$TiO_2$ catalyst.

The PdNi bimetallic catalyst is the least active for hydrogen peroxide synthesis, with a synthesis activity of 33 mol$H_2O_2$/h/$kg_{cat}$. Additionally, hydrogenation activity is the lowest of the gold-free bimetallic catalysts at 70 mol$H_2O_2$/h/$kg_{cat}$. This is consistent with previous work by Maity *et al.* who investigated the activity of Pd, Au and Ni containing nanostructured bulk materials for the direct synthesis of hydrogen peroxide.[67] The PdNi material was found to be inactive towards hydrogen peroxide hydrogenation and decomposition and selectivity

towards hydrogen peroxide in excess of 90 %. The low hydrogenation activity of the PdNi catalyst presented in this work could be attributed to preparation conditions, as the reduction of Ni precursors using solution phase reductants has been reported to be less favourable both thermodynamically and kinetically than Au or Pd precursors.[68,69] Discrepancies between precursor reduction rates is known to yield core-shell nanoparticles, and in the case of PdAu bimetallic catalysts, core-shell structures have been shown to less active for hydrogen peroxide synthesis and hydrogenation versus alloyed nanoparticle catalysts.[70,13] Indeed, in Sections 4.3.2 to 4.3.4 it is shown that careful control of preparation conditions is critical in preparing highly selective catalysts, which suggests that further exploration of these conditions could yield a PdNi catalyst with comparable activity for the direct synthesis of hydrogen peroxide to that of PdAu bimetallic catalysts.

*4.7.*
*4.7. Discussion*

The preparation of highly active and selective catalysts for direct hydrogen peroxide synthesis is intimately related to the reactions that hydrogen and oxygen readily undergo on metal surfaces.

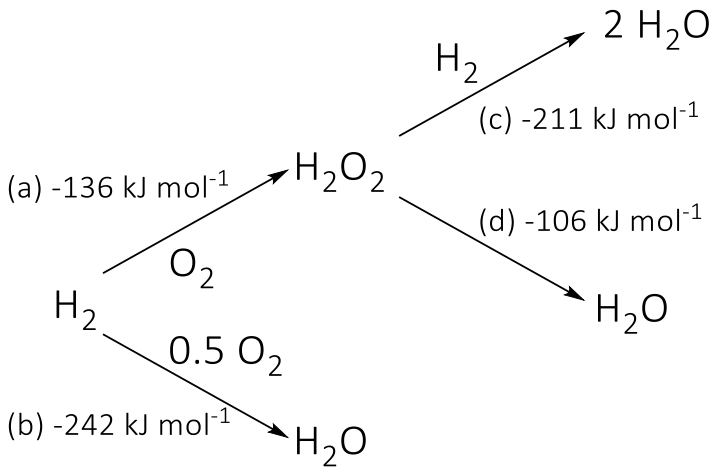


**Figure 4-28 - Catalytic reaction pathways and enthalpies for reactions of $H_2$ and $O_2$**

Referring to the reaction scheme in Figure 4-28, hydrogen peroxide is an intermediate in the two step formation of water by either hydrogenation (c) or decomposition (d). Therefore, in producing hydrogen peroxide, the rates of steps (b), (c) and (d) must be minimised and the rate of (a) maximised. The hydrogen peroxide hydrogenation activity of catalysts acts as a useful evaluator for the rates of (b), (c) and (d). Experimentally, in evaluating catalysts in the presence of hydrogen peroxide under a hydrogen atmosphere, the resultant hydrogen peroxide loss is representative of the sum of the reactions (c) and (d). Previous work has found that the decomposition rate of hydrogen peroxide (d) is considerably slower than (c) and therefore minimising the hydrogenation rate (c) is the most effective method to improve catalyst selectivity.

In the case of Pd catalysed direct synthesis, it is thought that competing reactions occur on separate sites. Ouyang *et al.* investigated $PdAu/TiO_2$ catalysts by *in situ* diffuse reflectance infrared Fourier transform spectroscopy of CO adsorption (CO-DRIFTS) and concluded that monatomic or Pd clusters are considerably more active for hydrogen peroxide synthesis than hydrogenation.[62] Similarly, Han and co-workers prepared hydroxyapatite supported Pd catalysts with varying particle size, from >20 nm down to atomically dispersed Pd species, and found that Pd cluster catalysts were most active for hydrogen peroxide synthesis, with

increased particle size resulting increased hydrogenation activity and therefore a reduction in selectivity.[31]

Critical to the application of the structure-activity relationship of Pd containing catalysts is fine control during catalyst preparation. Indeed, catalysts prepared by wet impregnation, an industrially applicable and low-cost preparation technique, results in a wide range of nanoparticulate species. For PdAu/$TiO_2$ catalysts, this includes monometallic particles and bimetallic particles of varying composition, which is further complicated by particle size effects. Under this regime, conventional wisdom indicates that an ideal catalyst will feature small nanoparticles of uniform composition which features small and well dispersed Pd domains.

The nanostructured morphology observed in the optimised 0.5 wt% Pd 0.5 wt% Au/$TiO_2$ catalysts prepared in this work suggest that other variables may influence hydrogen peroxide synthesis activity and selectivity. In the stabiliser free catalysts, active metal surface area appears to dominate catalyst activity. The 0.5 wt% Pd 0.5 wt% Au/$TiO_2$ catalyst prepared using $NaBH_4$ in absence of stabilisers, has a hydrogen peroxide hydrogenation activity of 1250 mol$H_2O_2$/h/$kg_{cat}$, i.e. three times greater than the analogous nanochain catalyst prepared using $NH_3BH_3$, which for all intent and purpose is formed from parent nanoparticles of comparable size and composition. The hydrogen peroxide synthesis activity of the $NaBH_4$ reduced catalyst was inferior to that of the $NH_3BH_3$ reduced analogue, which can be considered a consequence of the catalysts high hydrogenation activity. In comparison, the stabiliser free $N_2H_4$ reduced catalyst displayed lower hydrogen peroxide synthesis and hydrogenation activity than the analogous catalysts prepared using $NH_3BH_3$ or $NaBH_4$. This can be reasonably attributed to metal nanostructuring presented in Section 4.4.6.2, in which it is shown that the in the case of the $N_2H_4$ reduced catalyst, nanoparticles agglomerate into collapsed chain structures of low surface area. The hydrogenation activity and surface area of the stabiliser free catalysts both follow the trend $NaBH_4$ > $NH_3BH_3$ > $N_2H_4$, which suggests that in the absence of stabiliser, the hydrogenation rate is dependent upon the surface availability of hydrogenation sites.

Morphology alone, however, cannot reasonably explain the unusual selectivity of the catalysts presented in Section 4.3.2 and 4.3.3. The addition of PVP during catalyst preparation results in a disproportionate decrease in catalyst hydrogenation activity versus synthesis activity, and therefore a selectivity improvement. It is well known that polymeric stabilisers remain on a catalyst surface after preparation and therefore the PVP can be thought to play two roles.[53] The

first is control of nanochain morphology during preparation. PVP has been previously reported to be an effective structure directing agent in the formation of monometallic Pd and Au nanochain materials.[37,38,61] Qualitative analysis of the agglomerate structures by STEM suggest the presence of PVP results in more branching. In the case of the stabiliser free nanochain catalyst, nanoparticle chains were found to terminate with globules formed from the unstructured agglomeration of the parent particles. Owing to the low metal loading and agglomerate density, it is difficult to quantitatively investigate such variations.

The second role of PVP is to modulate activity through electronic interactions with the active metal surface. Xian *et al.* previously investigated the interaction between PVP and Pd nanoparticles using IR spectroscopy and XPS, and found that pyrrolidone units coordinate to the surface of the nanoparticles principally through the carbonyl oxygen providing electron density, as evidenced by shifts in the C=O IR stretch and peak splitting in the O1s XPS region.[71] PVP-Au interactions have also been explored both theoretically and experimentally: Tsunoyama *et al.* reported the preparation of PVP stabilised Au nanoparticles for aerobic oxidations.[72] Here, the authors observed, using CO-DRIFTS, that increasing PVP content resulted in the formation of a more negatively charged Au surface as evidenced by the red shift of the IR peak. Likewise Haruta and co-workers computationally evaluated the structure of PVP bound $Au_{13}$ clusters and showed that, whilst the energy of interaction between the PVP and cluster was comparable to that of physisorption, encapsulation by PVP resulted in increased cluster charge density which was thought to promote anionic $O_2$, an intermediate in aerobic oxidation.[73]

The activity modulation effect of stabilisers on nanoparticle activity is also seen in this work. In Section 4.4.2, it is shown that at sufficiently high concentrations, PAA stabilised PdAu/$TiO_2$ catalysts are entirely selective towards the synthesis of hydrogen peroxide. Furthermore, in Section 4.4.6.1 it is presented that the PAA stabilised catalysts contain well dispersed metal nanoparticles, and not agglomerate nanostructures as seen in the PVP stabilised analogues. This indicates that the selectivity of the PAA stabilised PdAu catalysts cannot be a result of the morphology of the active metal species. The effect of PAA on hydrogenation activity is further supported by additional experiments which found that the addition of PAA to the reaction mixture resulted in the complete suppression of the hydrogenation pathway. The nature of the interaction between PAA and PdAu surface is however unknown, as in contrast to PVP, previous work using PAA as a nanoparticle stabiliser is rare. Jaine *et al.* reported the

preparation of Pd colloids using PVP, PVA and PAA as polymeric stabilisers, and found that the diameter of the resultant nanoparticles decreased from 4.4 nm in the case of PVP, to 2.5 nm for PVA and 2.3 nm for PAA.[18]

### *4.8. Conclusions*

Whilst the factors involved in preparing selective catalysts have been identified, the origin of their cumulative effect on hydrogen peroxide hydrogenation activity cannot currently be explained.

STEM analysis of the catalysts prepared using $NaBH_4$, $NH_3BH_3$ and $N_2H_4$, in the presence and absence of PVP, have enabled isolation of the factors leading to the formation of chain nanostructures, yielding catalysts with maximum hydrogen peroxide synthesis and minimum hydrogenation activity. Nanochains were found to form in the presence of $NH_3BH_3$ only, thought to be due to the presence of ammonium cations due to its decomposition during metal precursor reduction. This was investigated by preparing catalysts in the presence of $NH_4Cl$ as an external source of ammonium cations, and yielded catalysts that were more active for hydrogen peroxide synthesis and less active for hydrogenation than those prepared in the absence of $NH_4Cl$. Crucially they were also observed by SEM to form nanochain agglomerates, supporting the hypothesis that reductant decomposition products influence colloidal nanoparticle stability and therefore metal nanostructure of the resultant catalyst..

Catalyst reusability was also investigated. XC72R carbon supported catalysts were stable upon reuse, where as those supported on P25 $TiO_2$ were not. Upon reuse the hydrogen peroxide hydrogenation activity of the $TiO_2$ supported catalysts increased and therefore selectivity decreased. XPS analysis of the fresh and used catalysts showed that the surface Pd and Au concentrations were greatly diminished for the $PdAu/TiO_2$ catalyst upon reuse, consistent with leaching of the active metal surface into solution. The increased hydrogen peroxide hydrogenation activity after reuse can be attributed to the dispersion of highly active solution phase metal species back onto the support.

In contrast, the Pd and Au surface concentrations remain constant for the XC72R supported catalyst, suggesting that the choice of support can influence stability and prevent dissolution of the supported metal catalyst into the reaction mixture. The carbon supported catalysts also have a significant portion of Pd(II) present in the metal nanostructure, which is unusual for catalysts prepared from colloidal nanoparticles without heat treatment. Pd(II) is known to be

more selective towards hydrogen peroxide synthesis than Pd(0), and the variable oxidation state found in the catalyst may contribute to maintaining high selectivity upon reuse. Identification of the precise origin of stability of this catalyst however requires further work.

## *4.9. References*

1 V. Haensel, US2479110A, 1947.
2 B. Choi, H. Yoon, I. S. Park, J. Jang and Y. E. Sung, *Carbon N. Y.*, 2007, **45**, 2496–2501.
3 L. Ouyang, L. Tan, J. Xu, P.-F. Tian, G.-J. Da, X.-J. Yang, D. Chen, F. Tang and Y.-F. Han, *Catal. Today*, 2015, **248**, 28–34.
4 F. Liguori, C. Moreno-Marrodan and P. Barbaro, *Cuihua Xuebao/Chinese J. Catal.*, 2015, **36**, 1157–1169.
5 F. Zimmerman, US2226149A, 1939.
6 J. Franzer, US1934795A, 1929.
7 J. K. Edwards, S. J. Freakley, R. J. Lewis, J. C. Pritchard and G. J. Hutchings, *Catal. Today*, 2015, **248**, 3–9.
8 J. K. Edwards, A. F. Carley, A. A. Herzing, C. J. Kiely and G. J. Hutchings, *Faraday Discuss.*, 2008, **138**, 225–239.
9 J. K. Edwards, A. Thomas, A. F. Carley, A. A. Herzing, C. J. Kiely and G. J. Hutchings, *Green Chem.*, 2008, **10**, 388–394.
10 J. K. Edwards, B. Solsona, P. Landon, A. F. Carley, A. Herzing, M. Watanabe, C. J. Kiely and G. J. Hutchings, *J. Mater. Chem.*, 2005, **15**, 4595.
11 J. C. Pritchard, Q. He, E. N. Ntainjua, M. Piccinini, J. K. Edwards, A. A. Herzing, A. F. Carley, J. A. Moulijn, C. J. Kiely and G. J. Hutchings, *Green Chem.*, 2010, **12**, 915.
12 N. Dimitratos, J. A. Lopez-Sanchez, D. Morgan, A. F. Carley, R. Tiruvalam, C. J. Kiely, D. Bethell and G. J. Hutchings, *Phys. Chem. Chem. Phys.*, 2009, **11**, 5142.
13 R. C. Tiruvalam, J. C. Pritchard, N. Dimitratos, J. A. Lopez-Sanchez, J. K. Edwards, A. F. Carley, G. J. Hutchings and C. J. Kiely, *Faraday Discuss.*, 2011, **152**, 63.
14 J. A. Lopez-Sanchez, N. Dimitratos, P. Miedziak, E. Ntainjua, J. K. Edwards, D. Morgan, A. F. Carley, R. Tiruvalam, C. J. Kiely and G. J. Hutchings, *Phys. Chem. Chem. Phys.*, 2008, **10**, 1921.
15 J. Pritchard, L. Kesavan, M. Piccinini, Q. He, R. Tiruvalam, N. Dimitratos, J. A. Lopez-Sanchez, A. F. Carley, J. K. Edwards, C. J. Kiely and G. J. Hutchings, *Langmuir*, 2010, **26**, 16568–16577.
16 J. A. Lopez-Sanchez, N. Dimitratos, N. Glanville, L. Kesavan, C. Hammond, J. K. Edwards, A. F. Carley, C. J. Kiely and G. J. Hutchings, *Appl. Catal. A Gen.*, 2011, **391**, 400–406.
17 J. Polte, *CrystEngComm*, 2015, **17**, 6809–6830.
18 J. E. Jaine and M. R. Mucalo, *J. Colloid Interface Sci.*, 2012, **375**, 12–22.
19 M. Morad, M. Sankar, E. Cao, E. Nowicka, T. E. Davies, P. J. Miedziak, D. J. Morgan, D. W. Knight, D. Bethell, A. Gavriilidis and G. J. Hutchings, *Catal. Sci. Technol.*, 2014, **4**, 3120–3128.
20 L. Abis, S. J. Freakley, G. Dodekatos, D. J. Morgan, M. Sankar, N. Dimitratos, Q. He, C. J. Kiely and G. J. Hutchings, *ChemCatChem*, 2017, **9**, 2914–2918.
21 M. Crespo-Quesada, J. M. Andanson, A. Yarulin, B. Lim, Y. Xia and L. Kiwi-Minsker, *Langmuir*, 2011, **27**, 7909–7916.
22 J. Pritchard, M. Piccinini, R. Tiruvalam, Q. He, N. Dimitratos, J. A. Lopez-Sanchez, D. J. Morgan, A. F. Carley, J. K. Edwards, C. J. Kiely and G. J. Hutchings, *Catal. Sci. Technol.*, 2013, **3**, 308–317.
23 J. K. Edwards, A. F. Carley, A. A. Herzing, C. J. Kiely and G. J. Hutchings, *Faraday Discuss.*, 2008, **138**, 225–239.
24 J. Edwards, B. Solsona, P. Landon, A. Carley, A. Herzing, C. Kiely And G. Hutchings,

*J. Catal.*, 2005, **236**, 69–79.
25 J. K. Edwards, A. Thomas, B. E. Solsona, P. Landon, A. F. Carley and G. J. Hutchings, *Catal. Today*, 2007, **122**, 397–402.
26 Y. Xia, X. Xia and H. C. Peng, *J. Am. Chem. Soc.*, 2015, **137**, 7947–7966.
27 S. Iqbal, S. A. Kondrat, D. R. Jones, D. C. Schoenmakers, J. K. Edwards, L. Lu, B. R. Yeo, P. P. Wells, E. K. Gibson, D. J. Morgan, C. J. Kiely and G. J. Hutchings, *ACS Catal.*, 2015, **5**, 5047–5059.
28 J. A. Lopez-Sanchez, N. Dimitratos, P. Miedziak, E. Ntainjua, J. K. Edwards, D. Morgan, A. F. Carley, R. Tiruvalam, C. J. Kiely and G. J. Hutchings, *Phys. Chem. Chem. Phys.*, 2008, **10**, 1921.
29 J. A. Lopez-Sanchez, N. Dimitratos, C. Hammond, G. L. Brett, L. Kesavan, S. White, P. Miedziak, R. Tiruvalam, R. L. Jenkins, A. F. Carley, D. Knight, C. J. Kiely and G. J. Hutchings, *Nat. Chem.*, 2011, **3**, 551–556.
30 T. Teranishi and M. Miyake, *Chem. Mater.*, 1998, **10**, 594–600.
31 P. Tian, L. Ouyang, X. Xu, C. Ao, X. Xu, R. Si, X. Shen, M. Lin, J. Xu and Y.-F. Han, *J. Catal.*, 2017, **349**, 30–40.
32 J. S. Jirkovský, I. Panas, E. Ahlberg, M. Halasa, S. Romani and D. J. Schiffrin, *J. Am. Chem. Soc.*, 2011, **133**, 19432–19441.
33 D. R. Jones, S. Iqbal, P. J. Miedziak, D. J. Morgan, J. K. Edwards, Q. He and G. J. Hutchings, *Top. Catal.*, 2018, **61**, 833–843.
34 S. a. Kondrat, P. J. Miedziak, M. Douthwaite, G. L. Brett, T. E. Davies, D. J. Morgan, J. K. Edwards, D. W. Knight, C. J. Kiely, S. H. Taylor and G. J. Hutchings, *ChemSusChem*, 2014, **7**, 1326–1334.
35 H.-L. Jiang and Q. Xu, *J. Mater. Chem.*, 2011, **21**, 13705.
36 K. G. Thomas, S. Barazzouk, B. I. Ipe, S. T. S. Joseph and P. V. Kamat, *J. Phys. Chem. B*, 2004, **108**, 13066–13068.
37 G.-T. Fu, R. Wu, C. Liu, J. Lin, D.-M. Sun and Y.-W. Tang, *RSC Adv.*, 2015, **5**, 18111–18115.
38 J. N. Zheng, M. Zhang, F. F. Li, S. S. Li, A. J. Wang and J. J. Feng, *Electrochim. Acta*, 2014, **130**, 446–452.
39 N. Agarwal, S. J. Freakley, R. U. McVicker, S. M. Althahban, N. Dimitratos, Q. He, D. J. Morgan, R. L. Jenkins, D. J. Willock, S. H. Taylor, C. J. Kiely and G. J. Hutchings, *Science*, 2017, **358**, 223–227.
40 D. I. Enache, J. K. Edwards, P. Landon, B. E. Solsona, A. F. Carley, A. A. Herzing, M. Watanabe, C. J. Kiely and D. W. Knight, *Science*, 2006, **311**, 362–365.
41 Z. Jiang, W. Zhang, L. Jin, X. Yang, F. Xu, J. Zhu and W. Huang, *J. Phys. Chem. C*, 2007, **111**, 12434–12439.
42 F. Menegazzo, M. Signoretto, M. Manzoli, F. Boccuzzi, G. Cruciani, F. Pinna and G. Strukul, *J. Catal.*, 2009, **268**, 122–130.
43 J. Panpranot, K. Phandinthong, P. Praserthdam, M. Hasegawa, S. ichiro Fujita and M. Arai, *J. Mol. Catal. A Chem.*, 2006, **253**, 20–24.
44 V. R. Choudhary, C. Samanta and T. V. Choudhary, *Appl. Catal. A Gen.*, 2006, **308**, 128–133.
45 P. Centomo, C. Meneghini, S. Sterchele, A. Trapananti, G. Aquilanti and M. Zecca, *ChemCatChem*, 2015, **7**, 3712–3718.
46 Z. Khan, N. F. Dummer and J. K. Edwards, *Philos. Trans. R. Soc. A Math. Phys. Eng. Sci.*, 2018, **376**.
47 M. Sankar, Q. He, M. Morad, J. Pritchard, S. J. Freakley, J. K. Edwards, S. H. Taylor, D. J. Morgan, A. F. Carley, D. W. Knight, C. J. Kiely and G. J. Hutchings, *ACS Nano*,

2012, **6**, 6600–6613.
48 J. Edwards, B. Solsona, P. Landon, A. Carley, A. Herzing, C. Kiely and G. Hutchings, *J. Catal.*, 2005, **236**, 69–79.
49 C. Samanta and V. R. Choudhary, *Appl. Catal. A Gen.*, 2007, **330**, 23–32.
50 A. Rodríguez-Gómez, F. Platero, A. Caballero and G. Colón, *Mol. Catal.*, 2018, **445**, 142–151.
51 Y. Li, E. Boone and M. A. El-Sayed, *Langmuir*, 2002, **18**, 4921–4925.
52 A. Villa, D. Wang, G. M. Veith, F. Vindigni and L. Prati, *Catal. Sci. Technol.*, 2013, **3**, 3036.
53 A. Villa, D. Wang, D. S. Su and L. Prati, *ChemCatChem*, 2009, **1**, 510–514.
54 J. K. Edwards, B. Solsona, E. N. N, A. F. Carley, A. A. Herzing, C. J. Kiely and G. J. Hutchings, *Science*, 2009, **323**, 1037–1041.
55 Z. P. Li, B. H. Liu, K. Arai and S. Suda, *J. Alloys Compd.*, 2005, **404**–**406**, 648–652.
56 W. X. Yin, Z. P. Li, J. K. Zhu and H. Y. Qin, *J. Power Sources*, 2008, **182**, 520–523.
57 K. Yamada, K. Asazawa, K. Yasuda, T. Ioroi, H. Tanaka, Y. Miyazaki and T. Kobayashi, *J. Power Sources*, 2003, **115**, 236–242.
58 X. B. Zhang, S. Han, J. M. Yan, M. Chandra, H. Shioyama, K. Yasuda, N. Kuriyama, T. Kobayashi and Q. Xu, *J. Power Sources*, 2007, **168**, 167–171.
59 U. B. Demirci and P. Miele, *Energy Environ. Sci.*, 2009, **2**, 627–637.
60 H. Jia and L. Zheng, *CrystEngComm*, 2012, **14**, 2920–2925.
61 D. F. Zhang, L. Y. Niu, L. Jiang, P. G. Yin, L. D. Sun, H. Zhang, R. Zhang, L. Guo and C. H. Yan, *J. Phys. Chem. C*, 2008, **112**, 16011–16016.
62 L. Ouyang, G. J. Da, P. F. Tian, T. Y. Chen, G. Da Liang, J. Xu and Y. F. Han, *J. Catal.*, 2014, **311**, 129–136.
63 J. K. Edwards, J. Pritchard, L. Lu, M. Piccinini, G. Shaw, A. F. Carley, D. J. Morgan, C. J. Kiely and G. J. Hutchings, *Angew. Chemie Int. Ed.*, 2014, **53**, 2381–2384.
64 S. J. Freakley, Q. He, J. H. Harrhy, L. Lu, D. A. Crole, D. J. Morgan, E. N. Ntainjua, J. K. Edwards, A. F. Carley, A. Y. Borisevich, C. J. Kiely and G. J. Hutchings, *Science*, 2016, **351**, 965–968.
65 D. Ding, X. Xu, P. Tian, X. Liu, J. Xu and Y. F. Han, *Chinese J. Catal.*, 2018, **39**, 673–681.
66 H. Xu, D. Cheng and Y. Gao, *ACS Catal.*, 2017, **7**, 2164–2170.
67 S. Maity and M. Eswaramoorthy, *J. Mater. Chem. A*, 2016.
68 O. Metin, V. Mazumder, S. Ozkar and S. Sun, *J. Am. Chem. Soc*, 2010, **132**, 1468.
69 S. K. Singh, Y. Iizuka and Q. Xu, *Int. J. Hydrogen Energy*, 2011, **36**, 11794–11801.
70 D. Ferrer, A. Torres-Castro, X. Gao, S. Sepúlveda-Guzmán, U. Ortiz-Méndez and M. José-Yacamán, *Nano Lett.*, 2007, **7**, 1701–1705.
71 J. Xian, Q. Hua, Z. Jiang, Y. Ma and W. Huang, *Langmuir*, 2012, **28**, 6736–6741.
72 H. Tsunoyama, N. Ichikuni, H. Sakurai and T. Tsukuda, *J. Am. Chem. Soc.*, 2009, **131**, 7086–7093.
73 M. Okumura, Y. Kitagawa, T. Kawakami and M. Haruta, *Chem. Phys. Lett.*, 2008, **459**, 133–136.

# 5. Carbons as Catalyst Supports and Heterogeneous Additives for the Direct Synthesis of Hydrogen Peroxide

## *5.1. Introduction*

Supported precious metal catalysts are well known to effectively catalyse a range of reactions such as the upgrading of biomass or the production of commodity chemicals by oxidation or hydrogenation.[1,2,3] One such application is the direct synthesis of hydrogen peroxide from molecular hydrogen and oxygen.[4]

A critical consideration in the preparation of heterogeneous catalysts is the choice of support material. In the case of the direct synthesis of hydrogen peroxide, metal oxides such as $TiO_2$, $SiO_2$, $Al_2O_3$ and $Fe_2O_3$ have been thoroughly explored as supports.[5,6,7,8] Complex metal oxides such as zeolites have also been found to be appropriate supports.[9,10] Carbon is a support which is cheap and abundant and therefore represents an environmentally friendly alternative to metal oxides.[4,11] Carbon is an incredibly versatile material, displaying a wide range of textural, chemical and conductive properties, and these factors have been shown to influence catalytic activity.[12,13,14]

As a first example, Choi *et al.* investigated Pt supported on nitrogen doped graphene for methanol electrooxidation and found that, in comparison to commercially available carbon blacks, the graphene supported catalyst was considerably more active and resistant to deactivation.[15] Conversely, Rintoul and co-workers published a comparison of Ru/C catalysts for ammonia decomposition and found that graphitic carbon was considerably more active than activated carbons, carbon blacks and carbon nanomaterials.[16] Interestingly the activity of the catalysts was inconsistent with the surface area, porosity or Ru particle size, suggesting that other unknown factors influence catalyst activity.

Carbon supported PdAu catalysts have been shown to be highly active for the direct synthesis of hydrogen peroxide from molecular hydrogen and oxygen.[17] Edwards *et al.* previously reported that the selectivity of impregnation prepared PdAu/C catalysts towards the direct synthesis of hydrogen peroxide can be significantly improved through functionalisation of the carbon support using acid pre-treatment prior to catalyst preparation.[18] This data suggests that the choice of carbon may influence catalyst activity; however, no such investigation has been previously reported for the direct synthesis of hydrogen peroxide. The aim of this work is

therefore to assess the catalytic activity and structure of carbon supported PdAu bimetallic catalysts for the direct synthesis of hydrogen peroxide.

## *5.2. Results*

### *5.2.1. Carbon Supported PdAu Catalysts Prepared by Impregnation*

Initially, 2.5 wt% Pd 2.5 wt% Au/C catalysts were prepared by wet impregnation supported on commercially available synthetic graphite. For comparison a catalyst was also prepared using P25 $TiO_2$ as the support. The hydrogen peroxide synthesis and hydrogenation activity of these catalysts are presented in Figure 5-1. The $TiO_2$ supported reference catalyst is highly active for direct synthesis, 97 mol$H_2O_2$/h/$kg_{cat}$. In comparison the graphite supported catalysts are inferior with activities of 42 and 11 mol$H_2O_2$/h/$kg_{cat}$.

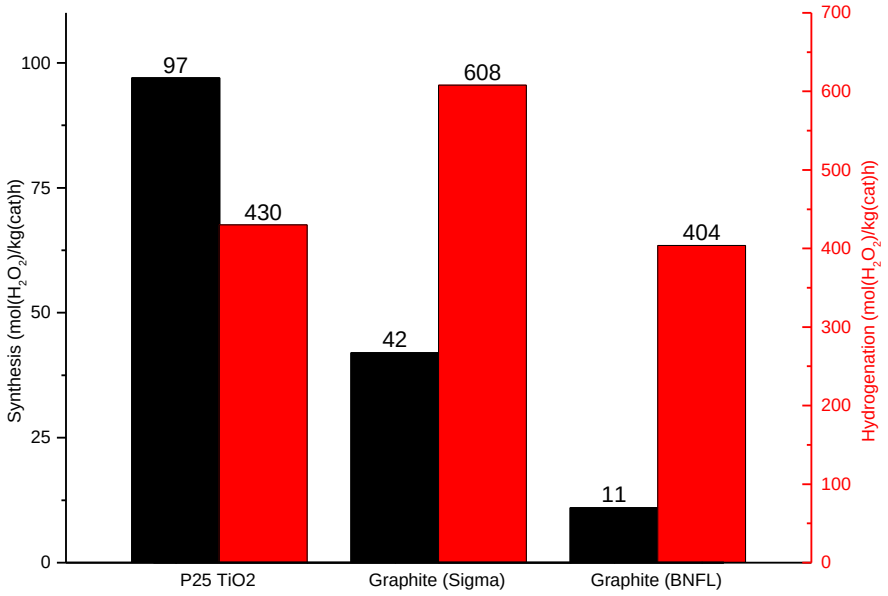


**Figure 5-1 - Hydrogen Peroxide Synthesis and Hydrogenation Activity of PdAu catalysts prepared by impregnation supported on P25 $TiO_2$ and graphite.**

**Reaction Conditions – Hydrogen peroxide synthesis: 5 % $H_2/CO_2$ (2.9 MPa) and 25 % $O_2/CO_2$ (1.1 MPa), 8.5 g solvent (2.9 g $H_2O$, 5.6 g MeOH) 0.01 g catalyst, 2 °C, 1200 rpm, 30 min. Hydrogen peroxide hydrogenation: 5 % $H_2/CO_2$ (2.9 MPa), 8.5 g solvent (2.22 g $H_2O$, 5.6 g MeOH and 0.68 g 50 wt% $H_2O_2$), 0.01 g catalyst, 2 °C, 1200 rpm, 30 min.**

The catalysts were also interrogated for their hydrogen peroxide hydrogenation activity. The graphite (Sigma) supported catalyst has the highest hydrogenation activity, 608 $molH_2O_2/h/kg_{cat}$ whilst the P25 $TiO_2$ and graphite (BNFL) supported catalysts have comparable activities of 430 and 404 $molH_2O_2/h/kg_{cat}$. Given the low activity of the graphite (BNFL) supported catalyst for direct synthesis, the hydrogenation values for the catalysts suggest that factors other than the hydrogenation of hydrogen peroxide are responsible for the catalysts low activity, such as metal nanostructuring. Pritchard *et al.* previously interrogated PdAu catalysts by scanning transmission electron microscopy (STEM).[19] The authors reported that $TiO_2$ supported nanoparticles underwent morphological change upon heat treatment, wetting the support such that the metal-surface interaction was maximised. In contrast, for carbon supported catalysts, the PdAu nanoparticles remained roughly spherical after heat treatment, indicative of the poor interaction with the support. The poor interaction between the carbon support material and nanoparticle surface suggests that the choice of carbon has a minimal electronic effect on the structure of the nanoparticles and therefore inadequately explains the activity disparity between carbon supported catalysts.

The activities of carbon supported PdAu catalysts have been previously evaluated by Edwards *et al.* for hydrogen peroxide direct synthesis.[18] The authors showed that a catalyst prepared by an analogous method to this work, albeit on the carbon black material Darco G60, had a hydrogen peroxide synthesis activity of 110 $molH_2O_2/h/kg_{cat}$, and a selectivity of 80 %. The activity of the previously reported G60 supported catalyst is considerably higher than the graphite supported carbon catalysts presented in Figure 5-1, indicating that the choice of carbon support does influence the activity of the resultant catalyst.

Given the low activity of graphite supported PdAu catalysts previously presented in Figure 5-1, further catalysts were prepared on commercial carbon blacks. The hydrogen peroxide synthesis and hydrogenation activity of the carbon black supported 2.5 wt% Pd 2.5 wt%Au catalysts are presented in Figure 5-2.

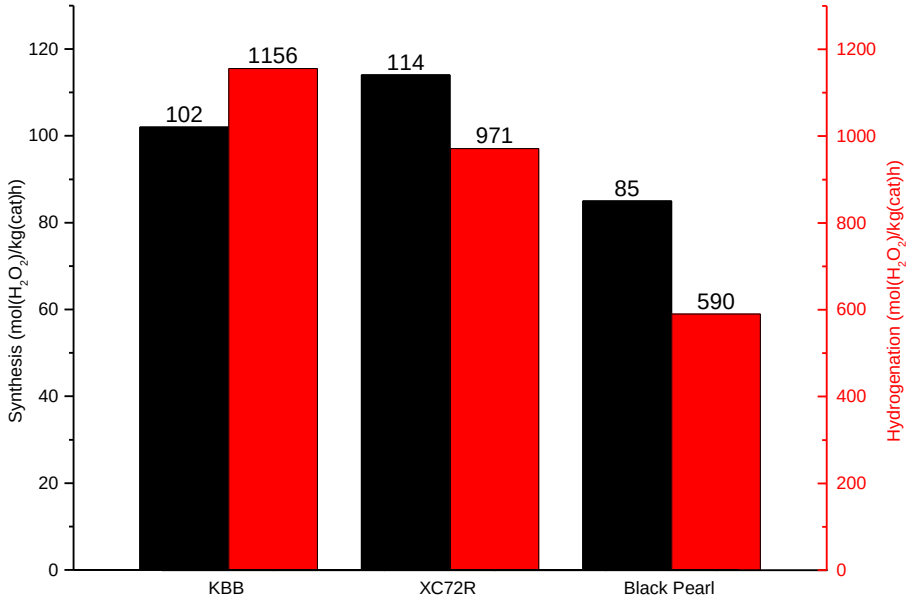


**Figure 5-2 - Hydrogen peroxide synthesis and hydrogenation activity of PdAu catalysts prepared by impregnation supported on commercial carbon blacks.**

**Reaction Conditions – Hydrogen peroxide synthesis: 5 % $H_2/CO_2$ (2.9 MPa) and 25 % $O_2/CO_2$ (1.1 MPa), 8.5 g solvent (2.9 g $H_2O$, 5.6 g MeOH) 0.01 g catalyst, 2 °C, 1200 rpm, 30 min. Hydrogen peroxide hydrogenation: 5 % $H_2/CO_2$ (2.9 MPa), 8.5 g solvent (2.22 g $H_2O$, 5.6 g MeOH and 0.68 g 50 wt% $H_2O_2$), 0.01 g catalyst, 2 °C, 1200 rpm, 30 min.**

In all cases the hydrogen peroxide synthesis activities of the carbon black supported catalysts are considerably greater than the graphite analogues. The XC72R and KBB supported catalysts have similar synthesis activities, 102 and 114 mol$H_2O_2$/h/$kg_{cat}$ respectively, whilst the Black Pearl supported catalyst is marginally less active at 85 mol$H_2O_2$/h/$kg_{cat}$. Interestingly, the carbon black supported catalysts are more active for hydrogen peroxide hydrogenation than the graphite supported or reference catalyst. The XC72R and KBB supported catalysts are highly active for hydrogen peroxide hydrogenation with activities of 1156 and 971 mol$H_2O_2$/h/$kg_{cat}$ whilst the activity of the Black Pearl supported catalyst is roughly half that of the KBB supported analogue, 590 mol$H_2O_2$/h/$kg_{cat}$.

Hydrogenation activity is indicative of the propensity of the catalyst to destroy hydrogen peroxide produced under batch synthesis conditions via hydrogenation. The hydrogenation of hydrogen peroxide is the dominant non-productive reaction pathway during hydrogen peroxide synthesis and therefore must be minimised through catalyst optimisation to yield selective catalysts. In this regard, the Black Pearl supported catalyst is superior to the other carbon supported catalysts with a balance of synthesis and hydrogenation activity. The Black Pearl supported catalyst is 25 % less active for hydrogen peroxide synthesis in comparison to

the KBB and XC72R supported analogues but also 50% less active for hydrogen peroxide hydrogenation, indicating that it is more selective.

Given the variance in activity of graphite and carbon black supported PdAu catalysts, further catalysts were prepared using carbon nanomaterials. Carbon nanotubes have been shown to be effective supports in producing highly active catalysts for a range of oxidation and hydrogenation reactions.[20,21,22] A series of 2.5 wt% Pd 2.5 wt% Au/C catalysts were prepared on multi-walled carbon nanotubes (MWCNT) and graphene nanoplatelets (SDP 500), as well as oxygen functionalised analogues of these materials, to probe the effect of surface groups on catalyst activity. The hydrogen peroxide synthesis and hydrogenation activity of carbon nanomaterial supported catalysts is presented in Figure 5-3.

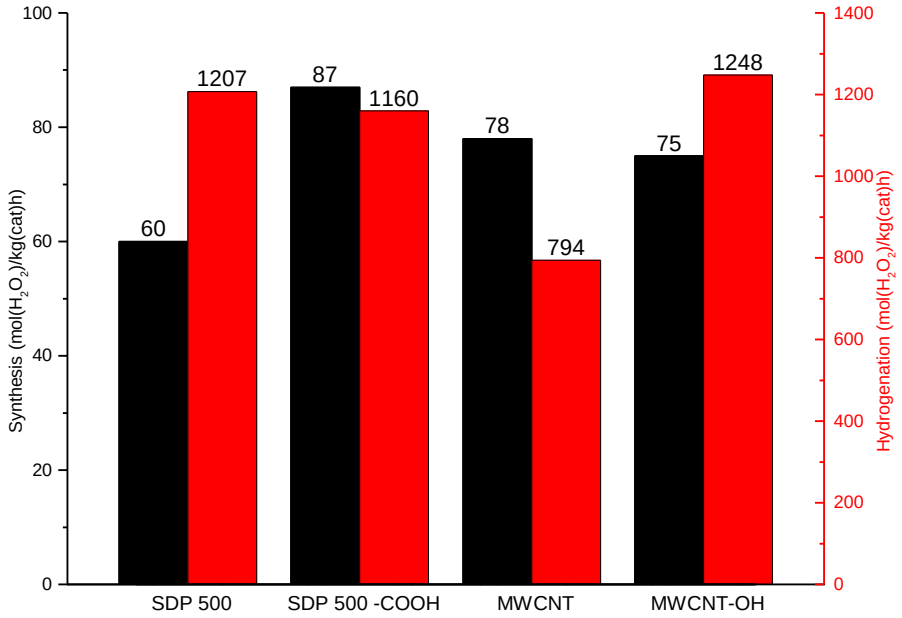


**Figure 5-3 - Hydrogen peroxide synthesis and hydrogenation activity of PdAu catalysts prepared by impregnation supported on carbon nanomaterials.**

**Reaction Conditions – Hydrogen peroxide synthesis: 5 % $H_2/CO_2$ (2.9 MPa) and 25 % $O_2/CO_2$ (1.1 MPa), 8.5 g solvent (2.9 g $H_2O$, 5.6 g MeOH) 0.01 g catalyst, 2 °C, 1200 rpm, 30 min. Hydrogen peroxide hydrogenation: 5 % $H_2/CO_2$ (2.9 MPa), 8.5 g solvent (2.22 g $H_2O$, 5.6 g MeOH and 0.68 g 50 wt% $H_2O_2$), 0.01 g catalyst, 2 °C, 1200 rpm, 30 min.**

The carboxylic acid functionalised graphene nanoplatelet (SDP 500-COOH) supported catalyst has the highest activity of the functionalised nanocarbons, 87 mol$H_2O_2$/h/$kg_{cat}$. In comparison, the catalyst supported on unfunctionalized parent material (SDP 500) is less active at 60 mol$H_2O_2$/h/$kg_{cat}$. Prati and co-workers previously investigated the functionalisation of carbon nanotubes in preparing active monometallic Pd and PdAu catalysts for alcohol oxidation and showed that functionalisation yielded decreased average

metal nanoparticle diameter and increased activity through surface area effects.[23] Guha *et al.* reported similar effects in Pt/CNT catalysts, finding that acid treatment of CNTs yielded decreased Pt particle size in the prepared catalyst.[24] The author's attribute the decreased nanoparticle diameter to the incorporation of nitrate or sulphate groups on the surface of the carbon as evidenced by XPS and potentiometric titration.

The increased activity of the SDP500-COOH supported catalyst in comparison to the SDP500 supported parent catalyst can be considered an amalgamation of two phenomena. Previous work has shown that the presence of solution phase strong or weak acids during reaction has a profound effect on hydrogen peroxide synthesis activity.[25] The presence of acidic functional groups on the surface of the support could therefore be considered as a heterogeneous source of acidic sites that results in increased the synthesis rate. It has also been shown that acid functionalised metal oxides are effective in preparing highly active catalysts for hydrogen peroxide synthesis.[26,27] Particularly in the case of catalysts prepared by impregnation, the presence of surface functionality results in improved metal precursor dispersion which yields smaller nanoparticles upon heat treatment.

The presence of acid during reaction has been shown to result in improved hydrogen peroxide synthesis activity through the suppression of hydrogen peroxide hydrogenation.[28] In the case of the SDP 500 derived catalysts, the hydrogen peroxide hydrogenation activity of the raw and carboxylic acid functionalised catalysts are comparable, 1207 and 1160 $molH_2O_2/h/kg_{cat}$, which suggests that the functional groups alter nanoparticle microstructure during catalyst preparation as opposed to playing an stabilising role during reaction.

The hydroxyl functionalised and unfunctionalized MWCNT supported catalysts have similar hydrogen peroxide synthesis activities, 75 and 78 $molH_2O_2/h/kg_{cat}$ respectively, which suggests that the presence of hydroxyl groups during reaction has minimal effect on catalyst activity. The acid dissociation constant, pKa, of a group is a quantitative measure of the equilibrium between acid and base form in solution. Guideline pKa values for hydroxyl and carboxylic acid groups are 17 and 4 respectively.[29] As a result the contribution of carboxylic acid groups to solution phase acidity is order of magnitudes larger than that of hydroxyl groups and any solution phase stabilisation by surface hydroxyl groups can be considered minimal.

The MWCNT catalysts were also evaluated for hydrogen peroxide hydrogenation. Interestingly the hydroxyl functionalised analogue is considerably more active for hydrogenation than the unfunctionalized counterpart, 1248 and 794 mol$H_2O_2$/h/$kg_{cat}$ respectively which indicates that the despite having similar synthesis activities, using unfunctionalized MWCNTs as the support yields a more selective catalyst.

#### *5.2.1.1. Brunauer–Emmett–Teller Surface Area Analysis*

To better understand the physical characteristics of the carbons used in this work, the 2.5 wt% Pd 2.5 wt% Au/C catalysts prepared by wet impregnation were interrogated using BET surface area analysis. For comparison, the 2.5 wt% Pd 2.5 wt% Au/$TiO_2$ reference catalyst used in Section 5.2.1. was also analysed. Using the wet impregnation preparation method, metal precursors are dispersed on a support material which decompose upon heat treatment to yield supported metal nanoparticles. Therefore, thorough dispersion of the metal precursor is prerequisite in affording small well dispersed nanoparticles in the final catalyst which suggests that support surface area is important in improving the dispersion of the precursors and therefore improving catalyst activity.

The surface area of the wet impregnation catalysts are presented in Table 5-1. The graphite (BNFL) supported catalyst has the lowest surface area, 7 $m^2$/g, whilst the Black Pearl derived catalyst the greatest at 2600 $m^2$/g. The low surface area of the graphite (BNFL) catalyst is consistent with the poor activity of the impregnation prepared catalysts suggesting that the surface area of the material is too low to effectively support dispersed nanoparticles.

**Table 5-1 - BET surface areas of 2.5 wt% Pd 2.5 wt% Au/C and $TiO_2$ catalysts prepared by wet impregnation**

| Support | BET Surface Area ($m^2/g$) |
|---|---|
| P25 $TiO_2$ | 50 |
| Graphite (Sigma) | 190 |
| Graphite (BNFL) | 7 |
| KBB | 1100 |
| XC72R | 250 |
| Black Pearl | 2600 |
| SDP 500 | 500 |
| SDP 500-COOH | 510 |
| MWCNT | 1500 |
| MWCNT-OH | 1480 |

Comparison of the hydrogen peroxide synthesis and hydrogenation activities and surface area of the catalyst materials suggests that the two are only weakly correlated. For example, in the case of the carbon black supported catalysts, 2.5 wt% Pd 2.5 wt% Au/XC72R is most active with a synthesis activity of 114 $molH_2O_2/h/kg_{cat}$. The KBB and Black Pearl supported catalysts have similarly high activities of 102 and 85 $molH_2O_2/h/kg_{cat}$ respectively. The KBB supported catalyst has a surface area 4 times greater than the XC72R supported analogue, and 10 times greater than the Black Pearl supported catalyst, which suggests that the assumption that increased support surface area improves nanoparticle dispersion and therefore increased catalyst activity, is incorrect.

The hydrogenation activity of the carbon black supported catalysts is similarly unconnected to the support surface area. The Black Pearl supported catalyst, with highest surface area, has the lowest hydrogenation activity of the series, 590 $molH_2O_2/h/kg_{cat}$, however the KBB catalyst of intermediate surface area displays the largest activity, 1156 $molH_2O_2/h/kg_{cat}$.

Analysis of the carbon nanomaterial derived catalysts also suggests that factors other than surface area modulate catalyst activity. The carbon nanomaterials used in this work were prepared commercially using plasma discharge. In this manufacturing method a methane rich

gas mixture is passed through a dielectric barrier discharge (DBD) reactor producing a non-thermal plasma. The plasma decomposes, yielding carbon nanoparticles, which are then isolated. Surface modification of the carbon material is achieved using a second pass through a reactor in an oxygen rich atmosphere.[30] Because of the non-thermal nature of the treatment, the surface area of the functionalised and raw carbon materials remains roughly constant and therefore cannot be responsible for the variation in activity of the impregnation prepared catalysts. For example, the catalysts supported on raw and carboxylic acid functionalised SDP 500 carbon have surface areas of 500 and 510 $m^2/g$ respectively. The SDP 500-COOH supported catalyst is however 30 % more active for hydrogen peroxide synthesis in comparison to the parent carbon SDP 500 with an activity of 87 versus 60 $molH_2O_2/h/kg_{cat}$.

The MWCNT and MWCNT-OH supported catalysts displayed also similar surface areas of 1500 and 1480 $m^2/g$. Interestingly, the hydrogen peroxide synthesis activity of the functionalised and raw carbon supported catalysts remains unchanged at 75 and 78 $molH_2O_2/h/kg_{cat}$; however, the MWCNT-OH supported catalyst displays considerably higher hydrogenation activity, 1248 versus 794 $molH_2O_2/h/kg_{cat}$ for the parent MWCNT carbon.

*5.2.1.2.Scanning Electron Microscopy (SEM)*

In the preceding section it has been established for catalysts prepared by wet impregnation, the surface area of the support material is not responsible for the large range of hydrogen peroxide synthesis and hydrogenation activities of carbon supported PdAu catalysts. Alternatively, it can be suggested that the activity variation of the catalysts could be due to structural variations in the active metal nanostructure. To further investigate this effect the 2.5 wt% Pd 2.5 wt% Au/C catalysts were interrogated by SEM-BSE.

*5.2.1.2.1.SEM-BSE Microscopy of the 2.5 wt% Pd 2.5 wt% Au/$TiO_2$ Reference Catalyst*

SEM-BSE images of the reference catalyst 2.5 wt% Pd 2.5 wt% Au/$TiO_2$ are presented in Figure 5-4. The $TiO_2$ supported catalyst contains largely spherical particles with a diameter of 5-100 nm. Edwards *et al.* previously reported PdAu/$TiO_2$ for hydrogen peroxide synthesis prepared by an analogous impregnation method, which contained particle sizes of 5-400 nm, with the mono and bimetallic species of various compositions observed.[31] The absence of larger nanoparticles in the reference catalyst presented in Section 5.2.1 are likely due to the use of acidified metal precursor solutions, consistent with previous work by Hutchings and

co-workers that found that average particle size could be greatly reduced through the addition of acid during preparation.[32]

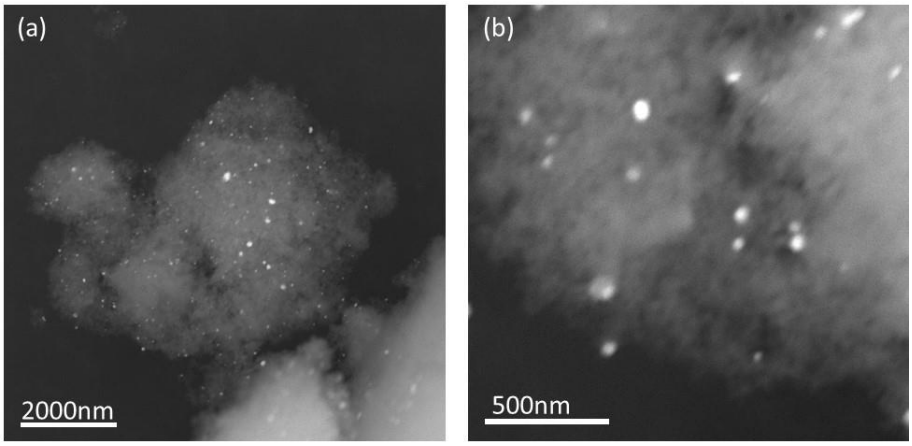


**Figure 5-4 - Low (a) and high (b) magnification SEM-BSE micrographs of 2.5 wt% Pd 2.5 wt% Au/$TiO_2$**

*5.2.1.2.2.SEM-BSE Microscopy of the 2.5 wt% Pd 2.5wt% Au/Graphite (Sigma) Catalyst*

The graphite (Sigma) catalyst was also investigated by SEM-BSE with representative images shown in Figure 5-5. The catalyst contains a wide range of particle sizes including the presence of micrometre sized PdAu particles. Large nanoparticles are thought to be inactive for hydrogen peroxide synthesis, owing to their low surface area-volume ratio, and as a result the presence of such particles is considered an inefficient use of costly precious metals. Curiously, many very small particles, 2-3 nm, were readily observed, in comparison to the reference catalyst in which only contained particles larger than 5 nm.

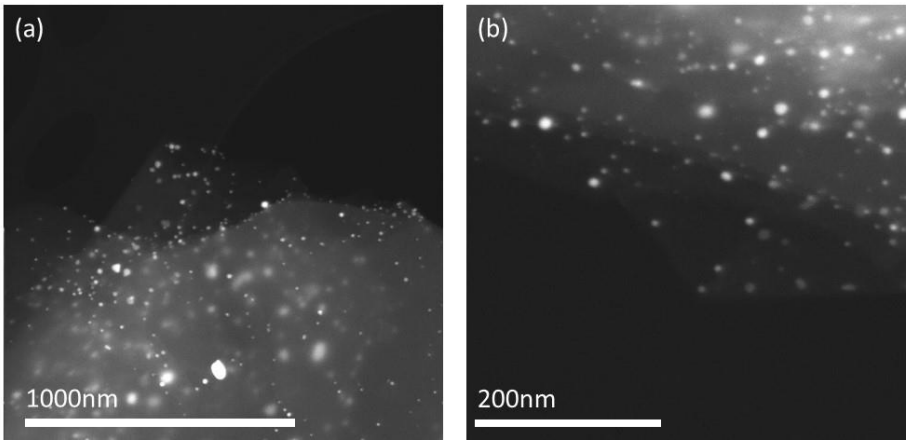


**Figure 5-5 - Low (a) and high (b) magnification SEM-BSE micrographs of 2.5 wt% Pd 2.5 wt% Au/Graphite (Sigma)**

The structure of the graphite (Sigma) catalyst is somewhat at odds with the catalyst activity reported in Section 5.2.1. Previous catalyst development work has largely concluded that

smaller nanoparticles are more active for hydrogen peroxide synthesis, however in this work it is shown that the graphite (Sigma) impregnation catalyst performed very poorly in comparison to the reference catalyst, despite containing relatively small, well dispersed nanoparticles.[17] The use of graphite as an additive negatively impacted hydrogen peroxide synthesis activity, which suggests that the poor activity of the graphite supported impregnation catalyst could be attributed to the presence of impurities active for the catalytic decomposition of hydrogen peroxide.

*5.2.1.2.3.SEM-BSE Microscopy of the 2.5 wt% Pd 2.5 wt% Au/Graphite (BNFL) Catalyst*

SEM-BSE Micrographs of the graphite (BNFL) supported catalyst are presented in Figure 5-6. The catalyst contains very large PdAu particles, 50-1000 nm in diameter. The dispersion of the nanoparticles is very poor; a significant proportion of the graphite particles were found to be devoid of metal and therefore catalytically inactive. Additionally, several large unsupported PdAu particles were found, typically 1-5 µm in diameter. The catalytic activity of such particles will be minimal due to low surface area and as a result, the amount of metal in the active nanoparticulate form varied greatly from the target loading.

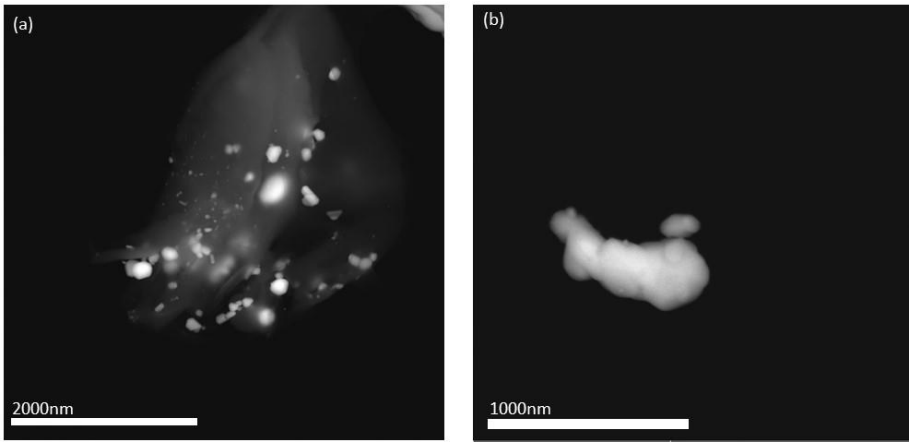


**Figure 5-6 - Low (a) magnification SEM-BSE micrographs of 2.5 wt% Pd 2.5 wt% Au/Graphite (BNFL). Image (b) of unsupported micrometre sized PdAu particle**

In Section 5.2.1, it was shown the graphite (BNFL) supported catalyst was very poorly active for hydrogen peroxide synthesis with an activity of 11 mol$H_2O_2$/h/$kg_{cat}$. This is consistent with the SEM-BSE data which shows that the catalyst contains a significant proportion of large particles are known to be less active for hydrogen peroxide synthesis.

*5.2.1.2.4.SEM-BSE Microscopy of the 2.5 wt% Pd 2.5 wt% Au/KBB Catalyst*

SEM-BSE images of the KBB supported PdAu catalyst are presented in Figure 5-7. The catalyst contains highly dispersed PdAu nanoparticles 2-10 nm in diameter and no larger agglomerated particles were observed, suggesting that high activity of the catalyst is due to the high active metal surface area and good dispersion, as little to no active metal is present as relatively inactive larger particles.

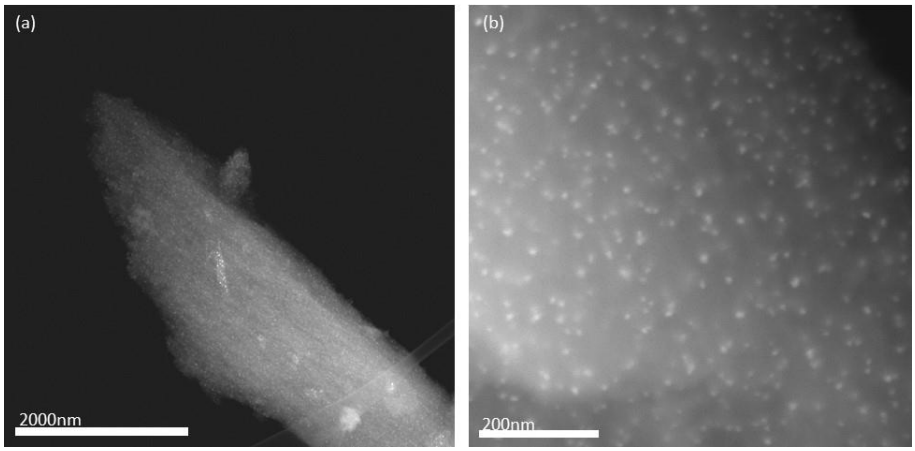


**Figure 5-7 -Low (a) and high (b) magnification SEM-BSE images of 2.5 wt% Pd 2.5 wt% Au/KBB**

The 2.5 wt% Pd 2.5 wt% Au/KBB catalyst is the most active impregnation catalyst for hydrogen peroxide hydrogenation, indicating that selectivity towards the direct synthesis pathway is poor. Tian *et al.* previously investigated particle size effects in monometallic Pd catalysts for the direct synthesis of hydrogen peroxide and reported that selectivity increased with decreasing average particle size achieving a maximum of 94 % for a 0.5 wt% Pd catalyst containing particles of 1.6 nm average diameter.[33] Catalyst selectivity fell with increasing metal loading; 2 wt% Pd and 5 wt% Pd catalysts achieve selectivity of 51 and 43%, respectively. The increases in metal loading resulted in an increase in average particle size to 2.2 nm for the 2 wt% Pd catalyst and 2.6 nm for the 5 wt% catalyst. which is consistent with the activity of the KBB supported catalyst presented in this work, which contains comparatively larger particles and shows high hydrogenation activity.

*5.2.1.2.5.SEM-BSE Microscopy of the 2.5 wt% P d2.5 wt% Au/XC72R Catalyst*

SEM-BSE images of 2.5 wt% Pd 2.5 wt% Au/XC72R are presented in Figure 5-8. The catalyst contains well dispersed particles 10-20 nm in diameter. In addition, no large particle agglomerates were observed. In Section 5.2.1, it is shown that the XC72R supported impregnation catalyst was the most active with a synthesis activity of 114 mol$H_2O_2$/h/$kg_{cat}$. Hydrogenation activity was lower than for the KBB supported analogue, which contains considerably smaller particles, suggesting that the presence of small particles may be detrimental in hydrogen peroxide synthesis due to increased activity for the hydrogenation pathway.

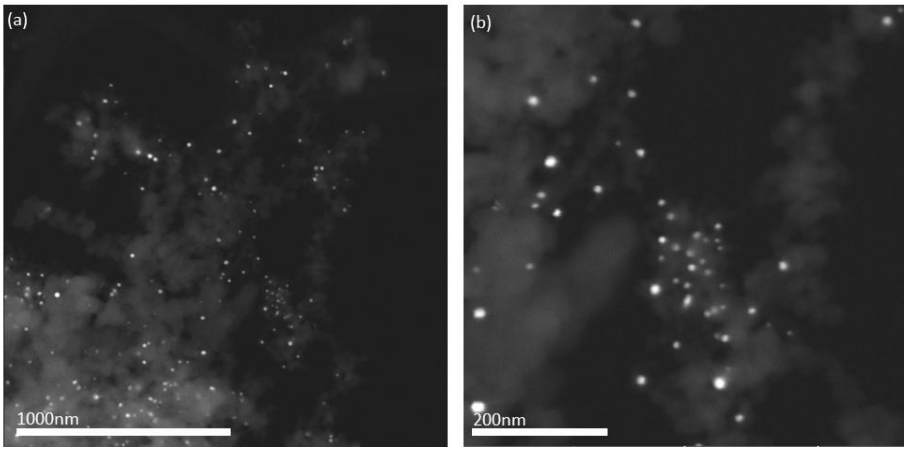


**Figure 5-8 - Low (a) and high (b) magnification SEM-BSE images of 2.5 wt% Pd 2.5 wt% Au/XC72R**

The superior performance of the XC72R supported catalyst can also be a consequence of the surface chemistry of the support. As an additive, KBB is highly detrimental to direct synthesis due to increased hydrogen peroxide hydrogenation/decomposition activity. Conversely, XC72R is a potent additive resulting in a significant increase in activity and a reduction in hydrogenation activity, indicating that the high activity of the XC72R supported impregnation catalyst may include some promoter contribution from the support.

*5.2.1.2.6.SEM-BSE Microscopy of the 2.5 wt% Pd 2.5 wt% Au/Black Pearl Catalyst*

SEM-BSE micrographs of the Black Pearl supported catalyst are shown in Figure 5-9 with the catalyst containing particles 2-20 nm in diameter. In this regard, the structure of the catalyst is intermediate to the KBB and XC72R supported catalysts with the former containing particles in the 3-10 nm range and the latter 10-20 nm. The 2.5 wt% Pd 2.5 wt%

Au/Black Pearl catalyst can be considered the optimum carbon supported catalyst prepared by impregnation owing to the balance between synthesis and hydrogenation activity.

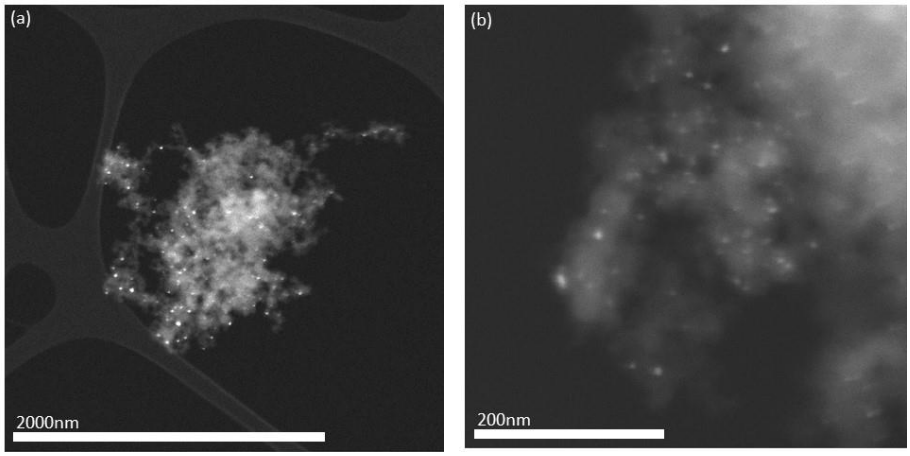


**Figure 5-9 - Low (a) and high (b) magnification SEM-BSE images of 2.5%Pd2.5%Au/Black Pearl**

In comparison with the most active catalyst, 2.5 wt% Pd 2.5 wt% Au /XC72R, the Black Pearl supported material is 20 % less active for hydrogen peroxide synthesis but crucially 40 % less active for hydrogen peroxide hydrogenation. The relative decrease in hydrogenation activity implies that the catalyst is more selective whilst maintaining appropriate activity for the direct synthesis pathway, and as a result is a superior catalyst. The comparatively low hydrogen peroxide hydrogenation activity also indicates that nanoparticle size is not the sole factor in determining activity. If either small (<10 nm) or large (>10 nm) nanoparticles were more active for the hydrogenation pathway, then the KBB or XC72R catalysts, which contain smaller and larger nanoparticles respectively, would exhibit decreased hydrogenation activity relative to the Black Pearl supported catalyst, which is not the case.

*5.2.1.2.7.SEM-BSE Microscopy of the 2.5 wt% Pd 2.5 wt% Au/SDP500 Catalyst*

SEM-BSE micrographs of the SDP500 supported PdAu impregnation catalyst are shown in Figure 5-10. The catalyst contains small nanoparticles, 3-10 nm in diameter. The nanoparticles are well dispersed on the support with nanoparticles thoroughly distributed across the surface of the support and an absence of naked support particles, in contrast to several other carbon supports used in this work.

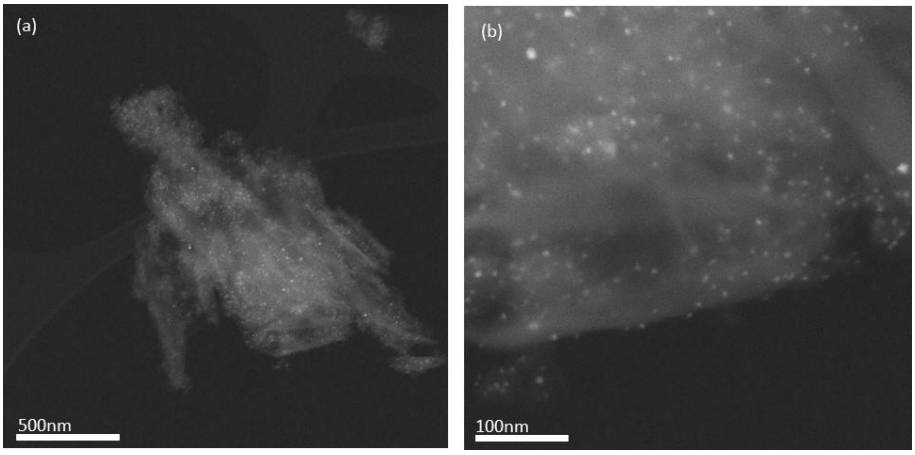


**Figure 5-10 - Low (a) and high (b) magnification SEM-BSE images of 2.5 wt% Pd 2.5 wt% Au/SDP 500**

The structure and activity of the SDP500 catalyst suggests that particle size effects cannot reasonably explain the activity of catalysts prepared by impregnation. Both the SDP500 and KBB supported catalysts contain well dispersed nanoparticles 3-10 nm in diameter, whilst the former has a hydrogen peroxide synthesis activity of 60 mol$H_2O_2$/h/$kg_{cat}$ and the latter 102 mol$H_2O_2$/h/$kg_{cat}$. Interestingly, the two catalysts have comparable hydrogenation activities, 1207 and 1156 mol$H_2O_2$/h/$kg_{cat}$ respectively, indicating that the poor activity of the SDP500 supported catalyst is not due to its activity for destructive pathways such as hydrogen peroxide hydrogenation or decomposition.

*5.2.1.2.8.SEM-BSE Microscopy of the 2.5 wt% Pd 2.5 wt% Au/SDP500-COOH Catalyst*

SEM-BSE images of the SDP 500-COOH supported impregnation catalyst are presented in Figure 5-11. In contrast to the carbon black supported catalysts, metal dispersion is very poor. Unsupported metal particles as large as 5 µm are observed as well as naked support particles, however the remaining supported metal is present as nanoparticles 7-15 nm in diameter. The catalyst was comparably active to the carbon black supported catalysts which are absent of large particulate agglomerates, indicating that in the case of SDP500 supported catalyst, the metal that is present as smaller nanoparticles is highly active for hydrogen peroxide synthesis and hydrogenation.

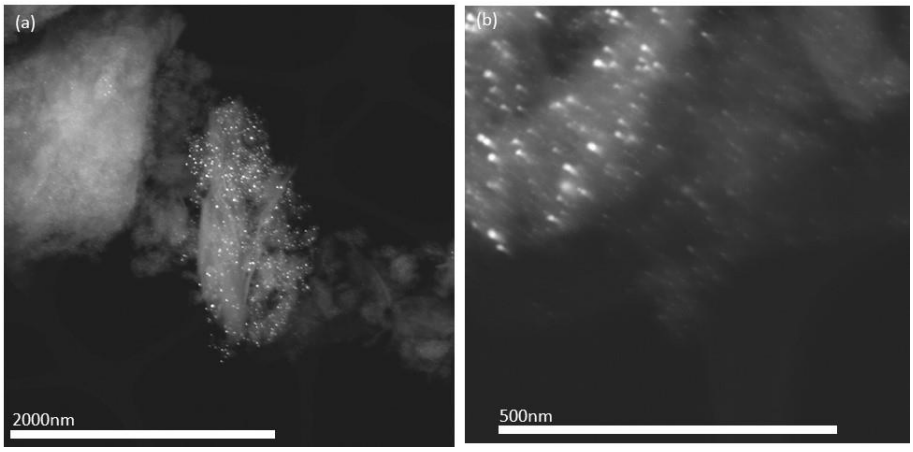


**Figure 5-11 - Low (a) and high (b) magnification SEM-BSE images of 2.5 wt% Pd 2.5 wt% Au/SDP 500-COOH**

Comparison of the SDP500 and SDP500-COOH supported catalysts further highlights a disparity between nanoparticle size and catalyst activity. As shown in Section 5.2.1.2.7, the SDP500 supported analogue contains nanoparticles 3-10 nm in diameter and a complete absence of larger metallic species. In contrast, the SDP500-COOH catalyst shown in Figure 5-11 displays a mixture of very large, relatively inactive particles and nanoparticles 7-15 nm in diameter. The SDP500-COOH supported catalyst is however more active for hydrogen peroxide synthesis than the analogous SDP500 supported catalyst, 87 versus 60 mol$H_2O_2$/h/$kg_{cat}$. In addition, the hydrogenation activity of SDP500-COOH catalyst is comparable to that of the catalyst supported on the parent carbon, 1160 and 1207 mol$H_2O_2$/h/$kg_{cat}$ respectively, indicating that the SDP500-COOH supported material is highly active for both direct synthesis and hydrogenation, despite containing larger nanoparticles than the SDP500 supported catalyst.

*5.2.1.2.9.SEM-BSE Microscopy of the 2.5 wt% Pd 2.5 wt% Au/MWCNT Catalyst*

Similar metal nanostructures were observed for the MWCNT supported catalyst, presented in Figure 5-12. The carbon nanotubes, approximately 12 nm in diameter, form entangled agglomerate structures 5-10 μm in size, containing micron sized metal nanoparticles. Smaller nanoparticles, 5-20 nm are readily present on nanotubes freely suspended at the periphery of the support structure.

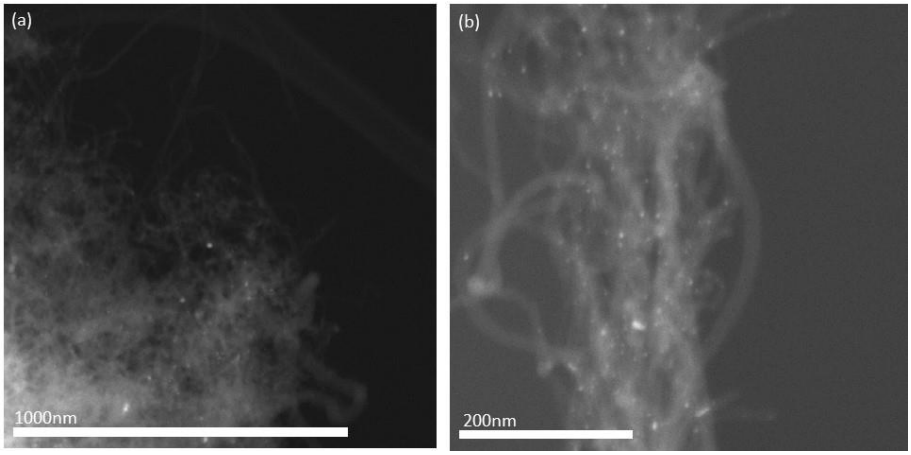


**Figure 5-12 - Low (a) and high (b) magnification SEM-BSE images of 2.5 wt% Pd 2.5 wt% Au/MWCNT**

The presence of both large and small particles suggests that metal precursor dispersion during preparation is poor and this could largely be attributed to the unique structure of the support material. BET surface area analysis reveals that the $N_2$ adsorption surface area of the support is many times greater than the $TiO_2$ reference material but the formation of micrometre sized metal particles indicates that the fraction of that surface area available to absorb solution phase metal precursors is considerably lower.

*5.2.1.2.10.SEM-BSE Microscopy of the 2.5 wt% Pd 2.5 wt% Au/MWCNT-OH Catalyst*

SEM-EDX analysis of the PdAu catalyst prepared on the hydroxyl functionalised nanotube support MWCNT-OH shows that it exhibits a bimodal particle distribution, as seen in Figure 5-13. Like the unfunctionalized parent carbon, small nanoparticles 5-20 nm in diameter are routinely observed immobilised on unbundled carbon nanotubes at the edges of the support particles. Interestingly, regular 100-200 nm metal particles can also be seen readily dispersed within the support structure.

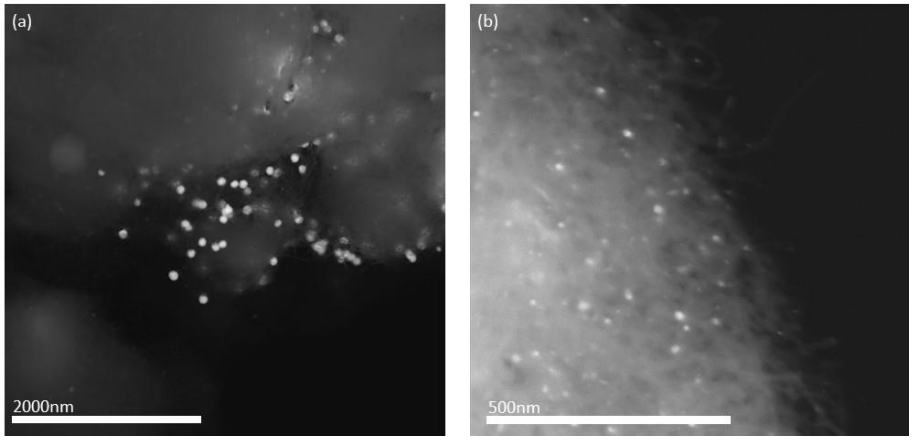


**Figure 5-13 - Low (a) and high (b) magnification SEM-BSE images of 2.5 wt% Pd 2.5 wt% Au/MWCNT-OH**

Unlike the parent carbon MWCNT, micron sized metal particles were not observed, which suggests that the presence of surface hydroxyl groups improves metal precursor dispersion and supresses the formation of larger nanoparticles. In Section 5.2.1 it was presented that the MWCNT and MWCNT-OH supported impregnation catalyst had comparable hydrogen peroxide synthesis activities, but hydroxyl functionalised analogue was significantly more active for hydrogen peroxide hydrogenation. The hydrogenation activity of the MWCNT-OH supported catalyst suggests that the 100-200 nm particles are more active for hydrogenation than the low surface area micrometre scale agglomerates present in the MWCNT supported catalyst, as both catalysts contain similarly sized small particles in addition to the larger PdAu species.

*5.2.1.3.X-Ray Photoelectron Spectroscopy (XPS) of 2.5 wt% Pd 2.5 wt% Au/C Catalysts Prepared by Wet Impregnation*

The chemical structure of the carbon supported PdAu catalysts was also investigated by X-ray photoelectron spectroscopy (XPS) to determine elemental surface concentration and oxidation state. Previous work has found that Pd(II) is more selective towards the direct synthesis of hydrogen peroxide than Pd(0) and therefore the catalytic activities presented in Section 5.2.1 may be a consequence of variation in Pd oxidation state.[34]

The Au(4f) spectra of the catalysts prepared by wet impregnation are presented in Figure 5-14. The Au(4f) binding energy of the catalysts varies minimally. The average binding energy was 83.7eV with a range of 0.4eV. This is consistent with Au(0) values previously reported for supported bimetallic PdAu catalysts, indicating that in all cases Au is present solely in the metallic state.[35]

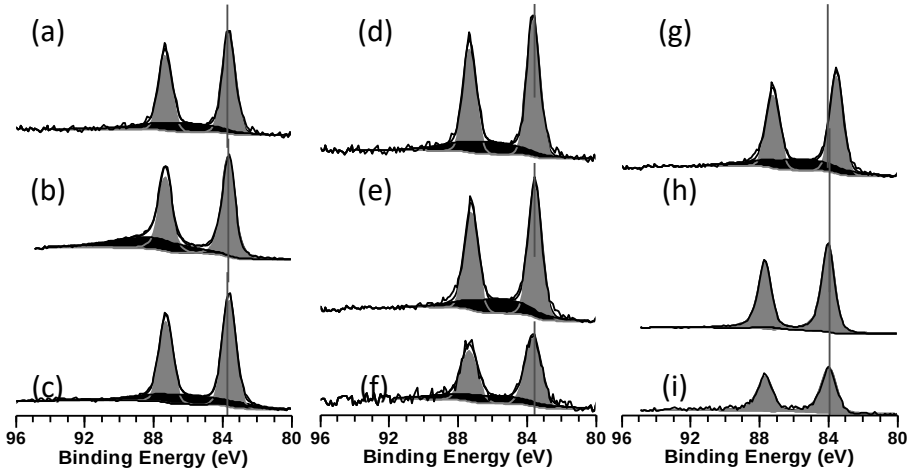


**Figure 5-14 – Au(4f) spectra of 2.5 wt% Pd 2.5 wt% Au catalysts supported on graphite (Sigma) (a), Graphite (BNFL) (b), KBB (c), XC72R (d), Black Pearl (e), SDP 500 (f), SDP 500-COOH (g), MWNCT (h) and MWCNT-OH (i). Grey and black shading indicative of Au and C contributions respectively.**

In contrast, Pd oxidation state varies significantly with differing support for impregnation prepared catalysts as shown in Figure 5-15. All the catalysts exhibited characteristic binding energies of approximately 335eV, corresponding to metallic Pd(0) species.[36] The presence of a shoulder at 338eV is indicative of the presence of Pd(II), typically PdO, suggesting imperfect alloy formation during preparation.[27]

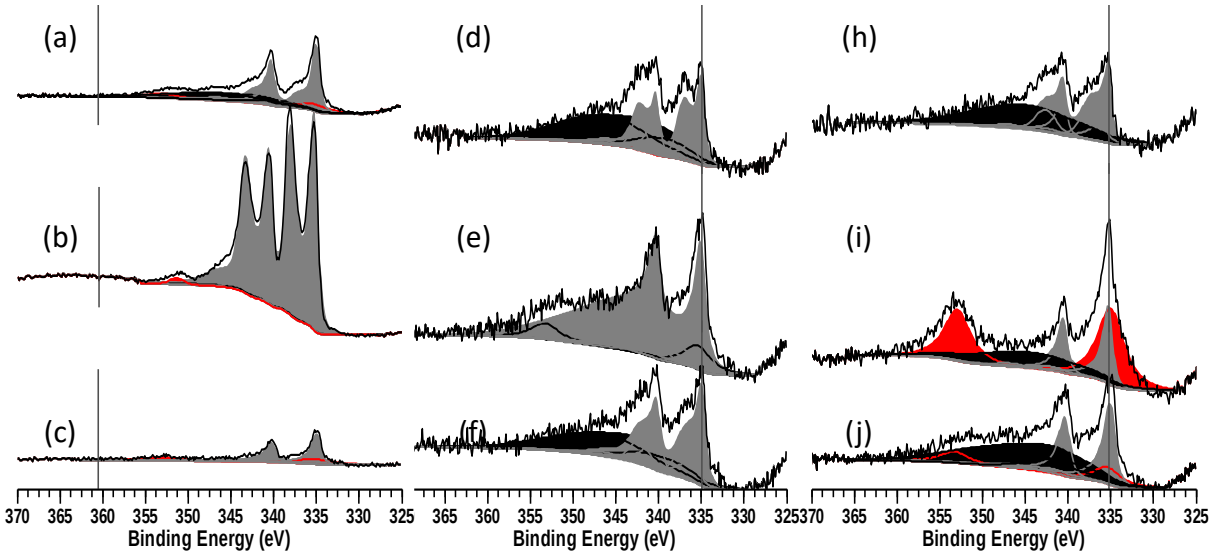


**Figure 5-15 – Pd(3d) spectra of 2.5 wt% Pd 2.5 wt% Au catalysts supported on Graphite (Sigma) (a), Graphite (BNFL) (b), KBB (c), XC72R (d), Black Pearl (e), SDP 500 (f), SDP 500-COOH (g), MWNCT (h) and MWCNT-OH (i). Grey, red and black shading indicative of Pd, Au and C contributions respectively.**

Quantified Pd(0)/Pd(II) ratios and Pd/Au surface concentrations of the carbon supported catalysts are presented in Table 5-2. The two graphite-supported PdAu catalysts exhibit different Pd(0)/Pd(II) ratios, the graphite (BNFL) supported catalyst containing proportionally more Pd(II). Additionally, the graphite (BNFL) supported catalyst has a Pd/Au ratio of 26.5, considerably larger than the theoretical ratio of 1.8. This is likely a sample error in characterising the catalyst by XPS. Analysis of the catalyst structure by SEM shows that the catalyst contained micrometre sized particles, both supported and unsupported. In the case of the XPS data presented here, the spot size of the beam used to record the XPS spectra was 400µm in diameter, comparable to the diameter of the metal particles. This results in a sampling bias, wherein an insufficiently small number of particles are interrogated during XPS data collection to be considered an accurate representation of the bulk sample. The presence of a sampling error is supported by the XPS derived Pd and C surface concentrations which correspond to a Pd weight loading of 28 wt%, an order of magnitude

greater than the target loading of 2.5 wt%, indicating that the XPS sampling area contains considerably more metal than the bulk catalyst.

The SDP500 and SDP500 COOH supported PdAu catalysts also have high Pd/Au surface ratios, 7.3 and 10 respectively but the Pd surface concentrations are 0.22 and 0.2 at%, close to the theoretical concentration of 0.3 at%. In contrast to the graphite supported catalyst, the deviation of the actual Pd/Au ratio from the theoretical ratio can be attributed to weak Au(4f) signals. The SDP500 and SDP500 COOH supported catalysts have XPS derived Au surface concentration of 0.03 and 0.02 at%, significantly lower than the theoretical value of 0.16, indicating size-dependent composition effects in the metal nanoparticles.

**Table 5-2- Tabulated XPS derived surface concentrations of Pd, Au, C, O and N of 2.5 wt% Pd 2.5 wt% Au catalysts supported on carbon prepared by wet impregnation.**

| Support | XPS Derived Surface Concentration (at%) | | | | | Pd/Au Ratio | Pd Oxidation State (%) | |
|---|---|---|---|---|---|---|---|---|
| | Pd | Au | C | O | N | | Pd(0) | Pd(II) |
| Graphite | 0.55 | 0.14 | 95.28 | 3.48 | - | 3.9 | 89 | 11 |
| BNFL | 4.25 | 0.16 | 92.33 | 0.15 | 0.15 | 26.5 | 63 | 37 |
| KBB | 0.3 | 0.13 | 89.41 | 9.92 | - | 2.3 | 100 | 0 |
| XC72R | 0.19 | 0.06 | 98.16 | 1.18 | - | 3 | 64 | 36 |
| Black Pearl | 0.29 | 0.11 | 85.9 | 14.09 | - | 2.6 | 65 | 35 |
| SDP 500 | 0.22 | 0.03 | 93.65 | 5.98 | - | 7.3 | 63 | 37 |
| SDP 500-COOH | 0.2 | 0.02 | 92.85 | 5.47 | 0.33 | 10 | 68 | 32 |
| MWCNT | 0.18 | 0.39 | 99 | 0.43 | 0.21 | 0.46 | 100 | 0 |
| MWCNT-OH | 0.22 | 0.16 | 95.69 | 3.73 | - | 1.4 | 100 | 0 |

The MWCNT and MWNCT-OH supported catalysts have Pd/Au ratios below the theoretical ratio, 0.46 and 1.4 respectively. The relatively high concentration of Au is apparent by the presence of Au(4d) peaks at 335eV in the Pd(3d) spectra, which were particularly intense in the case of the MWCNT supported catalyst.

In considering the activity of the catalysts for both hydrogen peroxide synthesis and hydrogenation, several trends are observed regarding the role of Pd/Au surface concentration or Pd oxidation state. The XC72R and KBB supported catalysts are most active, with hydrogen peroxide synthesis activities of 114 and 102 mol$H_2O_2$/h/$kg_{cat}$ and hydrogenation activities of 1156 and 971 mol$H_2O_2$/h/$kg_{cat}$ respectively. The XC72R and KBB supported

catalysts have surface Pd/Au ratios of 3 and 2.4, similar to the theoretical ratio of 1.8 and considerably smaller than those of less active catalysts. In comparison, the SDP500 supported analogue has a hydrogen peroxide synthesis activity of only 60 mol$H_2O_2$/h/$kg_{cat}$ but a hydrogenation activity of 1207 mol$H_2O_2$/h/$kg_{cat}$. The XPS derived Pd/Au ratio of the SDP500 supported catalyst, 7.3, is consistent with Pd enrichment of the nanoparticle surface, which is indicative of the formation of larger Pd domains highly active for hydrogenation.[33]

Pd oxidation state has been previously shown to influence hydrogen peroxide hydrogenation activity and therefore selectivity of monometallic catalysts towards hydrogen peroxide synthesis.[31] The XC72R supported catalyst was also found to contain both Pd(0) and Pd(II) in a 2:1 ratio suggesting the formation of monometallic PdO species in addition to alloyed PdAu species. PdO nanoparticles are known to be less active for hydrogen peroxide synthesis than alloyed PdAu analogues, suggesting that some metal is present on the surface of the catalyst as a relatively non-productive moiety.[5]

Comparison of the Pd oxidation state distribution of the impregnation prepared PdAu catalysts indicates that the formation of PdO phases alone is unable to explain the activity of the catalysts. Instead, it can be suggested that surface Pd enrichment and the presence of PdO yields catalysts that are less active for direct synthesis and less selective towards hydrogen peroxide formation. The SDP 500 and SDP500-COOH supported catalysts both exhibit low hydrogen peroxide synthesis and high hydrogenation activity. Like the XC72R supported catalysts, considerable surface concentrations of Pd(II) were observed, corresponding to the formation of monometallic PdO particles, however the Pd/Au surface ratio was elevated in both cases. This suggests that the presence of a Pd enriched surface, including both PdAu alloy phases and PdO, results in increased hydrogen peroxide hydrogenation activity and therefore reduced synthesis activity.

The O(1s) XPS region was also investigated to understand the effect of surface oxygen content and functionality on catalyst activity, presented in Figure 5-16.

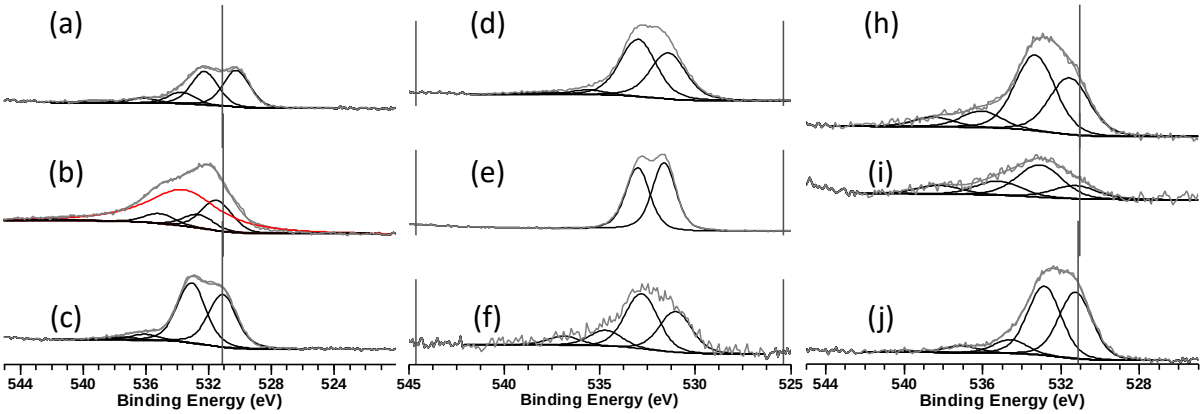


**Figure 5-16 - O(1s) spectra of 2.5 wt% Pd 2.5 wt% Au catalysts prepared by wet impregnation supported on Graphite (Sigma) (a), Graphite (BNFL) (b), KBB (c), XC72R (d), Black Pearl (e), SDP 500 (f), SDP 500-COOH (g), MWNCT (h) and MWCNT-OH (i). Black and Red composition indicative of O 1s and Pd 2p contributions.**

Previous work by Edwards *et al.* found that the activity of impregnation prepared carbon supported catalysts could be greatly improved by acid treating the support prior to catalyst preparation.[18] Davies and co-workers published complimentary work in which they studied the effect of acid treatment on highly ordered pyrolytic graphite (HOPG) using AFM, SEM and XPS, showing that treatment of the carbon surface with acids resulted in a significant increase in surface oxygen concentration.[37] Given that acid treatment is commonly used in the industrial manufacture of activated carbons, it is reasonable to suggest that the presence of oxygen containing support surface functional groups could play a role in determining catalyst activity.

The O(1s) spectra of the wet impregnation prepared catalysts are shown in Figure 5-16. Surface oxygen environments of carbonaceous materials have been previously studied such that general peak assignments can be made.[38–41] The fitted peaks can be attributed to five environments, C=O groups, present as quinonic groups (peak 1 - 531.5-532.4eV), C-OH and C-O-C groups (peak 2 - 532.5-533.4eV), C-O groups present in carboxylic acids and anhydrides (peak 3 - 535.5-536.4eV), chemisorbed water (peak 4 - 536.5-537.4eV) and oxygen (peak 5 - 338.0-339.5eV). The binding energies and relative peak areas of the fitted peaks are presented in Table 5-3. The areas of Peaks 1 and 2 have the greatest O1s contribution for all carbons, indicating that quinonic and hydroxyl functional groups are

prominent of the surface of the carbons. The relatively minor fitting contribution of Peak 3, corresponding to carboxylic acid groups, indicates that the presence of acidic groups is unlikely to be the origin of the catalyst activity variation.

**Table 5-3 - O1s XPS peak binding energies (B.E., eV) and relative peak areas (R.A., %) for the 2.5 wt% Pd 2.5 wt% Au/C catalysts prepared by wet impregnation.**

| Carbon | Peak 1 | | Peak 2 | | Peak 3 | | Peak 4 | | Peak 5 | |
|---|---|---|---|---|---|---|---|---|---|---|
| | B.E. (eV) | R. A (%) | B.E. (eV) | R. A (%) | B.E. (eV) | R. A (%) | B.E. (eV) | R. A (%) | B.E. (eV) | R. A (%) |
| Graphite | 530.2 | 38 | 532.3 | 41 | 533.8 | 13 | 536.2 | 5 | 539.1 | 3 |
| BNFL | 531.5 | 55 | 532.6 | 24 | 535.1 | 18 | - | - | 541.7 | 2 |
| KBB | 531.1 | 43 | 533.1 | 49 | 536.1 | 5 | 537.4 | 2 | 539.2 | 1 |
| XC72R | 531.0 | 34 | 532.8 | 46 | 534.7 | 13 | 536.9 | 7 | - | - |
| Black Pearl | 531.7 | 52 | 533.1 | 48 | - | - | - | - | - | - |
| SDP 500 | 531.4 | 41 | 533.0 | 51 | 535.6 | 4 | 537.6 | 2 | 539.2 | 1 |
| SDP 500-COOH | 531.6 | 36 | 533.3 | 48 | 536.1 | 10 | 538.5 | 6 | - | - |
| MWCNT | 531.3 | 47 | 533.1 | 21 | 535.2 | 13 | 538.2 | 13 | - | - |
| MWCNT-OH | 531.3 | 42 | 532.9 | 44 | 534.6 | 9 | 537.1 | 4 | 540.0 | 1 |

The relationship between oxygen content and catalyst activity is presented in Figure 5-17. The graph shows that no clear correlation between hydrogen peroxide synthesis activity and oxygen/carbon ratio, indicating that the presence of oxygen containing surface groups is not responsible for the activity of the catalysts. For instance, the graphite (Sigma) and MWNCT-OH supported catalysts both contain 3.9 at% surface oxygen, yet the synthesis activity of the former is 42 mol$H_2O_2$/h/$kg_{cat}$ and the latter 72 mol$H_2O_2$/h/$kg_{cat}$. Similarly, the SDP500 and SDP500-COOH supported PdAu catalysts exhibit synthesis activities of 60 and 87 mol$H_2O_2$/h/$kg_{cat}$ respectively despite having comparable oxygen/carbon surface ratios of 0.06 and 0.05. The hydrogen peroxide hydrogenation activity of the catalysts also shows no clear correlation with oxygen/carbon surface ratio. The graphite (Sigma) and MWCNT-OH supported catalysts exhibit similar surface oxygen concentrations but considerably different hydrogenation activities, 608 mol$H_2O_2$/h/$kg_{cat}$ and 794 mol$H_2O_2$/h/$kg_{cat}$ respectively.

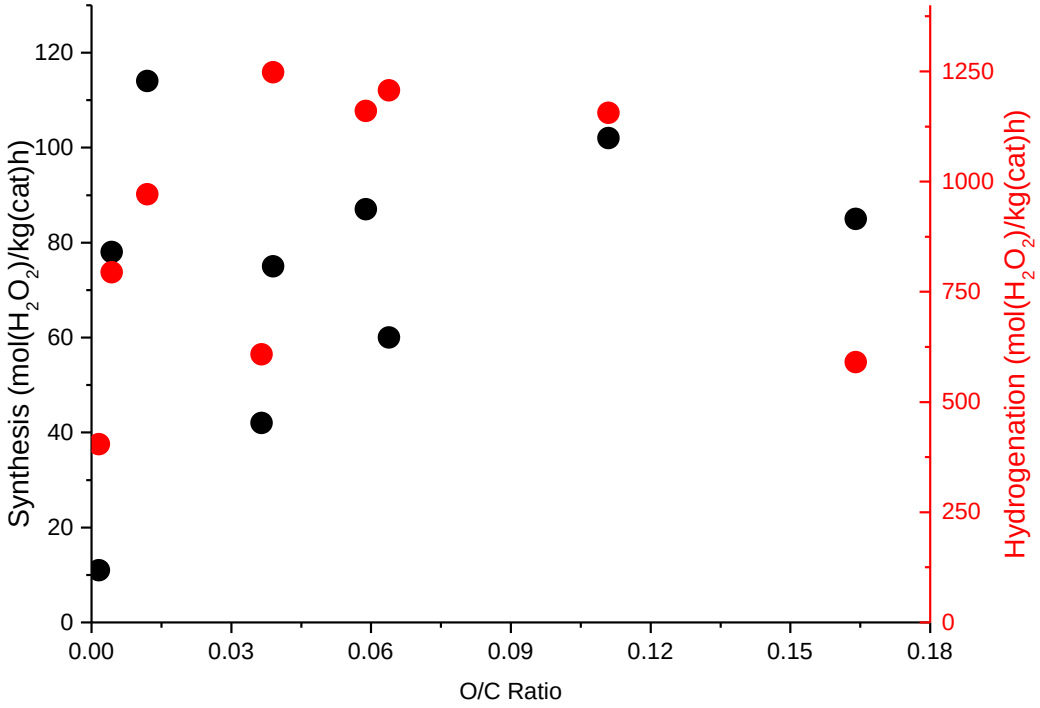


**Figure 5-17 - Hydrogen peroxide synthesis and hydrogenation activity versus surface oxygen/carbon ratio of the wet impregnation prepared 2.5 wt% Pd 2.5 wt% Au/C catalysts**

### *5.2.2. Carbon Supported PdAu Catalysts Prepared by Modified Sol Immobilisation*

The role of carbon supports in preparing active catalysts was then further investigated in the preparation of 0.5 wt% Pd 0.5 wt% Au/C catalysts by modified sol immobilisation. It is previously presented in Chapter 4. that small variations in sol immobilisation preparation protocols can significantly influence final catalyst activity. Indeed, it was shown that optimum conditions yielded $TiO_2$ and carbon supported catalysts that were entirely inactive towards hydrogen peroxide hydrogenation, and therefore completely selective for the direct synthesis of hydrogen peroxide.

Analogous to the work presented in Section 5.2.1, 0.5 wt% Pd 0.5 wt% Au catalysts were initially prepared on P25 $TiO_2$ and two commercially available synthetic graphites. The hydrogen peroxide synthesis and hydrogenation activity of these catalysts is presented in Figure 5-18.

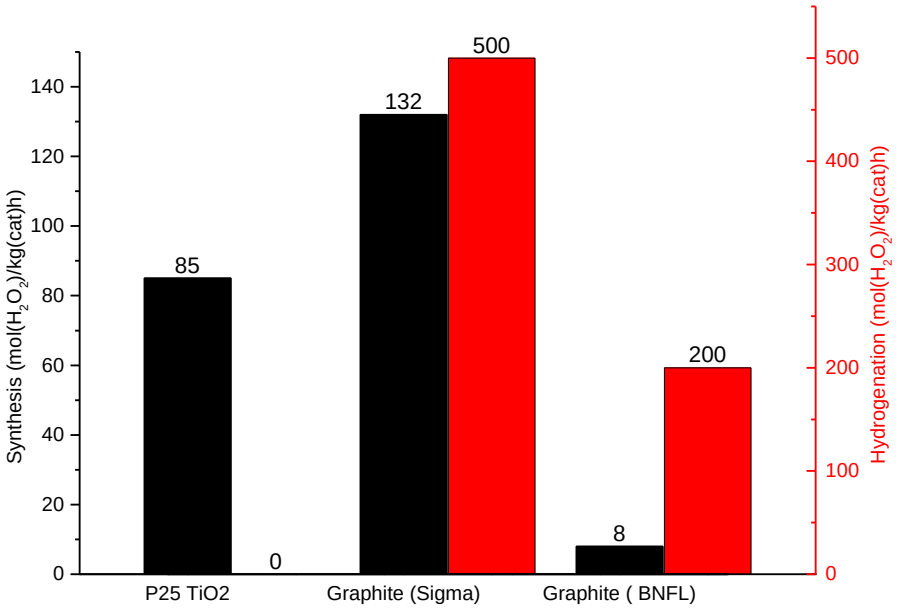


**Figure 5-18 - Hydrogen peroxide synthesis and hydrogenation activity of PdAu catalysts prepared by modified sol immobilisation supported on P25 $TiO_2$ and graphite**

**Reaction Conditions – Hydrogen peroxide synthesis: 5 % $H_2/CO_2$ (2.9 MPa) and 25 % $O_2/CO_2$ (1.1 MPa), 8.5 g solvent (2.9 g $H_2O$, 5.6 g MeOH) 0.01 g catalyst, 2 °C, 1200 rpm, 30 min. Hydrogen peroxide hydrogenation: 5 % $H_2/CO_2$ (2.9 MPa), 8.5 g solvent (2.22 g $H_2O$, 5.6 g MeOH and 0.68 g 50 wt% $H_2O_2$), 0.01 g catalyst, 2 °C, 1200 rpm, 30 min.**

The graphite (Sigma) supported catalyst is the most active for hydrogen peroxide synthesis with an activity of 132 mol$H_2O_2$/h/$kg_{cat}$. In agreement with the data presented in 5.2.1. the graphite (BNFL) derived catalyst performed very poorly, with a synthesis activity of 8

mol$H_2O_2$/h/$kg_{cat}$, suggesting that this material is unsuitable as a catalyst support. The $TiO_2$ supported reference catalyst has intermediate activity, 85 mol$H_2O_2$/h/$kg_{cat}$.

The hydrogen peroxide hydrogenation activity of the catalysts is also shown in Figure 5-18. Interestingly the graphite (Sigma) catalyst, most active for direct synthesis, is also highly active for hydrogen peroxide hydrogenation indicating that catalyst selectivity is poor. In comparison, the graphite (BNFL) supported catalyst has reduced hydrogenation activity of 200 mol$H_2O_2$/h/$kg_{cat}$. As previously reported in Chapter 4, the $TiO_2$ supported catalyst prepared by modified sol immobilisation was inactive for hydrogen peroxide hydrogenation and decomposition, and highly selective towards the direct synthesis of hydrogen peroxide.

In Section 5.2.1, it is shown that the choice of carbon support influences the activity of catalysts prepared by impregnation. One factor in preparing active catalysts by impregnation is the dispersion of metal precursors prior to heat treatment. Carbon supports with low surface areas, or surface groups with unfavourable interactions with the metal precursors result in the formation of large metal precursor domains, yielding large nanoparticles upon heat treatment.

The effect of metal precursor-support interactions has been previously investigated by Wong *et al.*, who showed that varying the pH of the preparation slurry resulted in electrostatic adsorption of charge complimentary cationic metal precursors.[42] Control of preparation pH greatly improved the dispersion of the precursors which translated into a reduction in average particle size. In the case of PtPd/$SiO_2$ nanoparticles, average particle diameter was observed to be 1.0 nm in comparison to 9.4 nm for the catalyst prepared by conventional wet impregnation.

The use of the sol immobilisation preparation method mitigates particle size effects through the production of a metal colloid prior to immobilisation. In Chapter 4, it is shown that catalysts prepared using the modified sol immobilisation protocol yield highly unusual nanochain agglomerate structures. Although the structure of the agglomerates is dependent upon preparation conditions, the metal nanostructure is independent of the choice of support material and formed of nanoparticles with constant size and composition. Preparing catalysts by sol immobilisation also requires thorough washing, ensuring the removal of any water-soluble contaminants remaining from the support manufacturing process which may also alter activity of the catalysts.

Sol immobilisation catalysts were also prepared using commercial carbon blacks. The hydrogen peroxide synthesis and hydrogenation activities of the catalysts are shown in Figure 5-19.

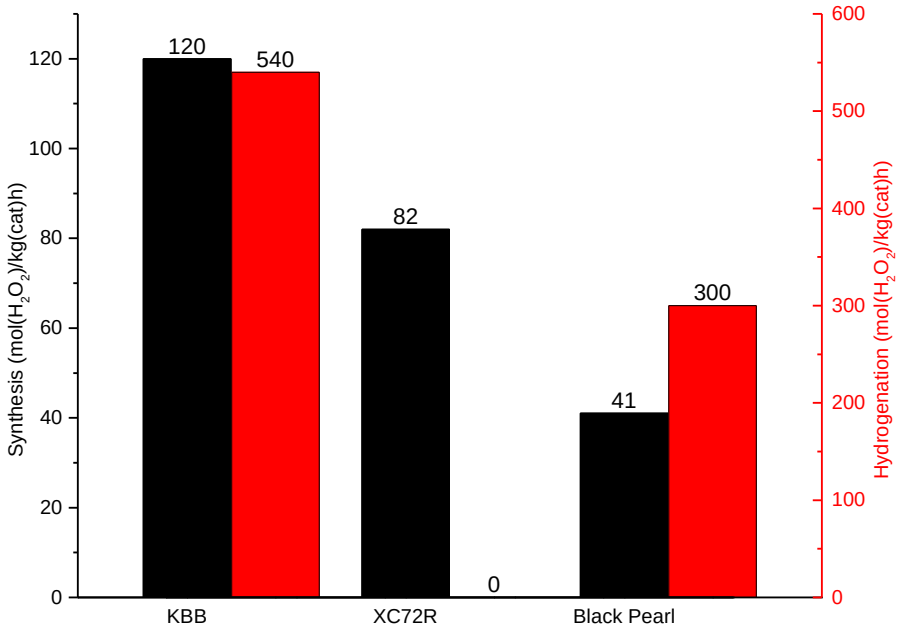


**Figure 5-19 - Hydrogen peroxide synthesis and hydrogenation activity of PdAu catalysts prepared by modified sol immobilisation supported on commercial carbon blacks**

**Reaction Conditions – Hydrogen peroxide synthesis: 5 % $H_2/CO_2$ (2.9 MPa) and 25 % $O_2/CO_2$ (1.1 MPa), 8.5 g solvent (2.9 g $H_2O$, 5.6 g MeOH) 0.01 g catalyst, 2 °C, 1200 rpm, 30 min. Hydrogen peroxide hydrogenation: 5 % $H_2/CO_2$ (2.9 MPa), 8.5 g solvent (2.22 g $H_2O$, 5.6 g MeOH and 0.68 g 50 wt% $H_2O_2$), 0.01 g catalyst, 2 °C, 1200 rpm, 30 min.**

The hydrogen peroxide synthesis activity of the catalysts follows the series KBB > XC72R > Black Pearl, corresponding to a maximum and minimum of 120 and 41 mol$H_2O_2$/h/$kg_{cat}$ respectively. The range of hydrogen peroxide synthesis activities was 79 mol$H_2O_2$/h/$kg_{cat}$, considerably greater than the impregnation catalysts prepared on the same carbons, 29 mol$H_2O_2$/h/$kg_{cat}$.

The large range of activities for the carbon black supported catalysts suggests that, in the case of sol immobilisation catalysts, the choice of support plays a significant role in determining activity and selectivity. The hydrogen peroxide hydrogenation activities of the sol immobilisation prepared catalysts were also determined. In agreement with the results presented in Chapter 4, the XC72R supported PdAu catalyst has a hydrogenation activity of 0 mol$H_2O_2$/h/$kg_{cat}$, indicating that the hydrogenation pathway is deactivated. The KBB and Black Pearl supported catalysts have hydrogenation activities of 540 and 300 mol$H_2O_2$/h/$kg_{cat}$

respectively. The hydrogenation activity of the carbon black supported catalysts were considerably lower than the impregnation prepared analogues. In the case of the KBB supported sol immobilisation catalyst, the reduced hydrogenation activity is accompanied by increased synthesis activity compared to the analogous impregnation catalyst, which suggests that controlled agglomeration of the PdAu nanoparticles can results in increased selectivity towards hydrogen peroxide and improve hydrogen peroxide yield.

Further 0.5 wt% Pd 0.5 wt% Au/C catalysts were prepared on carbon nanomaterials using the modified sol immobilisation preparation method. The hydrogen peroxide synthesis and hydrogenation activity of these catalysts is presented in Figure 5-20.

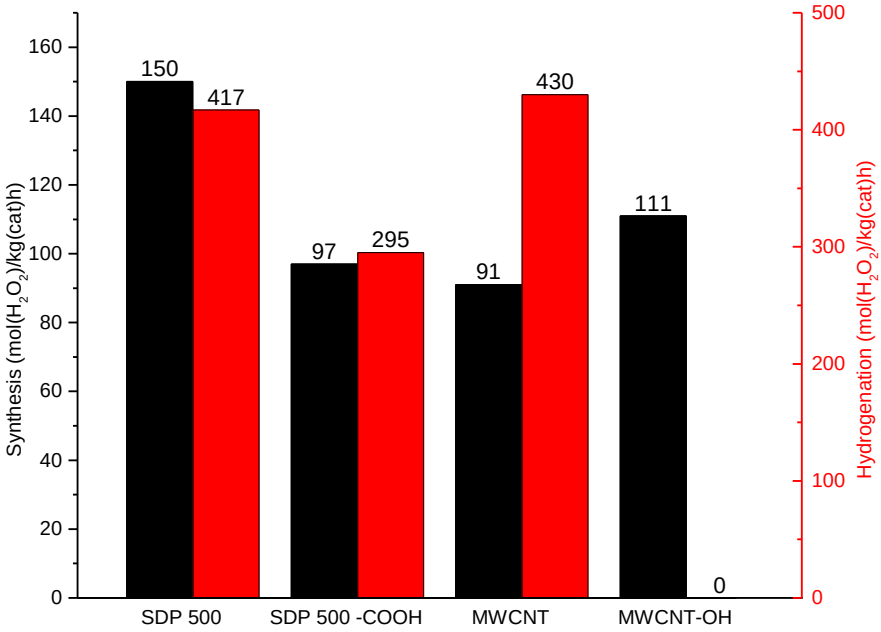


**Figure 5-20 - Hydrogen peroxide synthesis and hydrogenation activity of PdAu catalysts prepared by sol immobilisation supported on carbon nanomaterials**

**Reaction Conditions – Hydrogen peroxide synthesis: 5 % $H_2/CO_2$ (2.9 MPa) and 25 % $O_2/CO_2$ (1.1 MPa), 8.5 g solvent (2.9 g $H_2O$, 5.6 g MeOH) 0.01 g catalyst, 2 °C, 1200 rpm, 30 min. Hydrogen peroxide hydrogenation: 5 % $H_2/CO_2$ (2.9 MPa), 8.5 g solvent (2.22 g $H_2O$, 5.6 g MeOH and 0.68 g 50 wt% $H_2O_2$), 0.01 g catalyst, 2 °C, 1200 rpm, 30 min.**

The SDP 500 supported catalyst was highly active for hydrogen peroxide synthesis, 150 mol$H_2O_2$/h/$kg_{cat}$. The synthesis activity of this catalyst is comparable to the most active sol immobilisation catalyst presented in the preceding chapter which, prepared using conventional protocols, contains small, well dispersed nanoparticles rather than low surface area agglomerates. This implies that metal surface area limitations can be overcome by selecting appropriate supports in preparing active catalysts for hydrogen peroxide synthesis.

Interestingly the catalyst prepared on carboxylic acid functionalised SDP 500-COOH was less active than its unfunctionalized counterpart for hydrogen peroxide synthesis with an activity of 97 mol$H_2O_2$/h/$kg_{cat}$. This is contrary to the activity of the wet impregnation prepared catalysts presented in Figure 5-3, which shows that the SDP 500-COOH supported catalyst was more active for hydrogen peroxide synthesis. The difference in activity between the sol immobilisation and impregnation prepared SDP500 catalysts suggests that the presence of surface carboxylic acid groups, beneficial in preparing active impregnation catalysts, are detrimental in the preparation of sol immobilisation catalysts. The SDP 500-COOH supported catalyst also has reduced hydrogenation activity in comparison to the unfunctionalized SDP-500 analogue, 295 and 417 mol$H_2O_2$/h/$kg_{cat}$ respectively. The consistent drop in both synthesis and hydrogenation activity of approximately 30 % upon support functionalisation could be attributed to the surface groups adversely impacting the adsorption of the metal colloid during preparation, yielding a catalyst that is less active for both pathways.

The MWCNT and MWCNT-OH supported catalysts also exhibit unusual activity. In Section 5.2.1, the impregnation prepared MWCNT-OH supported catalyst is more active for hydrogen peroxide hydrogenation than the unfunctionalized counterpart, despite having comparable synthesis activity. This indicates that in the case of catalysts prepared by wet impregnation, the introduction of surface hydroxyl groups is detrimental to the selectivity of resultant catalyst. In the case of sol immobilisation prepared catalysts, the opposite trend is observed, shown in Figure 5-20. The MWCNT and MWCNT-OH supported catalysts have hydrogen peroxide synthesis activities of 91 and 110 mol$H_2O_2$/h/$kg_{cat}$. This was accompanied by a complete deactivation of the hydrogenation pathway, decreasing from 430 to 0 mol$H_2O_2$/h/$kg_{cat}$ for the hydroxyl functionalised support. Previous work has shown that the selectivity of supported PdAu catalysts greatly increases with the deactivation of the hydrogenation pathway.[18] The activity of the MWCNT supported catalysts prepared by sol immobilisation further expand the data presented in Chapter 4, which shows that catalysts prepared on XC72R carbon are also inactive for hydrogen peroxide hydrogenation. Comparison of the activity of the impregnation and sol immobilisation prepared catalysts in this chapter shows that the that the surface environment of the support greatly influences catalyst activity and that the optimal support is dependent upon the preparation protocol.

*5.2.2.1.X-Ray Photoelectron Spectroscopy (XPS) of Carbon Supported PdAu Catalysts Prepared by Modified Sol Immobilisation*

The carbon supported catalysts prepared by sol immobilisation were also characterised by XPS to determine whether their activity was also a consequence of Pd surface enrichment and Pd oxidation state. The Au(4f) spectra of the different carbon supported catalysts are presented in Figure 5-21. The catalysts contain Au(0) only, with an average Au(4f7/2) binding energy of 83.6 and a range of 0.48eV. This is slightly lower than the bulk Au(0) binding energy of 84.0 eV, which has been previously ascribed to charge transfer between Au and Pd in bimetallic alloy nanoparticles.[43]

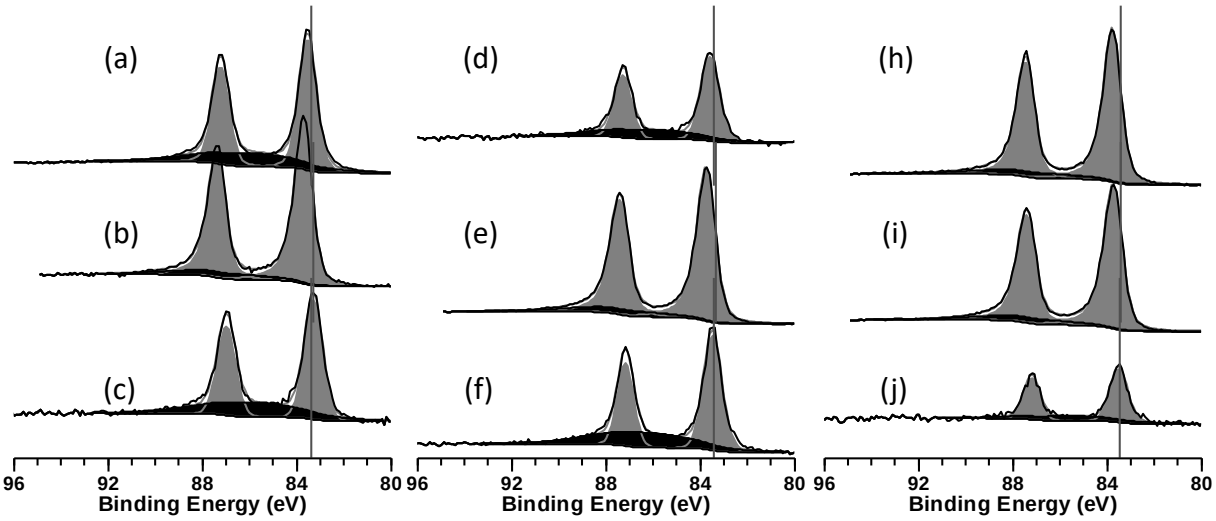


**Figure 5-21 - Au(4f) spectra of 0.5 wt% Pd 0.5 wt% Au Catalysts prepared by modified sol immobilisation supported on Graphite (Sigma) (a), Graphite (BNFL) (b), KBB (c), XC72R (d), Black Pearl (e), SDP 500 (f), SDP 500-COOH (g), MWNCT (h) and MWCNT-OH (i). Grey and black shading indicative of Au and C contribution**

In contrast to the impregnation prepared catalysts, the catalysts prepared by sol immobilisation exhibit a primary Pd(3d5/2) binding energy at 335 eV, consistent with the reported value for Pd(0), as shown in Figure 5-22.[44] Significant overlap was observed with the Au(4d5/2) peak, which was fitted using the relative intensity of the Au(4d3/2) peak found at 353 eV. The Pd/Au surface ratio and Pd oxidation state distributions are presented in Table 5-4. Unlike the catalysts prepared by wet impregnation, Pd is present entirely in its metallic state, suggesting that the resultant nanoparticles are composed of bimetallic alloys and that PdO monometallic particles are absent.

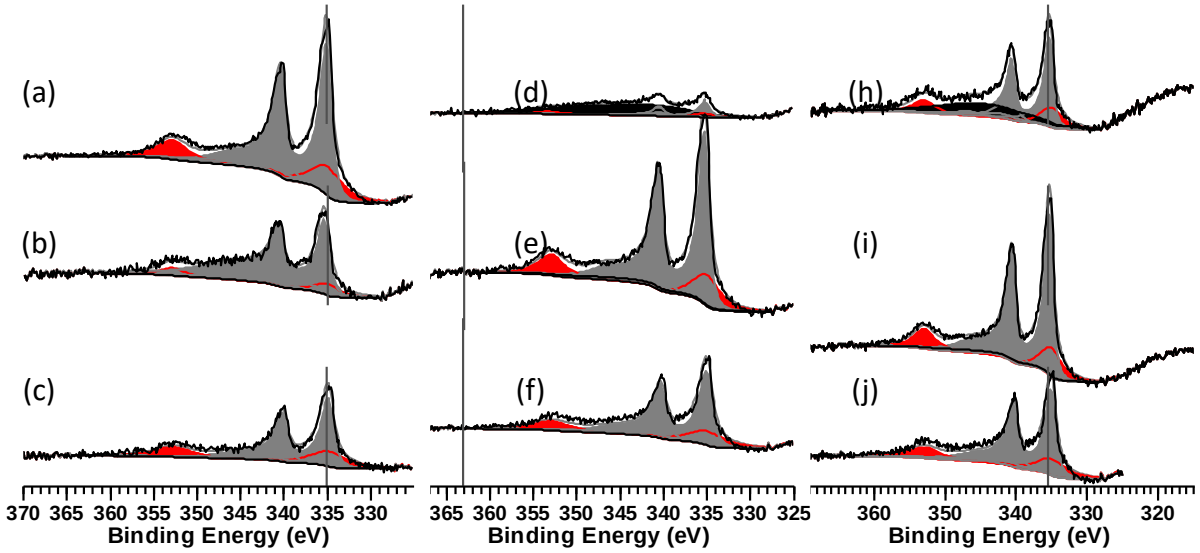


**Figure 5-22 – Pd(3d) spectra of 0.5 wt% Pd 0.5 wt% Au Catalysts prepared by modified sol immobilisation supported on Graphite (Sigma) (a), Graphite (BNFL) (b), KBB (c), XC72R (d), Black Pearl (e), SDP 500 (f), SDP 500-COOH (g), MWNCT (h) and MWCNT-OH (i). Grey, red and black shading indicative of Pd, Au and C contributions respectively.**

The catalysts prepared by modified sol immobilisation also have Pd/Au surface ratios much closer to the theoretical ratio of 1.85. The composition of the catalysts is consistent with the data presented in Chapter 4, which found that the surface structure of the PdAu parent colloid was unchanged upon immobilisation on either $TiO_2$ or XC72R carbon. The XPS spectra of the sol immobilisation prepared catalysts shown in this work, indicates that supporting the colloidal PdAu nanochains on various carbons also has negligible effect on the surface structure.. Although the Pd/Au surface ratios are largely consistent between supports, the concentration of Pd and Au relative to the support C peak varies significantly. This is consistent with the nanostructure of the analogous catalysts, determined by STEM in Chapter 4, which shows that the PdAu assemblies are poorly dispersed on the support owing to the low loading and high degree of agglomeration, including the presence of metal-free support particles. The discrepancy in XPS derived Pd and Au surface concentrations in this work is therefore a result of variations in the particle frequency during data collection and therefore are not representative of the bulk loading.

**Table 5-4 - Tabulated XPS derived surface concentrations of Pd, Au, C, O and N of 0.5 wt% Pd 0.5 wt% Au catalysts supported on carbon prepared by modified sol immobilisation**

| Support | XPS Derived Surface Concentration (at%) | | | | | Pd/Au Ratio | Pd Oxidation State (%) | |
|---|---|---|---|---|---|---|---|---|
| | Pd | Au | C | O | N | | Pd(0) | Pd(II) |
| Graphite | 0.96 | 0.4 | 93.47 | 3.74 | 0.85 | 2.4 | 99 | 1 |
| BNFL | 0.33 | 0.12 | 98.25 | 0.22 | 1.02 | 2.8 | 100 | 0 |
| KBB | 0.35 | 0.17 | 88.63 | 9.82 | 0.96 | 2.1 | 100 | 0 |
| XC72R | 0.07 | 0.04 | 97.83 | 1.39 | 0.22 | 1.8 | 100 | 0 |
| Black Pearl | 0.1 | 0.05 | 89.03 | 10.97 | 0.65 | 2 | 100 | 0 |
| SDP 500 | 0.41 | 0.2 | 92.14 | 6.77 | 0.39 | 2.1 | 100 | 0 |
| SDP 500-COOH | 0.28 | 0.16 | 92.42 | 5.11 | 0.45 | 1.8 | 100 | 0 |
| MWCNT | 0.68 | 0.33 | 97.94 | 0.47 | 0.39 | 2.1 | 100 | 0 |
| MWCNT-OH | 0.05 | 0.03 | 96.03 | 3.82 | 0.32 | 1.7 | 100 | 0 |

Analysis of the activity data presented in Section 5.2.2 suggests that the origin of the activity of the carbon supported sol immobilisation catalysts lies firmly in the nature of the support. Previous work by Kiely and co-workers investigated the nanostructure of $TiO_2$ and carbon supported PdAu bimetallic catalysts prepared by an analogous sol immobilisation method, and showed that, in the case of $TiO_2$ supported catalysts, the PdAu nanoparticles wetted the surface of the support providing intimate contact through the strong metal support interaction.[4] In contrast, carbon supported PdAu nanoparticles remained spherical, indicative of the relatively unfavourable interaction between the two.

In the case of the catalysts presented in this work, enhancement of the electronic properties of the PdAu surface through a metal support interaction would manifest as a shift in the Pd(3d) or Au(4f) binding energy, however such a shift is not observed using XPS. This indicates that the activity variation of the sol immobilisation prepared catalysts is not a result of electronic interactions between the active PdAu nanostructure and the surface of the support.

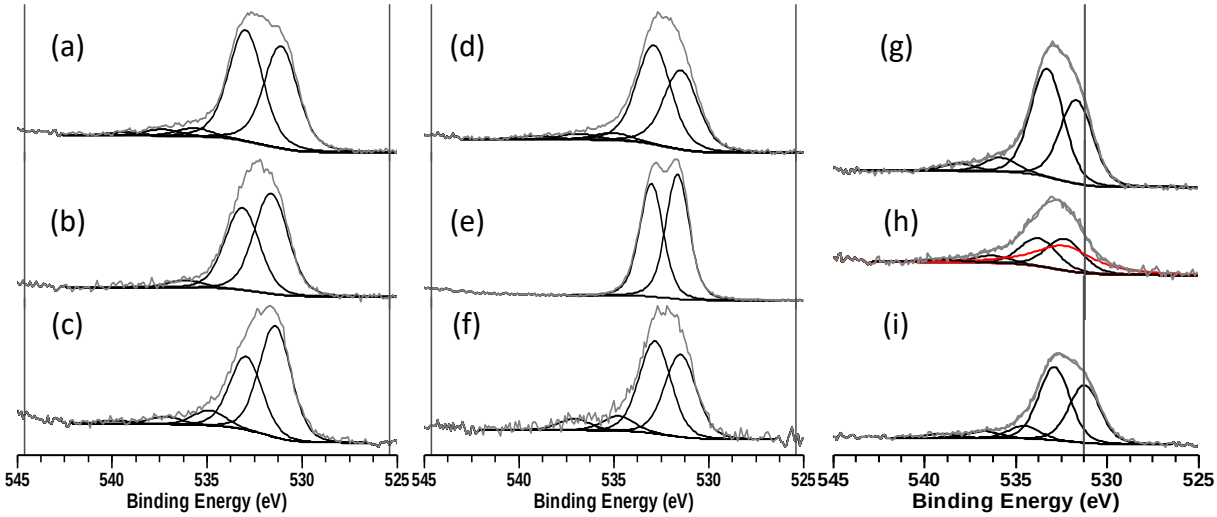


**Figure 5-23 - O(1s) spectra of 0.5 wt% Pd 0.5 wt% Au catalysts prepared by modified sol immobilisation supported on Graphite (Sigma) (a), Graphite (BNFL) (b), KBB (c), XC72R (d), Black Pearl (e), SDP 500 (f), SDP 500-COOH (g), MWNCT (h) and MWCNT-OH (i). Black and Red components correspond to O(1s) and Pd(2p) contributions respectively.**

To better understand the role of surface oxygen on catalyst activity, XPS narrow scans of the O1s region were recorded, shown in Figure 5-23. The O1s peaks of the modified sol immobilisation catalysts were deconvoluted into general oxygen environments analogous to the described assignments in Section 5.2.1.3 for the wet impregnation prepared catalysts, with the binding energies and relative contributions presented in . The O1s spectra contain significant contributions from peaks at ~531.5 and 533.0 eV, attributed to quinonic and hydroxyl functionalities respectively. In all cases, the contribution of peak 3 at 355.5 eV, corresponding to carboxylic groups, was diminished in comparison to the analogous wet impregnation prepared catalysts, consistent with reduction of surface carboxylic acid groups by the ammonia-borane used to reduce the metal precursors during catalyst preparation.

**Table 5-5 - O1s XPS Peak Binding Energies (B.E., eV) and Relative Peak Areas (R.A., %) for the 0.5 wt% Pd 0.5 wt% Au/C Catalysts Prepared By Modified Sol Immobilisation**

| Carbon | Peak 1 | | Peak 2 | | Peak 3 | | Peak 4 | | Peak 5 | |
|---|---|---|---|---|---|---|---|---|---|---|
| | B.E. (eV) | R.A (%) | B.E. (eV) | R.A (%) | B.E. (eV) | R.A (%) | B.E. (eV) | R.A (%) | B.E. (eV) | R.A (%) |
| Graphite | 531.4 | 53 | 532.9 | 35 | 534.9 | 7 | 537.2 | 4 | 539.9 | 2 |
| BNFL | 531.6 | 53 | 533.1 | 43 | 536.1 | 4 | - | 0 | - | 0 |
| KBB | 531.1 | 44 | 532.9 | 48 | 535.7 | 4 | 537.4 | 3 | 539.3 | 1 |
| XC72R | 531.4 | 41 | 532.8 | 46 | 534.8 | 7 | 537.0 | 6 | - | 0 |
| Black Pearl | 531.6 | 51 | 532.9 | 49 | - | 0 | - | 0 | - | 0 |
| SDP 500 | 531.5 | 41 | 532.9 | 51 | 535.0 | 4 | 536.8 | 3 | 539.0 | 2 |
| SDP 500-COOH | 531.7 | 39 | 533.2 | 51 | 535.8 | 7 | - | 3 | 538.1 | 0 |
| MWCNT | 532.3 | 46 | 533.8 | 40 | 536.3 | 10 | - | 4 | 539.0 | 0 |
| MWCNT-OH | 531.2 | 37 | 532.9 | 48 | 534.5 | 8 | 536.7 | 4 | 539.1 | 2 |

The correlation between catalyst activity and surface oxygen content is presented in Figure 5-24. The hydrogen peroxide synthesis activity of the catalysts shows a volcano trend, with the maximum synthesis activity corresponding to the SDP-500 supported catalyst containing 6.77 at% oxygen. The BNFL graphite, which contains only 0.12 at% oxygen, performed poorly with a synthesis activity of 8 mol$H_2O_2$/h/$kg_{cat}$ whilst the Black Pearl supported catalyst, which displays the greatest surface oxygen concentration (10.97 at%), also performs poorly with a synthesis activity of 40 mol$H_2O_2$/h/$kg_{cat}$. In contrast, the relationship between oxygen content and hydrogenation activity is considerably less well defined. The graphite and MWCNT-OH supported catalysts both contain roughly 3.8 at% surface oxygen, yet the hydrogenation activity of the former is 500 mol$H_2O_2$/h/$kg_{cat}$, versus 0 mol$H_2O_2$/h/$kg_{cat}$ for the latter. The XC72R supported catalyst is another outlier, as it also exhibits no hydrogenation activity, yet contains less than half the surface concentration of the MWCNT-OH supported catalyst, which was also inactive for hydrogen peroxide hydrogenation.

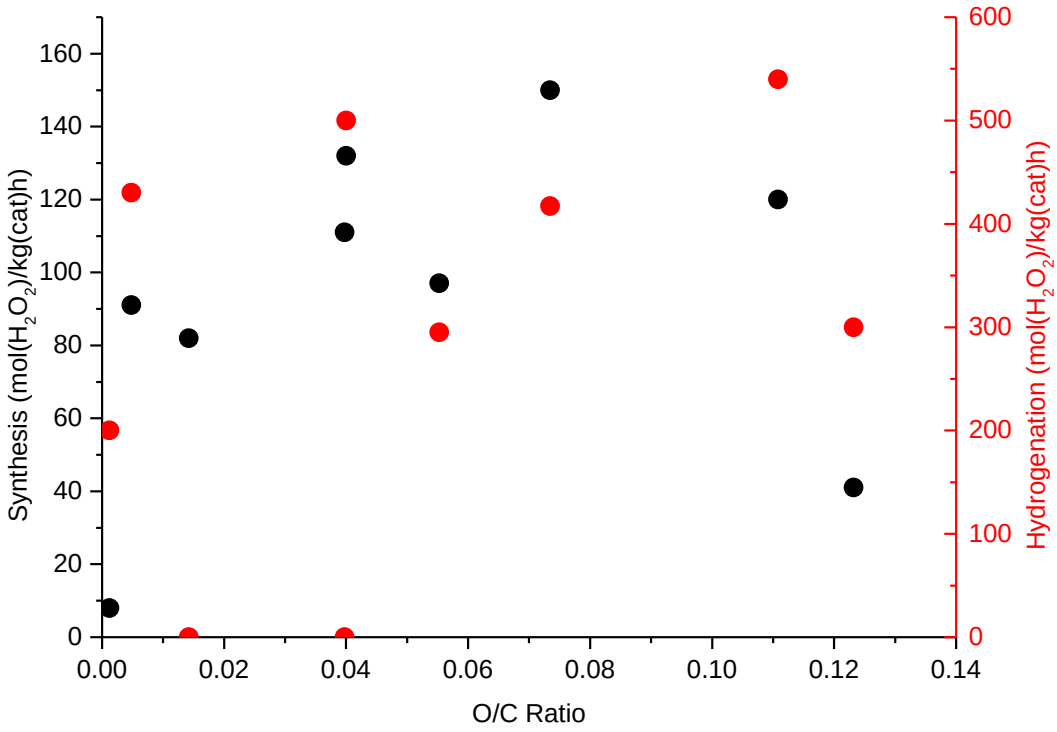


**Figure 5-24 - Hydrogen peroxide synthesis and hydrogenation activity versus surface oxygen/carbon ratio of the modified sol immobilisation prepared 0.5 wt% Pd 0.5 wt% Au/C catalysts**

The disparity between the relationships of synthesis and hydrogenation activity versus oxygen content suggests that the promotion effect of surface oxygen content is not a consequence of a deactivation of the hydrogenation pathway, but rather another effect.

### *5.2.3. Carbons as Heterogeneous Additives*

In Sections 5.2.1 and 5.2.2, it is shown that the activity of PdAu catalysts prepared by impregnation and sol immobilisation varied significantly by choice of support material. There is a disparity between the two preparation methods, as supports appropriate for impregnation catalysts yielded poorly performing sol immobilisation catalysts and vice versa.

The activity of the sol immobilisation catalysts ranged from 8 to 150 mol$H_2O_2$/h/$kg_{cat}$. The large range of activities is surprising considering that the nature of the preparation requires the preparation colloidal nanochain agglomerates prior to immobilisation. In this respect the support could be considered strictly as a carrier of the active metal phase, playing no role in directing the structure of the PdAu agglomerates. Previous work by Kiely and co-workers has found that the metal-support interaction between PdAu nanoparticles and carbon is minimal in comparison to metal oxide supported PdAu catalysts and therefore it is reasonable to suggest that the activity of the sol immobilisation prepared catalysts is not a consequence of nanoparticle size or composition.[19] The activity of the raw and functionalised SDP500 and MWCNT supported catalysts suggests that surface functionalisation of the carbon nanomaterials could result in changes in catalyst activity. To better understand the effect of support surface functional groups on catalyst activity, the support materials were screened as heterogeneous additives using a 2.5 wt% Pd 2.5 wt% Au/$TiO_2$ reference catalyst prepared by wet impregnation. The hydrogen peroxide synthesis and hydrogenation activity of the reference catalyst is presented in Figure 5-25.

Previous work has shown that catalysts prepared using wet impregnation contain latent chloride ions from the metal chloride precursors and these halides are potent promoters for hydrogen peroxide synthesis.[45,10] To prevent such an effect masking the additive properties of the carbon materials, the reference catalyst was washed thoroughly after preparation to remove residual chloride contaminants.

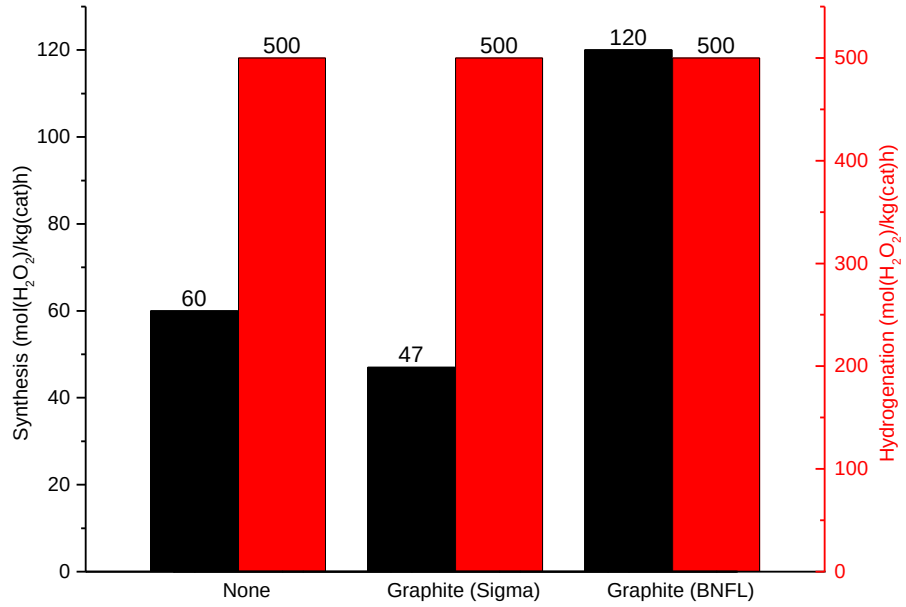


**Figure 5-25 - Hydrogen peroxide synthesis and hydrogenation activity of 2.5 wt% Pd 2.5 wt% Au/$TiO_2$ in the presence and absence of graphite additive**

**Reaction Conditions – Hydrogen peroxide synthesis: 5 % $H_2/CO_2$ (2.9 MPa) and 25 % $O_2/CO_2$ (1.1 MPa), 8.5 g solvent (2.9 g $H_2O$, 5.6 g MeOH) 0.01 g catalyst, 0.01 g additive, 2 °C, 1200 rpm, 30 min. Hydrogen peroxide hydrogenation: 5 % $H_2/CO_2$ (2.9 MPa), 8.5 g solvent (2.22 g $H_2O$, 5.6 g MeOH and 0.68 g 50 wt% $H_2O_2$), 0.01 g catalyst, 0.01 g additive, 2 °C, 1200 rpm, 30 min.**

The washed catalyst has a hydrogen peroxide synthesis and hydrogenation activity of 60 and 500 mol$H_2O_2$/h/$kg_{cat}$ respectively, less active than the unwashed analogue reported in Section 5.2.1., which has synthesis and hydrogenation activities of 97 and 430 mol$H_2O_2$/h/$kg_{cat}$.

The addition of graphite (Sigma) to the reaction mixture results in a decrease in hydrogen peroxide synthesis activity from 60 to 47 mol$H_2O_2$/h/$kg_{cat}$. In the presence of the graphite additive, the hydrogenation activity of the catalyst remained constant at 500 mol$H_2O_2$/h/$kg_{cat}$, indicating that hydrogenation of the formed hydrogen peroxide is not responsible for the synthesis activity decrease. Curiously, the addition of graphite (BNFL) results in an increase in hydrogen peroxide synthesis activity to 120 mol$H_2O_2$/h/$kg_{cat}$, and no change in hydrogenation rate, remaining constant at 500 mol$H_2O_2$/h/$kg_{cat}$. In Sections 5.2.1 and 5.2.2, graphite (BNFL) is a poor support for either sol immobilisation or impregnation prepared catalysts owing to the low hydrogen peroxide synthesis activity of the resultant catalysts. This is contrary to the use of graphite as an additive, suggesting that the necessary properties of the graphite as a support are incongruent with those as an additive. A similar trend is also observed in the case of graphite (Sigma), in which the material yields relatively active sol immobilisation catalysts yet is a poor support for impregnation catalysts and a poor additive.

Carbon blacks were also investigated as additives. The hydrogen peroxide synthesis and hydrogenation activities of 2.5 wt% Pd 2.5 wt% Au/$TiO_2$ in the presence of carbon black additives are shown in Figure 5-26.

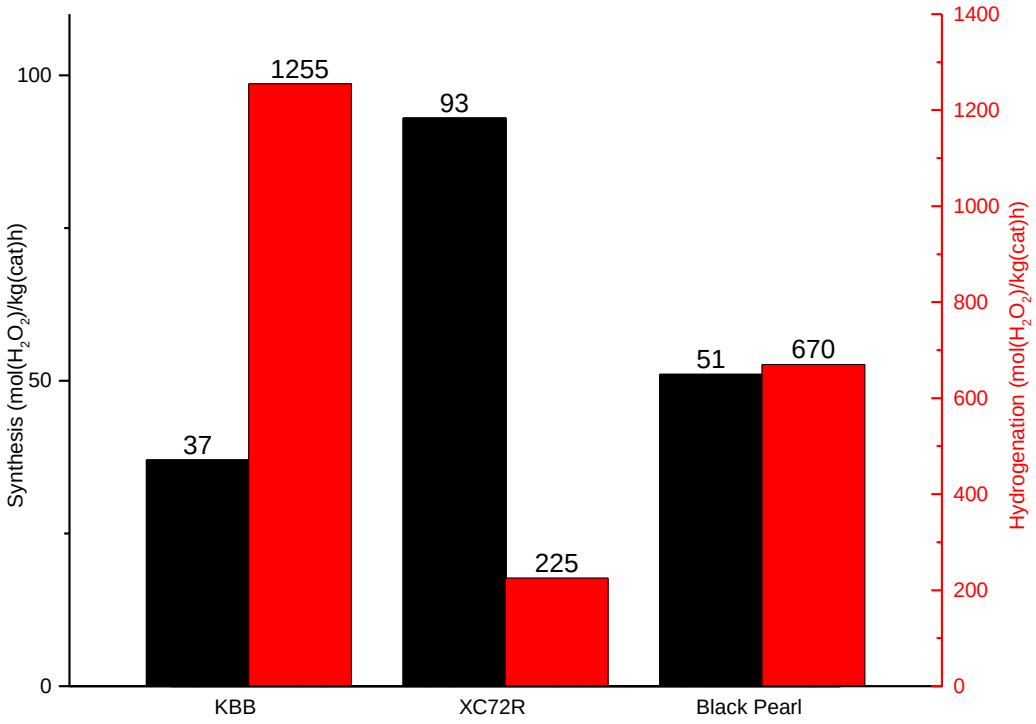


**Figure 5-26 - Hydrogen peroxide synthesis and hydrogenation activity of 2.5 wt% Pd 2.5 wt% Au/$TiO_2$ in the presence of commercial carbon blacks**

**Reaction Conditions – Hydrogen peroxide synthesis: 5 % $H_2/CO_2$ (2.9 MPa) and 25 % $O_2/CO_2$ (1.1 MPa), 8.5 g solvent (2.9 g $H_2O$, 5.6 g MeOH) 0.01 g catalyst, 0.01 g additive, 2 °C, 1200 rpm, 30 min. Hydrogen peroxide hydrogenation: 5 % $H_2/CO_2$ (2.9 MPa), 8.5 g solvent (2.22 g $H_2O$, 5.6 g MeOH and 0.68 g 50 wt% $H_2O_2$), 0.01 g catalyst, 0.01 g additive, 2 °C, 1200 rpm, 30 min.**

The addition of XC72R to the reaction results in a significant increase in hydrogen peroxide synthesis activity, 93 mol$H_2O_2$/h/$kg_{cat}$ compared to 60 mol$H_2O_2$/h/$kg_{cat}$ in the absence of additive. This is accompanied by a suppression of the hydrogen peroxide hydrogenation activity, indicating that the presence of XC72R diminishes the destruction of formed hydrogen peroxide under batch conditions. The decreased hydrogenation activity in the presence of XC72R indicates that the material is suitable to act as a heterogeneous additive for the direct synthesis of hydrogen peroxide as well as a catalyst support. Such a decrease in hydrogen peroxide hydrogenation could be attributed to the presence of surface groups known to stabilise hydrogen peroxide, like acids or halides/pseudohalides. Hydrogen peroxide stabilising groups have been exhaustively studied in the solution phase, and immobilised on metal oxide and carbon supports.[10,28,46,47]

The converse trend is observed in the case of KBB, which reduces hydrogen peroxide synthesis activity from 60 to 37 mol$H_2O_2$/h/$kg_{cat}$ and increases hydrogenation activity more than twofold from 500 to 1255 mol$H_2O_2$/h/$kg_{cat}$. This indicates that KBB effectively catalyses hydrogen peroxide decomposition or hydrogenation, which could be due to the presence of metal impurities from the manufacturing process which are not effectively removed by washing prior to use as an additive. The presence of highly active impurities is consistent with the activity of the KBB supported catalysts prepared by impregnation and sol immobilisation, which both have high hydrogenation activities relative to other catalysts in the series. Black Pearl also negatively impacts catalyst performance when used as an additive, as hydrogen peroxide synthesis activity decreased minimally to 51 mol$H_2O_2$/h/$kg_{cat}$ in the presence of the carbon, whilst hydrogenation activity rose to 670 mol$H_2O_2$/h/$kg_{cat}$.

Carbon nanomaterials were also tested as heterogeneous additives for the direct synthesis of hydrogen peroxide. The hydrogen peroxide synthesis and hydrogen activities of these reactions are presented in Figure 5-27.

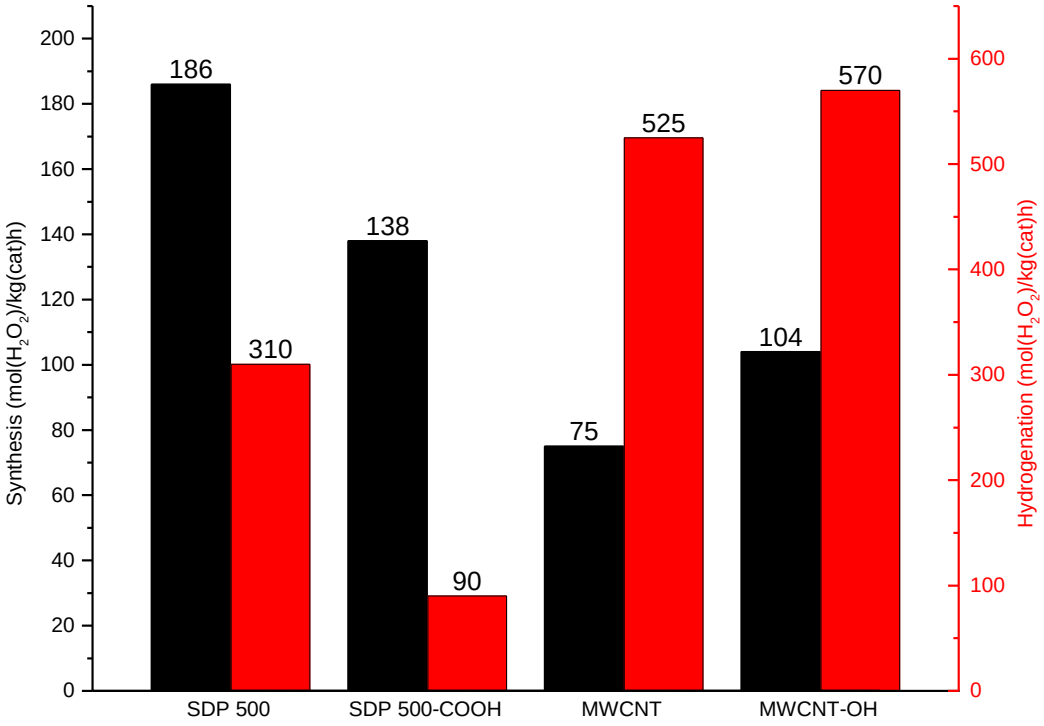


**Figure 5-27 - Hydrogen peroxide synthesis and hydrogenation activity of 2.5 wt% Pd 2.5 wt% Au/$TiO_2$ in the presence of carbon nanomaterials.**

**Reaction Conditions – Hydrogen peroxide synthesis: 5 % $H_2/CO_2$ (2.9 MPa) and 25 % $O_2/CO_2$ (1.1 MPa), 8.5 g solvent (2.9 g $H_2O$, 5.6 g MeOH) 0.01 g catalyst, 0.01 g additive, 2 °C, 1200 rpm, 30 min. Hydrogen peroxide hydrogenation: 5 % $H_2/CO_2$ (2.9 MPa), 8.5 g solvent (2.22 g $H_2O$, 5.6 g MeOH and 0.68 g 50 wt% $H_2O_2$), 0.01 g catalyst, 0.01 g additive, 2 °C, 1200 rpm, 30 min.**

Remarkably, the addition of SDP 500 to the reaction tripled the activity of the catalyst from 60 to 189 mol$H_2O_2$/h/$kg_{cat}$ and reduced hydrogen peroxide hydrogenation activity from 500 to 310 mol$H_2O_2$/h/$kg_{cat}$. The addition of SDP500 results in a 300 % increase in synthesis activity but only a 40 % decrease in hydrogenation activity suggesting that the promotional effect of the carbon occurs through a mechanism other than deactivation of the hydrogenation pathway. The presence of SDP 500-COOH similarly promotes synthesis activity to 138 mol$H_2O_2$/h/$kg_{cat}$ and reduces hydrogenation activity even further, to 90 mol$H_2O_2$/h/$kg_{cat}$, an 80 % reduction in hydrogenation activity in comparison to the catalyst in the absence of additive. The activity improvement found in using SDP 500 and SDP 500-COOH is unparalleled in comparison with the other carbons tested. The reduction in hydrogenation activity seen in the SDP 500-COOH promoted reaction is consistent with acidification of the reaction medium, which improves selectivity and synthesis activity through modulation of the hydrogenation pathway.

Blanco-Brieva *et al.* previously investigated the surface acidification of silica nanoparticles for use as a support for direct hydrogen peroxide synthesis.[47] Monometallic Pd catalysts supported on sulfonic and phosphoric acid functionalised silicas were found to be highly active for the direct synthesis of hydrogen peroxide, yielding a 6.5 wt% $H_2O_2$ solution in 3h, with selectivity of 55 %. The carboxylic acid functionalised silica performed poorly in comparison, yielding only a 2 wt% solution with a 20 % selectivity, which suggests that carboxylic acids are unsuitable for the acidic promotion of hydrogen peroxide synthesis and therefore that other factors are responsible for the additive activity of SDP500-COOH.

Park *et al.* previously reported the remarkable activity of catalysts supported on tungstic acid derived heteropolyacids (HPAs).[48] HPAs are highly acidic polyoxometalate clusters and have previously been used for acid-base catalysis and isomerisation reactions.[30] The authors showed that monometallic Pd/HPA catalysts were considerably more active for hydrogen peroxide synthesis than metal oxide supported analogues. Curiously however, the hydrogenation activity of the HPA supported catalyst was larger than $TiO_2$ supported catalysts, suggesting that the synthesis rate enhancement was not a product of hydrogenation pathway deactivation. The increased hydrogen peroxide synthesis and hydrogenation activity of HPA supported catalysts is consistent with the observations for the use of MWCNT carbons as additives in this work. The addition of unfunctionalized MWCNT carbon increases synthesis activity to 75 mol$H_2O_2$/h/$kg_{cat}$, but minimally increases hydrogenation

activity from 500 to 525 mol$H_2O_2$/h/$kg_{cat}$, indicating that the increase in synthesis activity is not due to a decrease in the hydrogenation activity. In a similar fashion, the hydroxyl modified MWCNT-OH increases both hydrogen peroxide synthesis and hydrogenation activity even further to 104 and 570 mol$H_2O_2$/h/$kg_{cat}$ respectively.

*5.2.3.1.X-Ray Photoelectron Spectroscopy (XPS) of Carbon Additives*

The carbon materials were interrogated by XPS to further understand their chemical composition and determine whether the disparity between the activity of the carbons as supports and additives is due to variation in surface composition of the materials. The XPS derived elemental surface concentrations are presented in Table 5-6.

**Table 5-6 - Tabulated XPS derived surface concentrations of C, O and N of carbon support/additive materials**

| Carbon | XPS Derived Concentration (at%) | | |
|---|---|---|---|
| | C | O | N |
| Graphite | 98.86 | 1.14 | - |
| BNFL | 99.72 | 0.11 | 0.17 |
| KBB | 89.18 | 10.82 | - |
| XC72R | 99.42 | 0.57 | - |
| Black Pearl | 88.44 | 11.56 | - |
| SDP 500 | 93.07 | 6.93 | - |
| SDP 500-COOH | 94.75 | 5.03 | 0.23 |
| MWCNT | 99.16 | 0.55 | 0.28 |
| MWCNT-OH | 94.77 | 5.23 | - |

The carbon support materials contain only carbon, oxygen and nitrogen in concentrations above the detection limit of XPS. The surface oxygen concentrations of the supports/additives and analogous impregnation and sol immobilisation prepared catalysts are shown in Table 5-7. Comparison of the surface oxygen concentrations of the impregnation catalysts and parent supports indicates that there is no clear correlation between the two. In the case of the graphite (Sigma) and XC72R supported impregnation catalysts, surface oxygen contents are three and two times larger than that of the support material respectively. Likewise, the graphite (BNFL) and Black Pearl supported impregnation catalysts also display increased oxygen surface concentrations relative to the raw carbons, to a lesser extent. Conversely, the KBB, SDP 500 and MWCNT derived impregnation catalysts exhibit a decrease in surface oxygen concentration relative to the carbon support materials. The wide

variation in oxygen concentrations of the impregnation prepared catalysts can be attributed to several effects.

**Table 5-7 - Tabulated XPS derived surface oxygen concentrations of raw carbon supports, impregnation prepared catalysts and sol immobilisation prepared catalysts, and percentage change between supports and catalysts**

| Carbon | XPS Derived Surface O Concentration (at%) | | | Surface Oxygen Content % Change Versus Support | |
|---|---|---|---|---|---|
| | Support | Impregnation Catalyst | Sol Immobilisation Catalyst | Impregnation Catalyst | Sol Immobilisation Catalyst |
| Graphite | 1.14 | 3.48 | 3.74 | 205 | 228 |
| BNFL | 0.11 | 0.15 | 0.22 | 36 | 100 |
| KBB | 10.82 | 9.92 | 9.82 | -8 | -9 |
| XC72R | 0.57 | 1.18 | 1.39 | 107 | 144 |
| Black Pearl | 11.56 | 14.09 | 10.97 | 22 | -5 |
| SDP 500 | 6.93 | 5.98 | 6.77 | -14 | -2 |
| SDP 500-COOH | 5.03 | 5.47 | 5.11 | 8 | 2 |
| MWCNT | 0.55 | 0.43 | 0.47 | -22 | -15 |
| MWCNT-OH | 5.23 | 3.73 | 3.82 | -29 | -27 |

In Section 5.2.1.3, it was shown by XPS that some of the impregnation prepared catalysts contain both Pd(0) and Pd(II) oxidation states, with the presence of Pd(II) being attributed to the formation of either monometallic PdO species, or surface oxidation of Pd domains in PdAu alloy nanoparticles. Formation of PdO species or surface oxidation of Pd domains should result in a contribution of these oxygen environments to the O 1s XPS region for the impregnation catalysts. Previous work by Simko and co-workers found that the O 1s binding energy of bulk powdered PdO is 530.5 eV, which suggests that in the case of the impregnation prepared catalysts, the contribution of PdO species to the O 1s spectra overlaps with the contribution from quinonic oxygen groups on the support and cannot be reasonably deconvoluted.[49]

The Pd(0)/Pd(II) ratios of the impregnation prepared catalysts determined by the Pd 3d spectra are however a reasonable indicator of the variation between the oxygen content of the impregnation prepared catalysts and the support materials. The impregnation catalysts which contain Pd(II) species also have increased surface oxygen concentrations relative to their parent carbon materials, which suggests that the formation of PdO species is responsible for

the increased surface oxygen concentrations of these catalysts versus the raw carbon materials.

XPS analysis of the KBB and MWCNT supported impregnation catalysts in Section 5.2.1.3 shows that these catalysts contain Pd solely in the Pd(0) oxidation state. In these cases, the surface oxygen concentrations of the catalysts are less than that of the support materials. The reduced surface oxygen content of these catalysts relative to the analogous support materials is likely due to the heat treatment regime used in the preparation of the catalysts. The impregnation prepared catalysts were treated under flowing 99 % pure nitrogen. The nitrogen gas will commonly contain water and oxygen impurities, and therefore the heat treatments proceed under mildly oxidative conditions. It can be suggested that under these conditions, easily oxidizable groups are removed by either combustion or oxidative decarboxylation which results in a decrease in surface oxygen content of the catalysts in comparison to the support materials.

The surface oxygen concentrations of the sol immobilisation prepared catalysts are also shown in

Table 5-7. Similar to the impregnation catalysts, the sol immobilisation prepared catalysts show a wide range of surface oxygen concentrations which vary considerably from the analogous oxygen concentrations of the parent carbons. It was shown in Section 5.2.2.1, that unlike the impregnation catalysts, the sol immobilisation catalysts all contain Pd in the Pd(0) oxidation state, and therefore any increase in surface oxygen content cannot be attributed to the formation of PdO species. Likewise, the sol immobilisation catalysts were not heat treated prior to use, and therefore any decrease in surface oxygen concentration is not due to the removal of easily oxidizable surface groups due to heat treatment.

XPS analysis of the sol immobilisation catalysts indicates the presence of surface nitrogen, not present in the case of the carbon supports. The presence of nitrogen in the sol immobilisation catalysts can be attributed to the polyvinylpyrrolidone (PVP) stabiliser used in the preparation of the colloidal PdAu nanoparticles prior to immobilisation on the carbon supports. Given the nitrogen XPS contributions from the PVP stabiliser, it follows that the carbonyl groups of the polymeric stabiliser must also contribute towards the O 1s spectra of the sol immobilisation catalysts. Such an effect is observed for the graphite (Sigma), graphite

(BNFL) and XC72R supported catalysts, which all exhibit increased oxygen surface concentrations relative to the support materials.

The KBB, Black Pearl and MWCNT supported sol immobilisation catalysts exhibit decreased surface oxygen concentrations in comparison to the analogous support materials. This can be ascribed to reduction of oxygen containing surface groups by the $NH_3BH_3$ used to reduce the metal precursors during nanoparticle preparation. As described in Chapter 2, $NH_3BH_3$ is used in a superstoichiometric ratio relative to the metal precursors to ensure complete reduction of the metal salts. Remaining reductant is therefore still present in the colloidal solution upon addition of the carbon support during preparation, and is known to readily reduce a number of oxygen containing functionalities, such as aldehydes, ketones and carboxylic acids, all of which were shown in Section 5.2.2.1 to be present on the surface of the support to a varying degree.

Narrow scans of the O 1s region of the carbon support materials were also recorded, to further investigate the relative abundance of different oxygen environments, presented in Figure 5-28. The O 1s peaks were fitted in a manner analogous to those described in Sections 5.2.1.3 and 5.2.2.1 for the wet impregnation and sol immobilisation prepared catalysts respectively.

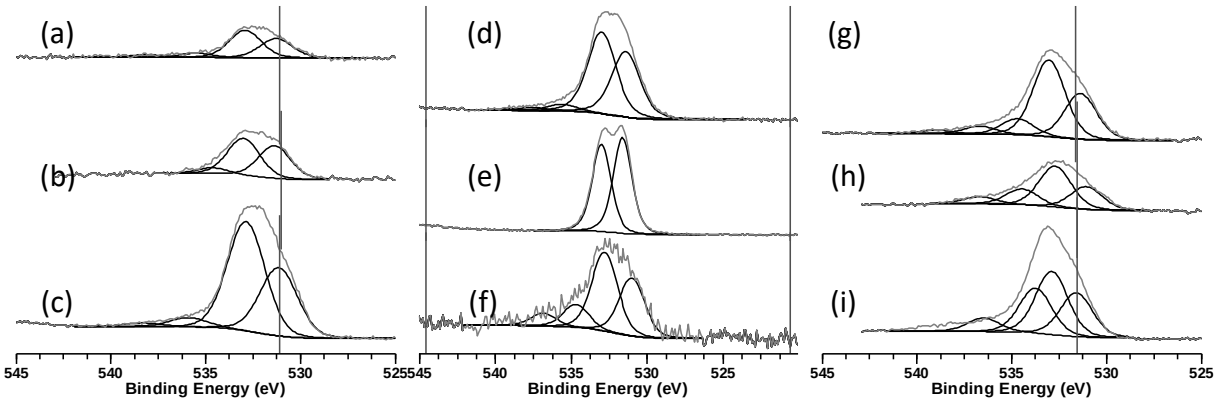


**Figure 5-28 - O(1s) spectra of carbon support/additive materials. Graphite (Sigma) (a), Graphite (BNFL) (b), KBB (c), XC72R (d), Black Pearl (e), SDP 500 (f), SDP 500-COOH (g), MWNCT (h) and MWCNT-OH (i).**

The carbon support materials all feature O 1s contributions at 531.5-532.4 eV consistent with the presence of quinonic carbonyl species, with the second significant peak at 532.5-533.4 eV corresponding to C-O bonds in alcohols and ether environments. The KBB support, and the carbon nanomaterials SDP500 and MWCNT (and their functionalised derivatives) feature a

peak at 535.5-536.4 eV indicative of C-O bonds in carboxylic and anhydride groups. In all cases the contribution of this peak to the overall O 1s spectrum is larger for the raw carbons than in the case of the sol immobilisation prepared catalyst, suggesting that the catalyst preparation method results in a modification of the support surface, likely due to reduction of the surface groups by $NH_3BH_3$ remaining from the formation of the colloidal PdAu nanoparticles.

In Section 5.2.2.1, it was shown that for sol immobilisation prepared catalysts, the oxygen/carbon surface ratio correlates with hydrogen peroxide synthesis activity, with the most active catalysts exhibiting surface oxygen concentrations around 6 at%, and decreasing or increasing the surface oxygen concentration resulting in a decrease in synthesis activity. Conversely, the wet impregnation prepared catalysts showed no trend between surface oxygen concentration and activity in Section 5.2.1.3, which can be attributed to the structure of the catalysts. In the case of wet impregnation catalysts, varying the carbon support yields catalysts with different nanoparticle sizes, oxidation states and surface compositions, which are known to influence catalyst activity.

The relationship between surface oxygen/carbon ratio and activity in the presence of the carbon additive materials is shown in Figure 5-29.

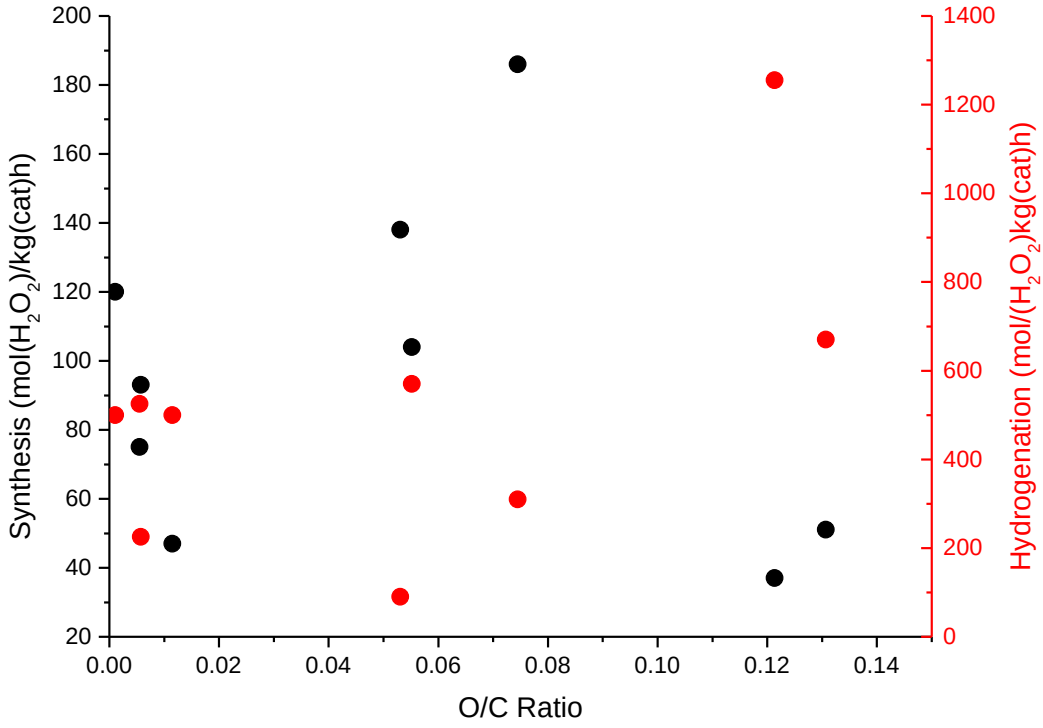


**Figure 5-29 - Hydrogen peroxide synthesis and hydrogenation activity of 2.5 wt% Pd 2.5 wt% Au/$TiO_2$ catalyst in the presence of carbon additive versus surface oxygen/carbon ratio of the carbon additive material**

Similar to the previously observed trend for sol immobilisation prepared catalysts, the SDP500 derived materials are most active as additives, with the parent SDP500 carbon increasing the hydrogenation peroxide synthesis activity of the 2.5 wt% Pd 2.5 wt% Au/$TiO_2$ reference catalyst from 60 mol$H_2O_2$/h/$kg_{cat}$ to 186 mol$H_2O_2$/h/$kg_{cat}$. Likewise, the addition of the functionalised SDP500-COOH carbon to the reaction results in an increase in synthesis activity to 138 mol$H_2O_2$/h/$kg_{cat}$. In agreement with the sol immobilisation prepared catalysts, the SDP500 carbons both exhibit intermediate surface oxygen concentrations of approximately 7 and 5 at% respectively.

The KBB carbon, exhibiting a surface oxygen concentration of 11 at%, was particularly detrimental to the activity of the catalyst, with the presence of the additive decreasing hydrogen peroxide synthesis activity from 60 to 37 mol$H_2O_2$/h/$kg_{cat}$, and increasing hydrogenation activity from 500 to 1255 mol$H_2O_2$/h/$kg_{cat}$. This suggests that the presence of the KBB carbon facilitates the decomposition of formed hydrogen peroxide under batch conditions, resulting in a decrease in hydrogen peroxide yield in comparison to the reference catalyst alone.

The fact that a number of carbon materials exhibit similar surface oxygen concentrations yet very different effects on catalyst activity, suggest that the surface oxygen groups are not responsible for the activity modulation of the additives and therefore there is no correlation between additive oxygen content and catalyst activity. For example, the MWCNT and XC72R carbons both display only 0.5 at% surface oxygen concentrations, but the hydrogen peroxide synthesis activity of the catalyst increases from 60 mol$H_2O_2$/h/$kg_{cat}$ to 75 mol$H_2O_2$/h/$kg_{cat}$ in the presence of the former and 93 mol$H_2O_2$/h/$kg_{cat}$ the latter. The two carbons also have considerably different effects on the hydrogen peroxide hydrogenation activity of the catalyst, as the addition of MWCNT carbon increases hydrogenation minimally from 500 to 525 mol$H_2O_2$/h/$kg_{cat}$ and the XC72R carbon decreases the hydrogenation activity to 225 mol$H_2O_2$/h/$kg_{cat}$.

## *5.3. Discussion*

### *5.3.1. 2.5 wt% Pd 2.5 wt% Au/C Catalysts Prepared by Wet Impregnation*

For PdAu supported nanoparticles, the synthesis and hydrogenation activity of impregnation prepared catalysts has been previously attributed to particle size effects. Edwards *et al.* previously showed that acid pre-treatment of carbon supports resulted in a decrease in average particle diameter and eliminated the formation of very large (70 nm+) particles for PdAu bimetallic catalysts, which resulted in a complete deactivation of the hydrogenation pathway and therefore an increase in direct synthesis activity in comparison to the untreated supports.[18] Lunsford and co-workers observed an analogous particle size effect for monometallic Pd/C catalysts, finding that smaller Pd particles resulted in increased hydrogen peroxide synthesis activity.[50] The authors attribute the increased catalyst activity to increased $H_2$ association on Pd(110) planes, which are more prevalent on smaller Pd nanoparticles than larger ones. Fu *et al.* studied the activity of monometallic Pd catalysts supported on fluorinated carbons, and found that the degree of fluorination resulted in minimal change in particle size, but a large change in catalyst activity, suggesting factors other than particle size determine that activity of carbon supported catalyst[51]

The activity of the wet impregnation prepared catalysts shown in this work suggests that nanoparticle size is not the predominant factor in determining catalyst activity. The KBB supported catalyst contains highly dispersed nanoparticles 2-10 nm in diameter and no larger agglomerates. In comparison, the XC72R supported catalyst contains consistently larger particles, 10-20 nm, which are also well dispersed on the support. The XC72R supported catalyst, containing larger PdAu nanoparticles, was however the most active, with a hydrogen peroxide synthesis activity of 114 mol$H_2O_2$/h/$kg_{cat}$, whilst the KBB supported analogue containing smaller nanoparticles, exhibited a synthesis activity of 102 mol$H_2O_2$/h/$kg_{cat}$. The catalysts prepared from the carbon nanomaterials SDP-500 and MWCNT, and their functionalised derivatives, exhibited particle diameters between the ranges of the two most active catalysts XC72R and KBB, yet were in all cases less active for hydrogen peroxide synthesis.

Previous work by Choudhary *et al.* has claimed that oxidation state, and not particle size, is the determinant factor in preparing highly active monometallic Pd catalysts.[34] Further work has suggested that in the case of the bimetallic catalysts, the presence of Pd(II), as determined by XPS, is indicative of the formation of PdO species during catalyst preparation.[27] The

presence of PdO is critical to catalyst activity because monometallic Pd species are considerably less selective for hydrogen peroxide synthesis than PdAu alloys.[52] In addition, the Pd/Au ratio of homogenously alloyed bimetallic nanoparticles is known to affect the hydrogen peroxide hydrogenation activity of a catalyst, and therefore synthesis activity. The presence of PdO species therefore results in separate bimetallic nanoparticles that are more gold rich than the desired Pd/Au ratio and less active.[6] Edwards and co-workers have previously suggested that the presence of Pd(II) is necessary in preparing highly selective PdAu catalysts for hydrogen peroxide synthesis, showing that the formation of Pd(II) phases upon catalyst heat treatment could instead be a result of the oxidation of surface Pd in alloyed bimetallic catalysts.[19] Follow up work found that the presence of Pd(II) species in highly dispersed PdAu bimetallic alloy catalysts correlated with a significant decrease in hydrogen peroxide hydrogenation activity.[18]

For the catalysts prepared by wet impregnation presented in this work, the relationship between Pd oxidation state and catalyst activity cannot be clearly established. Generally, the PdAu/C catalysts contain either solely Pd(0), or a combination of Pd(0) and Pd(II) in a 2:1 ratio, and any oxidation state-activity trend is subtle at best. For example, the XC72R supported catalyst is 10 % more active than its KBB supported analogue, with hydrogen peroxide synthesis activities of 102 and 114 mol$H_2O_2$/h/$kg_{cat}$ respectively, yet the KBB supported catalyst contains only Pd(0) and the XC72R analogue a mixture of Pd(0) and Pd(II). The hydrogenation activity of the XC72R supported catalyst is however 20 % lower than the KBB supported analogue, 971 mol$H_2O_2$/h/$kg_{cat}$ for the former versus 1156 mol$H_2O_2$/h/$kg_{cat}$ for the latter. The relationship between Pd oxidation state and catalyst hydrogenation activity does not extend to all the other impregnation catalysts prepared in this work. The catalyst prepared on MWCNT and its derivative MWCNT-OH have comparable hydrogen peroxide synthesis activities, 78 and 75 mol$H_2O_2$/h/$kg_{cat}$ respectively, yet the former has a hydrogenation activity of 794 mol$H_2O_2$/h/$kg_{cat}$, and the latter 1248 mol$H_2O_2$/h/$kg_{cat}$. It is determined by XPS that the catalysts both solely contain Pd(0), indicating that oxidation state variation cannot be responsible for the increase in hydrogenation activity of the MWCNT-OH supported catalyst relative to the MWCNT supported parent catalyst. It is however shown that catalysts have low synthesis activity and high hydrogenation activity (and therefore perform very poorly) if they contain Pd(II) and display a high Pd/Au surface ratio. The combination of these two factors indicates that

thorough alloying of Pd and Au during preparation is critical in preparing active catalysts, as PdAu nanoparticles formed in the presence of PdO phases exhibit surface compositions that are poorly active for hydrogen peroxide synthesis.

The surface oxygen functionality of the impregnation catalysts has also been investigated by XPS. Previous work has shown that surface functionality of carbon support materials is critical in preparing active monometallic Pd, Au and PdAu catalysts for a variety of applications.[53–60] Surface oxygen concentration varies between 0.15 at% for the graphite (BNFL) supported catalyst and 14.09 at% for the Black Pearl supported catalysts. In all cases, fitted XPS peaks corresponding to quinonic and hydroxyl functional groups were most intense, followed by contributions from carboxylic acids and chemisorbed oxygen and water. The low concentration of carboxylic acid groups on the surface of the supports precludes acid stabilisation from being responsible in the origin of catalyst activity variation, which has been previously claimed for carbon supported PdAu catalysts.[18]

It Section 5.2.1.3, it is shown that there is no relationship between the oxygen content of the support material and the activity of the impregnation catalysts for either hydrogen peroxide synthesis or hydrogenation, which is consistent with the physical and chemical structure of the catalysts as determined by electron microscopy and XPS. Whilst the effect of parameters such as particle size, composition and oxidation state have been discussed at great length in literature, in the case of the catalysts presented in this work, it is not possible to isolate any one variable as the cause of the activity of the catalysts. The catalysts prepared by wet impregnation all contain PdAu particles of different diameters, compositions and oxidation states which makes identifying the primary elements directing catalyst activity difficult.

*5.3.2.0.5 wt% Pd 0.5 wt% Au/C Catalysts Prepared by Modified Sol Immobilisation*

Catalysts were also prepared on the same carbon materials using a modified sol immobilisation method. In preparing catalysts by sol immobilisation, a colloidal metal solution is prepared and then subsequently immobilised on the support material. The principle benefit of the sol immobilisation method in comparison to wet impregnation is that the size, composition and oxidation state of the PdAu nanoparticles is determined by the formation of the metal sol and therefore independent of the interaction between the metal and the support. Kiely and co-workers previously reported the preparation of supported alloyed PdAu nanoparticles by sol immobilisation, showing that unlike the impregnation method, sol

immobilisation yields catalysts containing homogenously alloyed nanoparticles of constant composition.[4] Analysis of the sol immobilisation catalysts prepared in this work confirms that the oxidation state and surface composition of active metal surface is constant regardless of support material. In Chapter 4, it was shown by STEM that the diameter of colloidal nanoparticles remains unchanged upon immobilisation on a support material. Given the constant surface composition, oxidation state and particle diameter of the supported PdAu catalysts prepared in this work, the activity variation of the catalysts can be considered a consequence of the support material.

Activity of the sol immobilisation prepared catalysts varies significantly for both hydrogen peroxide synthesis and hydrogenation pathways. The SDP500 and graphite(BNFL) supported PdAu/C catalysts were the most and least active catalysts for direct synthesis with activities of 150 and 8 mol$H_2O_2$/h/$kg_{cat}$ respectively. The low activity of the graphite(BNFL) supported catalyst can be attributed to a combination of low surface area, only 7 $m^2$/g, and lack of surface functionalisation as determined by XPS, which may impede chemisorption of the stabilised PdAu colloid on the surface of the support. The activity of the SDP500 supported catalyst is comparable to most active sol immobilisation catalysts previously reported in literature. Pritchard *et al.* previously investigated the preparation of PdAu/C catalysts by sol immobilisation for hydrogen peroxide synthesis, showing that a 1 wt% PdAu/C catalyst with 1.85:1 Pd:Au molar ratio exhibits hydrogen peroxide synthesis and hydrogenation activities of 158 and 546 mol$H_2O_2$/h/$kg_{cat}$ respectively.[17]

The hydrogenation activities of the catalysts prepared in this work varies considerably, from 540 mol$H_2O_2$/h/$kg_{cat}$ for the KBB supported catalyst to 0 mol$H_2O_2$/h/$kg_{cat}$ in the case of the XC72R and MWCNT-OH supported analogues. The MWCNT-OH supported catalyst is more active for hydrogen peroxide synthesis than the XC72R supported catalyst, with activities of 111 and 82 mol$H_2O_2$/h/$kg_{cat}$ respectively, and as a result it is the best performing catalyst in this work. Hutchings and co-workers previously reported that a PdAu/C catalyst prepared by sol immobilisation displayed hydrogen peroxide synthesis and hydrogenation activities of 143 and 650 mol$H_2O_2$/h/$kg_{cat}$.[19] In comparison, the MWCNT-OH supported catalyst prepared in this work, was 23 % less active for direct synthesis, but completely inactive for hydrogenation. The cost of hydrogen is a critical factor in determining the industrial viability of the direct synthesis of hydrogen peroxide, and therefore using highly selective catalysts is vital to the economic feasibility of the process.

In Section 5.2.2.1, it is shown that the hydrogen peroxide synthesis activity of the carbon supported catalysts correlates with the oxygen content of the carbons such that a volcano trend is observed, with the most active catalysts containing intermediate surface oxygen concentration. Interestingly, hydrogenation activity does not correlate with surface oxygen content in a similar manner. Most commonly, increases in hydrogen peroxide synthesis activity are accompanied by decreases in hydrogenation activity. The relationship between hydrogen peroxide synthesis and hydrogenation activity is particularly prevalent for the evaluation of catalysts under batch conditions, as the contact time between hydrogen peroxide and the catalyst is sufficiently long for considerable hydrogen peroxide decomposition to take place. Several examples exist of catalysts exhibiting increased hydrogen peroxide synthesis activity through other mechanisms, where hydrogenation activity remains constant or even increases. Freakley *et al.* previously reported the activity of Pd and Au exchanged heteropolyacids (HPAs) for hydrogen peroxide direct synthesis, and found that the catalysts were considerably more active for direct synthesis than a 2.5 wt% Pd 2.5 wt% Au/C reference catalyst but also more active for hydrogen peroxide hydrogenation, indicating that the origin of activity of the HPA supported catalysts lies in a factor other than deactivation of the hydrogenation pathway.[61] This is consistent with my unpublished work on HPAs as heterogeneous additives, which has found that the addition of HPAs in the presence of a $PdAu/TiO_2$ reference catalyst results in a significant increase in hydrogen peroxide synthesis activity as well as hydrogen activity.

### *5.3.3. Carbons as Heterogeneous Additives*

The various carbon supports were also evaluated for their use as heterogeneous additives in Section 5.2.3. Changes in the hydrogen peroxide synthesis and hydrogenation activity of a 2.5 wt% Pd 2.5 wt% $Au/TiO_2$ reference catalyst in the presence of carbon additives indicates either an interaction between the carbon additive and active metal surface or formed hydrogen peroxide in solution. The most active additive is SDP500, which increased the synthesis activity of the reference catalyst from 60 to 186 $molH_2O_2/h/kg_{cat}$, whilst the worst additive is KBB, decreasing synthesis activity to 37 $molH_2O_2/h/kg_{cat}$. Using KBB as an additive results in a 250 % increase in hydrogenation activity to 1255 $molH_2O_2/h/kg_{cat}$ versus 500 $molH_2O_2/h/kg_{cat}$ for the reference catalyst alone. The high hydrogenation activity of KBB as an additive is consistent with the KBB supported catalysts prepared by impregnation and sol immobilisation; in both cases the catalysts have the highest hydrogenation activities of

their respectively series. The hydrogenation activity of the KBB material, either as additive or catalyst support, is likely due to the presence of basic surface sites highly active for hydrogen peroxide decomposition.[62]

The activity of the remaining carbon additives can be divided into two groups. The first group consists of carbons that increase hydrogen peroxide synthesis activity and decrease hydrogenation activity relative to the use of the reference catalyst alone. Carbons that exhibit this pattern of activity include the carbon nanomaterial SDP500, its functionalised derivative SDP500-COOH, and the carbon black XC72R. The activity of these additives is consistent with previous work on solution phase acid and halide additives, which also increase hydrogen peroxide synthesis activity through a similar reduction in hydrogenation/decomposition activity, and therefore the activity of these additives could be attributed to the presence of stabilising surface groups.[46,28] The activity of the SDP500 derived additives suggest that other factors may also play a role in additive activity. For example, the presence of SDP500-COOH increases hydrogen peroxide synthesis activity to 138 mol$H_2O_2$/h/$kg_{cat}$ versus 60 mol$H_2O_2$/h/$kg_{cat}$ for the reference catalyst and significantly decreases hydrogenation activity from 500 to 90 mol$H_2O_2$/h/$kg_{cat}$. In comparison, SDP500 is an even more potent additive, increasing hydrogen peroxide synthesis activity to 186 mol$H_2O_2$/h/$kg_{cat}$, but only decreases hydrogenation activity to 310 mol$H_2O_2$/h/$kg_{cat}$ which indicates that the reduction of hydrogenation/decomposition activity alone cannot explain the increased synthesis activity in the presence of the additives.

The second group of additives includes graphite (BNFL) and the MWCNT derived carbons. These carbons exhibit a beneficial effect on hydrogen peroxide synthesis activity, whilst resulting in minimal change in hydrogenation activity. The addition of MWCNT-OH yields a 73 % increase in hydrogen peroxide synthesis activity to 104 mol$H_2O_2$/h/$kg_{cat}$ in comparison to the reference catalyst, but also increases hydrogenation activity by 15 % to 570 mol$H_2O_2$/h/$kg_{cat}$. Likewise, MWCNT increases synthesis and hydrogenation activity by 25 % and 5 % respectively compared to the reference catalyst alone. The activity of the graphite(BNFL) carbon is particularly unusual, increasing synthesis activity to 120 mol$H_2O_2$/h/$kg_{cat}$ and resulting in no change in hydrogenation activity. XPS of the graphite(BNFL) catalysts shows that the carbon contains minimal oxygen or nitrogen functionality, and therefore the presence of surface groups cannot be reasonably invoked to explain the activity of the material as an additive.

## *5.4. Conclusions*

In this chapter, carbon supported catalysts have been characterised and evaluated for hydrogen peroxide synthesis and hydrogenation. Catalysts were prepared by wet impregnation on a range of graphites, activated carbons and carbon nanomaterials. The activity of the catalysts is highly dependent upon the choice of carbon support, with the most active catalysts exhibiting comparable activity to catalysts reported in literature prepared by analogous methods. The structure of the catalysts is investigated by SEM and it is shown that PdAu particle diameter varies by  support, with the formation of small particles likely due to favourable interactions between the support surface groups and the metal precursors. Determination of BET surface area of the supports showed that neither nanoparticle diameter nor catalyst activity correlated in any meaningful way with support surface area. The oxygen functionalities of the catalyst material is investigated by XPS, and it is shown that the carbon surface contains predominantly quinonic and hydroxy surface groups for all the carbons used in this work. XPS is also used to determine the Pd oxidation state and Pd/Au surface ratios, with catalysts rich in Pd(II) with Pd rich surfaces typically more active for hydrogen peroxide hydrogenation. It is suggested that due to the stark differences in catalyst structure and composition, no one factor is responsible for the variation in activity, but rather that particle size, oxidation state and surface Pd/Au ratio all contribute to catalyst activity.

Catalysts were also prepared on the same carbons using a modified sol immobilisation technique. The catalysts are more active for hydrogen peroxide synthesis and less active for hydrogenation than the wet impregnation catalysts on a per metal basis. Interestingly the XC72R and MWCNT-OH supported catalysts are completely inactive for hydrogen peroxide hydrogenation whilst remaining comparable synthesis activity to catalysts previously reported in literature. The origin of the activity of the catalysts was investigated using XPS. As the catalysts were all prepared from a parent PdAu colloid, they all contain Pd and Au in the same oxidation state, with a constant Pd/Au surface ratio. Previous work suggests that nanoparticle diameter remains constant upon immobilisation of the colloid on a support, and therefore the sol immobilisation catalysts can be considered a like-for-like comparison of support effects. The oxygen content of the supports was found to exhibit a volcano trend with hydrogen peroxide synthesis activity, with maximum activity corresponding to approximately 6 at% oxygen on the support surface. The relationship between hydrogenation activity and oxygen functionality is less well defined, suggesting that improvements in catalyst activity

are derived from a mechanism other than a decrease in hydrogenation activity frequently purported in literature.

The carbon supports were also evaluated as heterogeneous additives using a reference 2.5 wt% Pd 2.5 wt% Au/$TiO_2$ catalyst. SDP500, SDP500-COOH and graphite(BNFL) are highly active as additives, increasing hydrogen peroxide synthesis activity by at least a factor of 2 in comparison to the activity of the reference catalyst alone. Several carbons exhibit increased hydrogen peroxide synthesis but little to no decrease in hydrogenation activity, suggesting that the mechanism of promotion is different from that previously observed for acid or halide stabilisers. Furthermore, the activity of the additives does not correlate with the use of the same materials as supports for either wet impregnation or sol immobilisation prepared catalysts, which could be attributed to modification of the support surface during catalyst preparation.

## *5.5. References*

1 S. Iqbal, S. A. Kondrat, D. R. Jones, D. C. Schoenmakers, J. K. Edwards, L. Lu, B. R. Yeo, P. P. Wells, E. K. Gibson, D. J. Morgan, C. J. Kiely and G. J. Hutchings, *ACS Catal.*, 2015, **5**, 5047–5059.
2 N. Dimitratos, A. Villa, D. Wang, F. Porta, D. Su and L. Prati, *J. Catal.*, 2006, **244**, 113–121.
3 C. Li, Z. Shao, M. Pang, C. T. Williams, X. Zhang and C. Liang, *Ind. Eng. Chem. Res.*, 2012, **51**, 4934–4941.
4 R. C. Tiruvalam, J. C. Pritchard, N. Dimitratos, J. A. Lopez-Sanchez, J. K. Edwards, A. F. Carley, G. J. Hutchings and C. J. Kiely, *Faraday Discuss.*, 2011, **152**, 63.
5 J. K. Edwards, B. Solsona, P. Landon, A. F. Carley, A. Herzing, M. Watanabe, C. J. Kiely and G. J. Hutchings, *J. Mater. Chem.*, 2005, **15**, 4595.
6 J. K. Edwards, A. F. Carley, A. A. Herzing, C. J. Kiely and G. J. Hutchings, *Faraday Discuss.*, 2008, **138**, 225–239.
7 J. K. Edwards, A. F. Carley, A. A. Herzing, C. J. Kiely and G. J. Hutchings, *Faraday Discuss.*, 2008, **138**, 225–239.
8 T. Ishihara, Y. Ohura, S. Yoshida, Y. Hata, H. Nishiguchi and Y. Takita, *Appl. Catal. A Gen.*, 2005, **291**, 215–221.
9 G. Li, J. Edwards, A. F. Carley and G. J. Hutchings, *Catal. Commun.*, 2007, **8**, 247–250.
10 V. R. Choudhary, S. D. Sansare and A. G. Gaikwad, *Catal. Letters*, 2002, **84**, 81–87.
11 G. Zhao, L. Jiang, Y. He, J. Li, H. Dong, X. Wang and W. Hu, *Adv. Mater.*, 2011, **23**, 3959–3963.
12 Z. Liu, B. Guo, L. Hong and T. H. Lim, *Electrochem. commun.*, 2006, **8**, 83–90.
13 H. Watanabe, S. Asano, S. I. Fujita, H. Yoshida and M. Arai, *ACS Catal.*, 2015, **5**, 2886–2894.
14 H. Sun, Y. Wang, S. Liu, L. Ge, L. Wang, Z. Zhu and S. Wang, *Chem. Commun.*, 2013, **49**, 9914.
15 B. Choi, H. Yoon, I. S. Park, J. Jang and Y. E. Sung, *Carbon N. Y.*, 2007, **45**, 2496–2501.
16 L. Li, Z. H. Zhu, Z. F. Yan, G. Q. Lu and L. Rintoul, *Appl. Catal. A Gen.*, 2007, **320**, 166–172.
17 J. Pritchard, L. Kesavan, M. Piccinini, Q. He, R. Tiruvalam, N. Dimitratos, J. A. Lopez-Sanchez, A. F. Carley, J. K. Edwards, C. J. Kiely and G. J. Hutchings, *Langmuir*, 2010, **26**, 16568–16577.
18 J. K. Edwards, B. Solsona, E. N. N, A. F. Carley, A. A. Herzing, C. J. Kiely and G. J. Hutchings, *Science (80-. ).*, 2009, **323**, 1037–1041.
19 J. Pritchard, M. Piccinini, R. Tiruvalam, Q. He, N. Dimitratos, J. A. Lopez-Sanchez, D. J. Morgan, A. F. Carley, J. K. Edwards, C. J. Kiely and G. J. Hutchings, *Catal. Sci. Technol.*, 2013, **3**, 308–317.
20 S. Song, Y. Wang and P. K. Shen, *J. Power Sources*, 2007, **170**, 46–49.
21 G. P. Soares, M. F. R. Pereira, O. S. G. P. Soares, J. J. M. Órfão and M. F. R. Pereira, *Ind. Eng. Chem. Res.*, 2010, **49**, 7183–7192.
22 D. U. Xianlong, L. I. U. Yongmei, W. Jianqiang, C. A. O. Yong and F. A. N. Kangnian, *Chinese J. Catal.*, 2013, **34**, 993–1001.
23 A. Villa, D. Wang, P. Spontoni, R. Arrigo, D. Su and L. Prati, *Catal. Today*, 2010, **157**, 89–93.
24 A. Guha, W. Lu, T. A. Zawodzinski and D. A. Schiraldi, *Carbon N. Y.*, 2007, **45**,

1506–1517.
25 V. R. Choudhary, C. Samanta and P. Jana, *Appl. Catal. A Gen.*, 2007, **332**, 70–78.
26 A. G. Gaikwad, S. D. Sansare and V. R. Choudhary, *J. Mol. Catal. A Chem.*, 2002, **181**, 143–149.
27 G. Blanco-Brieva, E. Cano-Serrano, J. M. Campos-Martin and J. L. G. Fierro, *Chem. Commun.*, 2004, **4**, 1184–1185.
28 C. Samanta and V. R. Choudhary, *Catal. Commun.*, 2007, **8**, 73–79.
29 D. R. Lide, *J. Am. Chem. Soc.*, 2005, **127**, 4542–4542.
30 M. Besson, P. Gallezot and C. Pinel, *Chem. Rev.*, 2014, **114**, 1827–1870.
31 J. Edwards, B. Solsona, P. Landon, A. Carley, A. Herzing, C. Kiely and G. Hutchings, *J. Catal.*, 2005, **236**, 69–79.
32 M. Morad, M. Sankar, E. Cao, E. Nowicka, T. E. Davies, P. J. Miedziak, D. J. Morgan, D. W. Knight, D. Bethell, A. Gavriilidis and G. J. Hutchings, *Catal. Sci. Technol.*, 2014, **4**, 3120–3128.
33 P. Tian, L. Ouyang, X. Xu, C. Ao, X. Xu, R. Si, X. Shen, M. Lin, J. Xu and Y.-F. Han, *J. Catal.*, 2017, **349**, 30–40.
34 V. R. Choudhary, C. Samanta and T. V. Choudhary, *Appl. Catal. A Gen.*, 2006, **308**, 128–133.
35 Y. Ryabenkova, Q. He, P. J. Miedziak, N. F. Dummer, S. H. Taylor, A. F. Carley, D. J. Morgan, N. Dimitratos, D. J. Willock, D. Bethell, D. W. Knight, D. Chadwick, C. J. Kiely and G. J. Hutchings, *Catal. Today*, 2013, **203**, 139–145.
36 M. L. Cubeiro and J. L. G. Fierro, *Appl. Catal. A Gen.*, 1998, **168**, 307–322.
37 E. Bouleghlimat, P. R. Davies, R. J. Davies, R. Howarth, J. Kulhavy and D. J. Morgan, *Carbon N. Y.*, 2013, **61**, 124–133.
38 H. Darmstadt, C. Roy and S. Kaliaguine, *Carbon N. Y.*, 1994, **32**, 1399–1406.
39 E. Desimoni, G. I. Casella and A. M. Salvi, *Carbon N. Y.*, 1992, **30**, 521–526.
40 E. Desimoni, G. I. Casella, A. M. Salvi, T. R. I. Cataldi and A. Morone, *Carbon N. Y.*, 1992, **30**, 527–531.
41 U. Zielke, K. J. Hüttinger and W. P. Hoffman, *Carbon N. Y.*, 1996, **34**, 983–998.
42 A. Wong, Q. Liu, S. Griffin, A. Nicholls and J. R. Regalbuto, *Science (80-. ).*, 2017, **358**, 1427–1430.
43 R. Liu, Y. Yu, K. Yoshida, G. Li, H. Jiang, M. Zhang, F. Zhao, S. ichiro Fujita and M. Arai, *J. Catal.*, 2010, **269**, 191–200.
44 J. A. Lopez-Sanchez, N. Dimitratos, P. Miedziak, E. Ntainjua, J. K. Edwards, D. Morgan, A. F. Carley, R. Tiruvalam, C. J. Kiely and G. J. Hutchings, *Phys. Chem. Chem. Phys.*, 2008, **10**, 1921.
45 J. Edwards, B. Solsona, P. Landon, A. Carley, A. Herzing, C. Kiely and G. Hutchings, *J. Catal.*, 2005, **236**, 69–79.
46 C. Samanta and V. R. Choudhary, *Appl. Catal. A Gen.*, 2007, **330**, 23–32.
47 G. Blanco-Brieva, M. Montiel-Argaiz, F. Desmedt, P. Miquel, J. M. Campos-Martin and J. L. G. Fierro, *Top. Catal.*, 2017, **60**, 1151–1155.
48 S. Park, S. H. Lee, S. H. Song, D. R. Park, S. H. Baeck, T. J. Kim, Y. M. Chung, S. H. Oh and I. K. Song, *Catal. Commun.*, 2009, **10**, 391–394.
49 M. C. Militello and S. J. Simko, *Surf. Sci. Spectra*, 1994, **3**, 395–401.
50 Q. Liu, J. C. Bauer, R. E. Schaak and J. H. Lunsford, *Angew. Chemie - Int. Ed.*, 2008, **47**, 6221–6224.
51 F. Fu, K. T. Chuang and R. Fiedorow, *Stud. Surf. Sci. Catal.*, 1992, **71**, 33–41.
52 J. K. Edwards, S. J. Freakley, A. F. Carley, C. J. Kiely and G. J. Hutchings, *Acc.*

*Chem. Res.*, 2013, 845–854.
53 X. Wan, C. Zhou, J. Chen, W. Deng, Q. Zhang, Y. Yang and Y. Wang, *ACS Catal.*, 2014, **4**, 2175–2185.
54 G. M. Scheuermann, L. Rumi, P. Steurer, W. Bannwarth and R. Mulhaupt, *J. Am. Chem. Soc.*, 2009, **131**, 8262–8270.
55 B. Kim and W. M. Sigmund, *Langmuir*, 2004, **20**, 8239–8242.
56 X. Gu, W. Qi, X. Xu, Z. Sun, L. Zhang, W. Liu, X. Pan and D. Su, *Nanoscale*, 2014, **6**, 6609–6616.
57 L. Jiang and L. Gao, *Carbon N. Y.*, 2003, **41**, 2923–2929.
58 X. Wu, Y. Xing, D. T. Pierce and J. X. Zhao, *ACS Appl. Mater. Interfaces*, 2017, acsami.7b12539.
59 G. Goncalves, P. A. A. P. Marques, C. M. Granadeiro, H. I. S. Nogueira, M. K. Singh and J. Grácio, *Chem. Mater.*, 2009, **21**, 4796–4802.
60 T. Sun, Z. Zhang, J. Xiao, C. Chen, F. Xiao, S. Wang and Y. Liu, *Sci. Rep.*, 2013, **3**, 1–6.
61 S. J. Freakley, R. J. Lewis, D. J. Morgan, J. K. Edwards and G. J. Hutchings, *Catal. Today*, 2015, **248**, 10–17.
62 C. Samanta, *Appl. Catal. A Gen.*, 2008, **350**, 133–149.